3-5-2010

Roles of Serine 101, Histidine 310 and Valine 464 in the Reaction Catalyzed by Choline Oxidase from Arthrobacter Globiformis

Steffan Finnegan
Georgia State University

ROLES OF SERINE 101, HISTIDINE 310 AND VALINE 464 IN THE REACTION CATALYZED BY CHOLINE OXIDASE FROM *ARTHROBACTER GLOBIFORMIS*

by

STEFFAN FINNEGAN

Under the Direction of Giovanni Gadda

ABSTRACT

The enzymatic oxidation of choline to glycine betaine is of interest because organisms accumulate glycine betaine intracellularly in response to stress conditions, as such it is of potential interest for the genetic engineering of crops that do not naturally possess efficient pathways for the synthesis of glycine betaine, and for the potential development of drugs that target the glycine betaine biosynthetic pathway in human pathogens. To date, one of the best characterized enzymes belonging to this pathway is the flavin-dependent choline oxidase from *Arthrobacter globiformis.* In this enzyme, choline oxidation proceeds through two reductive half-reactions and two oxidative half-reactions. In each of the reductive half-reactions the FAD cofactor is reduced to the anionic hydroquinone form (2 e^- reduced) which is followed by an oxidative half-reaction where the reduced FAD cofactor is reoxidized by molecular oxygen with formation and release of hydrogen peroxide.

In this dissertation the roles of selected residues, namely histidine at position 310, valine at position 464 and serine at position 101, that do not directly participate in catalysis in the reaction catalyzed by choline oxidase have been elucidated. The effects on the overall reaction kinetics of these residues in the protein matrix were investigated by a combination of steady state kinetics,

rapid kinetics, pH, mutagenesis, substrate deuterium and solvent isotope effects, viscosity effects as well as X-ray crystallography.

A comparison of the kinetic data obtained for the variant enzymes to previous data obtained for wild-type choline oxidase are consistent with the valine residue at position 464 being important for the oxidative half-reaction as well as the positioning of the catalytic groups in the active site of the enzyme. The kinetic data obtained for the serine at position 101 shows that serine 101 is important for both the reductive and oxidative half-reactions. Finally, the kinetic data for histidine at position 310 suggest that this residue is essential for both the reductive and oxidative half-reactions.

INDEX WORDS: Choline oxidase, Flavin oxidation, Oxygen reactivity, Proton-transfer network, Chemical mechanism, Flavoprotein.

ROLES OF SERINE 101, HISTIDINE 310 AND VALINE 464 IN THE REACTION CATALYZED BY CHOLINE OXIDASE FROM *ARTHROBACTER GLOBIFORMIS*

by

STEFFAN FINNEGAN

A Dissertation Submitted in Partial Fulfillment of the Requirements for the Degree of Doctor of Philosophy

in the College of Arts and Sciences

Georgia State University

2010

ROLES OF SERINE 101, HISTIDINE 310 AND VALINE 464 IN THE REACTION CATALYZED BY CHOLINE OXIDASE FROM *ARTHROBACTER GLOBIFORMIS*

by

STEFFAN FINNEGAN

Committee Chair: Dr. Giovanni Gadda

Committee: Dr. Markus W. Germann

Dr. Aimin Liu

Electronic Version Approved by:

Office of Graduate Studies

College of Arts and Sciences

Georgia State University

May 2010

TABLE OF CONTENTS

LIST OF TABLES

LIST OF FIGURES

LIST OF SCHEMES

CHAPTER I

INTRODUCTION

1.1 Flavin dependent enzymes

Flavin dependent enzymes or flavoenzymes are enzymes that utilize the chemically versatile compound 7,8-dimethyl-10-alkylisoalloxazine or simply flavin (**Figure 1.1**) as a noncovalently or covalently bound cofactor for catalysis. The predominant form of flavin found in nature is flavin adenine dinucleotide (FAD), and to a lesser degree flavin mononucleotide (FMN).

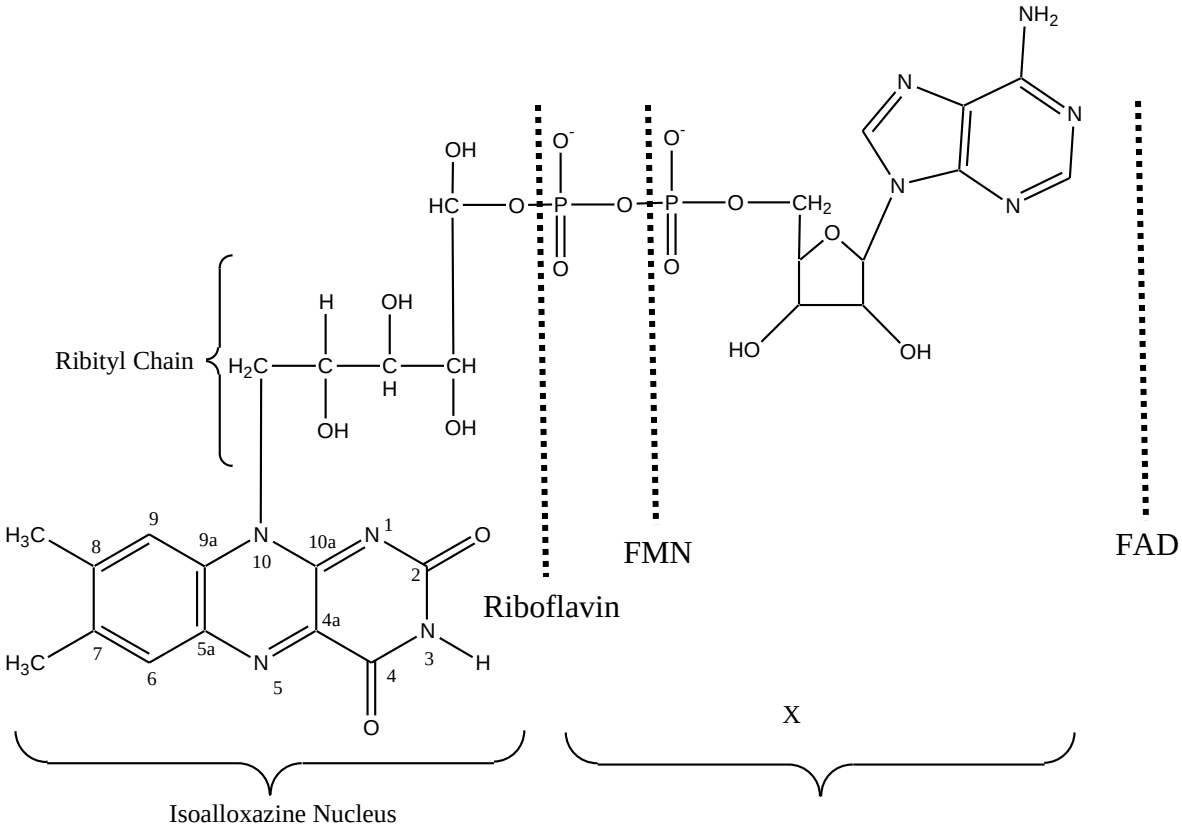

Figure 1.1. Structures of Riboflavin (X=H), FMN (X = PO_3^{2-}), and FAD (X = ADP)**.**

Although synthesis of riboflavin, the precursor of all biological relevant flavins, only occurs in some lower organisms and plants, an estimated 1-3% of all prokaryotic and eukaryotic genes are thought to encode for flavin binding proteins. In humans, riboflavin is an essential nutrient

required for FMN and FAD synthesis. FMN and FAD synthesis begin with flavokinase phosphorylating riboflavin to generate FMN, which then can be adenylated to form FAD by FAD synthetase (*1-3*). The abundance of flavin binding proteins in nature is likely due to the wide array of biochemical reactions that can be catalyzed by flavin dependent enzymes (**Figure 1.2**).

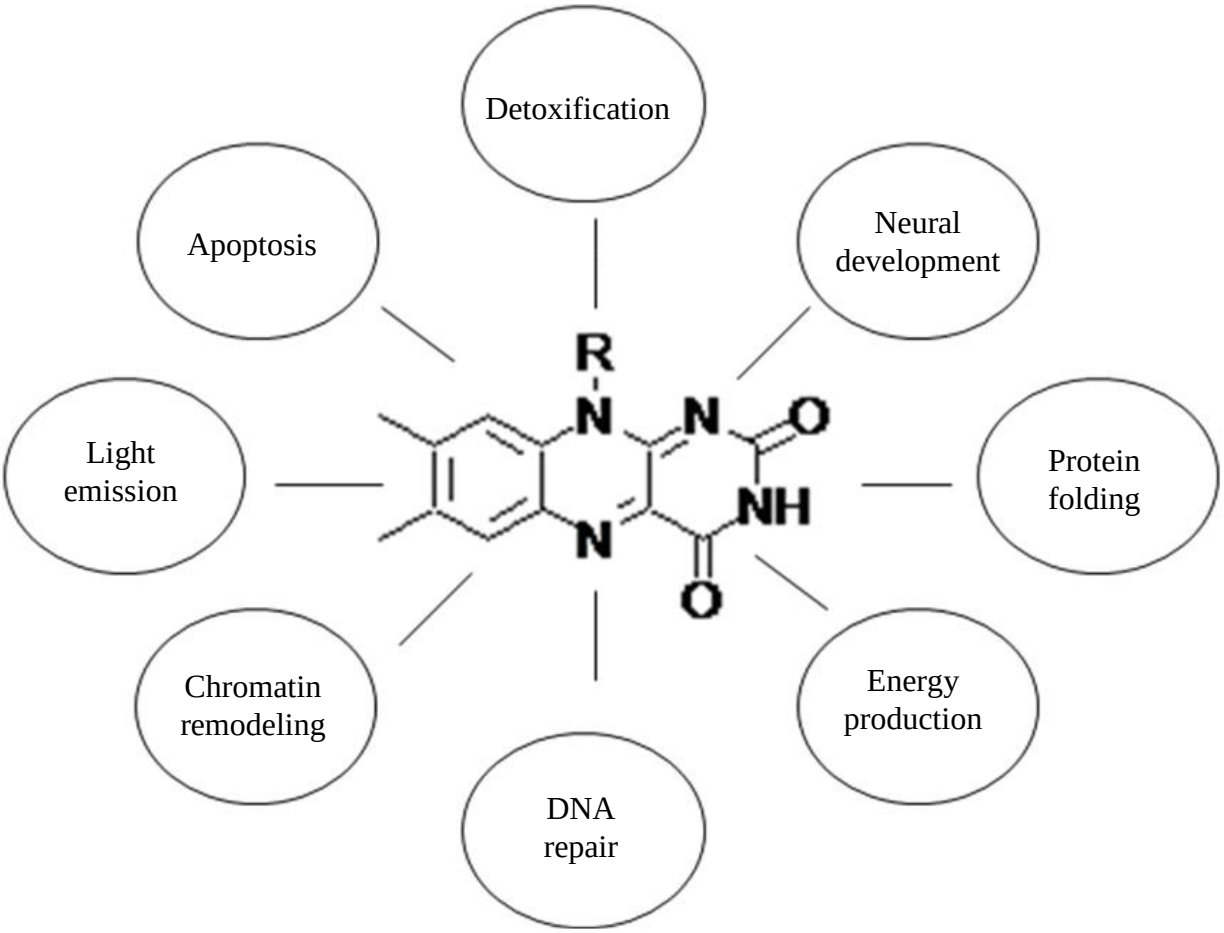

Figure 1.2. Sample of Biological Functions that Involve Flavoenzymes (*4-10*). (Modified from ref. (*11*))

The chemical versatility of flavoenzymes arises from the flavin cofactor having the ability to couple one- and two-electron transfer processes between substrates and various electron carriers as well as functioning as electrophile and nucleophile (*12*). Flavoenzymes generally achieve

catalysis through two half-reactions, a reductive half-reaction in which the flavin cofactor is either one- or two-electron reduced followed by an oxidative half-reaction in which the flavin is re-oxidized (**Scheme 1.1**).

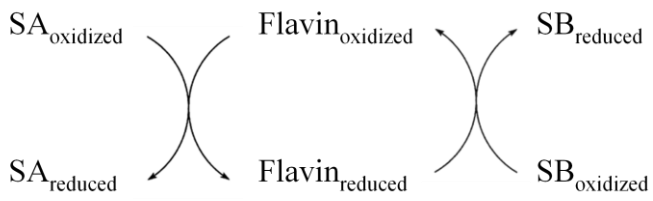

Scheme 1.1. Generalized Flavin Catalytic Cycle. SA and SB are Substrate A and B Respectively.

Flavin can exist in three different redox states, the oxidized, the semiquinoid (1 e^- reduced), and the fully reduced (2 e^- reduced) species (**Figure 1.3**). Additionally, the semiquinoid and the fully reduced states exist in both a neutral and an anionic form. Each of these 5 flavin states is accompanied with unique spectral properties (**Figure 1.4**) (*13*). These large spectral differences between the various flavin oxidation states make it possible to monitor events occurring during catalysis using the flavin itself as a spectral probe.

The semiquinoid species of the free flavin can either be in a neutral (blue) or anionic (red) form, with a pK_a of ~8.5 in solution (*14-15*). However, upon association of the flavin with the apoprotein forming the holoenzyme, this pK_a value is often shifted beyond the pH-range where the flavoenzymes are stable and therefore only one form of the semiquinone will be stabilized and detectable. Glucose oxidase was the first reported flavoenzyme where the pK_a of the semiquinone remained in the pH-range where the enzyme was stable, thus allowing both forms of the semiquinone to be spectrally characterized (**Figure 1.4**) (*13*).

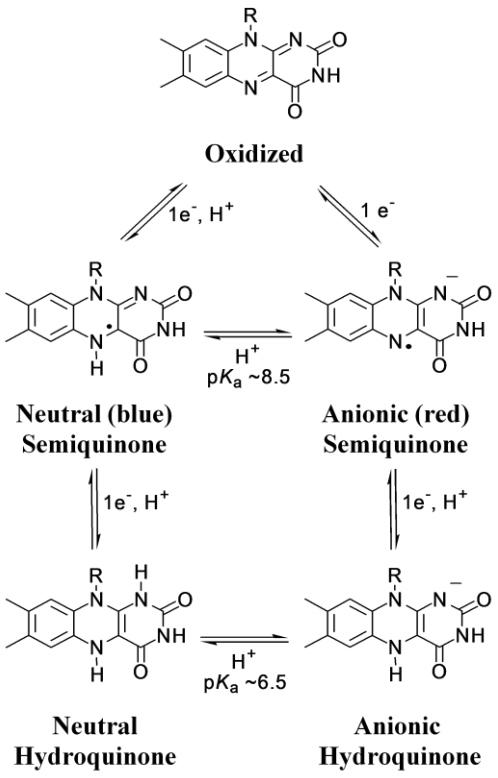

Figure 1.3. Redox and Ionization States of Flavins. (Modified from ref. (*16*))

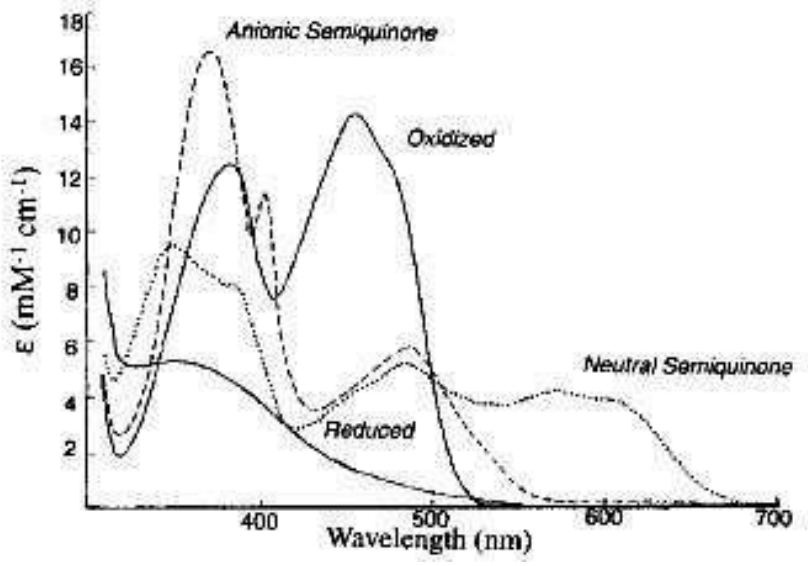

Figure 1.4. Spectra of Glucose Oxidase in the Oxidized, Semiquinone (Anionic and Neutral), and Fully Reduced States (*13*).

The spectroscopic properties of flavins have allowed for a detailed kinetic characterization of many flavoenzymes, making them one of the best studied classes of enzymes. In addition, these kinetic studies have often been supplemented with structural studies. In recent years, structural studies of flavoenzymes have gained momentum as seen by the increase of entries in the Protein Databank that now contains ~1400 structures of proteins containing flavin as compared to ~200 in the year 2000.

Generally, flavoenzymes can be grouped into a relatively small number of subclasses, where members within the same subclass share several common properties, including the type of reactions that they catalyze. The most common grouping of flavoenzymes is based on the reactivity of their reduced form with dioxygen (*17*). Using these criteria there are four well defined groups of flavoenzymes.

1. Oxidases – react rapidly with oxygen to yield H_2O_2 and oxidized enzyme.
2. Monooxygenases – react rapidly with oxygen to yield H_2O, oxidized enzyme and a substrate with an inserted single oxygen atom.
3. Electron transferases – react slowly with oxygen to yield an oxygen radical paired with the neutral flavoenzyme semiquinone radical.
4. Dehydrogenases – react poorly with oxygen to yield $O_2^{-\cdot}$.

Enzymes belonging to each of these classes of have been found to share several common properties. However, each class has been further sub-characterized based on these additional properties.

Oxidases. The flavin dependent oxidases react with oxygen in their reduced form by transferring a hydride equivalent to reform the oxidized flavin cofactor and hydrogen peroxide. A common feature of all the flavin dependent oxidases is that they stabilize the red anionic one-electron reduced semiquinone (*18-22*) as well as having the ability to form a stable flavin N(5)-sulfite adduct (*19-20*). These features both imply the presence of a positive charge proximal to the negative charge formed at the N(1)-C(2)=O locus of the flavin isoalloxazine ring as a result of flavin reduction. Indeed, the emergence of X-ray crystallographic structures of flavin dependent oxidases has shown the presence of a positively charged residue close to N(1)-C(2)=O region of the flavin cofactor, e.g. His466 in choline oxidase and Lys230 in glycolate oxidase (*23-25*). Amongst the most intensively studied flavin dependent oxidases are: choline oxidase (*24, 26-38*), cholesterol oxidase (*39-61*), glycolate oxidase (*23-25*), sarcosine oxidase, D-amino acid oxidase (*62-69*) and glucose oxidase (*70-75*).

Monooxygenases. Contrary to the oxidases, the flavin dependent monooxygenases activate oxygen through a detectable flavin hydro-peroxide intermediate. Upon formation the flavin hydroperoxide intermediate transfers an oxygen atom to the substrate with the formation of a C(4a)-hydroxyflavin, which returns to its oxidized state upon dehydration. However, even in the absence of the substrate, the flavin hydroperoxide converts slowly to H_2O_2 and oxidized flavin (*76*).

Electron transferases. The flavin-dependent electron transferases react slowly with oxygen to yield an oxygen radical and the neutral flavoenzyme semiquinone radical in the absence of a physiological electron acceptor (*76*). Additionally, in contrast to the flavoenzymes that react rapidly with oxygen, the flavin-dependent electron transferases do not readily form N(5)-sulfite

adducts. Amongst the best characterized flavoprotein electron transferases are flavodoxin (*23-25*), NADPH-cytochrome P-450 reductase (*77*), and ferredoxin-$NADP^+$ reductase (*78-83*).

Dehydrogenases. The flavin-dependent dehydrogenases react poorly, if at all, with molecular oxygen. They utilize a specific electron acceptor such as $NADP^+$ to oxidize the organic substrate. Amongst the best studied flavin-dependent dehydrogenases are the acyl-CoA dehydrogenases. These enzymes oxidize the organic substrate by transferring a hydride equivalent to the oxidized flavin, which subsequently transfers these electrons to the final electron acceptor, $NAD(P)^+$ (*84*).

1.2 Selected structural features of flavoenzymes with different oxygen reactivity

Flavoenzymes are known to have a variety of folding topologies such as the $(\alpha/\beta)_8$-barrel and the PHBH-fold (*24, 85-88*). However, these folding features do not correlate with enzyme function (**Table 1.1**). Topologically similar flavoenzymes can catalyze significantly different reactions as exemplified by the similar overall folding observed in cholesterol oxidase (*89*), fumarate reductase (*90*) and *p*-hydroxybenzoate hydroxylase (*91*). Furthermore, flavoenzymes with dissimilar overall folding topologies can catalyze similar reactions. As such, the overall folding topology cannot be used to distinguish between oxidases and monooxygenases, a finer and more detailed analysis of the active site is required. This correlates well to the findings from sequence and structure analyses of FAD-containing enzymes performed by O. Dym and D. Eisenberg (*92*) that showed that the major determinant of the catalytic function is the flavin protein-microenvironment immediately surrounding the isoalloxazine ring of the flavin cofactor rather than the overall protein folding.

Table 1.1. Overall Fold of Selected Flavoenzymes

Flavoenzyme (PDB file)	Cofactor	Folding topology	Ref
Choline Oxidase (2JBV)	FAD	PHBH	(*24*)
Glucose Oxidase (1CF3)	FAD	PHBH	(*85*)
Cholesterol Oxidase (1COY)	FAD	PHBH	(*93*)
Cellobiose Dehydrogenase (1NAA)	FAD	PHBH	(*94*)
Pyranose 2-Oxidase (1TT0)	FAD	PHBH	(*95*)
D-Amino Acid Oxidase (2E48)	FAD	PHBH	(*96*)
Polyamine Oxidase (1B37)	FAD	PHBH	(*97*)
Monomeric Sarcosine Oxidase (1L9F)	FAD	PHBH	(*98*)
p-Hydroxybenzoate Hydroxylase (1PHH)	FAD	PHBH	(*91*)
p-Hydroxyphenylacetate Hydroxylase (2JBR)	FMN	Tetrameric	(*99*)
Flavocytochrome b_2 (1FCB)	FMN	$(\alpha/\beta)_8$ Barrel	(*100*)
Glycolate Oxidase (1GOX)	FMN	$(\alpha/\beta)_8$ Barrel	(*101*)
Trimethylamine Dehydrogenase (2TMD)	FMN	$(\alpha/\beta)_8$ Barrel	(*86*)
Dihydroorotate Dehydrogenase (2DOR)	FMN	$(\alpha/\beta)_8$ Barrel	(*88*)
Old yellow Enzyme (1OYB)	FMN	$(\alpha/\beta)_8$ Barrel	(*102*)

In the flavin-dependent monooxygenases, the reaction of reduced flavin with oxygen proceeds through a detectable reaction-intermediate such as C(4a)-(hydro)peroxides and C(4a)-hydroxides (*103*). The stabilization of these reaction intermediates is key for monooxygenase reactivity and is generally achieved by desolvation of a highly defined hydrophobic cavity in front of the C(4a) atom of the flavin. A typical example of this desolvation is seen in the monooxygenase component (C_2) of *p*-hydroxyphenylacetate hydroxylase (*99*), where nine

hydrophobic residues define a hydrophobic cavity in front of the C(4a) atom and in phenylacetone monooxygenase (*104*) where 5 residues create a similar cavity on the *re* side of the flavin. Other monooxygenases with similar cavities in front of the C(4a)-N5 locus of the flavin are *p*-hydroxybenzoate hydroxylase (*91*), 3-hydroxybenzoate hydroxylase (*105*) and tryptophan 7-halogenase (*106*).

A structural comparison of the active sites of the flavin dependent oxidases revealed no such well defined hydrophobic cavities (*103*). However when surveying several well characterized flavin-dependent oxidases a recurring motif consisting of a non-polar site and a positive charge in close proximity to the C(4a)-N5 locus of the flavin cofactor (**Figure 1.5**) was observed (see Chapter IV for survey details) (*24, 85, 107-108*). In choline oxidase, the positive charge required for oxygen activation is provided by the positively charged trimethylammonium moiety of the substrate (*32, 109*) and the non-polar region is provided by the side chain of the hydrophobic residue Val464, which is ~5.5 Å away from the flavin C(4a) atom (See Chapter IV). A similar motif is seen in glucose oxidase and monomeric sarcosine oxidase. In glucose oxidase the side chain of the hydrophobic residue Val560 is ~4.7 Å away from the side chain of His516, which has been shown to provide the positive charge that is required to activate molecular oxygen for reaction with the reduced flavin cofactor (*107, 110-111*), and ~6.3 Å away from the C(4a) atom of the flavin cofactor. Similarly, in monomeric sarcosine oxidase the hydrophobic residue Phe256 is ~4 Å away from the positive charge provided by the side chain of Lys265, which is required for oxygen activation (*49*), and ~6 Å from the C(4a) atom of the flavin. The importance of the positive charge can also be seen in D-amino acid oxidase and in monoamine oxidase A, where it has been shown that the rate of the reaction of the reduced flavin with molecular oxygen

is increased almost an order of magnitude upon binding of the positively charged product or product analog (*112-113*).

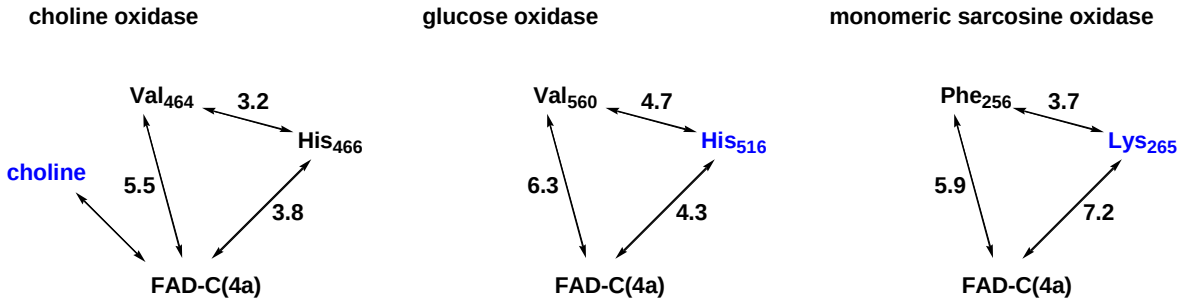

Figure 1.5. Flavin Dependent Enzymes Displaying a Hydrophobic Residue Close to a Positive Charge that is Required for Oxygen Activation Close to the FAD-C(4a)-N5 Region.

When expanding the structural analysis to encompass flavoenzymes that have not been as comprehensively characterized, several flavin-dependent oxidases are found with a similar motif consisting of a non-polar region close to a positive charge and the C(4a) atom of the flavin as exemplified by the flavoenzymes shown in **Figure 1.6** (see Chapter IV for survey details) (*24, 85, 107-108*).

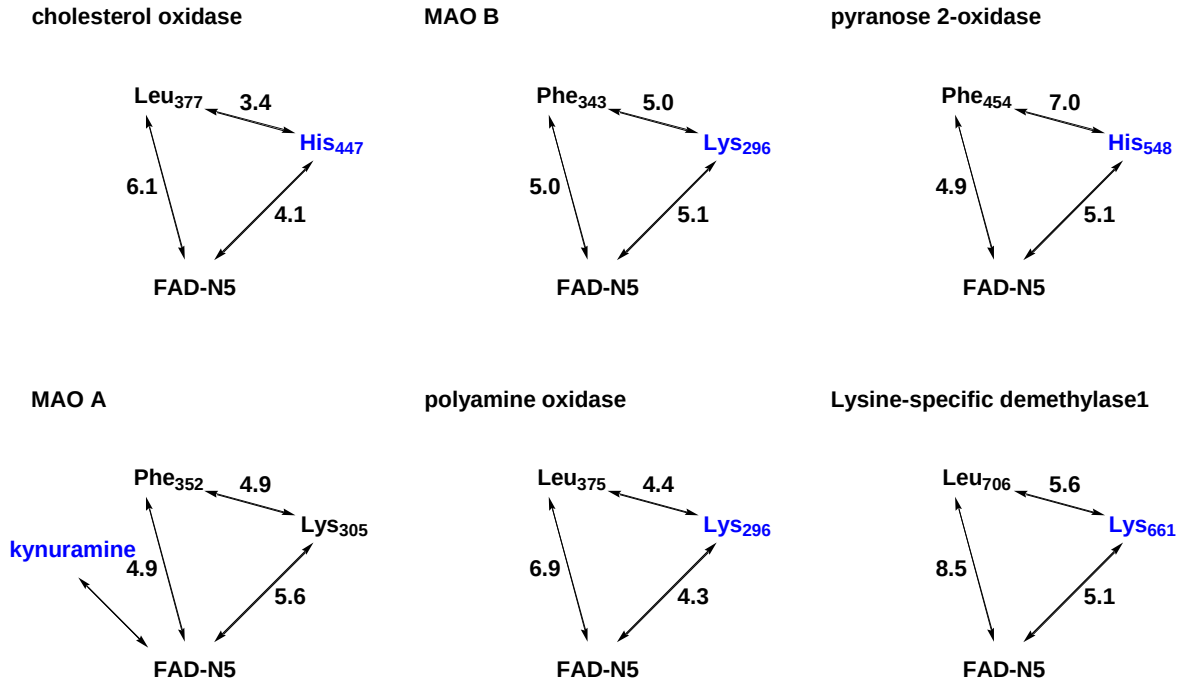

Figure 1.6. Flavin Dependent Enzymes Displaying a Hydrophobic Residue Close to a Positive Charge Close to the FAD-N5 Atom (*24, 101, 114-116*).

A structural and kinetic comparison of glycolate oxidase and flavocytochrome b_2 revealed that flavoenzymes with structurally homologous and highly conserved active sites can have vastly different reactivities with oxygen. The major differences between these two flavoenzymes are the presence of a leucine (Leu230) residue and the backbone nitrogen of Ala198 close to the C(4a) atom of the flavin cofactor in flavocytochrome b_2 whereas in glycolate oxidase it is a tryptophan (Trp108) and the methyl side-chain of alanine79 that is close to the C(4a)-atom (*87, 100*). Thus, the polarity and orientation of the sidechain of this region appears to be the predominant difference between these two flavoenzymes.

Consistent with the importance of the cavity in front of the C(4a)-N5 locus of the FAD isoalloxazine ring for oxygen reactivity are findings from recent studies on the enzymes belonging to the L-2-hydroxy acid oxidase family, which are FMN dependent enzymes. The members of the L-2-hydroxy acid oxidase family that display poor oxygen reactivity have been shown to have a constrained environment around the N5 position of the FMN cofactor (*117*). To further elaborate on the importance of the residues lining the cavity in front of the C(4a)-N5 locus of the flavin it is key to look at a study of L-galactono-γ-lactone dehydrogenase. The study showed that upon mutation of the alanine residue at position 113, which is positioned near the C(4a) locus of the isoalloxazine ring, to a glycine residue oxygen reactivity was increased 400-fold and effectively changing a dehydrogenase to a catalytically competent oxidase (*118*). In L-galactono-γ-lactone dehydrogenase, a bigger cavity is sufficient to allow for better oxygen reactivity likely due to improved oxygen accessibility.

In summary, it appears that the monooxygenases have a highly defined hydrophobic cavity in front of the C(4a) atom of the flavin with optimum geometry for encapsulating and stabilizing the C4-hydroperoxyflavin, and thus allowing monooxygenation reactions to be catalyzed.

Conversely, in the oxidases no such highly defined cavity is observed, most likely due to the oxidases having less stringent requirements for optimum reaction of the reduced flavin with molecular oxygen. These structurally different oxidases do seem to have some commonly recurring structural features, such as a non-polar region or a positive charge close to the C(4a)-atom of the flavin cofactor. A summary of common structural features of the surveyed flavoenzymes are shown in **Table 1.2.**

Table 1.2. Structural Features of Selected Flavoenzymes Important for Oxygen Reactivity

Flavoenzyme	Positive charge	Effect of positive charge on k_{cat}/K_{oxygen}	Non-polar residue	Ref
Choline Oxidase	Substrate	~80 fold increase	Val464	(*24*, *108*)
Glucose Oxidase	His516	~100 fold increase	Val560	(*85*, *107*)
Cholesterol Oxidase	His447		Leu377	(*93*)
Pyranose 2-Oxidase	His548		Phe454	(*95*)
D-Amino Acid Oxidase	Product analog		Ile230	(*96*)
Polyamine Oxidase	Lys296		Leu375	(*97*)
Monomeric Sarcosine Oxidase	Lys265	~8000 fold increase	Phe256	(*49*, *98*)
Glycolate Oxidase	Lys236		Trp110	(*119*)
Monoamine oxidase A	Product/Lys305	~10 fold increase	Phe352	(*86*)
Monoamine oxidase B	Product/Lys296	~10 fold increase	Phe343	(*116*)
Old yellow Enzyme	His196		Phe250	(*102*)

1.3 Oxygen reactivity

1.3.1. General oxygen chemistry

Molecular oxygen, O_2, can exist in both the singlet ($^1\Delta_g$) (i.e. no unpaired electrons) and the triplet ($^3\sum_g$) (i.e. unpaired electrons) spin state. Triplet oxygen is the most stable form of the oxygen. The electron configuration of triplet oxygen has two unpaired electrons occupying two antibonding molecular orbitals. The unpaired electrons in these two degenerate orbitals can have the same spin, so the total spin of the molecule is 1. Due to this non-zero spin molecular oxygen

in its triplet state has a magnetic moment and as such liquid oxygen is paramagnetic. Molecular oxygen in its singlet ground spin state, there are no unpaired electrons and as such the total spin is zero. Singlet oxygen is many times more reactive than triplet oxygen and readily reacts with other singlet molecules, which comprise the majority of all compounds, and is therefore rapidly depleted. Contrary to this is molecular oxygen in its triplet ground state, for which chemical reactions between reactants in their triplet and singlet spin states are forbidden by Wigner's spin selection rule (*120*). The conservation of spin allows triplet oxygen to readily react with molecules in a doublet state, such as radicals, to form a new radical.

Thus, the triplet multiplicity is the actual reason why most reactions of oxygen with organic substances, although being exergonic, do not readily proceed at room temperature but only upon heating or in the presence of catalysts that activate O_2 via a series of one-electron transfer reactions (*121*). **Figure 1.7** shows the reduction potentials of O_2 at pH 7.0. These reduction potentials indicate that the limiting step in O_2 reduction is the first single electron transfer (*122*). Furthermore the negative standard reduction potential for the one electron transfer to O_2 makes it a non-spontaneous process with electron donors of higher standard potentials.

$$O_2 \xrightarrow{-0.33V} O_2^{-\cdot} \xrightarrow{+0.89V} H_2O_2 \xrightarrow{+0.38V} H_2O + {}^{\cdot}OH \xrightarrow{+2.31V} 2H_2O$$

Figure 1.7. Standard Reduction Potentials for O_2 (*123*).

In order to overcome this restriction that contribute to the kinetically inertness of O_2, enzymes have evolved to utilize cofactors such as transition metals, flavins or hemes to enhance their reactivity with oxygen. A survey of the different mechanisms by which enzymes reduce O_2

does not yield a single principle by which this is achieved. However, broad generalizations can be made and some general principles can be deduced.

One method employed by enzymes is to have a reduced metal-center, most frequently Fe^{2+} or Cu^{1+} (*124*). The triplet oxygen binds to the metal-center and upon binding the electron orbitals of the oxygen overlap with those of the metal-center and the unpaired electrons are no longer distinguishable, meaning that the unpaired electrons do not belong to neither the metal-center nor oxygen, but rather to the metal-oxygen complex as a whole. It is spin allowed for such a complex to react with singlet reactants to yield singlet oxidized products as long as the number of unpaired electrons in the metal-oxygen complex remains constant. In this type of enzyme enhanced oxygen reactivity, the reaction with oxygen typically proceeds by an ionic mechanism (*125*). A second method by which enzymes can overcome the spin-forbidden reaction of molecular oxygen with singlet reactants is to have the initial reaction being a free radical mechanism in which a single electron is transferred from a reduced cofactor to oxygen resulting in the formation of two free radicals that can either recombine or react further. This type of reaction is exemplified by the reaction of a reduced flavin with molecular oxygen. In flavin dependent enzymes, the reduction of O_2 is spin prohibited. A proposed mechanism by which oxygen, in its triplet state, reacts with reduced flavin, in its singlet state, proceeds via a single electron being transferred from the reduced flavin to O_2 to form a caged radical pair consisting of a flavin semiquinone and a superoxide anion. This radical pair can then follow different routes resulting in the generation of deprotonated hydrogen peroxide, the insertion of an oxygen atom into a substrate via a peroxy-flavin intermediate or simply produce oxygen radicals (**Figure 1.8**). The flavin-dependent monooxygenases all proceed via a detectable peroxy-flavin intermediate. However, in the flavin-dependent oxidases the route by which the caged radical pair decays to

hydrogen peroxide and oxidized flavin is not as clear. It can either go directly to the end product or through an intermediate as in the monooxygenases. So far, only two flavin dependent oxidases have experimental evidence that this reaction proceeds through an intermediate. Both pyranose-2-oxidase and choline oxidase have shown the presence of a C(4a)-oxygen-adduct (*24, 126-127*).

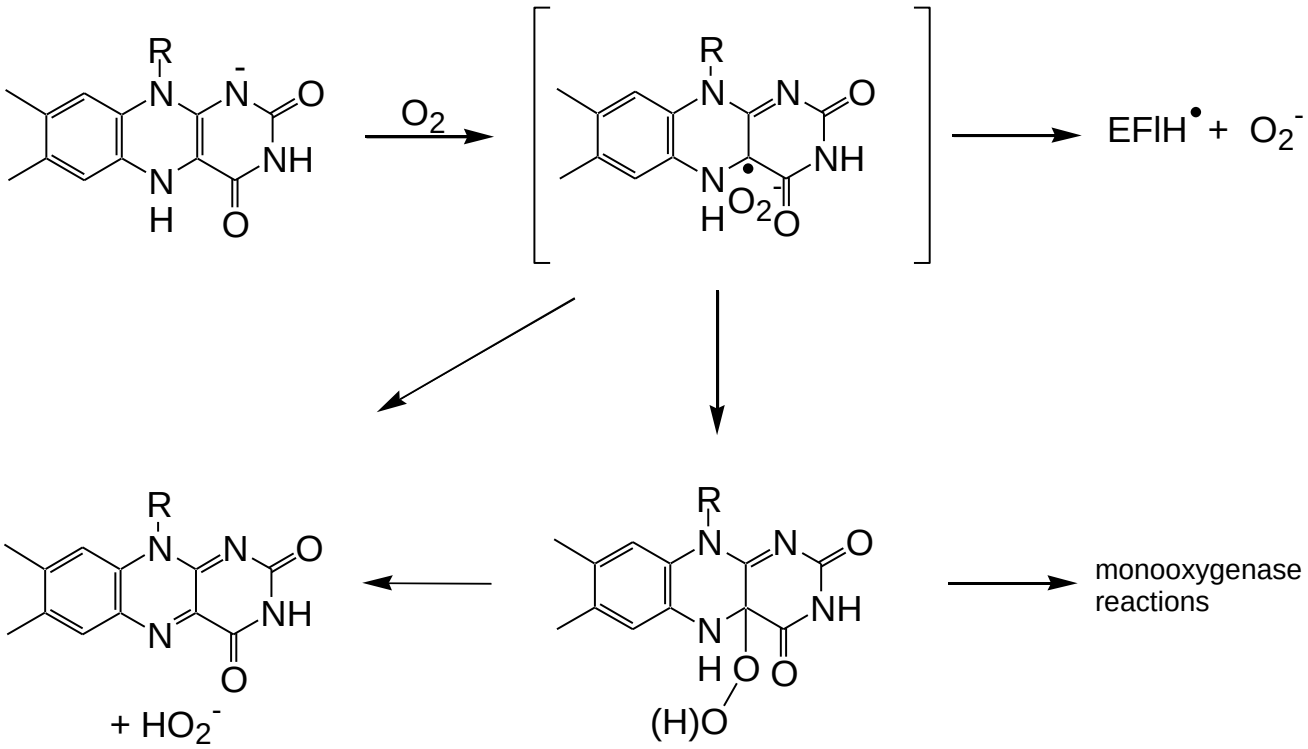

Figure 1.8. Flavin Dependent Oxygen Reduction Pathways. **(**modified from (*103*))

1.3.2. Enzymes and oxygen

Generally, all the known enzymes that have molecular oxygen as one of their substrates can be divided in to two main categories:

1. Oxygenases.
2. Oxidases.

Oxygenases catalyze reactions that result in the incorporation of one (monooxygenases) or both (dioxygenases) of the oxygen atoms into an organic substrate. In the oxidases molecular

oxygen functions as an electron acceptor and is reduced to a superoxide radical, hydrogen peroxide, or water. A common feature of all enzymes activating molecular oxygen for reaction is that they are conjugated proteins with a metal or flavin prosthetic group. Oxidases as well as oxygenases have either or both types of prosthetic groups.

1.3.1.1.Metal-containing oxygenases

Iron is by far the most frequently used metal cofactor in oxygenases (*124, 128*), either as part of a heme group as in tryptophan 2,3-dioxygenase and indolamine 2,3-dioxygenase (*124*). Alternatively, iron may be in a non-heme form as seen in protocatechuate 3,4-dioxygenase (*129-130*) and lipoxygenase (*124, 131-132*).

1.3.1.1.1. Heme-dependent oxygenases

For the cofactor in heme-dependent proteins to interact directly with molecular oxygen the iron must be in its ferrous state and possess an available sixth coordination site.
There are four known types of interactions of heme-proteins and molecular oxygen:

1. Transport (hemoglobin) (*133*)
2. Reduction (cytochrome oxidase) (*134*)
3. Monooxygenation (cytochrome P-450) (*135*)
4. Dioxygenation (tryptophan oxygenase) (*136*)

Hemoglobin does not chemically activate molecular oxygen but reversibly binds it and transports it from the lungs to the rest of the tissues where it releases the oxygen for cellular use. Cytochrome oxidase is a membrane bound copper-heme protein (*137*) that acts as a terminal

electron acceptor catalyzing the electron flow from oxygen as it gets reduced to water. Contrary to these types of heme-containing proteins, are the heme-dependent monooxygenases and dioxygenases which activate oxygen and catalyze its insertion into organic substrates.

In the current hypothesis for how iron-dependent oxygenases, in which the iron cofactor is directly involved, activate molecular oxygen, the iron has to be reduced to the Fe^{2+} state prior to oxygen binding and involves an electron transfer from Fe^{2+} to the bound oxygen to form a oxyferrous intermediate, which is or will lead to the activated oxygen species. This type of mechanism has been established for most iron-dependent dioxygenases such as indoleamine 2,3-dioxygenase (*138*), however, not all oxygenases proceed through this type of mechanism. Protocatechuate 3,4-dioxygenase is an example of an iron-dependent oxygenase that must proceed through a mechanism that does not directly involve an electron-transfer from iron to oxygen as evidenced by the absence of a valency change in the iron cofactor (*139*).

As an example of the mechanism of oxygen activation that directly involves the iron cofactor, a closer look at indoleamine 2,3-dioxygenase is prudent, as it is one of the best characterized heme-dependent enzymes. Indoleamine 2,3-dioxygenase catalyzes the oxidative ring cleavage of indoleamine derivatives via an ordered sequential mechanism with the indoleamine derivative binding before oxygen in accordance to the mechanism shown in **Scheme 1.2** (*140-141*).

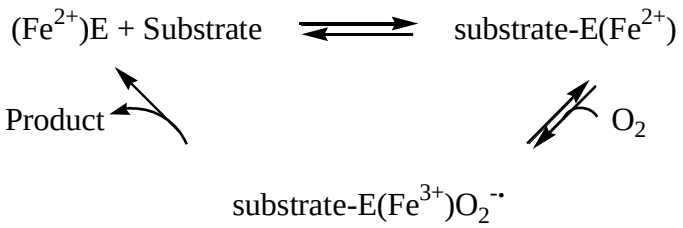

Scheme 1.2. Reaction Mechanism of Indoleamine 2,3-dioxygenase.

In vitro, indoleamine 2,3-dioxygenase requires methylene blue and a system to generate $O_2^{\bullet-}$ for maximum activity (*140*). As seen in **Scheme 1.2**, the oxygenated intermediate contains a ($Fe^{3+}O_2^{\bullet-}$)-complex, and the resting enzyme has been shown to have its iron cofactor in the Fe^{3+} state. As a consequence, the intermediate complex can be formed from the resting enzyme and $O_2^{\bullet-}$ directly but not with molecular oxygen directly. Experimentally it has been shown that the product is released from the Fe^{2+} enzyme, which can then undergo a second turnover with O_2 (*142-143*). Upon binding of O_2, an electron is transferred from Fe^{2+} to form the $Fe^{3+}O_2^{\bullet-}$ reaction intermediate bound in the active site of the enzyme.

Cytochrome P-450 is an example of an iron-dependent monooxygenase. The term cytochrome P-450 (P450) refers to a group of heme-proteins that have a sulfur atom ligated to the iron (*144*). Cytochrome P-450 activates molecular oxygen to catalyze the monooxygenation of unactivated hydrocarbons (R-H). A generalized reaction scheme for the reaction catalyzed by cytochrome P-450 is shown in **Scheme 1.3** (*145*).

$$\text{R-H} + O_2 + \text{NAD(P)H} \longrightarrow \text{R-OH} + H_2O + \text{NAD(P)}^+$$

Scheme 1.3. Generalized Reaction Catalyzed by Cytochrome P-450.

P450's catalyze the oxidation of a vast number of substrates with substantially different involvement of electron transfer from NAD(P)H to form the reaction products. However, all P450's generally follow the simplified mechanism shown in **Scheme 1.4**.

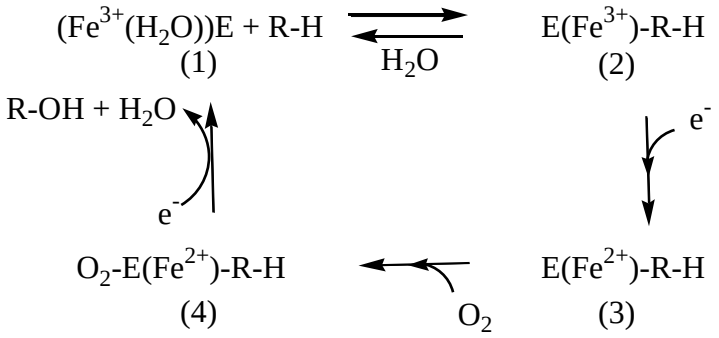

Scheme 1.4. Simplified Catalytic Mechanism for Cytochrome P-450 (*124, 144*).

The resting state of P450 has a hexacoordinated low spin heme (species (1) in **Scheme 1.4**). The sixth axial ligand is a weakly bound H_2O molecule. Upon substrate binding, the water molecule is displaced to yield a pentacoordinated high spin heme (species (2) in **Scheme 1.4**) (*145*). The pentacoordinated ferric P450 is then reduced by its redox partner to give Fe^{2+} (species (3) in **Scheme 1.4**) to which oxygen binds to generate an oxyferrous intermediate (species (4) in **Scheme 1.4**). A second electron is then transferred from the redox partner to the oxyferrous intermediate to form a peroxo ($Fe\text{-}O\text{-}O^{2-}$) intermediate that is subsequently protonated to give a hydroperoxo ($Fe\text{-}O\text{-}O\text{-}H^{-}$) intermediate. This is followed by heterolytic cleavage of oxygen to form the oxyferryl ($Fe{=}O^{+\cdot}$) intermediate, which is the activated form of oxygen able to react with the hydrocarbon to form the hydroxylated hydrocarbon and water (*145*).

1.3.1.1.2. Iron non-heme oxygenases

In protocatechuate 3,4-dioxygenase the iron does not seem to be directly involved in oxygen activation. EPR studies of the free enzyme, the enzyme-substrate complex and the enzyme-substrate-oxygen complex revealed that the iron remains in the high-spin, Fe^{3+}

throughout the catalytic cycle. Molecular oxygen has not been found to complex with Fe^{3+}, and as such the most likely role of the iron cofactor is to activate the substrate rather than oxygen (*129*). A proposed mechanism for the reaction catalyzed by protocatechuate 3,4-dioxygenase involves an initial keto-enol tautomerization of the substrate resulting from the interaction of one of the hydroxyl groups with the Fe^{3+}. The activated keto form reacts with molecular oxygen to form $O_2^{\bullet-}$ that can then continue to form the enzyme-product complex. Resonance-Raman spectroscopy show no signs of a charge-transfer complex, consistent with there being no interactions between Fe^{3+} and $O_2^{\bullet-}$ (*146*).

1.3.1.1.3. Copper oxygenases

Enzymes utilizing copper as their metal cofactor achieve their catalytic power through the ability of copper to perform both oxidations and reductions as well as oxygen binding. Copper-dependent enzymes are not restricted to a single biological role, but catalyze a wide range of chemical reactions spanning from oxidative cleavage of heterocyclic rings (Quercetinase) (*147*), monooxygenation (dopamine β-hydroxylase) (*148*) to hydroxylation reactions (3,4-dihydroxyphenylethylsmine, ascorbate:oxygen oxidoreductase) (*149*). The diverse reactivity that copper-dependent enzymes have with oxygen is best exemplified by tyrosinase, which catalyzes two dissimilar reactions both involving molecular oxygen. Tyrosinase catalyzes the insertion of oxygen in the ortho position of monophenols (**Scheme 1.5**) and the dehydrogenation of *o*-diphenols (**Scheme 1.6**). As such, tyrosinase, is both a monophenol monooxygenase and a diphenol oxidase (*150*).

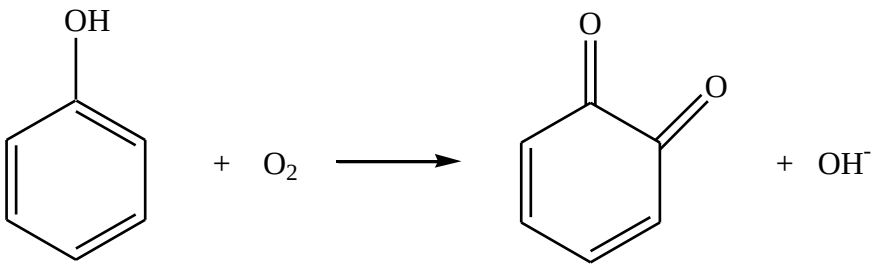

Scheme 1.5. Monooxygenation of Monophenols Catalyzed by Tyrosinase.

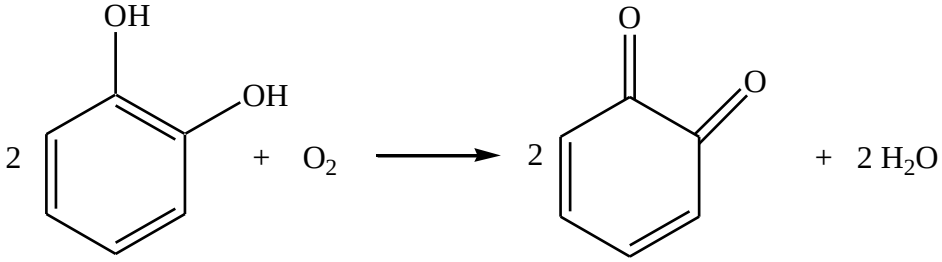

Scheme 1.6. Dehydrogenation of *o*-diphenols Catalyzed by Tyrosinase.

The active site of tyrosinase contains 2 Cu^{2+} metal ions (*151*) that during the catalytic cycle upon binding of either the mono- and di-phenol substrate are first reduced to Cu^{+}. The reduced enzyme then temporarily contains two reducing equivalents that are used for activation of molecular oxygen. Upon reduction of the copper cofactors, molecular oxygen is reversibly bound and the release of the oxidated phenol substrate ensues. Upon binding and oxidation of a second phenol substrate, oxygen is reduced to water and released from the active site of the enzyme (**Scheme 1.7**) (*150, 152*).

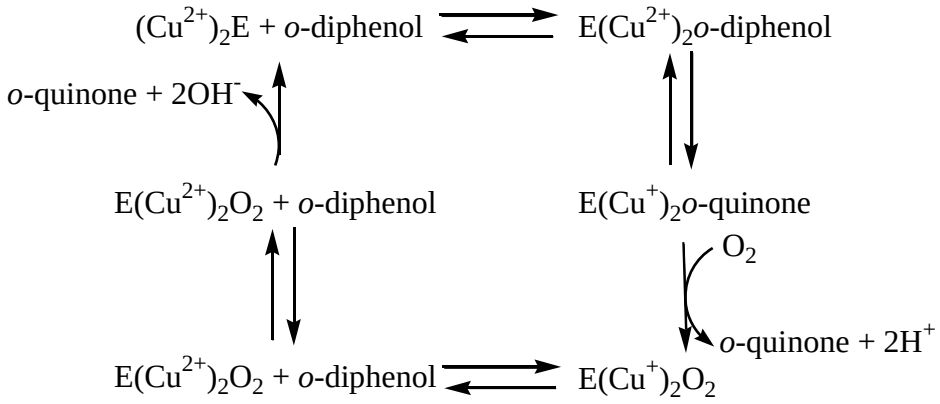

Scheme 1.7. Catalytic Cycle of Tyrosinase Reaction with *o*-diphenols.

It is assumed, that in the copper-dependent oxygenases oxygen activation proceeds via an electron transfer from reduced Cu^{2+} to oxygen to form a peroxo intermediate, which is the activated form of oxygen (*150, 153*).

1.3.1.2.Flavin-containing oxygenases

Currently, there are no known dioxygenases that only have flavin as a cofactor. The known flavin-containing dioxygenases, such as indoleamine 2,3-dioxygenase, utilize a metal cofactor to activate oxygen for reaction rather than flavin. Monooxygenases only containing flavin as a cofactor are a diverse group of enzymes that catalyze a wide range of oxygenation reactions while being highly regio- and enantioselective (*154*). To overcome the spin-forbidden reaction between molecular oxygen and carbon in the organic substrates, monooxygenases activate oxygen for reaction by creating an intermediate that can transfer oxygen. In order for the flavin to react in the flavin-dependent monooxygenases it must be in the electron rich reduced state (*155*). For most monooxygenases the flavin cofactor is reduced by NAD(P)H. However, in rare cases the flavin cofactor is reduced by the substrate itself. Such is the case for lactate

monoooxygenase, where the flavin is reduced as lactate is oxidized to pyruvate (*156*). Regardless of how the flavin is reduced, the first step in the reaction with oxygen is a single electron transfer from the reduced flavin to oxygen to form a caged radical pair consisting of superoxide and a flavin radical as shown in **Figure 1.8**. For most flavin-dependent monooxygenases, this is followed by the formation of a covalent adduct between oxygen and the C(4a) atom of the flavin radical. This leads to the formation of a C(4a)-hydroperoxyflavin intermediate, which is the reactive intermediate containing activated oxygen. In the flavin-dependent monooxygenases this highly unstable and reactive intermediate is stabilized long enough for it to transfer oxygen to the organic substrate rather than decaying to hydrogen peroxide and oxidized flavin as in the flavin-dependent oxidases thought to proceed through the formation of a C(4a) oxygen adduct (*157*). Depending on the protonation state of the peroxyflavin intermediate, either an electrophilic or a nucleophilic attack on the substrate will result in the transfer of a single atom of molecular oxygen to the substrate, while the other oxygen atom is reduced to water.

The range of reactions catalyzed by flavin-dependent monooxygenases span from hydroxylations, epoxidations, halogenations to organoboron oxidations (**Figure 1.9**) (*154*).

oethane species, which then further decays to nitrite and acetaldehyde (*158*).

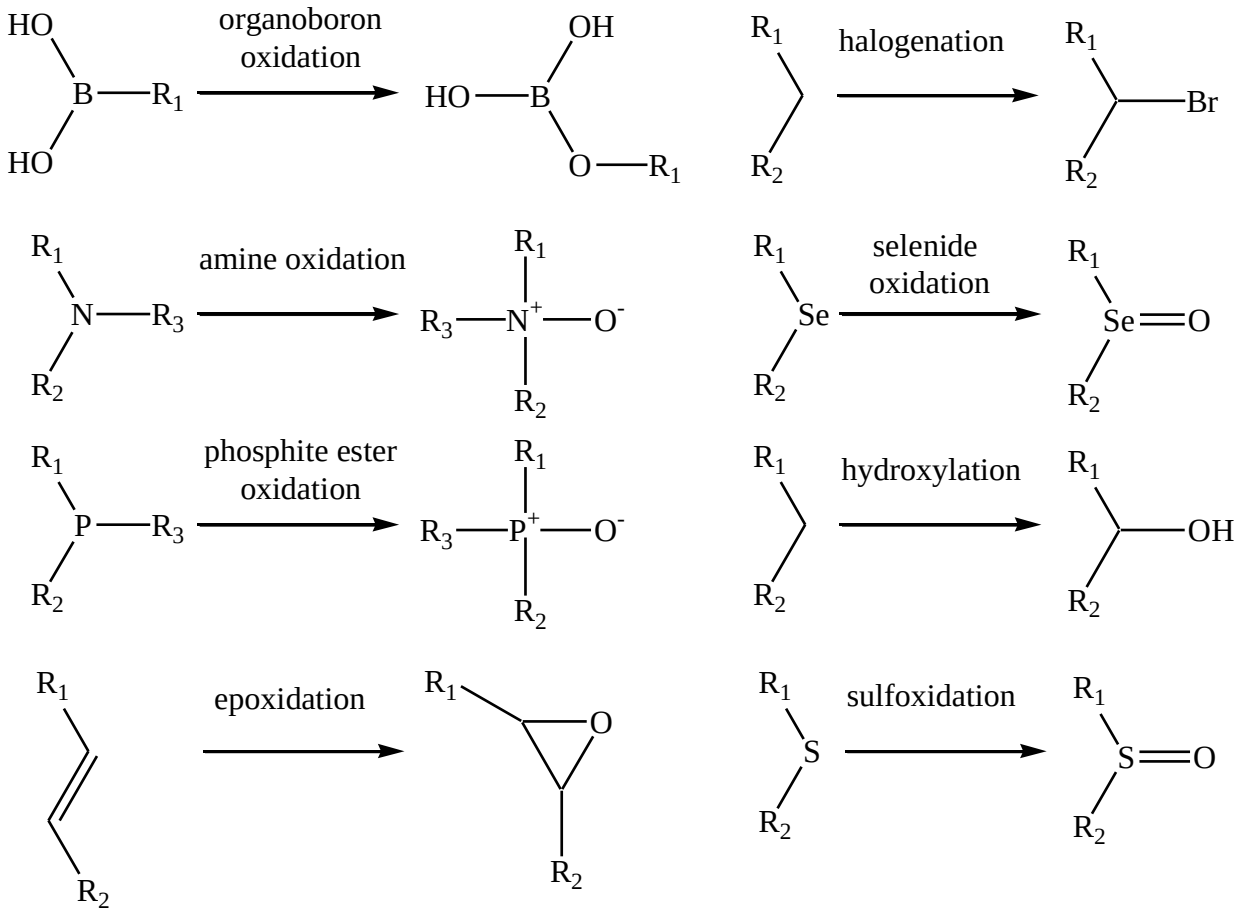

Figure 1.9. Reaction Types Catalyzed by Flavin-dependent Monooxygenases. (modified from (*154*)).

The flavin-dependent monooxygenases have been divided into several subclasses based on sequence and structural homology. Each subclass seems to only catalyze a limited range of oxygenation reactions suggesting that the types of reactions catalyzed is at least partially dependent on the overall folding topology (*154*).

Nitronate monooxygenase (NMO) distinguishes itself as a flavin dependent monooxygenase through its unusual kinetic mechanism involving a one electron reduced anionic semiquinone species. NMO proceeds through an oxidase-like mechanism in which the transfer of a single electron oxidizes the organic substrate and reduces the enzyme-bound flavin to an

anionic semiquinone species. While the substrate radical is still bound in the active site of the enzyme molecular oxygen reacts with the one electron reduced flavin to yield an enzyme-associated superoxide species. The substrate radical and the superoxide is proposed to collapse in the active site of the enzyme and form an α-peroxynitrate.

1.3.1.3.Metal-containing oxidases

In contrast to the metal-containing oxygenases, the oxidases primarily use copper rather than iron as a cofactor. The copper-dependent oxidases generally use a free radical mechanism to activate oxygen for reaction. Galactose oxidase is one of the best characterized copper-dependent oxidases. It is a mononuclear copper-containing oxidase, belonging to the tyrosyl radical family (*159*). The overall reaction catalyzed by galactose oxidase shown in **Scheme 1.8** is the oxidation of primary alcohols to the corresponding aldehydes (*160*), which in turn is oxidized to the corresponding carboxylates (*161*).

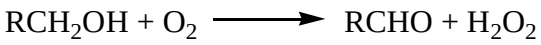

Scheme 1.8. The Overall Reaction Catalyzed by Galactose Oxidase.

The mechanism by which oxygen is reduced is the least-well understood aspect of galactose oxidase turnover. However, synthetic chemistry has provided 2 models for the coordination of oxygen in the oxygenated mononuclear copper complexes. The two distinct coordination modes are side-on (**Figure 1.10A**) (*162*) and end-on (**Figure 1.**Error! Reference source not found.**B**) (*163*).

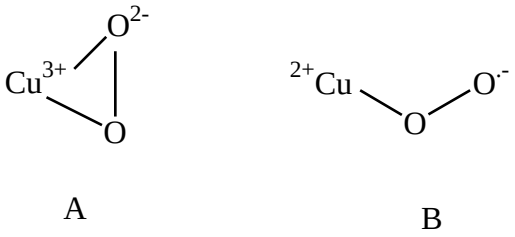

A B

Figure 1. Error! Reference source not found.**.** The Two Proposed Copper Oxygen Coordination Modes (A = Side-on, B = End-on)

The side-on coordination mode is what would be expected if there is strong metal-ligand covalent interactions and it will result in the formation of a Cu^{3+}-peroxide intermediate (*164*). Whereas the end-on coordination mode results in an intermediate with a Cu^{2+}-superoxide adduct (*164*). In a sterically congested active site, the end-on oxygen coordination mode is the most likely favored, due to the side-on mode requiring both metal coordination sites to be available in order to form. The active site in galactose oxidase has been shown to be highly coordinated and sterically restricted with His496, His581 and Tyr272 occupying three of four equatorial positions in the copper-protein complex (*165*). As such, oxygen activation is most likely accomplished by coordinating oxygen to copper in the end-on mode and the reaction proceeding through a Cu^{2+}-hydroperoxide intermediate. Based on the distribution of the valence electrons it is expected that the reaction in the end-on oxygen coordination mode will proceed through an outer sphere (oxygen centered) reaction mechanism (*164*). Upon formation, the Cu^{2+}-hydroperoxide adduct is protonated and subsequently hydrogen peroxide is displaced from the copper atom, which in turn is ready to undergo a second turnover.

1.3.1.4.Flavin-containing oxidases

The chemical basis for flavin-dependent O_2 reduction is not well understood. In summary, it is believed that the reaction proceeds by successive single electron transfers, the first of which is a single electron being transferred from the reduced flavin to O_2 to form a caged radical pair consisting of a semi-reduced flavin and a superoxide anion. From here the oxygen can be further reduced through several different pathways as summarized in **Figure 1.8**.

Free flavin by itself can reduce oxygen with a second order rate constant in the 10^2 $M^{-1}s^{-1}$ range, whereas the flavin-dependent enzymes display second order rate constants spanning from 10^1 $M^{-1}s^{-1}$ range (flavocytochrome b_2 (*17*)) to 10^6 $M^{-1}s^{-1}$ range (glucose oxidase (*166*)), indicative of the importance of the protein moiety in modulating the reactivity of the flavin cofactor with oxygen. However no clearly identifiable structural features seem to be recurring in the enzymes with high rate constants. For some of the fastest reacting flavin-dependent oxidases a preorganized electrostatic environment dominated by a positive charge close to the C(4a)-N5 locus of the flavin cofactor has been shown to be crucial for the fast reaction with oxygen. In the case of glucose oxidase it is a protonated histidine that provides the positive charge (*85, 110*). In cholesterol oxidase type I and II the need for a positive charge has also been demonstrated (*167-168*). In choline oxidase the positive charge in the active site required for efficient reaction with oxygen is provided by the positive charged head-group of choline and not by a residue in the active site (*31, 109*). Other examples of ligand binding enhancing oxygen reactivity are D-amino acid oxidase (*112*) and monoamine oxidase (*113*). In these two enzymes it is product binding that increases oxygen reactivity and in both cases the product or product analog is positively charged.

Other factors such as active site solvation, flavin stereochemistry and oxygen accessibility have been implicated in oxygen reactivity, however so far systematic effects arising

from these factors have not been well established. In some cases they have a positive effect on oxygen reactivity, whereas in others they have a detrimental effect (*103*).

Overall, it does not seem that there are general structural features that will always result in enhancement of oxygen reactivity in flavin-dependent oxidases, but rather several subtle factors with a combined effect that results in an enhanced oxygen reactivity being the main reason. Additionally it seems that there are multiple combinations possible to achieve enhanced oxygen reactivity, thereby making the identification of general principles elusive and problematic.

1.4. Choline Oxidase from *Arthrobacter globiformis*

For a recent comprehensive review on choline oxidase see "Hydride transfer made easy in the reaction of alcohol oxidation catalyzed by flavin-dependent oxidases" by G. Gadda published in *Biochemistry 47*, 13745-13753 (*169*). Choline oxidase from *Arthrobacter globiformis* is a homodimer with each subunit having a covalently attached FAD to His99 (*24*). This enzyme catalyzes the oxidation of choline to glycine betaine with betaine aldehyde as intermediate (*170*). The reaction proceeds through two reductive half-reactions and two oxidative half-reactions as shown in **Scheme 1.9**.

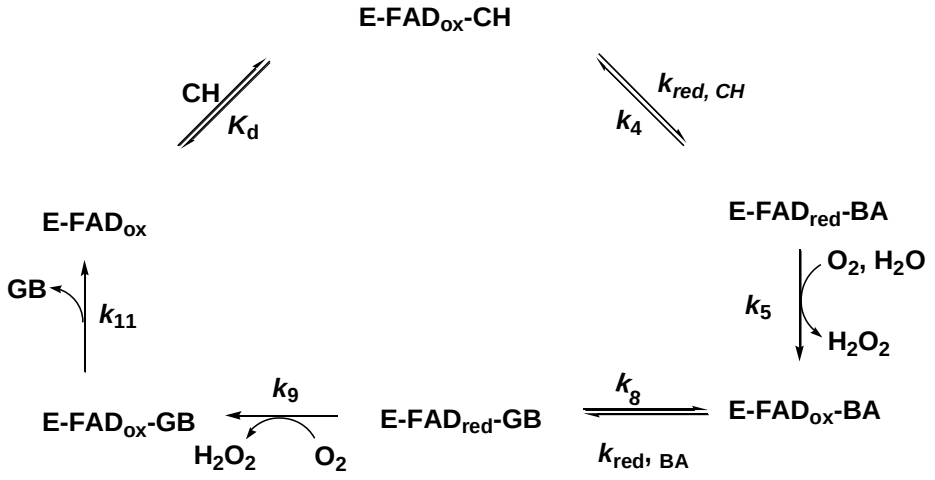

Scheme 1.9. Minimal Kinetic Mechanism of Choline Oxidase. (E-FAD_{ox} = Oxidized Enzyme Bound Flavin, -FAD_{red} = Reduced Enzyme Bound Flavin CH = Choline, BA = Betaine Aldehyde and GB = Glycine Betaine)

In the reductive half-reactions the FAD cofactor is reduced to the anionic hydroquinone form (2 e^- reduced) by choline and the aldehyde intermediate respectively. Each reductive half reaction is followed by an oxidative half-reaction where the reduced FAD cofactor is reoxidized by molecular oxygen with formation of hydrogen peroxide (*170-171*).

The first reductive half-reaction is initiated by a kinetically fast abstraction of the hydroxyl proton of choline, which results in the formation of a transient alkoxide intermediate (*37*). This is followed by a rate-limiting hydride ion transfer to N(5) atom of the flavin cofactor from the α-carbon of the alkoxide resulting in the oxidation of choline to betaine aldehyde and reduction of the flavin (*37*). Prior to the second reductive half-reaction, betaine aldehyde is hydrated to form *gem*-diol choline in the active site (*35*). The subsequent oxidation of the reduced flavin occurs while the active site is still occupied with the *gem*-diol choline intermediate (*38, 108-109*). In the second reductive half-reaction, the *gem*-diol choline is oxidized to the product, glycine betaine. In both oxidative half-reactions the oxidized flavin cofactor is reformed upon a transfer of a hydride equivalent from the reduced flavin to molecular oxygen (*32*). Each of these half-reactions has specific requirements, that choline oxidase must balance in order to achieve maximum overall rate of catalysis. In the wild-type choline oxidase this yields the following kinetic parameters in the pH independent region, k_{cat} = 60 s^{-1}, k_{cat}/K_m = 237,000 M^{-1} $s^{-1}$and k_{cat}/K_{oxygen} = 86,000 M^{-1} s^{-1} (*37*).

The alcohol oxidation catalyzed by choline oxidase from *Arthrobacter globiformis* has been intensively studied using structural (*24, 126*), biochemical (*30, 32, 34*), mutagenesis (*24, 26, 28, 30, 33, 108*) and mechanistic (*27, 35-38, 171-172*) techniques. Through these studies several residues have been identified to have specific roles in choline oxidase. The kinetic

parameters affected by substitution of His99, Glu312, His351, Val464 and His466 are summarized in **Table 1.3**.

Even though the positively charged His466 does not affect oxygen activation, it is important for catalysis. The positive charge has been shown to be involved in the stabilization of a negatively charged reduced flavin as well as of the transient alkoxide species (*30-31*). Additionally, His466 is likely involved in choline activation as seen by the 60- and 1000-fold lowered k_{cat} and $k_{cat}/K_{choline}$, respectively, in the pH independent region upon replacing the histidine with an alanine as compared to the wild-type enzyme (*31*).

Table 1.3. Kinetic Parameters Influenced by Substitution of Various Residues in Choline Oxidase.

Residue (variant investigated)	Kinetic parameter		Ref
	Large effect[1]	Minor or no effect	
His466[a] (H466A and H466D)	k_{cat}, $k_{cat}/K_{choline}$, K_{oxygen}, $K_{choline}$	k_{cat}/K_{oxygen}	(*31*)
His351[a] (H351A)	k_{cat}, k_{red}, K_d $k_{cat}/K_{choline}$, K_{oxygen}, $K_{choline}$	k_{cat}/K_{oxygen}	(*26*)
His99[a] (H99N)	k_{cat}, k_{red} $k_{cat}/K_{choline}$, K_{oxygen}, $K_{choline}$	k_{cat}/K_{oxygen}	(*28*)
Glu312[a] (E312D and E312Q)	k_{cat}, k_{red}, K_d $k_{cat}/K_{choline}$, K_{oxygen}, $K_{choline}$	k_{cat}/K_{oxygen}	(*24*)
Val464[a] (V464A and V464T)	k_{cat}, k_{cat}/K_{oxygen},	k_{red}	(*33*) (SF)
Positive charge on substrate[b]	k_{cat}, k_{cat}/K_{oxygen}, K_{oxygen}	$K_{choline}$	(*109*)

[a] The affected kinetic parameters were determined by investigating the variant enzymes where the residue of interest was replaced. [b] using 3,3-dimethyl-butanol instead of choline.

[1] A large effect on a kinetic parameter is defined here as it being more than 3-fold different as compared to the wild-type enzyme

His351 is also likely involved in choline activation as seen by the 60- and 350-fold lowered k_{cat} and $k_{cat}/K_{choline}$, respectively, in the pH independent region upon replacing the histidine with an alanine as compared to the wild-type enzyme (*26*). Furthermore, His351 has a profound effect on the substrate binding affinity as well as the rate of flavin reduction in the first reductive half-reaction with choline as the reductant as seen by the K_d value increasing 10 times and the k_{red} value decreasing 75 times (*26*).

Glu312 is involved in the preorganization of the enzyme-substrate complex as well as the initial binding and correct positioning of choline through interactions between its negatively charged side-chain and the positively charged trimethylammonium headgroup of choline (*24*).

Other than merely being the site of covalent attachment of the flavin cofactor to the protein moiety the FAD-histidyl covalent linkage between His99 and FAD is important for the optimal positioning of the flavin cofactor in the enzyme-alkoxide complex that is required for the environmentally assisted tunneling of the hydride ion in the oxidation of choline (*28*).

In summary, residues Glu312, His99, His351 and His466 do not contribute to oxygen activation, as indicated by site-directed mutagenesis studies where each of these four residues located in the active site of the enzyme were individually replaced. These studies revealed that the bimolecular rate constants for the reaction of the reduced flavin cofactor with oxygen (k_{cat}/K_{oxygen}) were not significantly altered in the mutant enzymes from the value of ~10^5 $M^{-1}s^{-1}$ of the wild-type (*24*, *26*, *28*, *30-32*).

Contrary to this, the substitution of the positively charged substrate through the use of the isosteric analogue of choline devoid of charge 3,3-dimethyl-butan-1-ol resulted in a two orders of magnitude decrease of the k_{cat}/K_{oxygen} value to ~10^3 $M^{-1}s^{-1}$, consistent with oxygen activation for reaction with the reduced flavin being largely exerted by the positive charge on enzyme-

bound ligand (*108-109*). Further evidence of the importance of this is seen in the pH studies of the His99Asn, His351Ala, His466Ala and wild-type forms of choline oxidase, which showed that the k_{cat}/K_{oxygen} values that are independent of pH, consistent with the fact that the trimethylammonium moiety of the choline cannot ionize (*26, 28, 31-32, 108*).

Further studies on choline oxidase from *Arthrobacter globiformis* are pertinent as they can help elucidate one of the puzzling unanswered questions in flavin chemistry, which is the chemical basis for the diverse oxygen reactivity in flavin-dependent enzymes.

1.5. Specific Goals

Flavin-dependent enzymes are in general amongst the most chemically versatile naturally occurring enzymes, as exemplified by the diverse reactivity of the reduced flavin with molecular oxygen. Depending upon the ability to react with oxygen and the product of oxygen reduction, three general classes of flavin-dependent enzymes have been distinguished (*103, 155*). Dehydrogenases have very poor, or no reactivity with oxygen, and utilize other electron acceptors for catalytic turnover. Monooxygenases and oxidases show high reactivity with oxygen, typically with second-order rate constants $\geq 10^5$ $M^{-1}s^{-1}$ (*155*). Free reduced flavin in aqueous solution react with molecular oxygen with a bimolecular rate constant of 250 $M^{-1}s^{-1}$ (*155*). It is the interactions between the flavin cofactor and the protein moiety that modulate the reactivity of the flavin. (*12, 103, 173*).

Based on the crystal structure of wild-type choline oxidase (*24*), three residues in the active site likely directly (or indirectly) affect the flavin microenvironment and as such potentially affect oxygen reactivity with the reduced flavin. These residues are Valine 464 (Val464), Histidine 310 (His310) and Serine 101 (Ser101). *The overall goal of this dissertation is the*

elucidation of the roles of these three residues on both the reductive and the oxidative half-reactions of choline oxidase.

Ser101 is located ~4 Å away from the N(5) atom of FAD cofactor and within hydrogen bonding distance to DMSO, a co-crystallized ligand found in the active site in the crystal structure of wild-type choline oxidase (*24*). The location of Ser101 allows me to propose that this residue affects the flavin microenvironment while being able to actively participate in the oxidation of choline. To elucidate the effect exerted by Ser101 on oxygen reactivity, kinetic characterization of a variant enzyme where the serine residue has been replaced with an alanine was carried out (Hongling, Y. submitted for publication, 2010). In order to attribute any determined kinetic differences between the variant enzyme and the wild-type enzyme to the removal of the hydroxyl group at position 101 rather than to structural differences, the crystal structure of the variant enzyme was also investigated.

The X-ray crystal structure of wild-type choline oxidase further revealed the presence of His310 ~2.9 Å away from His466 (*24*). The latter has been shown to provide a positive charge needed for catalysis (*30-31*). The crystal structure also suggested that the position of the side-chain of His310 is highly coordinated through hydrogen bonding to the side-chain of His466 ($His466^{N\delta1}$-$His310^{N\delta1}$) and the peptidyl main chain oxygen atoms of Threonine 380 and Valine 507 as shown in **Figure 1.5**. This high degree of coordination of His310 suggests the presence of a proton-transfer network between the protonated, conserved, active site residue His466 and His310 that enables efficient catalysis for both the oxidative and reductive half-reactions by optimizing the FAD micro-environment for each reaction type. This H-bonding pattern provides a possible proton relay system that enables efficient reduction and reoxidation of the covalently bound FAD cofactor by shuttling a proton to and from residue His466. This potential proton-

transfer network was perturbed through site directed mutagenesis of His310 and subsequently the variant enzymes were subjected to kinetic analysis and characterization in order to establish the presence of a proton-transfer network and its effect on the reaction catalyzed by choline oxidase.

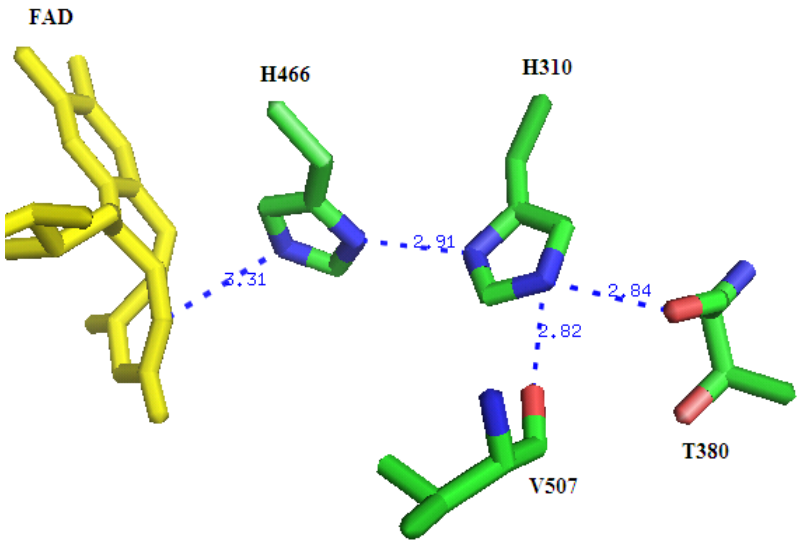

Figure 1.11. The Coordination of the Side-chain of His310 in the Crystal Structure of Wild-type Choline Oxidase (2JBV).

Finally, Val464 is seen to be the only hydrophobic residue in the active site in the X-ray crystal structure of choline oxidase (*24, 126*). Val464 is in the active site cavity close to the C(4a)-N(5) atoms of the flavin, with its hydrophobic side chain in van der Waals contact with the C(2) atom of the conserved His466. Findings from other flavin-dependent enzymes, such as glycolate oxidase and flavocytochrome b_2, show that steric interactions as well as hydrophobicity can profoundly affect oxygen reactivity with reduced flavin. In the case of glycolate oxidase and flavocytochrome b_2, two structurally homologous enzymes that share a highly conserved active site, the only obvious difference is a leucine in the FAD microenvironment in glycolate oxidase and a tryptophan in its place in flavocytochrome b_2 (*87, 100*). The difference in the micro-

environment of these two enzymes may be the cause for the rate constant for the reactivity of oxygen to drop from 8.5 x 10^4 $M^{-1}s^{-1}$ in glycolate oxidase to 2 $M^{-1}s^{-1}$ in flavocytochrome b_2 (*103*). Through X-ray crystallography, site-directed mutagenesis of position Val464 in choline oxidase, steady state and rapid kinetics approaches the role of the hydrophobic residue Val464 in the active site of choline oxidase was investigated.

Finally, the reaction of choline oxidation catalyzed by choline oxidase is very well characterized, *making it ideally suited to investigate the chemical basis of how flavin-dependent enzymes react with molecular oxygen.* As such, mechanistic data on Ser101, His310 and Val464 will provide important information about the roles of these active site residues in the reaction catalayzed by choline oxidase that may be relevance for a large number of flavin-dependent enzymes.

1.6.References

1. Fischer, M., and Bacher, A. (2005) Biosynthesis of flavocoenzymes, *Nat Prod Rep 22*, 324-350.
2. Schrecker, A. W., and Kornberg, A. (1950) Reversible enzymatic synthesis of flavin-adenine dinucleotide, *J Biol Chem 182*, 795-803.
3. Santos, M. A., Jimenez, A., and Revuelta, J. L. (2000) Molecular characterization of FMN1, the structural gene for the monofunctional flavokinase of Saccharomyces cerevisiae, *J Biol Chem 275*, 28618-28624.
4. Gross, E., Kastner, D. B., Kaiser, C. A., and Fass, D. (2004) Structure of Ero1p, source of disulfide bonds for oxidative protein folding in the cell, *Cell 117*, 601-610.

5. Forneris, F., Binda, C., Vanoni, M. A., Mattevi, A., and Battaglioli, E. (2005) Histone demethylation catalysed by LSD1 is a flavin-dependent oxidative process, *FEBS Lett 579*, 2203-2207.

6. White, H. B., 3rd, and Merrill, A. H., Jr. (1988) Riboflavin-binding proteins, *Annu Rev Nutr 8*, 279-299.

7. Susin, S. A., Lorenzo, H. K., Zamzami, N., Marzo, I., Snow, B. E., Brothers, G. M., Mangion, J., Jacotot, E., Costantini, P., Loeffler, M., Larochette, N., Goodlett, D. R., Aebersold, R., Siderovski, D. P., Penninger, J. M., and Kroemer, G. (1999) Molecular characterization of mitochondrial apoptosis-inducing factor, *Nature 397*, 441-446.

8. Murty, C. V., and Adiga, P. R. (1982) Pregnancy suppression by active immunization against gestation-specific riboflavin carrier protein, *Science 216*, 191-193.

9. Jorns, M. S., Wang, B., and Jordan, S. P. (1987) DNA repair catalyzed by Escherichia coli DNA photolyase containing only reduced flavin: elimination of the enzyme's second chromophore by reduction with sodium borohydride, *Biochemistry 26*, 6810-6816.

10. Dagley, S. (1987) Lessons from biodegradation, *Annu Rev Microbiol 41*, 1-23.

11. Joosten, V., and van Berkel, W. J. (2007) Flavoenzymes, *Curr Opin Chem Biol 11*, 195-202.

12. Massey, V. (2000) The chemical and biological versatility of riboflavin, *Biochem Soc Trans 28*, 283-296.

13. Massey, V., and Palmer, G. (1966) On the existence of spectrally distinct classes of flavoprotein semiquinones. A new method for the quantitative production of flavoprotein semiquinones, *Biochemistry 5*, 3181-3189.

14. Draper, R. D., and Ingraham, L. L. (1968) A potentiometric study of the flavin semiquinone equilibrium, *Arch Biochem Biophys 125*, 802-808.

15. Ehrenberg, A., Muller, F., and Hemmerich, P. (1967) Basicity, visible spectra, and electron spin resonance of flavosemiquinone anions, *Eur J Biochem 2*, 286-293.

16. Ghisla, S., and Massey, V. (1986) New flavins for old: artificial flavins as active site probes of flavoproteins, *Biochem J 239*, 1-12.

17. Massey, V. (2002) The reactivity of oxygen with flavoproteins, *International Congress Series 1233*, 3-11.

18. Massey, V., Muller, F., Feldberg, R., Schuman, M., Sullivan, P. A., Howell, L. G., Mayhew, S. G., Matthews, R. G., and Foust, G. P. (1969) The reactivity of flavoproteins with sulfite. Possible relevance to the problem of oxygen reactivity, *J Biol Chem 244*, 3999-4006.

19. Macheroux, P., Kieweg, V., Massey, V., Soderlind, E., Stenberg, K., and Lindqvist, Y. (1993) Role of tyrosine 129 in the active site of spinach glycolate oxidase, *Eur J Biochem 213*, 1047-1054.

20. Gadda, G., Wels, G., Pollegioni, L., Zucchelli, S., Ambrosius, D., Pilone, M. S., and Ghisla, S. (1997) Characterization of cholesterol oxidase from Streptomyces hygroscopicus and Brevibacterium sterolicum, *Eur J Biochem 250*, 369-376.

21. Gadda, G., and Fitzpatrick, P. F. (1998) Biochemical and physical characterization of the active FAD-containing form of nitroalkane oxidase from Fusarium oxysporum, *Biochemistry 37*, 6154-6164.

22. Fitzpatrick, P. F., and Massey, V. (1983) The reaction of 8-mercaptoflavins and flavoproteins with sulfite. Evidence for the role of an active site arginine in D-amino acid oxidase, *J Biol Chem 258*, 9700-9705.

23. Vrielink, A., Lloyd, L. F., and Blow, D. M. (1991) Crystal structure of cholesterol oxidase from Brevibacterium sterolicum refined at 1.8 A resolution, *J Mol Biol 219*, 533-554.

24. Quaye, O., Lountos, G. T., Fan, F., Orville, A. M., and Gadda, G. (2008) Role of Glu312 in binding and positioning of the substrate for the hydride transfer reaction in choline oxidase, *Biochemistry 47*, 243-256.

25. Lindqvist, Y. (1989) Refined structure of spinach glycolate oxidase at 2 A resolution, *J Mol Biol 209*, 151-166.

26. Rungsrisuriyachai, K., and Gadda, G. (2008) On the role of histidine 351 in the reaction of alcohol oxidation catalyzed by choline oxidase, *Biochemistry 47*, 6762-6769.

27. Quaye, O., and Gadda, G. (2009) Effect of a conservative mutation of an active site residue involved in substrate binding on the hydride tunneling reaction catalyzed by choline oxidase, *Arch Biochem Biophys 489*, 10-14.

28. Quaye, O., Cowins, S., and Gadda, G. (2009) Contribution of flavin covalent linkage with histidine 99 to the reaction catalyzed by choline oxidase, *J Biol Chem 284*, 16990-16997.

29. Hoang, J. V., and Gadda, G. (2007) Trapping choline oxidase in a nonfunctional conformation by freezing at low pH, *Proteins 66*, 611-620.

30. Ghanem, M., and Gadda, G. (2006) Effects of reversing the protein positive charge in the proximity of the flavin N(1) locus of choline oxidase, *Biochemistry 45*, 3437-3447.

31. Ghanem, M., and Gadda, G. (2005) On the catalytic role of the conserved active site residue His466 of choline oxidase, *Biochemistry 44*, 893-904.

32. Ghanem, M., Fan, F., Francis, K., and Gadda, G. (2003) Spectroscopic and kinetic properties of recombinant choline oxidase from Arthrobacter globiformis, *Biochemistry 42*, 15179-15188.

33. Finnegan, S., and Gadda, G. (2008) Substitution of an active site valine uncovers a kinetically slow equilibrium between competent and incompetent forms of choline oxidase, *Biochemistry 47*, 13850-13861.

34. Fan, F., Ghanem, M., and Gadda, G. (2004) Cloning, sequence analysis, and purification of choline oxidase from Arthrobacter globiformis: a bacterial enzyme involved in osmotic stress tolerance, *Arch Biochem Biophys 421*, 149-158.

35. Fan, F., Germann, M. W., and Gadda, G. (2006) Mechanistic studies of choline oxidase with betaine aldehyde and its isosteric analogue 3,3-dimethylbutyraldehyde, *Biochemistry 45*, 1979-1986.

36. Fan, F., and Gadda, G. (2007) An internal equilibrium preorganizes the enzyme-substrate complex for hydride tunneling in choline oxidase, *Biochemistry 46*, 6402-6408.

37. Fan, F., and Gadda, G. (2005) On the catalytic mechanism of choline oxidase, *J Am Chem Soc 127*, 2067-2074.

38. Fan, F., and Gadda, G. (2005) Oxygen- and temperature-dependent kinetic isotope effects in choline oxidase: correlating reversible hydride transfer with environmentally enhanced tunneling, *J Am Chem Soc 127*, 17954-17961.

39. Lyubimov, A. Y., Chen, L., Sampson, N. S., and Vrielink, A. (2009) A hydrogen-bonding network is important for oxidation and isomerization in the reaction catalyzed by cholesterol oxidase, *Acta Crystallogr D Biol Crystallogr 65*, 1222-1231.

40. Fujishiro, K., Ohta, T., Hasegawa, M., Yamaguchi, K., Mizukami, T., Uwajima, T., and Ota, T. (1990) Isolation and identification of the gene of cholesterol oxidase from Brevibacterium sterolicum ATCC 21387, a widely used enzyme in clinical analysis, *Biochem Biophys Res Commun 172*, 721-727.

41. Cheetham, P. S., Dunnill, P., and Lilly, M. D. (1982) The characterization and interconversion of three forms of cholesterol oxidase extracted from Nocardia rhodochrous, *Biochem J 201*, 515-521.

42. Doukyu, N., and Aono, R. (1999) Two moles of O2 consumption and one mole of H2O2 formation during cholesterol peroxidation with cholesterol oxidase from Pseudomonas sp. strain ST-200, *Biochem J 341 (Pt 3)*, 621-627.

43. Lim, L., Molla, G., Guinn, N., Ghisla, S., Pollegioni, L., and Vrielink, A. (2006) Structural and kinetic analyses of the H121A mutant of cholesterol oxidase, *Biochem J 400*, 13-22.

44. Smith, A. G., and Brooks, C. J. (1975) Studies of the substrate specificity of cholesterol oxidase from Nocardia erythropolis in the oxidation of 3-hydroxy steroids, *Biochem Soc Trans 3*, 675-677.

45. Smith, A. G., and Brooks, C. J. (1977) The mechanism of the isomerization of Cholest-5-en-3-one to cholest-4-en-3-one by cholesterol oxidase [proceedings], *Biochem Soc Trans 5*, 1088-1090.

46. Sampson, N. S., Kass, I. J., and Ghoshroy, K. B. (1998) Assessment of the role of an omega loop of cholesterol oxidase: a truncated loop mutant has altered substrate specificity, *Biochemistry 37*, 5770-5778.

47. Buckland, B. C., Lilly, M. D., and Dunnill, P. (1976) The kinetics of cholesterol oxidase synthesis by Nocardia rhodocrous, *Biotechnol Bioeng 18*, 601-621.

48. Piubelli, L., Pedotti, M., Molla, G., Feindler-Boeckh, S., Ghisla, S., Pilone, M. S., and Pollegioni, L. (2008) On the oxygen reactivity of flavoprotein oxidases: an oxygen access tunnel and gate in brevibacterium sterolicum cholesterol oxidase, *J Biol Chem 283*, 24738-24747.

49. Zhao, G., Bruckner, R. C., and Jorns, M. S. (2008) Identification of the oxygen activation site in monomeric sarcosine oxidase: role of Lys265 in catalysis, *Biochemistry 47*, 9124-9135.

50. Hassan-Abdallah, A., Zhao, G., Chen, Z. W., Mathews, F. S., and Schuman Jorns, M. (2008) Arginine 49 is a bifunctional residue important in catalysis and biosynthesis of monomeric sarcosine oxidase: a context-sensitive model for the electrostatic impact of arginine to lysine mutations, *Biochemistry 47*, 2913-2922.

51. Hassan-Abdallah, A., Zhao, G., and Jorns, M. S. (2008) Covalent flavinylation of monomeric sarcosine oxidase: identification of a residue essential for holoenzyme biosynthesis, *Biochemistry 47*, 1136-1143.

52. Saito, M., Kanno, M., Iizuka, H., and Suzuki, H. (2007) Kinetic studies on the role of Lys-171 and Lys-358 in the beta subunit of sarcosine oxidase from Corynebacterium sp. U-96, *J Biochem 141*, 799-815.

53. Hassan-Abdallah, A., Zhao, G., and Jorns, M. S. (2006) Role of the covalent flavin linkage in monomeric sarcosine oxidase, *Biochemistry 45*, 9454-9462.

54. Mukouyama, E. B., Oguchi, M., Kodera, Y., Maeda, T., and Suzuki, H. (2004) Low pKa lysine residues at the active site of sarcosine oxidase from Corynebacterium sp. U-96, *Biochem Biophys Res Commun 320*, 846-851.

55. Zhao, G., Song, H., Chen, Z. W., Mathews, F. S., and Jorns, M. S. (2002) Monomeric sarcosine oxidase: role of histidine 269 in catalysis, *Biochemistry 41*, 9751-9764.

56. Zhao, G., and Jorns, M. S. (2002) Monomeric sarcosine oxidase: evidence for an ionizable group in the E.S complex, *Biochemistry 41*, 9747-9750.

57. Nishiya, Y. (2000) A mutant sarcosine oxidase in which activity depends on flavin adenine dinucleotide, *Protein Expr Purif 20*, 95-97.

58. Wagner, M. A., and Jorns, M. S. (2000) Monomeric sarcosine oxidase: 2. Kinetic studies with sarcosine, alternate substrates, and a substrate analogue, *Biochemistry 39*, 8825-8829.

59. Wagner, M. A., Trickey, P., Chen, Z. W., Mathews, F. S., and Jorns, M. S. (2000) Monomeric sarcosine oxidase: 1. Flavin reactivity and active site binding determinants, *Biochemistry 39*, 8813-8824.

60. Willie, A., Edmondson, D. E., and Jorns, M. S. (1996) Sarcosine oxidase contains a novel covalently bound FMN, *Biochemistry 35*, 5292-5299.

61. Kawamura-Konishi, Y., and Suzuki, H. (1987) Kinetic studies on the reaction mechanism of sarcosine oxidase, *Biochim Biophys Acta 915*, 346-356.

62. Boselli, A., Piubelli, L., Molla, G., Sacchi, S., Pilone, M. S., Ghisla, S., and Pollegioni, L. (2004) On the mechanism of Rhodotorula gracilis D-amino acid oxidase: role of the active site serine 335, *Biochim Biophys Acta 1702*, 19-32.

63. Bresler, S. E., Vasil'eva, N. N., and Kazbekov, E. N. (1976) [Mechanism of action of D-amino acid oxidase. II. Evidence for the free radical mechanism of the reaction catalysed by the monomer form of the enzyme], *Mol Biol (Mosk) 10*, 501-506.

64. Bresler, S. E., Vasil'eva, N. N., and Kazbekov, E. N. (1976) [The mechanism of action of d-amino acid oxidase. I. Evidence for a free radical mechanism of the reaction catalyzed b a dimeric form of the enzyme], *Mol Biol (Mosk) 10*, 260-269.

65. Denu, J. M., and Fitzpatrick, P. F. (1994) Intrinsic primary, secondary, and solvent kinetic isotope effects on the reductive half-reaction of D-amino acid oxidase: evidence against a concerted mechanism, *Biochemistry 33*, 4001-4007.

66. Fitzpatrick, P. F., and Massey, V. (1982) The kinetic mechanism of D-amino acid oxidase with D-alpha-aminobutyrate as substrate. Effect of enzyme concentration on the kinetics, *J Biol Chem 257*, 12916-12923.

67. Harris, C. M., Molla, G., Pilone, M. S., and Pollegioni, L. (1999) Studies on the reaction mechanism of Rhodotorula gracilis D-amino-acid oxidase. Role of the highly conserved Tyr-223 on substrate binding and catalysis, *J Biol Chem 274*, 36233-36240.

68. Koster, J. F., and Veeger, C. (1968) On the catalytic mechanism of D-amino-acid oxidase, *Biochim Biophys Acta 151*, 11-19.

69. Yagi, K. (1971) Reaction mechanism of D-amino acid oxidase, *Adv Enzymol Relat Areas Mol Biol 34*, 41-78.

70. Porter, D. J., Voet, J. G., and Bright, H. J. (2000) Active site generation of a protonically unstable suicide substrate from a stable precursor: glucose oxidase and dibromonitromethane, *Biochemistry 39*, 11808-11817.

71. Hartnett, A. M., Ingersoll, C. M., Baker, G. A., and Bright, F. V. (1999) Kinetics and thermodynamics of free flavins and the flavin-based redox active site within glucose oxidase dissolved in solution or sequestered within a sol-gel-derived glass, *Anal Chem 71*, 1215-1224.

72. Porter, D. J., and Bright, H. J. (1977) Mechanism of oxidation of nitroethane by glucose oxidase, *J Biol Chem 252*, 4361-4370.

73. Weibel, M. K., and Bright, H. J. (1971) The glucose oxidase mechanism. Interpretation of the pH dependence, *J Biol Chem 246*, 2734-2744.

74. Bright, H. J., and Appleby, M. (1969) The pH dependence of the individual steps in the glucose oxidase reaction, *J Biol Chem 244*, 3625-3634.

75. Bright, H. J., and Gibson, Q. H. (1967) The oxidation of 1-deuterated glucose by glucose oxidase, *J Biol Chem 242*, 994-1003.

76. Massey, V. (1995) Introduction: flavoprotein structure and mechanism, *FASEB J 9*, 473-475.

77. Tamburini, P. P., and Schenkman, J. B. (1986) Differences in the mechanism of functional interaction between NADPH-cytochrome P-450 reductase and its redox partners, *Mol Pharmacol 30*, 178-185.

78. Tejero, J., Peregrina, J. R., Martinez-Julvez, M., Gutierrez, A., Gomez-Moreno, C., Scrutton, N. S., and Medina, M. (2007) Catalytic mechanism of hydride transfer between

NADP+/H and ferredoxin-NADP+ reductase from Anabaena PCC 7119, *Arch Biochem Biophys 459*, 79-90.

79. Nogues, I., Perez-Dorado, I., Frago, S., Bittel, C., Mayhew, S. G., Gomez-Moreno, C., Hermoso, J. A., Medina, M., Cortez, N., and Carrillo, N. (2005) The ferredoxin-NADP(H) reductase from Rhodobacter capsulatus: molecular structure and catalytic mechanism, *Biochemistry 44*, 11730-11740.

80. Carrillo, N., and Ceccarelli, E. A. (2003) Open questions in ferredoxin-NADP+ reductase catalytic mechanism, *Eur J Biochem 270*, 1900-1915.

81. Hermoso, J. A., Mayoral, T., Faro, M., Gomez-Moreno, C., Sanz-Aparicio, J., and Medina, M. (2002) Mechanism of coenzyme recognition and binding revealed by crystal structure analysis of ferredoxin-NADP+ reductase complexed with NADP+, *J Mol Biol 319*, 1133-1142.

82. Medina, M., Martinez-Julvez, M., Hurley, J. K., Tollin, G., and Gomez-Moreno, C. (1998) Involvement of glutamic acid 301 in the catalytic mechanism of ferredoxin-NADP+ reductase from Anabaena PCC 7119, *Biochemistry 37*, 2715-2728.

83. Aliverti, A., Bruns, C. M., Pandini, V. E., Karplus, P. A., Vanoni, M. A., Curti, B., and Zanetti, G. (1995) Involvement of serine 96 in the catalytic mechanism of ferredoxin-NADP+ reductase: structure--function relationship as studied by site-directed mutagenesis and X-ray crystallography, *Biochemistry 34*, 8371-8379.

84. Ghisla, S., and Thorpe, C. (2004) Acyl-CoA dehydrogenases. A mechanistic overview, *Eur J Biochem 271*, 494-508.

85. Hecht, H. J., Kalisz, H. M., Hendle, J., Schmid, R. D., and Schomburg, D. (1993) Crystal structure of glucose oxidase from Aspergillus niger refined at 2.3 A resolution, *J Mol Biol 229*, 153-172.

86. Barber, M. J., Neame, P. J., Lim, L. W., White, S., and Matthews, F. S. (1992) Correlation of x-ray deduced and experimental amino acid sequences of trimethylamine dehydrogenase, *J Biol Chem 267*, 6611-6619.

87. Stenberg, K., and Lindqvist, Y. (1997) Three-dimensional structures of glycolate oxidase with bound active-site inhibitors, *Protein Sci 6*, 1009-1015.

88. Rowland, P., Bjornberg, O., Nielsen, F. S., Jensen, K. F., and Larsen, S. (1998) The crystal structure of Lactococcus lactis dihydroorotate dehydrogenase A complexed with the enzyme reaction product throws light on its enzymatic function, *Protein Sci 7*, 1269-1279.

89. Yue, Q. K., Kass, I. J., Sampson, N. S., and Vrielink, A. (1999) Crystal structure determination of cholesterol oxidase from Streptomyces and structural characterization of key active site mutants, *Biochemistry 38*, 4277-4286.

90. Iverson, T. M., Luna-Chavez, C., Cecchini, G., and Rees, D. C. (1999) Structure of the Escherichia coli fumarate reductase respiratory complex, *Science 284*, 1961-1966.

91. Schreuder, H. A., Prick, P. A., Wierenga, R. K., Vriend, G., Wilson, K. S., Hol, W. G., and Drenth, J. (1989) Crystal structure of the p-hydroxybenzoate hydroxylase-substrate complex refined at 1.9 A resolution. Analysis of the enzyme-substrate and enzyme-product complexes, *J Mol Biol 208*, 679-696.

92. Dym, O., and Eisenberg, D. (2001) Sequence-structure analysis of FAD-containing proteins, *Protein Sci 10*, 1712-1728.

93. Li, J., Vrielink, A., Brick, P., and Blow, D. M. (1993) Crystal structure of cholesterol oxidase complexed with a steroid substrate: implications for flavin adenine dinucleotide dependent alcohol oxidases, *Biochemistry 32*, 11507-11515.

94. Hallberg, B. M., Henriksson, G., Pettersson, G., and Divne, C. (2002) Crystal structure of the flavoprotein domain of the extracellular flavocytochrome cellobiose dehydrogenase, *J Mol Biol 315*, 421-434.

95. Hallberg, B. M., Leitner, C., Haltrich, D., and Divne, C. (2004) Crystal structure of the 270 kDa homotetrameric lignin-degrading enzyme pyranose 2-oxidase, *J Mol Biol 341*, 781-796.

96. Kawazoe, T., Tsuge, H., Imagawa, T., Aki, K., Kuramitsu, S., and Fukui, K. (2007) Structural basis of D-DOPA oxidation by D-amino acid oxidase: alternative pathway for dopamine biosynthesis, *Biochem Biophys Res Commun 355*, 385-391.

97. Binda, C., Coda, A., Angelini, R., Federico, R., Ascenzi, P., and Mattevi, A. (1999) A 30-angstrom-long U-shaped catalytic tunnel in the crystal structure of polyamine oxidase, *Structure 7*, 265-276.

98. Trickey, P., Wagner, M. A., Jorns, M. S., and Mathews, F. S. (1999) Monomeric sarcosine oxidase: structure of a covalently flavinylated amine oxidizing enzyme, *Structure 7*, 331-345.

99. Alfieri, A., Fersini, F., Ruangchan, N., Prongjit, M., Chaiyen, P., and Mattevi, A. (2007) Structure of the monooxygenase component of a two-component flavoprotein monooxygenase, *Proc Natl Acad Sci U S A 104*, 1177-1182.

100. Xia, Z. X., and Mathews, F. S. (1990) Molecular structure of flavocytochrome b2 at 2.4 A resolution, *J Mol Biol 212*, 837-863.

101. Huang, Q., Liu, Q., and Hao, Q. (2005) Crystal structures of Fms1 and its complex with spermine reveal substrate specificity, *J Mol Biol 348*, 951-959.

102. Fox, K. M., and Karplus, P. A. (1994) Old yellow enzyme at 2 A resolution: overall structure, ligand binding, and comparison with related flavoproteins, *Structure 2*, 1089-1105.

103. Mattevi, A. (2006) To be or not to be an oxidase: challenging the oxygen reactivity of flavoenzymes, *Trends Biochem Sci 31*, 276-283.

104. Malito, E., Alfieri, A., Fraaije, M. W., and Mattevi, A. (2004) Crystal structure of a Baeyer-Villiger monooxygenase, *Proc Natl Acad Sci U S A 101*, 13157-13162.

105. Hiromoto, T., Fujiwara, S., Hosokawa, K., and Yamaguchi, H. (2006) Crystal structure of 3-hydroxybenzoate hydroxylase from Comamonas testosteroni has a large tunnel for substrate and oxygen access to the active site, *J Mol Biol 364*, 878-896.

106. Dong, C., Flecks, S., Unversucht, S., Haupt, C., van Pee, K. H., and Naismith, J. H. (2005) Tryptophan 7-halogenase (PrnA) structure suggests a mechanism for regioselective chlorination, *Science 309*, 2216-2219.

107. Su, Q., and Klinman, J. P. (1999) Nature of oxygen activation in glucose oxidase from Aspergillus niger: the importance of electrostatic stabilization in superoxide formation, *Biochemistry 38*, 8572-8581.

108. Gadda, G., Fan, F., and Hoang, J. V. (2006) On the contribution of the positively charged headgroup of choline to substrate binding and catalysis in the reaction catalyzed by choline oxidase, *Arch Biochem Biophys 451*, 182-187.

109. Gadda, G., Powell, N. L., and Menon, P. (2004) The trimethylammonium headgroup of choline is a major determinant for substrate binding and specificity in choline oxidase, *Arch Biochem Biophys 430*, 264-273.

110. Roth, J. P., Wincek, R., Nodet, G., Edmondson, D. E., McIntire, W. S., and Klinman, J. P. (2004) Oxygen isotope effects on electron transfer to O2 probed using chemically modified flavins bound to glucose oxidase, *J Am Chem Soc 126*, 15120-15131.

111. Roth, J. P., and Klinman, J. P. (2003) Catalysis of electron transfer during activation of O2 by the flavoprotein glucose oxidase, *Proc Natl Acad Sci U S A 100*, 62-67.

112. Porter, D. J., Voet, J. G., and Bright, H. J. (1977) Mechanistic features of the D-amino acid oxidase reaction studied by double stopped flow spectrophotometry, *J Biol Chem 252*, 4464-4473.

113. Tan, A. K., and Ramsay, R. R. (1993) Substrate-specific enhancement of the oxidative half-reaction of monoamine oxidase, *Biochemistry 32*, 2137-2143.

114. Mimasu, S., Sengoku, T., Fukuzawa, S., Umehara, T., and Yokoyama, S. (2008) Crystal structure of histone demethylase LSD1 and tranylcypromine at 2.25 A, *Biochem Biophys Res Commun 366*, 15-22.

115. Son, S. Y., Ma, J., Kondou, Y., Yoshimura, M., Yamashita, E., and Tsukihara, T. (2008) Structure of human monoamine oxidase A at 2.2-A resolution: the control of opening the entry for substrates/inhibitors, *Proc Natl Acad Sci U S A 105*, 5739-5744.

116. Binda, C., Wang, J., Pisani, L., Caccia, C., Carotti, A., Salvati, P., Edmondson, D. E., and Mattevi, A. (2007) Structures of human monoamine oxidase B complexes with selective noncovalent inhibitors: safinamide and coumarin analogs, *J Med Chem 50*, 5848-5852.

117. Sun, W., Williams, C. H., Jr., and Massey, V. (1996) Site-directed mutagenesis of glycine 99 to alanine in L-lactate monooxygenase from Mycobacterium smegmatis, *The Journal of biological chemistry 271*, 17226-17233.

118. Leferink, N. G., Fraaije, M. W., Joosten, H. J., Schaap, P. J., Mattevi, A., and van Berkel, W. J. (2009) Identification of a gatekeeper residue that prevents dehydrogenases from acting as oxidases, *The Journal of biological chemistry 284*, 4392-4397.

119. Murray, M. S., Holmes, R. P., and Lowther, W. T. (2008) Active site and loop 4 movements within human glycolate oxidase: implications for substrate specificity and drug design, *Biochemistry 47*, 2439-2449.

120. Wigner, E. P. (1959) *Group theory and its application to the quantum mechanics of atomic spectra / [by] Eugene P. Wigner ; translated from the German by J. J. Griffin* Academic Press.

121. Schweitzer, C., and Schmidt, R. (2003) Physical mechanisms of generation and deactivation of singlet oxygen, *Chem Rev 103*, 1685-1757.

122. Sawyer, D. T. (1991) *Oxygen Chemistry*.

123. Sawyer, D. T. (1990) *International Review of Experimental Pathology*, Vol. 31, Academic Press, INC.

124. Malmstrom, B. G. (1982) Enzymology of oxygen, *Annu Rev Biochem 51*, 21-59.

125. Hamilton, G. A. (1969) Mechanisms of two- and four-electron oxidations catalyzed by some metalloenzymes, *Adv Enzymol Relat Areas Mol Biol 32*, 55-96.

126. Orville, A. M., Lountos, G. T., Finnegan, S., Gadda, G., and Prabhakar, R. (2009) Crystallographic, spectroscopic, and computational analysis of a flavin C4a-oxygen adduct in choline oxidase, *Biochemistry 48*, 720-728.

127. Sucharitakul, J., Prongjit, M., Haltrich, D., and Chaiyen, P. (2008) Detection of a C4a-hydroperoxyflavin intermediate in the reaction of a flavoprotein oxidase, *Biochemistry 47*, 8485-8490.

128. Keevil, T. a. M., H. S. (1978) In *Methods of Enzymology*, pp 3 - 40.

129. Que, L., Jr., Lipscomb, J. D., Munck, E., and Wood, J. M. (1977) Protocatechuate 3,4-dioxygenase. Inhibitor studies and mechanistic implications, *Biochim Biophys Acta 485*, 60-74.

130. Davis, M. I., Orville, A. M., Neese, F., Zaleski, J. M., Lipscomb, J. D., and Solomon, E. I. (2002) Spectroscopic and electronic structure studies of protocatechuate 3,4-dioxygenase: nature of tyrosinate-Fe(III) bonds and their contribution to reactivity, *J Am Chem Soc 124*, 602-614.

131. Schneider, C., Pratt, D. A., Porter, N. A., and Brash, A. R. (2007) Control of oxygenation in lipoxygenase and cyclooxygenase catalysis, *Chem Biol 14*, 473-488.

132. Schneider, C., Boeglin, W. E., Yin, H., Stec, D. F., and Voehler, M. (2006) Convergent oxygenation of arachidonic acid by 5-lipoxygenase and cyclooxygenase-2, *J Am Chem Soc 128*, 720-721.

133. Wajcman, H., Kiger, L., and Marden, M. C. (2009) Structure and function evolution in the superfamily of globins, *C R Biol 332*, 273-282.

134. Chufan, E. E., Puiu, S. C., and Karlin, K. D. (2007) Heme-copper/dioxygen adduct formation, properties, and reactivity, *Acc Chem Res 40*, 563-572.

135. Koymans, L., Donne-op den Kelder, G. M., Koppele Te, J. M., and Vermeulen, N. P. (1993) Cytochromes P450: their active-site structure and mechanism of oxidation, *Drug Metab Rev 25*, 325-387.

136. Thackray, S. J., Mowat, C. G., and Chapman, S. K. (2008) Exploring the mechanism of tryptophan 2,3-dioxygenase, *Biochem Soc Trans 36*, 1120-1123.

137. Nicholls, P. a. C., B (1974) Cytochrome c Oxidase, In *Molecular Mechanisms of oxygen activation* (Hayaishi, O., Ed.), pp 479 - 534, Academic Press.

138. Hayaishi, O., Nozaki, M. and Abbott, M. T. (1975) In *Enzymes* (Boyer, P. d., Ed.), pp 119 - 189.

139. Wood, J. M. (1980) In *Metal ion Activation of dioxygen* (Spiro, T. G., Ed.), pp 163 - 180, Wiley, New York.

140. Taniguchi, T., Sono, M., Hirata, F., Hayaishi, O., Tamura, M., Hayashi, K., Iizuka, T., and Ishimura, Y. (1979) Indoleamine 2,3-dioxygenase. Kinetic studies on the binding of superoxide anion and molecular oxygen to enzyme, *J Biol Chem 254*, 3288-3294.

141. Sono, M., Taniguchi, T., Watanabe, Y., and Hayaishi, O. (1980) Indoleamine 2,3-dioxygenase. Equilibrium studies of the tryptophan binding to the ferric, ferrous, and CO-bound enzymes, *J Biol Chem 255*, 1339-1345.

142. Hirata, F., Ohnishi, T., and Hayaishi, O. (1977) Indoleamine 2,3-dioxygenase. Characterization and properties of enzyme. O2- complex, *J Biol Chem 252*, 4637-4642.

143. Hayaishi, O., Hirata, F., Ohnishi, T., Henry, J. P., Rosenthal, I., and Katoh, A. (1977) Indoleamine 2,3-dioxygenase: incorporation of 18O2-- and 18O2 into the reaction products, *J Biol Chem 252*, 3548-3550.

144. White, R. E., and Coon, M. J. (1980) Oxygen activation by cytochrome P-450, *Annu Rev Biochem 49*, 315-356.

145. Hamdane, D., Zhang, H., and Hollenberg, P. (2008) Oxygen activation by cytochrome P450 monooxygenase, *Photosynth Res 98*, 657-666.

146. Que, L., Jr., and Epstein, R. M. (1981) Resonance Raman studies on protocatechuate 3,4-dioxygenase-inhibitor complexes, *Biochemistry 20*, 2545-2549.

147. Antonczak, S., Fiorucci, S., Golebiowski, J., and Cabrol-Bass, D. (2009) Theoretical investigations of the role played by quercetinase enzymes upon the flavonoids oxygenolysis mechanism, *Phys Chem Chem Phys 11*, 1491-1501.

148. Klinman, J. P. (2006) The copper-enzyme family of dopamine beta-monooxygenase and peptidylglycine alpha-hydroxylating monooxygenase: resolving the chemical pathway for substrate hydroxylation, *J Biol Chem 281*, 3013-3016.

149. Kaufman, S., Bridgers, W. F., Eisenberg, F., and Friedman, S. (1962) The source of oxygen in the phenylalanine hydroxylase and the copamine-beta-hydroxylase catalyzed rections, *Biochem Biophys Res Commun 9*, 497-502.

150. Vanneste, W. H. a. z., A. (1974) Coper-containing oxygenases, In *Molecular Mechanisms of Oxygen Activation* (Hayaishi, O., Ed.), pp 371 - 404, Academic Press, New York and London.

151. Yasunobu, K. T., Mower, H. F. and Hayaishi, O. (1976) *Iron and Copper Proteins*, Plenum, New York.

152. Himmelwright, R. S., Eickman, N. C., LuBien, C. D., Lerch, K., Solomon, E. I. (1980) *J. Am. Chem. Soc. 102*, 7339 - 7344.

153. Ruegg, C., and Lerch, K. (1981) Cobalt tyrosinase: replacement of the binuclear copper of Neurospora tyrosinase by cobalt, *Biochemistry 20*, 1256-1262.

154. van Berkel, W. J., Kamerbeek, N. M., and Fraaije, M. W. (2006) Flavoprotein monooxygenases, a diverse class of oxidative biocatalysts, *J Biotechnol 124*, 670-689.

155. Massey, V. (1994) Activation of molecular oxygen by flavins and flavoproteins, *J Biol Chem 269*, 22459-22462.

156. Sutton, W. B. (1957) Mechanism of action and crystallization of lactic oxidative decarboxylase from Mycobacterium phlei, *J Biol Chem 226*, 395-405.

157. Entsch, B., and van Berkel, W. J. (1995) Structure and mechanism of para-hydroxybenzoate hydroxylase, *FASEB J 9*, 476-483.

158. Gadda, G., and Francis, K. (2010) Nitronate monooxygenase, a model for anionic flavin semiquinone intermediates in oxidative catalysis, *Arch Biochem Biophys 493*, 53-61.

159. Babcock, G. T., Espe, M., Hoganson, C., Lydakis-Simantiris, N., McCracken, J., Shi, W., Styring, S., Tommos, C., and Warncke, K. (1997) Tyrosyl radicals in enzyme catalysis: some properties and a focus on photosynthetic water oxidation, *Acta Chem Scand 51*, 533-540.

160. Avigad, G., Amaral, D., Asensio, C., and Horecker, B. L. (1962) The D-galactose oxidase of Polyporus circinatus, *J Biol Chem 237*, 2736-2743.

161. Kelleher, F. M., and Bhavanandan, V. P. (1986) Re-examination of the products of the action of galactose oxidase. Evidence for the conversion of raffinose to 6"-carboxyraffinose, *J Biol Chem 261*, 11045-11048.

162. Aboelella, N. W., Lewis, E. A., Reynolds, A. M., Brennessel, W. W., Cramer, C. J., and Tolman, W. B. (2002) Snapshots of dioxygen activation by copper: the structure of a 1:1 Cu/O(2) adduct and its use in syntheses of asymmetric Bis(mu-oxo) complexes, *J Am Chem Soc 124*, 10660-10661.

163. Fujisawa, K., Tateda, A., Miyashita, Y., Okamoto, K., Paulat, F., Praneeth, V. K., Merkle, A., and Lehnert, N. (2008) Structural and spectroscopic characterization of

mononuclear copper(I) nitrosyl complexes: end-on versus side-on coordination of NO to copper(I), *J Am Chem Soc 130*, 1205-1213.

164. Whittaker, J. W. (2005) The radical chemistry of galactose oxidase, *Arch Biochem Biophys 433*, 227-239.

165. Ito, N., Phillips, S. E., Stevens, C., Ogel, Z. B., McPherson, M. J., Keen, J. N., Yadav, K. D., and Knowles, P. F. (1991) Novel thioether bond revealed by a 1.7 A crystal structure of galactose oxidase, *Nature 350*, 87-90.

166. Roth, J. P., and Klinman, J. P. (2003) Catalysis of electron transfer during activation of O-2 by the flavoprotein glucose oxidase, *P Natl Acad Sci USA 100*, 62-67.

167. Coulombe, R., Yue, K. Q., Ghisla, S., and Vrielink, A. (2001) Oxygen access to the active site of cholesterol oxidase through a narrow channel is gated by an Arg-Glu pair, *J Biol Chem 276*, 30435-30441.

168. Kass, I. J., and Sampson, N. S. (1998) Evaluation of the role of His447 in the reaction catalyzed by cholesterol oxidase, *Biochemistry 37*, 17990-18000.

169. Gadda, G. (2008) Hydride transfer made easy in the reaction of alcohol oxidation catalyzed by flavin-dependent oxidases, *Biochemistry 47*, 13745-13753.

170. Ikuta, S., Imamura, S., Misaki, H., and Horiuti, Y. (1977) Purification and characterization of choline oxidase from Arthrobacter globiformis, *J Biochem 82*, 1741-1749.

171. Gadda, G. (2003) Kinetic mechanism of choline oxidase from Arthrobacter globiformis, *Biochim Biophys Acta 1646*, 112-118.

172. Gadda, G. (2003) pH and deuterium kinetic isotope effects studies on the oxidation of choline to betaine-aldehyde catalyzed by choline oxidase, *Biochim Biophys Acta 1650*, 4-9.

173. Ghisla, S., and Massey, V. (1989) Mechanisms of flavoprotein-catalyzed reactions, *Eur J Biochem 181*, 1-17.

CHAPTER II

CRYSTALLOGRAPHIC, SPECTROSCOPIC, AND COMPUTATIONAL ANALYSIS OF A FLAVIN C4A-OXYGEN ADDUCT IN CHOLINE OXIDASE.

(This chapter has been published verbatim in Orville, AM, Lountos, GT, Finnegan, S, Prabhakar, R, and Gadda, G., (2009), *Biochemistry 48(4)*, 720-8.)

2.1.Abstract

Flavin C4a-OOH and C4a-OH adducts are critical intermediates proposed in many flavoenzyme reaction mechanisms, but they are rarely detected even by rapid transient kinetics methods. We observe a trapped flavin C4a-OH or C4a-OO(H) adduct by single crystal spectroscopic methods and in the 1.86 Å resolution x-ray crystal structure of choline oxidase. The microspectrophotometry results shows that the adduct forms rapidly *in situ* at 100 K upon exposure to x-rays. Density functional theory calculations establish the electronic structures for the flavin C4a-OH and the C4a-OO(H) adducts, and estimate the stabilization energy of several active site hydrogen bonds deduced from the crystal structure. We propose that the enzyme-bound FAD is reduced in the x-ray beam. The aerobic crystals then form either a C4a-OH or a C4a-OO(H) adduct, but an insufficient proton inventory prevents their decay at cryogenic temperatures.

2.2.Introduction

Although flavins and flavoproteins were discovered in the 1930s, their remarkable functional diversity continues to be characterized. It is now estimated that up to 4% of microbial or eukarytotic proteins are flavoproteins, and more than 1100 flavoprotein structures are currently available from the Protein Data Bank. Flavin-dependent proteins catalyze a wide range of biochemical reactions including aerobic and anaerobic metabolism, light emission,

photosynthesis, DNA repair, plant phototropism, regulation of biological clocks, and the activation of oxygen for hydroxylation and oxidation reactions (*1*). This diversity derives from the flavin isoalloxazine ring system, which is ideally suited for oxidative or reductive reactions involving one or two electron transfer to and from other redox-active centers, as well as reactivity with molecular oxygen. Moreover, the isoalloxazine ring system can act as an electrophile or a nucleophile forming covalent adducts with either protein residues or reaction intermediates at the C4a, N5, C6, and C8M positions (see **Figure 2.4** for nomenclature). The flavin is also influenced by the protein active site, which extends the reaction diversity and facilitates catalysis along a particular flavoenzyme reaction coordinate. Thus, the interactions between the flavin, active site residues, and substrate molecules yield almost limitless combinations, and consequently remarkable diversity in flavoprotein function.

The reaction of molecular oxygen with reduced flavoenzymes is fundamental to all aerobic organisms and can be orders of magnitude faster or slower than the analogous reactions of flavins in solution (*2*). The outcome of the reaction also varies greatly, which has been used to segregate flavoenzymes into different classes. For example, the NAD(P)H-dependent monooxygenases cleave the dioxygen O-O bond with incorporation of one oxygen atom into an organic product and the other oxygen atom is then released as water. In contrast, the ubiquitous flavin-dependent oxidases use O_2 as a two-electron, two-proton acceptor to produce H_2O_2. A transient C4a-hydroperoxy-flavin species has been established by spectroscopic methods in *p*-hydroxybenzoate 3-hydroxylase (*3*), *p*-hydroxyphenylacetate 3-hydroxylase (*4*), luciferase (*5*), and microsomal flavin-containing monooxygenase (*6*). A similar species has also been detected in three oxidases via rapid kinetic studies of pyranose 2-oxidase (*7*), on a mutant form of NADH oxidase (*8*), and pulse radiolysis experiments with glucose oxidase (*9*). Because a C4a-oxygen

adduct is so rarely observed in oxidases, some authors recently proposed that flavin reoxidation in these enzymes proceeds preferentially by an outer-sphere electron transfer process, rather than through formation of a C4a-hydroperoxide intermediate (*10*). Regardless of the mechanism or enzyme family classification, to date there is no structurally defined flavin C4a-oxygen adduct in the Protein Data Bank.

Choline oxidase (E.C. 1.1.3.17) from *Arthrobacter globiformis* catalyzes the four-electron oxidation of choline to glycine betaine (*N*,*N*,*N*-trimethylglycine) via two sequential, FAD-dependent reactions in which betaine aldehyde is formed as an obligatory enzyme-bound intermediate (*11*). In each of the oxidative half-reactions, a molecule of O_2 is converted into H_2O_2. The midpoint reduction potentials for the FAD in choline oxidase are 211±2 mV and -65±2 mV for the FAD - FAD^{sq} and FAD^{sq} - $FADH^{-}$, respectively (*12*). These values are the highest determined to date for any flavoprotein, and are thought to be influenced by several active site characteristics, including a covalent linkage between the C8M position and His99. We recently determined the crystal structure of choline oxidase at 1.86 Å resolution under cryogenic conditions (*13*). A novel, but unexplained feature of the structure is the flavin cofactor, which exhibits a distorted isoalloxazine ring system and suggests the presence of a novel C4a-adduct. In this report, we show that a C4a-OH or C4a-OO(H) adduct forms in an x-ray dependent process under cryogenic conditions. The essential insights derive from single crystal microspectrophotometry concurrent with x-ray diffraction collected recently at the new single crystal spectroscopy facility located at the National Synchrotron Light Source (see **Figure 2. 1**), which is now available on a full-time basis to the general user population. The spectroscopic data also correlates very well with density functional theory (DFT) calculations and the high resolution x-ray crystal structure of the enzyme.

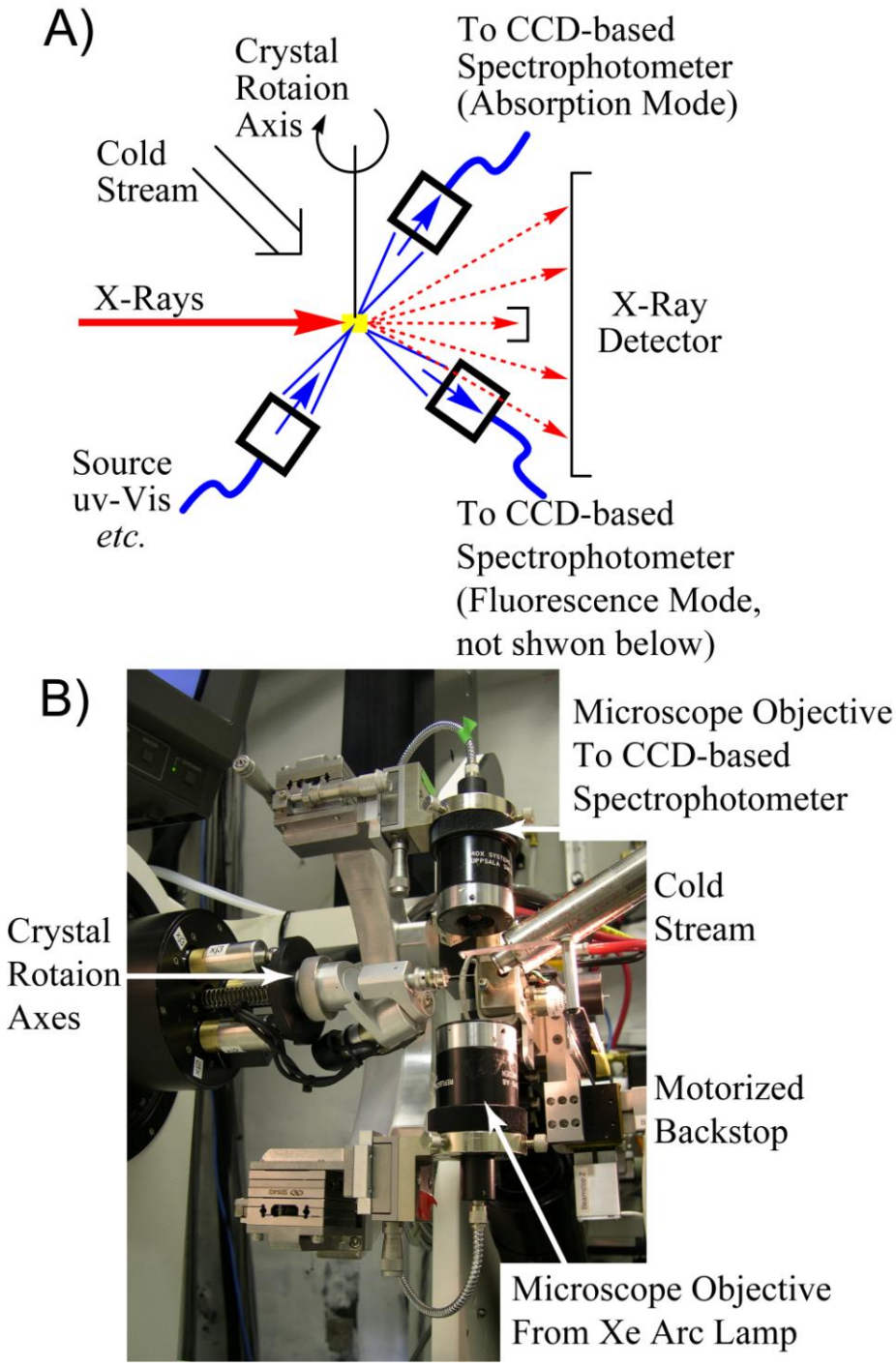

Figure 2.1. The Single Crystal Optical Absorption Spectroscopy Facility Installed at X26-C. **(A)** A Schematic Overview of the Facility. **(B)** A Photograph of the Current Installation at X26-C Approximately from the Perspective of the X-ray Detector Looking Toward the Crystal.

2.3.Materials and methods

Enzyme Purification, Crystallization, Structure Determination, and Model Refinement: Oxidized choline oxidase from *Arthrobacter globiformis* strain ATCC 8010 was expressed from pET/codA in Escherichia coli and purified to homogeneity as described previously (*13-15*). Crystals of choline oxidase were grown aerobically by hanging drop vapor diffusion from 1.2 - 1.8 M ammonium sulphate and 10% v/v dimethylsulfoxide (DMSO) in 0.1 M Bis-Tris propane, pH 8.5. Single crystals were transferred from the mother liquor into a cryoprotectant solution consisting of 3.4 M sodium malonate, pH 7.0 and allowed to soak for two minutes prior to flash freezing in liquid nitrogen (*13*). Several independent crystals were used for x-ray diffraction data sets and for single crystal microspectrophotometry. X-ray diffraction data was collected at either the SER-CAT facilities (22-ID and 22-BM) at the Advanced Photon Source at Argonne National Laboratory, or at beamlines X12-B, X25, X26-C or X29 of the National Synchrotron Light Source at Brookhaven National Laboratory. The crystal structure was determined by molecular replacement as previously described (*13*) using the coordinates of the crystal structure of glucose oxidase (1CF3, (*16*)) as a search model. Choline oxidase crystallizes with one homodimer in the asymmetric unit in space group $P4_32_12$ with a = b = 84.4 Å, and c = 343.5 Å. The high resolution data set extends to 1.86 Å resolution. Crystals of aerobic choline oxidase were also grown from 1.2 - 1.8 M ammonium sulfate and 10% v/v 1,4-dioxane in 0.1M Bis-Tris propane, pH 8.5. These conditions yield space group $P2_1$ with typical unit cell dimensions of a = 69.3 Å, b = 346.2 Å, c = 105.9 Å, β = 94.3° and four homodimer enzymes in the asymmetric unit.

Refinements and model adjustments for the active site FAD were carried out as described (*13*). All library files with restraints were prepared using the PRODRG server (http://davapc1.bioch.dundee.ac.uk/programs/prodrg/). Initially, the FAD was refined using

restraints to confer planarity on the entire isoalloxazine ring. Electron density maps at this point clearly revealed significant bending of the pyrimidine ring and the mF_o-DF_c maps contoured at 3σ returned negative features on the flat pyrimidine ring and a lobe of positive difference density protruded from the C4a position and the pyrimidine ring. The isoalloxazine was then manually adjusted to properly fit the pyrimidine ring into the electron density and the restraints were adjusted to remove planar restraints from the pyrimidine ring and sp^3 hybridization was conferred upon the C4a atom. Planar restraints were applied to the dimethylbenzene ring and the atoms of the piperazine ring. Electron density maps from the refinement indicated a good fit of the pyrimidine ring at this point, but the mF_o - DF_c maps revealed > 4σ positive difference features near the C4a atom. At this point, two series of refinements were performed. In one round, the sp^3 C4a atom was bonded to a single oxygen atom (FAD-C4a-O^-) and the model was refined. An FAD-C4a-O_2^- model was also refined. The resulting maps indicated that the O_2 moiety also fits the 2mF_o - DF_c maps quite well; however, the occupancy of the distal oxygen atom refined best with an occupancy value of 0.5. To check for model bias, 2mF_o-DF_c and mF_o-DF_c simulated annealing omit maps were prepared in CNS. The FAD, DMSO, residues His99, and His466 as well as all atoms within a 3.5 Å radius were removed from the model. The simulated annealing and map calculation was carried out with a starting temperature of 1000 K with data from 50.0-1.86 Å resolution.

Two additional models were also refined with *REFMAC5*. The first included a water molecule centered in the difference peak and unrestrained with respect to the FAD C4a atom. Upon convergence of the refinement of this model, the water molecule was only 1.6 Å from the C4a atom (**Table 2.1**) and there was continuous electron density between the two atoms.

Table 2.1. Selected Bond Distances and Angles in the X-ray Structure and DFT Optimized Models

Model Source	X-ray	X-ray	X-ray	DFT	DFT	DFT	DFT
Model	C4a, H_2O	C4a-OH	C4a-OO(H)	C4a-OH	C4a-OOH	FAD^{sq}	$FADH^-$
Bond Distances (Å)							
O_p-O_d	N.A.	N.A.	1.40	N.A.	1.48	N.A.	N.A.
C4a-O_p	1.63	1.45	1.42	1.43	1.42	N.A.	N.A.
C4a-C10a	1.47	1.47	1.46	1.52	1.51	1.44	1.43
C4a-C4	1.55	1.59	1.59	1.56	1.59	1.49	1.49
C4a-N5	1.51	1.47	1.48	1.43	1.43	1.32	1.33
Bond Angle (°)							
C4a-O_p-O_d	N.A.	N.A.	116.3	N.A.	108.8	N.A.	N.A.
C4-C4a-O_p	134.2	123.5	119.0	106.1	100.7	N.A.	N.A.
N5-C4a-O_p	88.9	100.7	105.4	109.2	110.7	N.A.	N.A.
C10a-C4a-O_p	104.1	107.4	110.9	110.3	110.9	N.A.	N.A.
C4-C4a-N5	123.5	120.8	122.9	111.8	113.3	122.3	121.3
C4-C4a-C10a	108.6	94.6	85.5	104.7	106.0	116.7	117.7
N5-C4a-C10a	97.8	110.7	111.3	114.3	114.5	120.5	117.7
Dihedral Angle (°)							
O_d-O_p-C4a-C4	N.A.	N.A.	169.7	N.A.	-171.9	N.A.	N.A.
O_d-O_p-C4a-N5	N.A.	N.A.	26.9	N.A.	68.1	N.A.	N.A.
O_d-O_p-C4a-C10	N.A.	N.A.	-93.6	N.A.	-60.1	N.A.	N.A.
O_p-C4a-N5-C5a	N.A.	-147.5	-156.0	-125.1	-134.0	N.A.	N.A.
O_p-C4a-C4-N3	N.A.	44.1	43.5	70.3	69.3	N.A.	N.A.
N3-C4-C4a-N5	174.0	175.5	179.5	-170.8	-172.5	164.0	162.0
C4-C4a-N5-C5a	69.0	71.8	63.1	117.8	113.8	164.1	164.1
C4a-N5-C5a-C6	-164.4	-168.9	-163.0	-179.1	-172.2	178.9	177.3
N5-C5a-C6-C7	-178.0	-177.9	-178.1	168.1	169.4	161.9	163.9
C2-N1-C10a-N10	96.0	94.9	107.6	162.1	167.3	176.6	175.7
N1-C10a-N10-C9a	-173.4	-173.1	175.7	-167.0	-159.6	173.5	168.5
C10a-N10-C9a-C9	-165.9	-164.4	-176.0	161.0	155.0	169.7	178.3
N10-C9a-C9-C8	-179.1	-179.1	-177.3	-171.9	-173.8	-173.6	-171.5
N3-C4-C4a-C10a	-68.4	-67.3	-68.0	-46.5	-46.2	-23.6	-27.2
N1-C10a-C4a-C4	60.4	59.7	73.5	51.2	47.7	20.8	22.8
C4-C4a-C10a-N10	-71.2	-72.9	-86.0	-128.9	-132.1	-155.7	-152.4
N1-C10a-C4a-N5	-170.7	-175.6	-162.9	173.9	173.2	-166.7	-166.3

However, since there is no H_2O-C4a bond, this model does not satisfy the observed sp^3 hybridization of the flavin C4a atom. The second alternative model consisted of a covalent FAD C4a-OH moiety, which refined to a 1.45 Å bond distance.

Single Crystal Microspectrophotometry: We built a Single Crystal μ-Spectroscopy Facility (SCμSF) at beamline X26-C at the National Synchrotron Light Source at Brookhaven National Laboratory for use by the general user population (see **Figure 2.1**). The microspectrophotometer components were from a 4DX-ray Systems AB (Sweden). We adapted it so that the microscopic optical axis and focal points were aligned with the crystal rotation axes of the diffractometer and x-ray beam at X26-C. The microscope objectives used parabolic mirrors to achieve 15x magnification and to minimize spherical or chromatic aberration in the wavelength range from approximately 150 – 10,000 nm. The objectives provide a 24mm working distance through a 0.4 numerical aperture, which allows for cryocooling and access for other microspectroscopic components. When coupled with a 50-micron quartz optical fiber, the incident spot size is approximately 25 μm in diameter. The transmitted light is collected from approximately 75 μm spot size. The incident light (350 - 850 nm) was from a 75W Xe research arc lamp (Newport Corp.). An Ocean Optics USB 4000 spectrophotometer (Dunedin, Florida) containing a 3648-element Toshiba linear CCD detector was used to collect the optical absorption spectra. The data were processed initially with the SpectraSuit software on either a Windows XP or LINUX operating system. The spectrophotometer was calibrated and microspectroscopy aligned with a Hg-Ar calibration laser. Typically, optical absorption spectra were collected by averaging ten spectra, each of which was collected with an approximately 70 ms integration time and a 10-pixle “box car” of the CCD detector array. Crystals were held at 100 K during x-ray diffraction and optical absorption spectroscopic data collection.

Computational Procedures: All calculations were performed using the Gaussian 03 program (*17*). The geometries of all the structures are optimized without any symmetry constraint using Density Functional Theory (DFT) based B3LYP method with the 6-31G(d) basis set in gas phase (*18-20*). The final energies were calculated using a large 6-31+G(d,p) basis set including diffuse and polarization functions. Since it was computationally unfeasible to calculate unscaled zero-point energy and thermal corrections on large models used in this study, they are not included. The dielectric effects (for $\varepsilon = 4.3$) from the surrounding protein were incorporated using the self-consistent reaction field method (*21*) at the B3LYP/(6-31G(d)) level. In order to retain the steric effect of the surrounding protein one hydrogen atom each in the backbones of His351 and His466 residues are kept frozen from the X-ray structure. This kind of approach is known to preserve some of the steric effect of the protein surroundings (*22*). The remaining degrees of freedom of all the structures are optimized. The initial models used in the DFT calculations were extracted from the crystal structure. Rather large models were used in the calculations (ca. 180 atoms) and included the FAD and active site residues His99, Asn100, Ser101, DMSO, Ile103, His351, His466, Asn510, and Pro511. The backbone atoms of residues His351 and His466 and the ribityl side chain of the FAD were omitted from the calculation.

2.4.Results and discussion

To investigate the single crystal spectroscopic properties of choline oxidase as a function of x-ray exposure, we harvested yellow crystals of oxidized enzyme from aerobic mother liquor. After transferring crystals to a cryoprotectant (3.5 M Na-Malonate), they were individually mounted in nylon loops and flash-cooled by plunging them into liquid N_2. The crystals were kept at 100 K during the optical absorption spectroscopic and x-ray diffraction and data collection. We performed several types of experiments with enzyme crystallized in space groups

$P4_32_12$ or $P2_1$ from ammonium sulfate. The exposure to 1 Å (12.398 KeV) x-ray photons (~4 x 10^{10} photon/s through a 200 ⌈m diameter collimated beam) was performed on stationary crystals or with crystals rotated through 180° at beamline X26-C of the National Synchrotron Light Source. The results are very reproducible and typical spectra are illustrated in **Figure 2.2**.

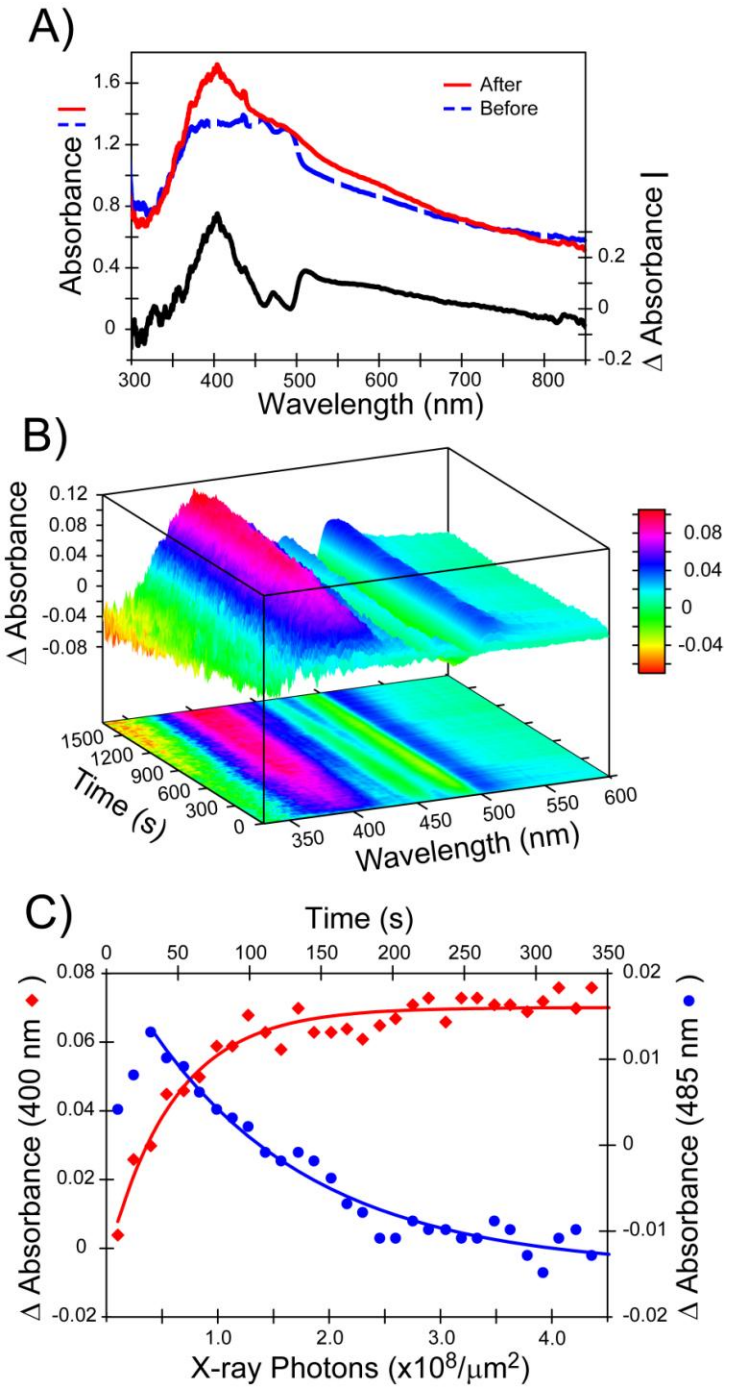

Figure 2.2. Spectroscopic Changes Observed in Single Crystals of Choline Oxidase upon X-ray Irradiation at 100 K. **(A)** Optical spectra measured from a single crystal of choline oxidase before (blue) or after (red) an x-ray diffraction data set was collected with 180° of phi-axis rotation. The difference between the two is shown with the black line and with the scale on the right. Each spectrum was recorded with the phi axis at 0° by averaging ten spectra obtained with a 70 ms integration time and the "box-car" set to 10 pixel-CCD elements. **(B)** The time-dependent change of the optical absorption spectrum of another choline oxidase crystal held stationary in the x-ray beam. Spectra were recoded every ten seconds with the instrument parameters as in (A). Six reference spectra were recoded before the x-ray shutter was opened, averaged, and then subtracted from each spectrum obtained after the x-ray shutter was opened. The lower panel of the 3-D plot is a projection of the time-dependent difference spectra. **(C)** Difference features at 400 and 485 nm from (B) were fit to the single exponential equation: $y = a*e^{(bt + c)}$, where t = time in seconds and for the 400 nm data points a = -0.074012, b = 0.021617, and c = 0.070048; whereas the first two data points were excluded for the 485 nm and fit with a = 0.036755, b = 0.0087557, and c = -0.0144.

The absorption spectrum of choline oxidase crystals at 100 K prior to x-ray exposure reveals two maxima centered at 460 nm and 485 nm. We and others have observed that single crystal spectra at low temperature are anisotropic and depend critically on crystal orientation, especially when planar chromophores such as flavins are present within the crystal (*23*-*24*). For example, AMO has collected single crystal spectra from several oxidized flavoenzymes (data not shown) including nitroalkane oxidase, xenobiotic reductase A, cholesterol oxidase, and thioredoxin reductase, which all yield two resolved peaks near 450 nm. Thus, the single crystal spectra of choline oxidase are better resolved than for the enzyme in solution at 300 K (for a typical example, see **Figure 2.3**), which yields a peak at 450 nm and a shoulder at about 480 nm.

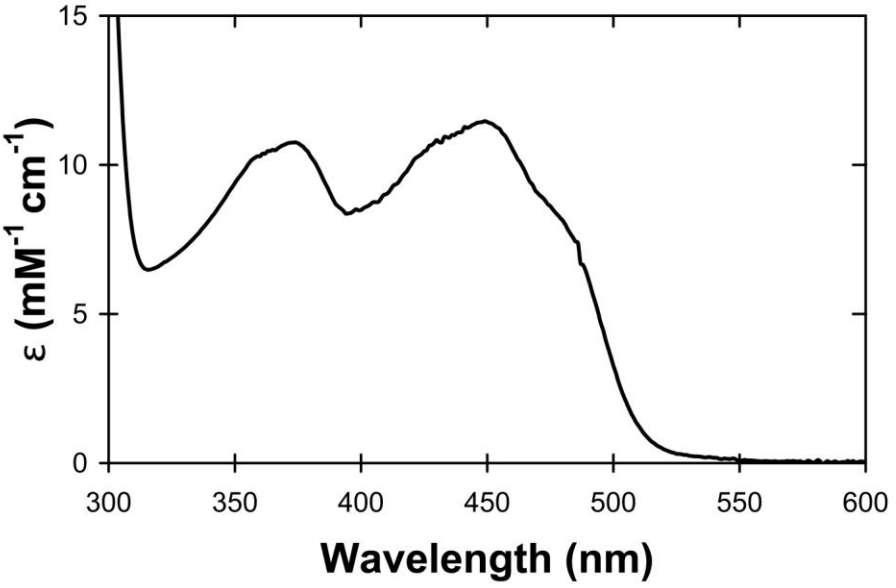

Figure 2.3. Optical Absorption Spectrum of 0.04 mM Choline Oxidase at Room Temperature and in a Solution of 0.05 M Bis-tris-propane pH 8.5, 0.6 M Ammonium Sulfate and 5% (v/v) Dimethylsulfoxide, which are Approximately the Crystallization Conditions.

After x-ray diffraction data collection, the optical spectrum of choline oxidase crystals yields a single absorption peak at approximately 400 nm and a broad shoulder extending to longer wavelengths. The difference spectra (after - before) clearly shows an absorption band with λ_{max} at 400 nm and features that extend from about 510 nm to longer wavelengths. The 400 nm feature represents the vast majority of the flavin species present in the region of the crystal exposed to x-rays and is remarkably similar to spectra obtained from transient flavin C4a-OO(H) or C4a-OH intermediates (*3-8*). The longer wavelength features indicate that a small fraction of the enzyme contains a FAD semiquinone species as previously observed for choline oxidase in solution (*25*).

We next evaluated the time-dependent process of adduct formation in a single crystal at 100 K. Spectra were collected every ten seconds from a stationary crystal of choline oxidase during exposure to the monochromatic synchrotron x-ray beam at X26-C. As illustrated in

Figure 2.2B-C, the difference feature at 400 nm increases in an exponential process with a $t_{1/2}$ of approximately 40 seconds. Thus, the appearance of the spectral feature at 400 nm is nearly complete within the time required to collect only a small fraction of the unique x-ray diffraction data (equivalent to less than 10° of crystal rotation), even at the relatively modest x-ray intensity of beamline X26-C of the NSLS. This process is also approximately commensurate with the decrease of the 460 and 485 nm features attributed to oxidized FAD ($t_{1/2}$ of approximately 100 seconds, **Figure 2.2C**). Optical spectra from enzyme in solution at room temperature show that the flavin semiquinone species (*i.e.* one electron reduced) has a spectrum that overlaps that of oxidized FAD (*25*). In contrast, the hydroquinone FAD species (*i.e.* reduced by 2 electrons), or the C4a-adduct observed here, each have very little absorbance in the 450 - 500 nm region. Consequently, the exponential decay at 485 nm appears to be slower than the appearance of the more remote 400 nm feature assigned to the C4a adduct. Together, the spectroscopic analyses of single crystals at low temperature show that the decrease in the concentration of oxidized FAD in the region of the crystal exposed x-rays is directly correlated to an increase of the concentration of the C4a-adduct.

The atomic structure and 1.86 Å resolution simulated-annealing omit electron density maps for the FAD are shown in **Figure 2.4**. The flavin isoalloxazine ring is not planar, as anticipated for oxidized choline oxidase, or bent along the N5-N10 axis as is often observed in reduced flavoproteins (*26*). The electron density for the dimethylbenzene and piperizine rings indicates that each ring is flat and that they are coplanar. However, the plane of the pyrimidine ring is at an approximately 120° angle to the plane of the other two rings (**Table 2.1**). The electron density for the pyrimidine ring indicates that it adopts a “half-boat” configuration in which the C4a atom is approximately 0.5 Å above the pyrimidine ring plane. Moreover,

throughout the refinement process a greater than 4σ positive difference peak associated with the C4a atom persisted. This feature clearly indicates that the C4a atom is sp^3 hybridized and, therefore, that a covalent flavin adduct is present in the crystal structure. The electron density for the difference feature is large enough to accommodate only one, or possibly two atoms in a covalently linked FAD C4a-adduct.

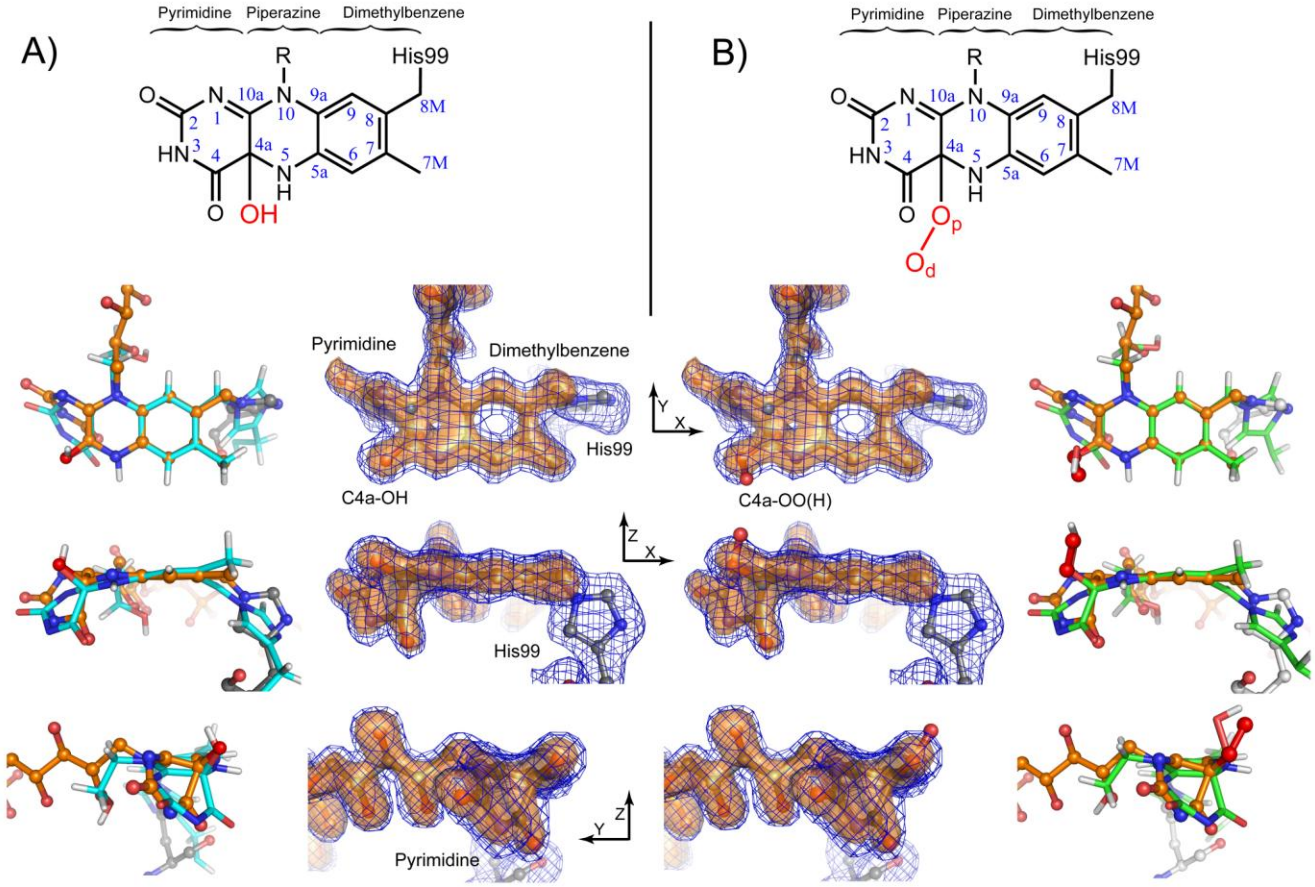

Figure 2.4. Comparison of the X-ray Structures with the DFT Optimized Modes for the FAD C4a-OH Adduct **(A)**, or the C4a-OO(H) adduct **(B)**. Orthogonal views of the simulated-annealing omit electron density maps (50 - 1.86 Å resolution) for the FAD isoalloxazine ring in choline oxidase **(lower central portions)**. The $mF_o - DF_c$ difference map (+3 σ) is shown with orange, translucent surface contours and the $2mF_o - DF_c$ map (1 σ) is displayed as a blue mesh. The FAD, C4a adduct, and DMSO were omitted from the model. For comparison, the refined C4a-OH and C4a-OO(H) atomic models are shown superimposed with C, N, and O atoms colored grey, blue and red, respectively. The arrows labeled X, Y and Z indicate the relative orientation of each image. An overlay of the x-ray structures with the DFT optimized modes for the FAD C4a-OH adduct and the C4a-OO(H) adduct **(lower outer portions)**. The refined crystal structure is shown with flavin C atoms and bonds in orange superimposed with the DFT

optimized C4a-OH (C atoms rendered with cyan sticks), or the C4a-OOH model (C atoms rendered with green sticks).

To our knowledge, the materials and aerobic crystallization conditions do not include any reagents that readily form a C4a adduct with oxidized FAD. Moreover, none of the reagents used to crystallize the enzyme alter the optical spectrum of oxidized choline oxidase indicating that the reagents do not perturb significantly the FAD electronic environment (see **Figure 2.3**). In contrast, reduced flavins in the semiquinone or hydroquinone states do react with O_2 and can form C4a-oxygen adducts (*2, 9*). Therefore, we followed a conservative approach and refined a FAD C4a-OH atomic model, which converged well with *REFMAC5* to yield a 1.45 Å C4a-O bond distance (**Figure 2.4A and Table 2.1**). Next we modeled an O_2 molecule bound to the C4a atom of reduced FAD. After refinement with *REFMAC5* the C4a-O_p and O_p-O_d bond lengths are 1.4 Å (**Figure 2.4B and Table 2.1**) with a C4a-O_p-O_d bond angle of 116°. Although the estimated coordinate error of the model is approximately 0.1 Å, these parameters agree well with those determined by quantum mechanical calculations for the model FAD-C4a-OOH intermediate in *p*-hydroxybenzoate 3-hydroxylase and phenol hydroxylase (*27-28*), as well as the DFT calculations discussed below. Therefore, the C4a-OH and C4a-OO(H) models for the FAD adduct in choline oxidase have reasonable geometry for sp^3 hybridization and the appropriate bond lengths and angles for a C4a-adduct. However, the observed electron density for the distal oxygen atom (O_d) is weaker than for the proximal atom oxygen (O_p) and consequently, the former atom also has a higher B-factor. This suggests that either the O_d atom may be partially disordered, possibly due to precession about the C4a-O_p bond, or that only one oxygen atom is present in the adduct.

The simulated-annealing omit maps provide the most unbiased view of the FAD adduct. During this procedure, the FAD, DMSO, and the C4a-adduct were omitted from the model. The resulting $mF_o - DF_c$ and $2mF_o - DF_c$ electron density maps (**Figure 2.4A-B**) calculated with reflections between 50 and 1.86 Å resolution were superimposed with refined models containing either the C4a-OH or the C4a-OO(H) adduct. This analysis prompts us to conclude that the FAD in choline oxidase is most likely a C4a-OH (hydroxy) flavin adduct. However, as discussed above, we can not unambiguously rule out the C4a-OO(H) (peroxy or hydroperoxy) adduct. The resolution of the structure, quality of the refined atomic models, and the fits to the observed electron density for choline oxidase are comparable to those of the recently reported dioxygen complexes of cytochrome $P450_{cam}$ (*29*), naphthalene dioxygenase (*30*), superoxide reductase (*31*), homoprotocatechuate 2,3-dioxygenase (*32*), and amine oxidase (*33*).

The x-ray crystal structure shows that the active sites are completely sequestered within each subunit of the dimeric enzyme such that there is no direct access of bulk solvent to the FAD isoalloxazine ring. Nevertheless, a DMSO molecule, an additive in the crystallization solution, is observed in the solvent excluded cavity within each active site (**Figure 2.5**). In addition to the covalent bond between the dimethylbenzene ring and His99, several deduced hydrogen bonds stabilize the isoalloxazine ring configuration and the C4a-OH (or C4a-OO(H)) adduct. For example, the FAD pyrimidine ring forms a network of hydrogen bonds with protein backbone atoms from Asn100, Cys102, Ile103, and Asn512. In addition there are side chain interactions between the pyrimidine ring and Asn100 and Ser101. Consequently, nearly every atom of the isoalloxazine ring with the potential to participate in hydrogen bonds, does so with either a protein residue or the DMSO. Furthermore, the structure indicates that the atoms of either C4a adduct are stabilized by hydrogen bonds with the side chains of His351 and Asn510. Finally, the

DMSO molecule is located adjacent to the C4a adduct and also hydrogen bonds with the side chain of Ser101 and the FAD N5 moiety.

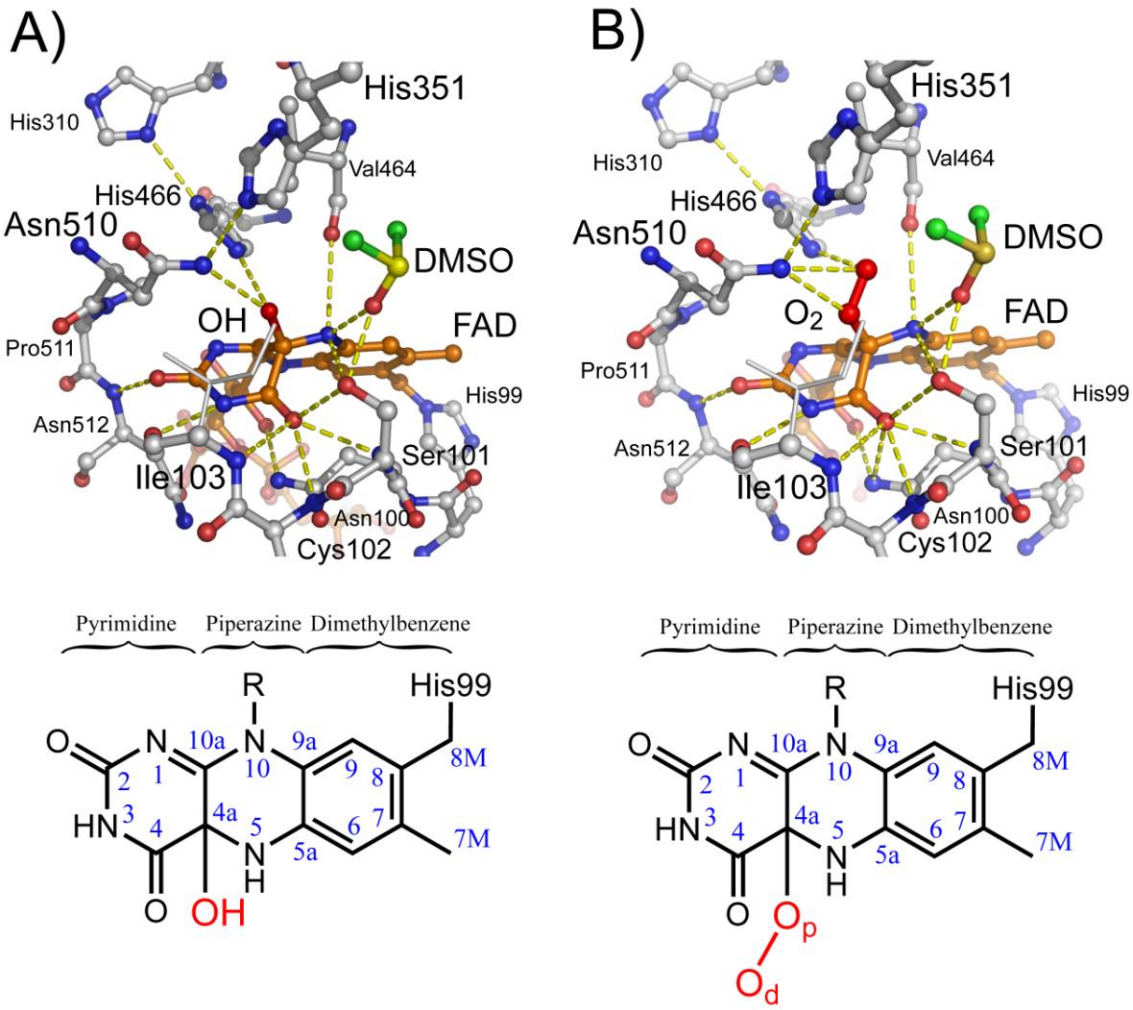

Figure 2.5. The Active Site Environment of Choline Oxidase Illustrating Potential Hydrogen Bonding Interactions (yellow dashes) that Stabilize the C4a-OH **(A)** or C4a-OO(H) **(B)** Adducts. Carbon atoms and bonds for the isoalloxazine ring and DMSO are shown in orange and green, respectively. For all the other atoms C, O, N and S atoms are colored grey, red, blue and yellow, respectively. The atom naming scheme for each adduct is shown at the bottom.

To gain a better understanding of the electronic structure of the unique isoalloxazine ring configuration observed in the x-ray structure of choline oxidase, we performed a number of DFT calculations. Each structure was optimized using Gaussian 03 program (*17*) at the B3LYP/6-

31G(d) level in the gas phase. The final energies were calculated using a large 6-31+G(d,p) basis set, which included dielectric effects (for ε = 4.3) from the surrounding protein using the self-consistent reaction field (IEFPCM) method at the B3LYP/6-31G(d) level. The largest calculations (ca. 180 atoms) included the FAD isoalloxazine ring and most of the first shell residues comprising the active site (**see Figure 2.5**; His99, Asn100, Ser101, Cys102, Ile103, His310, His351, His466, Asn510, Pro511, Asn512, and a DMSO molecule). Several flavin electronic states within the enzyme active site were computed including: *a)* one electron reduced flavin semiquinone (FAD^{sq}), *b)* a reduced flavin C4a hydroperoxy complex (FAD-C4a-OOH) *c)* a flavin C4a-hydroxy complex (FAD-C4a-OH), and *d)* flavin C4a-peroxy complex (FAD-C4a-OO^-). The metrics for observed x-ray structure and the DFT optimized structures for each flavin species are summarized in **Table 2.1**.

The DFT calculations unequivocally indicate that formation of the FAD C4a adduct, and the first shell hydrogen bond interactions with the flavin moiety are necessary to reproduce the observed x-ray structure (**Figures 2.4, 2.5 and 2.6**). Unfortunately, the accuracy of the DFT calculations and the uncertainty of the crystal structure do not support a clear discrimination between the C4a-OH or C4a-OO(H) structures. In contrast, gas-phase optimizations of protein-free flavin adducts yield less distorted FAD-C4a-OOH and FAD-C4a-OH structures (**Figure 2.6-D**). By comparison to these structures, we estimate that the energies required to stabilize the x-ray structure of the enzyme are approximately 29.1 kcal/mol for the FAD-C4a-OH adduct and 21.8 kcal/mol for the FAD-C4a-OOH adduct. Either of these total energetic contributions that stabilize the distorted flavin C4a adduct are consistent with the crystal structure and the numerous active site hydrogen bonds deduced between the distorted FAD and active site residues. In this context, our computational analysis suggests that the hydrogen bonding

interactions of the flavin with the side chains His99, Asn100, Ser101, Cys102, Ile103, Asn510, His466 and His351 (**Figure 2.5**) are essential for the stabilization of the distorted flavin C4a adduct. This is underscored by our additional computations (not shown) suggesting that removal of any of these residues *in silico* yields a more planar flavin C4a-adduct.

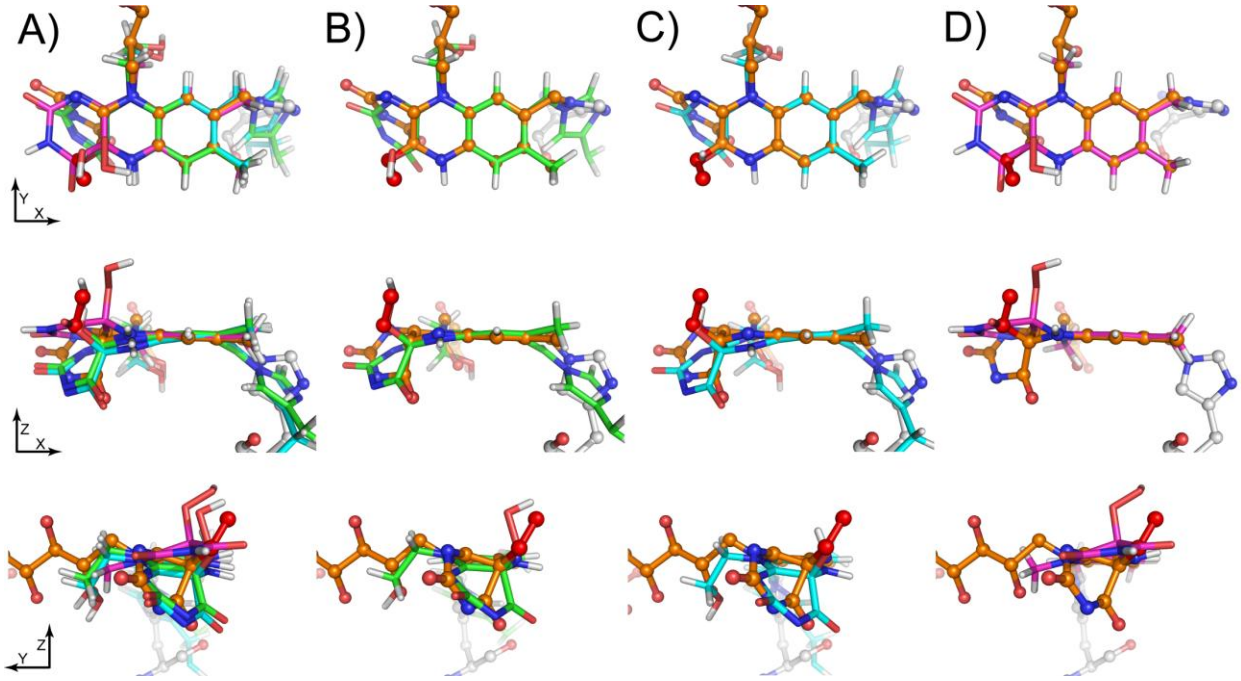

Figure 2.6. Overlay of Several DFT Optimized C4a Adducts and the Crystal Structure of Choline Oxidase. The three orthogonal views are shown in a similar orientation as that of **Figure 2.1**. **A)** The overlay of all four structures with the C atoms and bonds colored orange, green, cyan, or magenta for the crystal structure, the DFT optimized C4a-OOH adduct, the DFT optimized C4a-OH adduct, or the gas-phase optimized C4a-OOH adduct, respectively. **B)** The overlay of the crystal structure and the DFT optimized C4a-OOH adduct. **C)** The overlay of the crystal structure and the DFT optimized C4a-OH adduct. **D)** The overlay of the crystal structure and the gas-phase optimized C4a-OOH adduct.

Solvated electrons are generated in biological samples by synchrotron x-ray irradiation on the time scale of electronic transitions (see for example (*34*) and references therein). Rapid electron transfer over significant distances can be facilitated by aromatic side chains, protein backbone atoms, and protein secondary structure (*35*). Consequently, it is very likely that the FAD in choline oxidase is reduced in the x-ray beam. We propose that the high reduction

potential for the enzyme bound FAD provides a strong thermodynamic driving force to capture the solvated electrons (**Figure 2.7**, path *a*). This conclusion is consistent with the negative features observed in the difference spectra at 450 and 480 nm, as well as the 510 nm features ascribed to the FAD semiquinone as a minor, but persistent species. Our DFT calculations indicate that the unpaired electron in an anionic FAD semiquinone radical like that stabilized in choline oxidase is delocalized between the C4a (0.19e), C9 (0.18e), C7 (0.08e), C8 (-0.13e) and C8M (0.58e) atoms of the isoalloxazine ring system. Thus the spectroscopic results show that exposure of the crystal to the x-ray beam at low temperature is commensurate with a decrease in concentration of oxidized FAD in the sample.

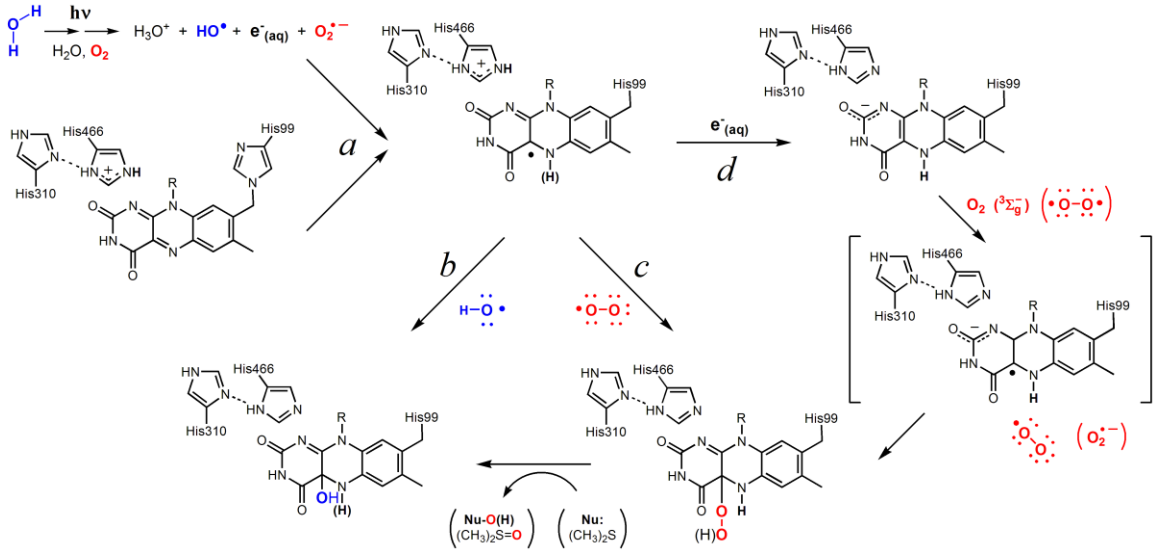

Figure 2.7. The proposed reaction scheme for the C4a adduct formation in single crystals of choline oxidase at 100 K. Radiolysis of solvent by x-rays yields solvated electrons and several types of reactive oxygen species (path *a*). An electron migrates to the high reduction potential FAD within the active site to yield the flavin semiquinone (path *a*). Either a hydroxyl radical (path *b*) or a superoxide radical (path *c*) then combines with the flavin semiquinone to form the C4a-OH or C4a-OO(H) species, respectively. It is also possible to form the C4a-OO(H) species via two electron reduction of the flavin, followed by reaction with O_2 (path *d*). Reaction of the flavin C4a-OOH species with an appropriate nucleophile (Nu:), such as dimethylsulfide, can also yield the C4a-OH adduct.

Hydroxyl and superoxide radicals, as well as other reaction products, are also generated in biological samples by x-ray exposure, but on a time scale of microseconds to milliseconds (*34*). However, the migration of hydroxyl and superoxide radicals, dioxygen, and protons within proteins at cryogenic temperatures are less well understood than electron transfer processes. Nevertheless, this raises the possibility that the adduct may form by one of several scenarios, which differ principally in the origin of the oxygen atom in the C4a-adduct (**Figure 2.7**). For example, our DFT calculations show that a hydroxyl radical does react with the C4a position of a FAD semiquinone yielding a flavin C4a-OH species, but only if the two radicals are near each other (ca. 2.0 - 2.2 Å), and only if the flavin N5 is unprotonated (**Figure 2.7**, path *b*). Similarly, our calculations indicate that a reaction between superoxide radical and the FAD semiquinone yielding a flavin C4a-OO(H) species is also possible (**Figure 2.7**, path *c*). Alternatively, the C4a-OO(H) adduct may derive from a reaction between a two-electron reduced flavin ($FADH^-$) and a ground-state O_2 (**Figure 2.7**, path *d*). Previous experimental and theoretical studies have demonstrated that a flavin C4a-OOH species can transfer an oxygen atom to dimethylsulfide to yield a flavin C4a-OH adduct and DMSO (*36-37*). Our crystallization conditions include 10% v/v DMSO, which likely has dimethylsulfide as a minor contaminant component. Consequently, a trace amount of dimethylsulfide could promote conversion of the C4a-OO(H) species into the C4a-OH adduct, but in this case the resulting oxygen atom in the observed adduct originates from O_2 rather than solvent. Each of the scenarios presented here requires that for an adduct to form, the appropriate reactants (with the exception of solvated electrons) must be either present or generated in the vicinity of the flavin isoalloxazine ring. Indeed, diffusion of bulky species over long-distances or through the protein and/or crystal matrix to the interior FAD C4a position is very unlikely at 100 K. In contrast, the proposed short-range migration of radical species, or

ground-state O_2 within the choline oxidase active site is analogous to the well documented results of carbon monoxide photodissociation of myoglobin-CO complexes (*38*-*39*).

Irrespective of the mechanism of formation of the flavin C4a-OH or C4a-OO(H) adduct, it seems likely that once formed, neither breaks down to release water or H_2O_2 because the cryogenic conditions do not establish the correct proton inventory on the surrounding residues and the flavin to facilitate product dissociation. In contrast, during catalytic turnover with choline (*11*), the enzyme coordinates the extraction of two protons and two electrons from the substrate with their subsequent delivery to O_2 to yield H_2O_2 (see **Figure 2.8**).

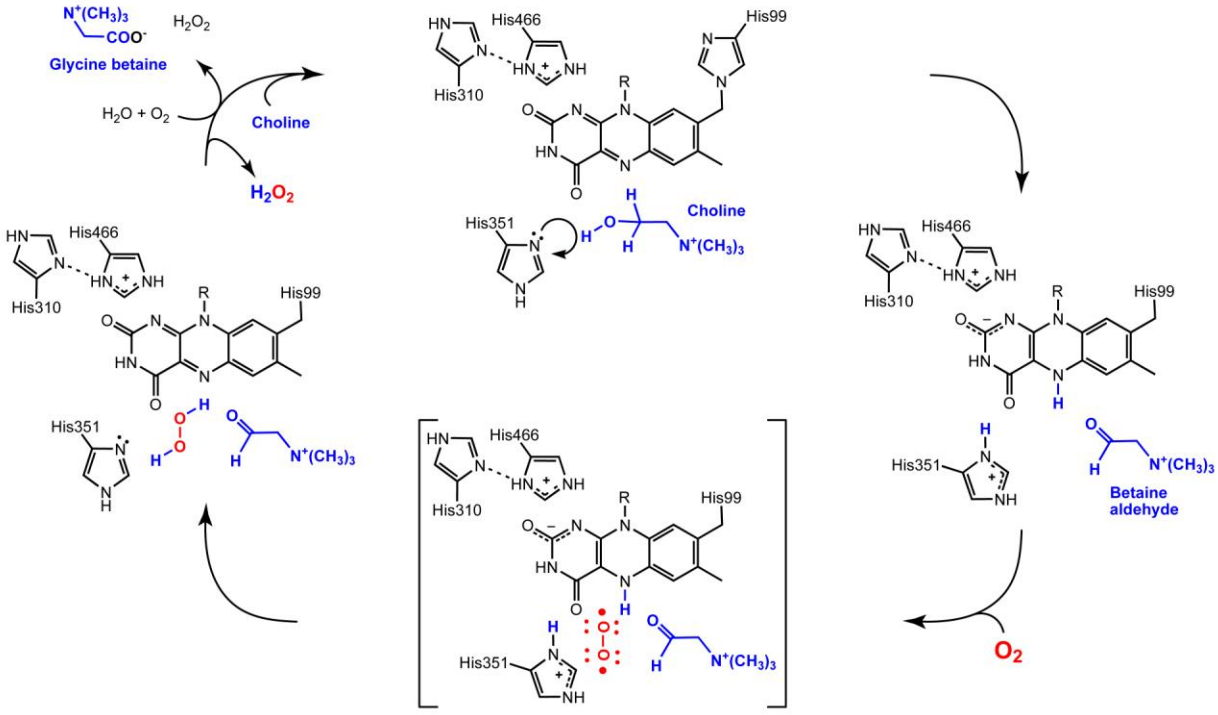

Figure 2.8. Proposed Reaction Mechanism for Choline Oxidase. In this scheme the active site base is indicated by His351 for the wild-type reaction. However, ongoing mutational studies suggest that the active site as a whole may serve as the general base for the reaction in some mutant isoforms of the enzyme.

Indeed, during the reductive half reaction, the net transfer and storage of two proton equivalents from the substrate to the active site base and the flavin N5 atom, is commensurate with the two-electron reduction of the flavin. In the subsequent oxidative half reaction, the two

electrons are transferred from the reduced flavin to O_2 along with the delivery of the two stored protons. Therefore, an incorrect proton inventory on the active site residues may stall the oxidative half-reaction. Thus the x-ray exposure at low temperature creates an improper proton inventory scenario that consequently yields the structure of choline oxidase containing the C4a-adduct.

Flavoenzyme mechanistic schemes often invoke FAD C4a-OO(H) or C4a-O(H) intermediates, but they have heretofore eluded structural characterization and have only rarely been detected by transient kinetic and spectroscopic techniques (*1-2, 9*). However, the structural environment in the active site of choline oxidase active site appears to be ideally suited to stabilize a C4a adduct involving an oxygen species. This study is therefore, the first direct observation by x-ray crystallography of a hydroxy-flavin or peroxo-flavin intermediate in any flavoenzyme, despite decades of effort by many researchers in the field, and numerous mechanistic proposals that invoke such a species. Our multidisciplinary experimental approach and correlation with complementary theoretical analysis thus provides direct evidence for an important oxygen intermediate in the reaction cycle of flavin-dependent enzymes.

2.5.Acknowledgment

This work was supported in part by a grant from the American Chemical Society Petroleum Research Fund (40310-G4), an American Heart Association Grant in Aid (0555286B), by the Offices of Biological and Environmental Research of the US Department of Energy, and the NIH (2 P41 RR012408) to A.M.O.; by an NSF CAREER Award (MCB-0545712), a grant from the American Chemical Society Petroleum Research Fund (37351-G4), and a Georgia State University Research Initiation Grant to G.G., a Molecular Basis Disease

Fellowship from Georgia State University to S.F., and a U.S. Department of Education GAANN Fellowship to G.T.L.

Data for this study were measured, in part, at beamlines X12B, X25, X26C, and X29 of the National Synchrotron Light Source, Brookhaven National Laboratory. Use of the National Synchrotron Light Source at Brookhaven National Laboratory was supported by the U.S. Department of Energy Office of Basic Energy Sciences, under Contract DE-AC02-98CH10886. Some of the x-ray diffraction data was also collected at the Southeast Regional Collaborative Access Team (SER-CAT) beamlines 22-ID and 22-BM at the Advanced Photon Source (APS), Argonne National Laboratory (SER-CAT supporting institutions may be found at: www.ser-cat.org/members.html). Use of the Advanced Photon Source was supported by the U.S. Department of Energy, Office of Science, Office of Basic Energy Sciences, under Contract No. W-31-109-Eng-38. We thank the SER-CAT staff at APS for assistance during data collection and Dr. Zhongmin Jin for assistance with the mail-in crystallography program. We are also grateful to the PXRR scientific staff at BNL for many helpful discussions, to Mr. Matt Cowan for assistance with the analysis and plotting of the time-dependent spectroscopic data of choline oxidase crystals, and to Ms. Mary Carlucci-Dayton for engineering and design assistance to mount the microspectrophotometer to beamline X26-C.

2.6.References

1. Massey, V. (2000) The chemical and biological versatility of riboflavin, *Biochem. Soc. Trans. 28*, 283-296.
2. Mattevi, A. (2006) To be or not to be an oxidase: challenging the oxygen reactivity of flavoenzymes, *Trends in biochemical sciences 31*, 276-283.

3. Entsch, B., Ballou, D. P., and Massey, V. (1976) Flavin-oxygen derivatives involved in hydroxylation by *p*-hydroxybenzoate hydroxylase, *J. Biol. Chem. 251*, 2550-2563.

4. Sucharitakul, J., Chaiyen, P., Entsch, B., and Ballou, D. P. (2006) Kinetic mechanisms of the oxygenase from a two-component enzyme, *p*-hydroxyphenylacetate 3-hydroxylase from *Acinetobacter baumannii*, *The Journal of biological chemistry 281*, 17044-17053.

5. Abu-Soud, H., Clark, A., Francisco, W., Baldwin, T., and Raushel, F. (1993) Kinetic destabilization of the hydroperoxy flavin intermediate by site- directed modification of the reactive thiol in bacterial luciferase, *J. Biol. Chem. 268*, 7699-7706.

6. Jones, K. C., and Ballou, D. P. (1986) Reactions of the 4a-hydroperoxide of liver microsomal flavin-containing monooxygenase with nucleophilic and electrophilic substrates, *J. Biol. Chem. 261*, 2553-2559.

7. Sucharitakul, J., Prongjit, M., Haltrich, D., and Chaiyen, P. (2008) Detection of a C4a-hydroperoxyflavin intermediate in the reaction of a flavoprotein oxidase, *Biochemistry 47*, 8485-8490.

8. Mallett, T. C., and Claiborne, A. (1998) Oxygen reactivity of an NADH oxidase C42S mutant: evidence for a C(4a)-peroxyflavin intermediate and a rate-limiting conformational change, *Biochemistry 37*, 8790-8802.

9. Massey, V. (1994) Activation of molecular oxygen by flavins and flavoproteins, *J. Biol. Chem. 269*, 22459-22462.

10. Prabhakar, R., Siegbahn, P. E. M., Minaev, B. F., and Agren, H. (2002) Activation of triplet dioxygen by glucose oxidase: Spin-orbit coupling in the superoxide ion, *Journal of Physical Chemistry B 106*, 3742-3750.

11. Fan, F., and Gadda, G. (2005) On the catalytic mechanism of choline oxidase, *J. Am. Chem. Soc. 127*, 2067-2074.

12. Ghanem, M., and Gadda, G. (2006) Effects of reversing the protein positive charge in the proximity of the flavin N(1) locus of choline oxidase, *Biochemistry 45*, 3437-3447.

13. Quaye, O., Lountos, G. T., Fan, F., Orville, A. M., and Gadda, G. (2008) Role of Glu312 in Binding and Positioning of the Substrate for the Hydride Transfer Reaction in Choline Oxidase, *Biochemistry 47*, 243-256.

14. Fan, F., Ghanem, M., and Gadda, G. (2004) Cloning, sequence analysis, and purification of choline oxidase from *Arthrobacter globiformis*: a bacterial enzyme involved in osmotic stress tolerance, *Arch. Biochem. Biophys. 421*, 149-158.

15. Gadda, G., Powell, N. L., and Menon, P. (2004) The trimethylammonium headgroup of choline is a major determinant for substrate binding and specificity in choline oxidase, *Arch. Biochem. Biophys. 430*, 264-273.

16. Wohlfahrt, G., Witt, S., Hendle, J., Schomburg, D., Kalisz, H. M., and Hecht, H. J. (1999) 1.8 and 1.9 Å resolution structures of the *Penicillium amagasakiense* and *Aspergillus niger* glucose oxidases as a basis for modelling substrate complexes, *Acta Crystallogr. D55*, 969-977.

17. Frisch, M. J., Trucks, G. W., Schlegel, H. B., Scuseria, G. E., Robb, M. A., Cheeseman, J. R., Montgomery, J., J. A., Vreven, T., Kudin, K. N., Burant, J. C., Millam, J. M., Iyengar, S. S., Tomasi, J., Barone, V., Mennucci, B., Cossi, M., Scalmani, G., Rega, N., Petersson, G. A., Nakatsuji, H., Hada, M., Ehara, M., Toyota, K., Fukuda, R., Hasegawa, J., Ishida, M., Nakajima, T., Honda, Y., Kitao, O., Nakai, H., Klene, M., Li, X., Knox, J. E., Hratchian, H. P., Cross, J. B., Bakken, V., Adamo, C., Jaramillo, J., Gomperts, R.,

Stratmann, R. E., Yazyev, O., Austin, A. J., Cammi, R., Pomelli, C., Ochterski, J. W., Ayala, P. Y., Morokuma, K., Voth, G. A., Salvador, P., Dannenberg, J. J., Zakrzewski, V. G., Dapprich, S., Daniels, A. D., Strain, M. C., Farkas, O., Malick, D. K., Rabuck, A. D., Raghavachari, K., Foresman, J. B., Ortiz, J. V., Cui, Q., Baboul, A. G., Clifford, S., Cioslowski, J., Stefanov, B. B., Liu, G., Liashenko, A., Piskorz, P., Komaromi, I., Martin, R. L., Fox, D. J., Keith, T., Al-Laham, M. A., Peng, C. Y., Nanayakkara, A., Challacombe, M., Gill, P. M. W., Johnson, B., Chen, W., Wong, M. W., Gonzalez, C., and Pople, J. A. (2004) Gaussian 03, Revision C1, Wallingford, CT.

18. Becke, A. D. (1988) Density-functional exchange-energy approximation with correct asymptotic behavior, *Physical Review. A 38*, 3098-3100.

19. Becke, A. D. (1993) Density-functional thermochemistry. III. The role of exact exchange, *J. Chem. Phys. 98*, 5648-5652.

20. Lee, C. T., Yang, W. T., and Parr, R. G. (1988) Development of the Colle-Salvetti correlation-energy formula into a functional of the electron-density, *Physical Review B 37*, 785-789.

21. Cances, E., Mennucci, B., and Tomasi, J. (1997) A new integral equation formalism for the polarizable continuum model: Theoretical background and applications to isotropic and anisotropic dielectrics, *Journal of Chemical Physics 107*, 3032-3041.

22. Prabhakar, R., Morokuma, K., and Musaev, D. G. (2005) A comparative study of various computational approaches in calculating the structure of pyridoxal 5 '-phosphate (PLP)-dependent beta-lyase protein. The importance of protein environment, *J. Comp. Chem. 26*, 443-446.

23. De la Mora-Rey, T., and Wilmot, C. M. (2007) Synergy within structural biology of single crystal optical spectroscopy and X-ray crystallography, *Current opinion in structural biology 17*, 580-586.

24. Siddiqui, M. S., and Stanley, R. J. (2005) A cryogenic optical waveguide spectrometer for the measurement of low-temperature absorption spectra of dilute biological samples, *Analytical biochemistry 337*, 121-129.

25. Ghanem, M., Fan, F., Francis, K., and Gadda, G. (2003) Spectroscopic and kinetic properties of recombinant choline oxidase from *Arthrobacter globiformis*, *Biochemistry 42*, 15179-15188.

26. Dixon, D. A., Lindner, D. L., Branchaud, B., and Lipscomb, W. N. (1979) Conformations and electronic structures of oxidized and reduced isoalloxazine, *Biochemistry 18*, 5770-5775.

27. Ridder, L., Harvey, J. N., Rietjens, I. M. C. M., Vervoort, J., and Mulholland, A. J. (2003) Ab initio QM/MM modeling of the hydroxylation step in p-hydroxybenzoate hydroxylase, *Journal of Physical Chemistry B 107*, 2118-2126.

28. Ridder, L., Mulholland, A. J., Rietjens, I. M. C. M., and Vervoort, J. (2000) A quantum mechanical/molecular mechanical study of the hydroxylation of phenol and halogenated derivatives by phenol hydroxylase, *J. Am. Chem. Soc. 122*, 8728-8738.

29. Schlichting, I., Berendzen, J., Chu, K., Stock, A. M., Maves, S. A., Benson, D. E., Sweet, R. M., Ringe, D., Petsko, G. A., and Sligar, S. G. (2000) The catalytic pathway of cytochrome p450cam at atomic resolution, *Science 287*, 1615-1622.

30. Karlsson, A., Parales, J. V., Parales, R. E., Gibson, D. T., Eklund, H., and Ramaswamy, S. (2003) Crystal structure of naphthalene dioxygenase: side-on binding of dioxygen to iron, *Science 299*, 1039-1042.

31. Katona, G., Carpentier, P., Niviere, V., Amara, P., Adam, V., Ohana, J., Tsanov, N., and Bourgeois, D. (2007) Raman-assisted crystallography reveals end-on peroxide intermediates in a nonheme iron enzyme, *Science 316*, 449-453.

32. Kovaleva, E. G., and Lipscomb, J. D. (2007) Crystal structures of Fe^{2+} dioxygenase superoxo, alkylperoxo, and bound product intermediates, *Science 316*, 453-457.

33. Wilmot, C. M., Hajdu, J., McPherson, M. J., Knowles, P. F., and Phillips, S. E. (1999) Visualization of dioxygen bound to copper during enzyme catalysis, *Science 286*, 1724-1728.

34. Xu, G., and Chance, M. R. (2007) Hydroxyl radical-mediated modification of proteins as probes for structural proteomics, *Chemical reviews 107*, 3514-3543.

35. Gray, H. B., and Winkler, J. R. (1996) Electron transfer in proteins, *Annual review of biochemistry 65*, 537-561.

36. Kemal, C., Chan, T. W., and Bruice, T. C. (1977) Reaction of $^3O_2$ with dihydroflavins. 1. N3,5-dimethyl-1,5- dihydrolumiflavin and 1,5-dihydroisoalloxazines, *J. Am. Chem. Soc. 99*, 7272-7286.

37. Bach, R. D., and Dmitrenko, O. (2003) Electronic Requirements for Oxygen Atom Transfer from Alkyl Hydroperoxides. Model Studies on Multisubstrate Flavin-Containing Monooxygenases, *J. Phys. Chem. B 107*, 12851-12861.

38. Srajer, V., Teng, T., Ursby, T., Pradervand, C., Ren, Z., Adachi, S., Schildkamp, W., Bourgeois, D., Wulff, M., and Moffat, K. (1996) Photolysis of the carbon monoxide

complex of myoglobin: nanosecond time-resolved crystallography, *Science 274*, 1726-1729.

39. Schotte, F., Lim, M., Jackson, T. A., Smirnov, A. V., Soman, J., Olson, J. S., Phillips, G. N., Jr., Wulff, M., and Anfinrud, P. A. (2003) Watching a protein as it functions with 150-ps time-resolved x-ray crystallography, *Science 300*, 1944-1947.

CHAPTER III

SUBSTITUTION OF AN ACTIVE SITE VALINE UNCOVERS A KINETICALLY SLOW EQUILIBRIUM BETWEEN COMPETENT AND INCOMPETENT FORMS OF CHOLINE OXIDASE

(This chapter has been published verbatim in Finnegan, S. and Gadda, G., (2008), *Biochemistry 47:* 13850-13861*)*

3.1. Abbreviations

Val464Ala, choline oxidase variant with valine 464 replaced with alanine; Val464Thr, choline oxidase variant with valine 464 replaced with threonine; His466Ala, choline oxidase variant with histidine 466 replaced with alanine.

3.2. Abstract

The enzymatic oxidation of choline to glycine betaine is of interest because organisms accumulate glycine betaine intracellularly in response to stress conditions. This is relevant for the genetic engineering of crops with economic interest that do not naturally possess efficient pathways for the synthesis of glycine betaine, and for the potential development of drugs that target the glycine betaine biosynthetic pathway in human pathogens. To date, the best characterized choline-oxidizing enzyme is the flavin-dependent choline oxidase from *Arthrobacter globiformis*, for which structural, mechanistic, and biochemical data are available. Here, we have replaced a hydrophobic residue (Val464) lining the active site cavity close to the N(5) atom of the flavin with threonine or alanine to investigate its role in the reaction of choline oxidation catalyzed by choline oxidase. The reductive half-reactions of the enzyme variants containing Thr464 or Ala464 were investigated using substrate and solvent kinetic isotope

effects, solvent viscosity effects, and proton inventories. Replacement of Val464 with threonine or alanine uncovered a kinetically slow equilibrium between a catalytically incompetent form of enzyme and an active species that can efficiently oxidize choline. In both variants, the active form of enzyme shows a decreased rate of hydroxyl proton abstraction from the alcohol substrate, with minimal changes in the subsequent rate of hydride ion transfer to the flavin. This study therefore establishes that a hydrophobic residue not directly participating in catalysis plays important roles in the reaction of choline oxidation catalyzed by choline oxidase.

3.3. Introduction

The four-electron, enzymatic oxidation of choline to glycine betaine (*N*,*N*,*N*-trimethylglycine) is of considerable interest because glycine betaine is a biocompatible solute that is accumulated in the cytoplasm of prokaryotic and eukaryotic organisms as a defensive mechanism to counteract deleterious stresses, such as extreme temperature changes or high osmotic pressures (*1*-*5*). This has significant relevance for the genetic engineering of specific stress tolerant crops of economic interest like tomato and rice that, by virtue of having inefficient biosynthetic pathways for the production of glycine betaine, are particularly vulnerable to stress conditions (*6*-*13*). Amassing large amounts of glycine betaine in the cytoplasm is particularly critical for bacteria, where adjustment of the cellular water content is attained by controlling the level of the intracellular solute pool due to lack of active water transport systems (*3*, *5*). Failure to do so in hyperosmotic environments immediately triggers fluxes of water across the cytoplasmic membrane resulting in dehydration and plasmolysis. Choline and its precursors phosphatidyl choline, phosphocholine and acetylcholine are very abundant at infection sites (*14*-*16*), where osmotic stress conditions are frequently observed (*17*). In a number of human

pathogens, including *Pseudomonas aeruginosa*, *Listeria monocytogenes*, *Vibrio cholerae*, *Enterococcus faecalis*, *Klebsiella pneumoniae*, or urophatogenic *Escherichia coli*, glycine betaine accumulates in the cytoplasm and allows growth in hyperosmotic minimal media of clinical isolates (*18-22*). Moreover, physiological responses to osmotic stress have recently gained attention with several studies showing that high osmolarity is one of the major environmental signals controlling the expression of genes associated with cellular invasion and virulence in a variety of human pathogenic microorganisms (*23-29*). In the model organism *E. coli*, the expression of a membrane-associated flavin-dependent, choline-oxidizing enzyme and a choline transporter for the production of glycine betaine are immediately up-regulated in media with high osmolality (*30-31*). Regulation of intracellular osmolality to hyperosmotic environments is also intimately connected to a number of physiological responses, such as increased heat and cold tolerance, regulation of the internal pH and ionic strength (*6, 9, 32-35*). Consequently, the study of the biophysical and mechanistic properties of flavin-dependent, choline-oxidizing enzymes has potential for the development of therapeutic agents that inhibit the biosynthesis of glycine betaine and render the bacteria either more susceptible to the immune system or to conventional treatments with antibiotics.

Two types of flavin-containing choline-oxidizing enzymes have been identified to date: a cytosolic, soluble choline oxidase (*36-38*) and a membrane-associated choline dehydrogenase (*21, 39-41*).

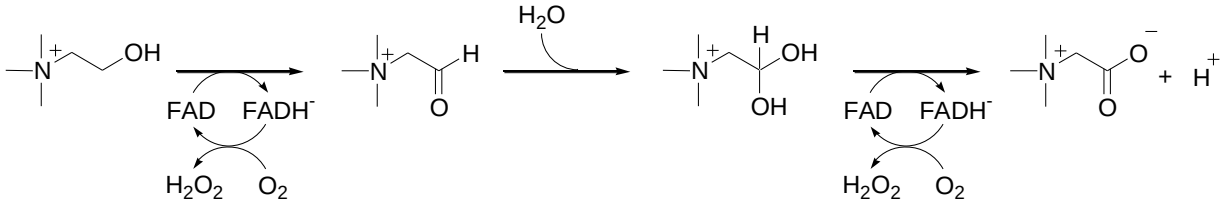

Scheme 3.1: The Flavin-mediated, Four-electron Oxidation of Choline to Glycine Betaine Catalyzed by Choline Oxidase.

These enzymes catalyze the identical oxidation of choline to glycine betaine via betaine aldehyde as intermediate, but prefer different primary electron acceptors (see **Scheme 3.1** for the reaction catalyzed by choline oxidase).

Indeed, the classification of the two enzymes is based on initial reports showing that choline oxidase readily reacts with O_2 (*42*) while choline dehydrogenase prefers electron acceptors other than O_2 (*43-44*). Difficulties of keeping choline dehydrogenase stable and active after extraction from its cellular source have hindered an in depth biochemical characterization of the enzyme (*43-44*). In contrast, due to the obtainment of large amounts of soluble, stable and active choline oxidase, significant progress in the understanding of the mechanistic, biochemical and structural properties of the flavin-dependent choline-oxidizing enzymes has been achieved (*42*, *45-56*).

The reductive half-reaction in which choline is oxidized to betaine aldehyde in choline oxidase has been characterized in detail in the wild-type enzyme (*42*, *45-56*). The reaction is initiated in the enzyme-substrate Michaelis complex by the removal of the hydroxyl proton of the alcohol substrate (**Scheme 3.2**), as suggested by kinetic isotope effects (*42*, *47*).

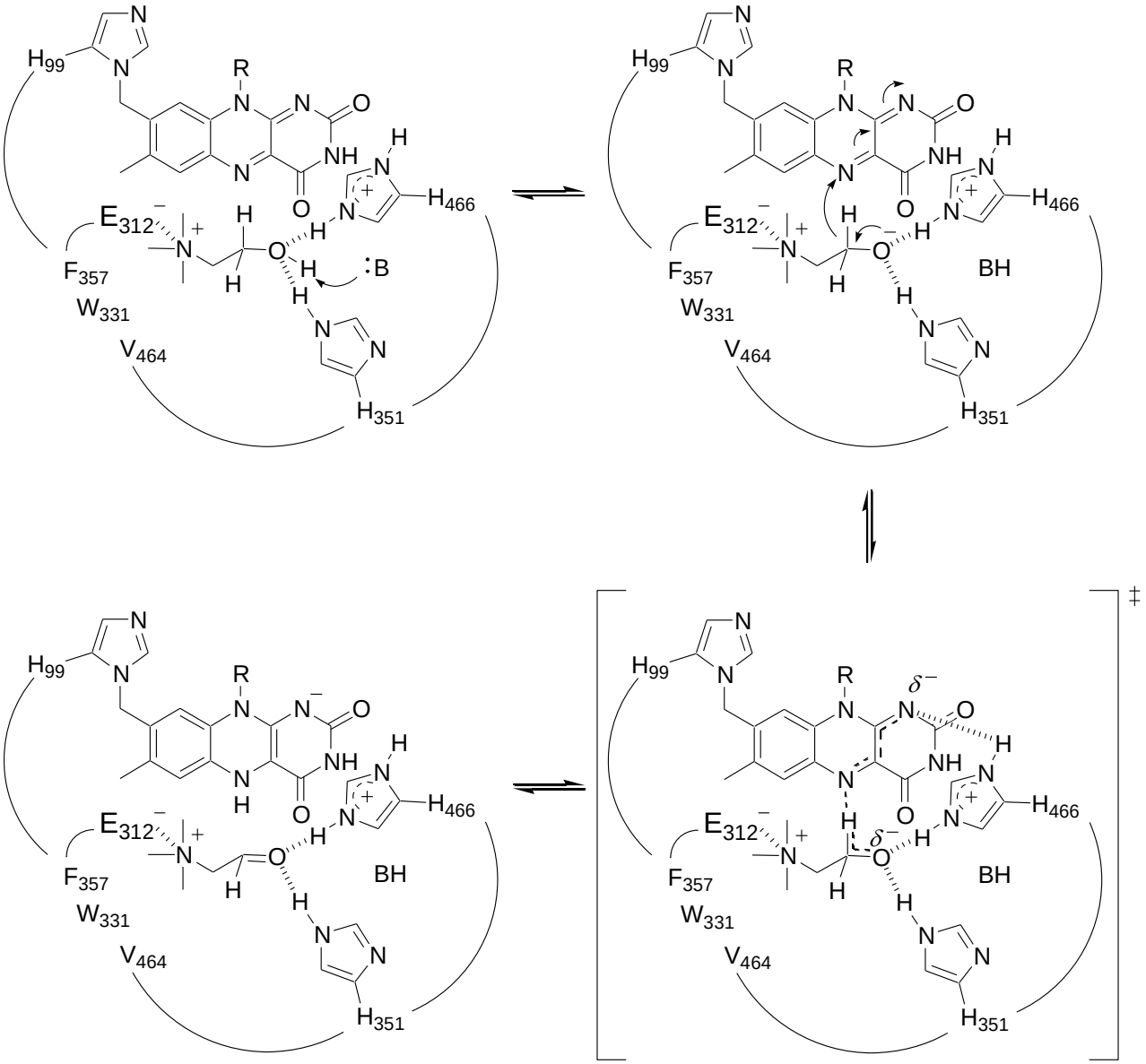

Scheme 3.2: Hydride Transfer Mechanism for the Oxidation of Choline to Betaine Aldehyde Catalyzed by Choline Oxidase.

Stabilization of the resulting choline alkoxide species is provided Stabilization of the resulting choline alkoxide species is provided by the side chains of His351, His466 and Glu312 (*49*, *54-55*). These electrostatic and hydrogen bonding interactions, along with the limited mobility of the flavin cofactor that is covalently linked through its C(8) methyl group to His99 (*54*), are major contributors to the preorganization of the enzyme-substrate complex for an

efficient oxidation reaction (*54*). Once activation and stabilization of the alkoxide species are achieved, a hydride ion tunnels from the alkoxide α-carbon to the N(5) atom of the flavin as a result of environmental vibrations of the reaction coordinate that permit a tunneling distance between the hydride donor and acceptor (*48*). The hydride donor and acceptor are brought in a configuration compatible with environmentally assisted tunneling through a conformational change of the enzyme-substrate complex that is mechanistically and kinetically distinct from the hydride transfer reaction, as suggested by temperature-dependent studies on the reaction catalyzed by the wild-type enzyme under reversible and irreversible catalytic regimes (*48*, *53*). Such a conformational change of the enzyme-substrate complex is also observed upon replacing the side chain of Glu312, which is important for the binding and positioning of the alcohol substrate in the active site of the enzyme, with an aspartate residue (*54*).

In the three-dimensional structure of choline oxidase recently solved to a resolution of 1.86 Å (*54*), the hydrophobic residue Val464 lines the active site cavity in proximity of the N(5) atom of the isoalloxazine ring of the flavin cofactor, with its side chain establishing a van der Waals contact with the C(2) atom of the conserved His466 (**Figure 3.1**). Such an arrangement suggests that, although Val464 does not directly participate in the reaction of choline oxidation catalyzed by the enzyme, it may play an important role in catalysis.

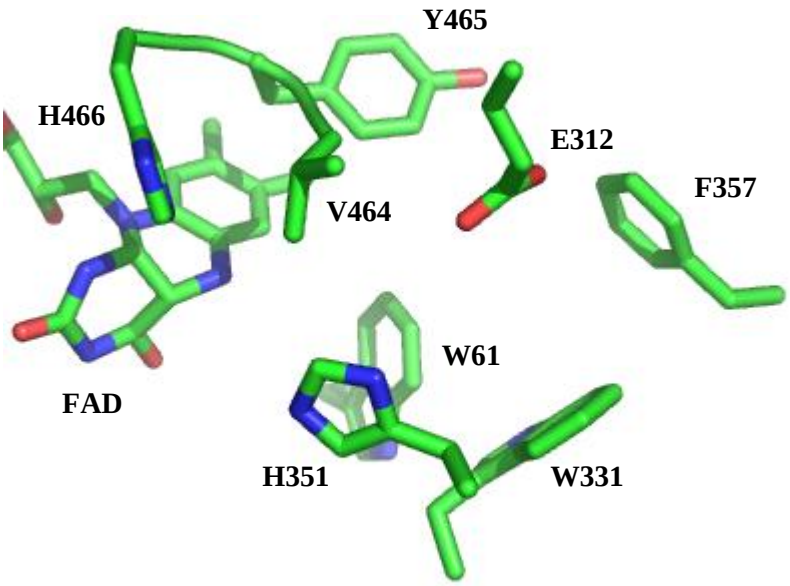

Figure 3.1. Close-up View of the Active Site of the Wild-type Form of Choline Oxidase Showing the Positioning of Val464 with Respect to the Isoalloxazine Ring of the Flavin and the Active Site Cavity (PDB entry 2jbv). Note the distortion of the flavin ring, which is due to the presence of a C(4a) flavin adduct (not shown here), whose identity is currently being investigated.

In this study, the effects of replacing Val464 with a hydrophilic residue (Thr) or an amino acid with a shorter side chain (Ala) on the hydrophobic packing needed for proper organization of the active site in the reductive half-reaction catalyzed by choline oxidase have been investigated. The enzyme variants Val464Thr and Val464Ala were prepared using site-directed mutagenesis and purified to homogeneity using ion exchange chromatography. The reductive half-reactions with choline as anaerobic substrate for the enzyme variants were investigated using an array of mechanistic probes including substrate and solvent kinetic isotope effects, solvent viscosity effects, and proton inventories. The results presented uncovered a kinetically slow equilibrium involving a catalytically incompetent form of enzyme and an active species that oxidizes choline. The active form of both enzyme variants showed lower rates of hydroxyl

proton abstraction from the alcohol substrate as compared to the wild-type enzyme, with minimal effects on the rates of the subsequent hydride transfer reaction.

3.4. Experimental procedures

Materials. Strain Rosetta(DE3)pLysS of *Escherichia coli* was from Novagen (Madison, WI). DNase was from Roche (Indianapolis, IN). The QuikChange site-directed mutagenesis kit was from Stratagene (La Jolla, CA). The QIAprep Spin Miniprep kit was from Qiagen (Valencia, CA). Oligonucleotides used for sequencing of the mutant genes were custom synthesized by Sigma Genosys (Woodland, TX). Choline chloride was from ICN Pharmaceutical Inc (Irvine, CA); 1,2-[$^{2}H_{4}$]-choline bromide (98%) and sodium deuterium oxide (99%) were from Isotec Inc. (Miamisburg, OH); glucose and glucose oxidase were from Sigma (St. Louis, MO); and Polyethylene glycol 6000 was from Fluka (St. Louis, MO). All other reagents were of the highest purity commercially available.

Site-Directed Mutagenesis. The variant forms of choline oxidase Val464Ala and Val464Thr were prepared using the pET/codAmg plasmid harboring the wild-type gene for choline oxidase as template for site-directed mutagenesis, as previously described (*45, 52, 54*). The presence of the desired mutations was confirmed by sequencing the entire mutagenized genes. *E. coli* strain Rosetta(DE3)pLysS competent cells were transformed with the mutant plasmids by electroporation. Host cells not containing the mutant plasmid showed no enzymatic activity with choline as a substrate.

Expression and Purification of the Val464Ala and Val464Thr Variants of Choline Oxidase. The mutant enzymes were expressed and purified to homogeneity using the same

procedure described previously for the purification of the wild-type enzyme (*45-46*). Typically, between 600 and 700 mg of purified enzymes were obtained from 5 L of cell culture. The enzymes maintained full enzymatic activity for at least six months upon storage in 20 mM Tris-Cl, pH 8.0, at -20 ^{o}C.

Spectroscopic Studies. The pH dependence of the UV-visible absorbance spectra for the Val464 variant enzymes were determined by titrating with sodium hydroxide as previously described for the His466Ala mutant enzyme (*49*).

Enzyme Assays. Pre-steady-state kinetic measurements were carried out using an SF-61DX2 HI-TECH KinetAsyst high performance stopped-flow spectrophotometer thermostated at 25 °C, in 50 mM sodium pyrophosphate, pH 10.0. The rate of flavin reduction was measured by monitoring the decrease in absorbance at 455 nm that results from the anaerobic mixing of choline oxidase with the organic substrate as previously described for the wild-type enzyme (*47*), except that 5 mM glucose and 0.5 μM glucose oxidase were present to scavenge possible trace amounts of oxygen. After anaerobic mixing in the stopped-flow spectrophotometer the final concentration of the enzymes was ~10 μM, whereas those of the organic substrates were between 0.05 to 10 mM, thereby maintaining pseudo-first order kinetic conditions. For the determination of the solvent kinetic isotope effects on the rate of flavin reduction, all of the reagents were prepared as described above except that D_2O was used to dissolve both the enzymes and substrates, and the pH of the buffered solution containing the enzyme was adjusted to 9.6 to account for the isotope effect on the ionization of sodium pyrophosphate (*57*). Solvent viscosity effects were measured in the presence of 8% (v/v) glucose or 0.0211g/mL PEG-6000 as

viscosigens, in both the tonometer containing the enzyme and the syringes containing the organic substrates. The resulting relative viscosities at 25 °C were 1.25 and 1.26 for glucose and PEG-6000 respectively, slightly above the value of 1.23 representing a 100% solution of D_2O (*58-59*). For proton inventories in solvents containing varying mole fractions of D_2O, the pD values were adjusted using DCl and NaOD based on the empirical relationship (equation 1) that exists between the pH-meter reading and the pD value at varying mole fractions of D_2O (n) (*57*). For each concentration of substrate, the rates of flavin reduction were recorded in triplicate, with measurements differing by ≤5%.

$$(\Delta pH)_n = 0.076n^2 + 0.3314n \qquad (1)$$

***Data Analysis*.** Kinetic data were fit with KaleidaGraph (Synergy Software, Reading, PA) and the Hi-Kinetic Studio Software Suite (Hi-Tech Scientific, Bradford on Avon, U.K.). Stopped-flow data traces were fit with equation 2, which describes a double-exponential process, in which k_{obs1} and k_{obs2} are the observed rate constants for the change in absorbance at 455 nm, *A* is the value of absorbance at time *t*, B and C are the amplitudes of the absorbance changes for the fast and slow observed phases, and D is an offset value that accounts for the non-zero absorbance value at infinite time. Pre-steady-state kinetic parameters were determined by using equations 3 and 4, which apply to the kinetic mechanism of **Scheme 3.3** (*see Results*). In equation 3, k_{obs1} is the observed first-order rate constant associated with the fast phase of flavin reduction at any given concentration of substrate, k_{red} is the limiting first-order rate constant for flavin reduction at saturating substrate concentrations, S is substrate concentration and K_d is the macroscopic dissociation constant for binding of the substrate to the active enzyme. In equation 4, k_{obs2} is the

observed first-order rate constant associated with the slow phase of flavin reduction at any given concentration of substrate, k_1 is the first-order rate constant for the conversion of the E^*_{ox} to E_{ox}, k_3 is the first-order rate constant for the conversion of $E^*_{ox}S$ to $E_{ox}S$, K_d* represents the macroscopic dissociation constant for binding of the substrate to the incompetent enzyme, and S is substrate concentration (see appendix for derivation of equation 4)(*60-61*). Data for the pH dependence of the UV-visible absorbance spectra were fit to equation 5, which describes a curve with two plateau regions at low (Y_L) and high (Y_H) pH connected by a decrease in absorbance with a slope of -1 followed by an increase with a slope of +1.

$$A = B\exp(-k_{obs1}t) + C\exp(-k_{obs2}t) + D \quad (2)$$

$$k_{obs1} = \frac{k_{red}S}{K_d + S} \quad (3)$$

$$k_{obs2} = \left(\frac{k_3 S + k_1 K_d^*}{S + K_d^*}\right) \quad (4)$$

$$Y = \frac{(Y_L \times 10^{-pK_{a1}} + Y_H \times 10^{-pH})}{(10^{-pK_{a1}} + 10^{-pH})} + \frac{(Y_H \times 10^{-pK_{a2}} + Y_L \times 10^{-pH})}{(10^{-pK_{a2}} + 10^{-pH})} \quad (5)$$

3.5. Results

Purification of the Val464Ala and Val464Thr Enzymes. Two variant forms of choline oxidase were engineered using site-directed mutagenesis to replace a valine at position 464 with alanine or threonine. The enzymes were independently expressed in *E. coli* strain Rosetta(DE3)pLysS, and purified by following the same protocol established for the wild-type enzyme (*45*). Upon purification, the variant enzymes displayed a covalently bound flavin cofactor in the form of a non-reactive, air-stable, anionic flavosemiquinone (data not shown).

The fully oxidized forms of the enzymes were obtained via slow oxidation of the flavosemiquinone by extensive dialysis at pH 6.0 and 4 ^{o}C, as previously reported for the wild-type and a number of active site mutant forms of choline oxidase (*42, 54-55*)**.** The specific activities of the resulting fully oxidized forms of the Val464Ala and Val464Thr enzymes were 0.3 μmol O_2 $min^{-1}mg^{-1}$ with 10 mM choline as substrate at pH 7.0. This value corresponds to a 25-fold decrease with respect to the specific activity of the wild-type enzyme (with a value of 8 μmol O_2 $min^{-1}mg^{-1}$) (*54*), suggesting that Val464 is an important residue for catalysis in choline oxidase.

Reductive Half-Reaction with Choline. The reductive half-reaction in which the Val464Ala or Val464Thr enzymes are reduced anaerobically with the substrate was investigated using a stopped-flow spectrophotometer by measuring the rates of decrease in absorbance at 455 nm as a function of the concentration of choline in 50 mM sodium pyrophosphate, pH 10.0 and 25 ^{o}C, under pseudo-first order conditions (i.e., 10 μM enzyme and ≥50 μM substrate). pH 10.0 has previously been shown to be in the pH independent region for the wild type as well as for various mutant forms of choline oxidase (*42, 49, 54-55*). As illustrated in the examples of **Figures 3.2A-B**, both investigated variant enzymes were reduced to the hydroquinone state in a biphasic pattern, with a fast phase accounting for approximately 60 to 70% of the total change in absorbance, contrary to the monophasic reduction observed for the wild type enzyme (*47*).

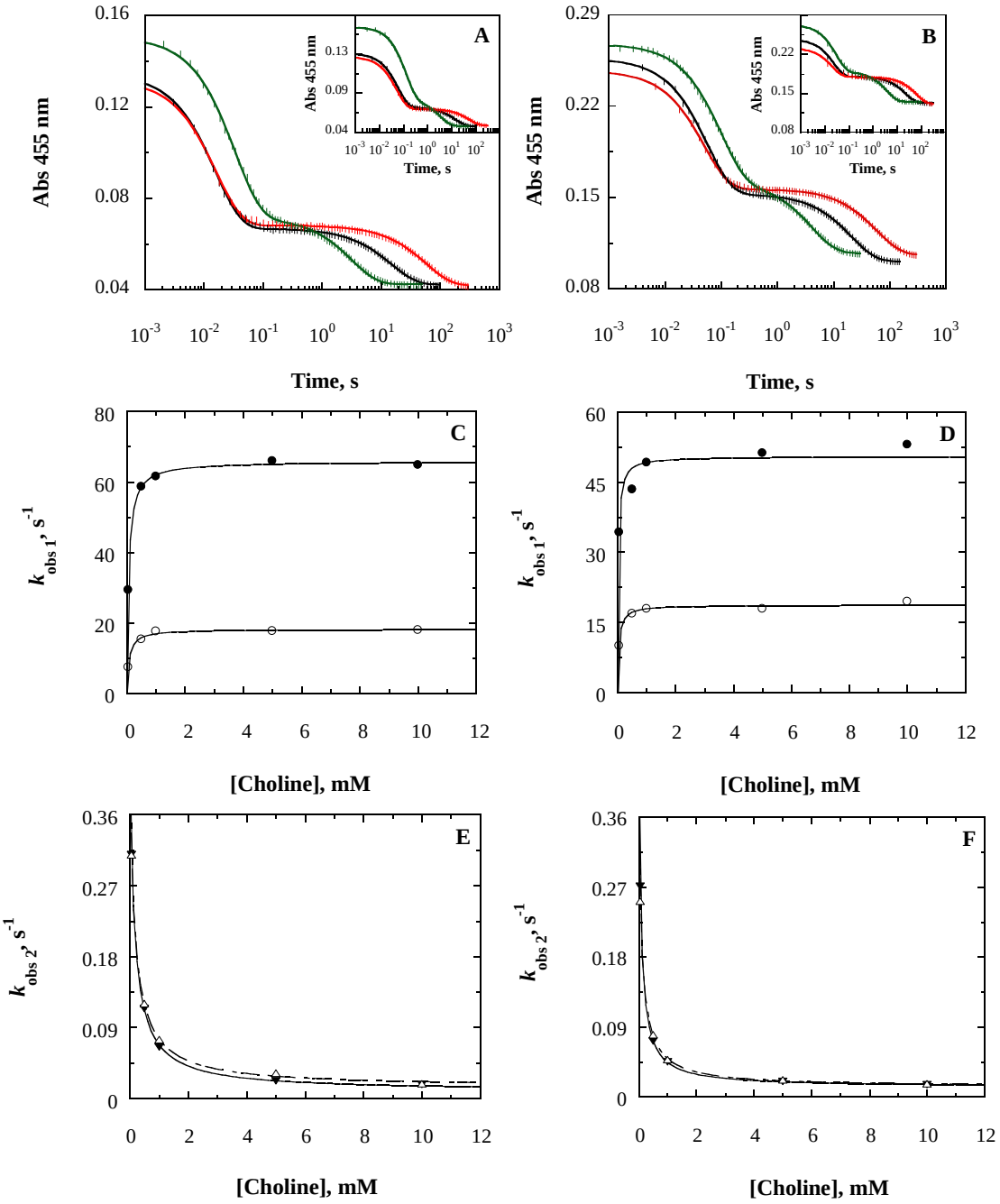
A
B
C
D
E
F
Abs 455 nm
Time, s
[Choline], mM
$k_{obs\,1}$, s^{-1}
$k_{obs\,2}$, s^{-1}

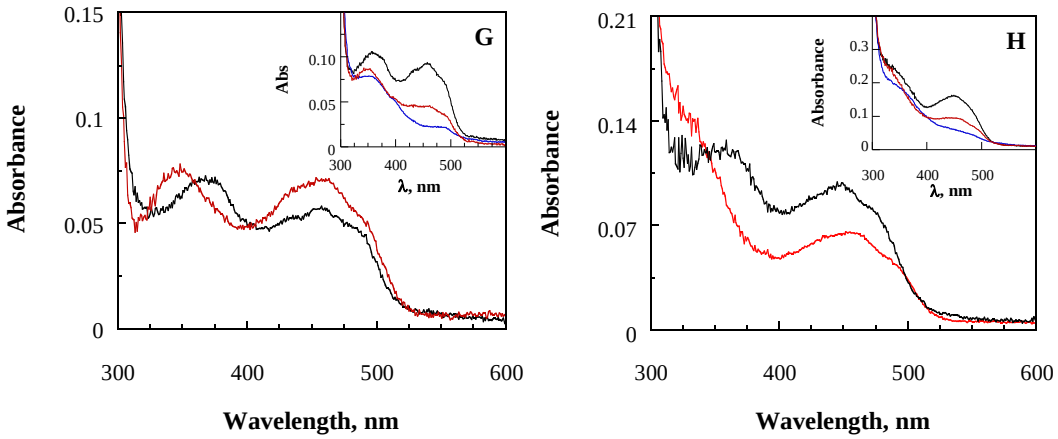

Figure 3.2. Anaerobic Reduction of the Val464Thr and Val464Ala Enzymes with Choline in 50 mM Sodium Pyrophosphate, pH 10.0 and 25 °C, Monitored at 455 nm in a Stopped-flow Spectrophotometer. Panel A shows the reduction traces for Val464Thr with 10 mM (red), 1 mM (black) and 0.05 mM (green) choline. *Inset*, reduction traces for the Val464Thr enzyme with 10 mM (red), 1 mM (black) and 0.05 mM (green) 1,2-[$^2H_4$]-choline. Panel B shows the reduction traces for Val464Ala with 10 mM (red), 1 mM (black) and 0.05 mM (green) choline. *Inset*, reduction traces for the Val464Ala enzyme with 10 mM (red), 1 mM (black) and 0.05 mM (green) 1,2-[$^2H_4$]-choline. All traces in panel A and B were fit with equation 2. Time indicated is after the end of flow, i.e., 2.2 ms. For clarity, one experimental point out of every ten is shown (vertical lines). Panel C shows the observed rates as a function of substrate concentration for the fast phase of flavin reduction with choline (●) and 1,2-[$^2H_4$]-choline (○) as substrates for Val464Thr. Panel D shows the observed rates as a function of substrate concentration for the fast phase of flavin reduction with choline (●) and 1,2-[$^2H_4$]-choline (○) as substrates for Val464Ala. The curves in panel C and D are fits of the data with equation 3. Panel E shows the observed rates for Val464Thr as a function of substrate concentration for the slow phase of flavin reduction with choline (▼) and 1,2-[$^2H_4$]-choline (△) as substrates. The curves for panel E and F are fits of the data with equation 4, eg. $y = \frac{0.009[s] + 0.072}{[s] + 0.183} \left(R^2 = 0.9997\right)$ with choline as a substrate for Val464Thr. Panel F shows the observed rates for Val464Ala as a function of substrate concentration for the slow phase of flavin reduction with choline (▼) and 1,2-[$^2H_4$]-choline (△) as substrates. Panel G shows the UV-visible absorbance spectra of the catalytically competent form (black) and of the incompetent form (red) of the Val464Thr enzyme in complex with choline at pH 10.0 and 25°C. *Inset*, UV-visible absorbance spectra determined with a PDA detector during the anaerobic reduction of the enzyme with 1 mM choline at 2.2 ms (black), 0.1 s (red), and 300 s (blue) after mixing the enzyme and the substrate in a stopped-flow spectrophotometer. Panel H shows the UV-visible absorbance spectra of the catalytically competent form (black) and of the incompetent form (red) of the Val464Ala enzyme in complex with choline at pH 10.0 and 25°C. *Inset*, UV-visible absorbance spectra determined with a PDA detector during the anaerobic reduction of the enzyme with 1 mM choline at 2.2 ms (black), 0.1 s (red), and 300 s (blue) after mixing the enzyme and the substrate in a stopped-flow spectrophotometer.

The relative amplitudes of the kinetic phases seen in the stopped-flow traces were independent of the concentration and the isotopic composition of the substrate, as similar results were obtained with 1,2-[$^2H_4$]-choline (**Figures 3.2A-B insets**), indicating that the kinetic behavior displayed by the Val464 variants is an intrinsic property of the enzymes that is unrelated to the substrate. The reductive half-reaction of the Val464Ala enzyme was also investigated at pH 6.0 where as illustrated in **Figure 3.3** it was reduced to the hydroquinone state in a biphasic pattern, with a fast phase accounting for approximately 45-50% of the total change in absorbance, as compared to the 60-70% at pH 10.0.

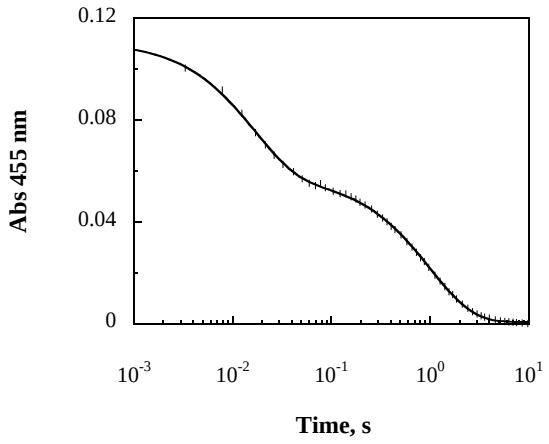

Figure 3.3. Example of an Anaerobic Reduction Trace of the Val464Ala Enzyme with 75 mM Choline in 50 mM Sodium Pyrophosphate, pH 6.0 and 25 °C, Monitored at 455 nm in a Stopped-flow. Data was fit with equation 2, $y = 0.053e^{-61.3[s]} + 0.057\ e^{-1.0[s]} + 0.001$ ($R^2 = 0.9998$).

With both the Val464Ala and Val464Thr enzymes, the observed rates for the fast phase of flavin reduction defined a rectangular hyperbola when plotted as a function of the concentration of choline (**Figures 3.2C-D**), as expected for an enzymatic kinetic process that reaches saturation. In contrast, a plot of the observed rates for the slow phase of flavin reduction as a function of the concentration of substrate yielded an inverse hyperbolic dependency, with

the observed rates decreasing to an asymptotic value with increasing concentration of choline (**Figures 3.2E-F**). These kinetic data are readily accounted for with the kinetic mechanism of **Scheme 3.3**, in which a catalytically competent and active form of the enzyme (E_{ox}) is in slow equilibrium with a catalytically incompetent[2] species of enzyme (E^{*}_{ox}). Upon forming a Michaelis complex with the substrate, the competent $E_{ox}S$ species will continue through catalysis yielding reduced flavin and betaine aldehyde. In contrast, the incompetent $E_{ox}{}^{*}S$ species will either slowly re-equilibrate through its free form devoid of bound substrate with the E_{ox} form or directly convert to the competent $E_{ox}S$ complex, which will subsequently proceed through catalysis.

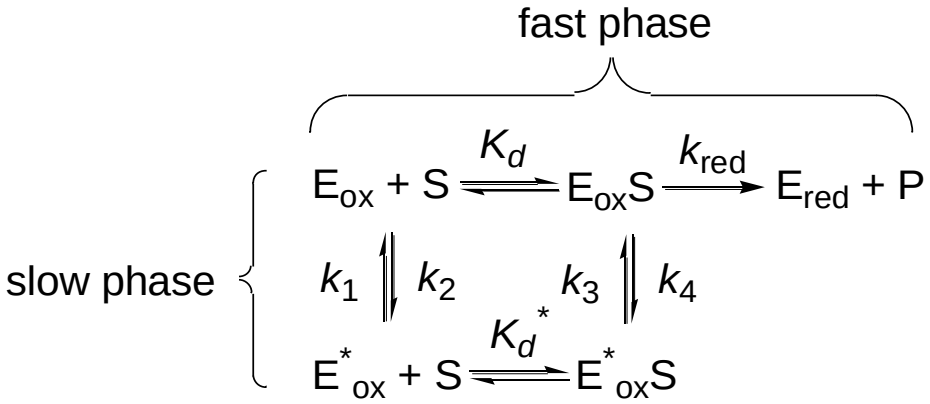

Scheme 3.3. Proposed Kinetic Mechanism for Choline Oxidation Catalyzed by the Val464Thr and Val464Ala Enzymes.

Since substrate binding to the enzyme is a rapid equilibrium process, the rate of re-equilibration of the two forms of choline oxidase is limited by the conformational change

[2] One of the two conformations of choline oxidase in which Val464 is replaced with alanine or threonine is defined in this study as incompetent, rather than inactive. The choice of the term stems from the kinetic mechanism of Scheme 3, which is the minimal mechanism that explains the experimental observations. Here, one species of enzyme is capable of oxidizing choline with a rate of hydride transfer that is not significantly different from that determined previously for the wild-type enzyme (i.e., $\geq$50.5 s^{-1} for Val464 variants; 93 s^{-1} for wild-type 47. Fan, F., and Gadda, G. (2005) On the catalytic mechanism of choline oxidase, *J. Am. Chem. Soc. 127*, 2067-2074.). This form of enzyme is defined here as either competent or active. The other form of enzyme present in solution in the Val464 variants is either not capable of oxidizing the substrate or it oxidizes choline at a rate that is significantly lower than the rates governing the re-equilibration of the two forms of enzyme. Since the two possibilities cannot be discerned, we opted to define this form of enzyme as incompetent rather than inactive.

involving both the free and enzyme-substrate complexes of the competent and incompetent forms of enzyme (defined by k_1, k_2, k_3 and k_4 in **Scheme 3.3**). According to this kinetic mechanism, the fast phase of flavin reduction seen in the stopped-flow traces represents the reduction of the $E_{ox}S$ species (k_{red} in **Scheme 3.3**), whereas the subsequent slow phase is due to the rate-limiting conformational change involving the two forms of enzyme. Fitting of the kinetic data[3] associated to the fast phase of flavin reduction to equation 3 allows for the determination of the first-order rate constant for flavin reduction (k_{red}), and the dissociation constant for the catalytically competent enzyme-substrate Michaelis complex (K_d) (*62*). Fitting of the kinetic data associated with the slow phase of flavin reduction to equation 4 allows for the determination of the first-order rate constants for the conversion of the incompetent form of enzyme to the competent form of enzyme (k_1 and k_3), and of the dissociation constant for the catalytically incompetent enzyme-substrate complex (K_d^*). Unfortunately, the requirement for pseudo-first order conditions in the anaerobic reduction of the enzyme with choline did not allow for concentrations of choline below 50 μM to be used, thereby preventing an accurate determination of the first-order rate constant for the conversion of the E^*_{ox} form of choline oxidase to the E_{ox} species (k_1). All the relevant kinetic parameters determined in the reductive half-reactions with choline as substrate for the choline oxidase variants containing alanine or threonine at position 464 as well as the previously determined values for the wild-type enzyme (*47*) are summarized in **Table 3.1.**

[3] The rationale for fitting the two phases seen in the reductive half-reaction catalyzed by the Val464Ala and Val464Thr enzymes with equations 3 and 4 is that with both enzymes the fast phase is more than 5000-fold faster at saturating concentration of substrate than the slow phase of flavin reduction (Table 3.1). This implies an accumulation of an enzyme form (i.e., E_{ox}^* and E_{ox}^*S) in the kinetic pathway at the end of the fast phase of reduction, allowing for the kinetic treatment of the two phases as being independent from one another *(62)*.

Table 3.1. Reductive Half-reaction of the Val464Thr, Val464Ala and Wild-type Enzymes with Choline as Substrate[a].

enzyme	k_{red}	K_d	k_1	k_2	k_3	k_4	K_d^*
	s^{-1}	μM	s^{-1}	s^{-1}	s^{-1}	s^{-1}	μM
Val464Ala	50.5 ± 2.4	≤50[b]	0.4 ± 0.01[b]	nd[c]	0.013 ± 0.001	nd[c]	≤80[b]
Val464Thr	65.8 ± 0.4	≤60[b]	0.4 ± 0.02[b]	nd[c]	0.009 ± 0.002	nd[c]	180 ± 10
Wild type (*47*)	93.1 ± 0.8	290 ± 10	no[d]	no[d]	no[d]	no[d]	no[d]

[a] Conditions: 50 mM sodium pyrophosphate, 25 °C, pH 10.0. [b] Better determinations could not be obtained due to the requirement of maintaining pseudo-first order conditions in which the [substrate] was ≥5-times the [enzyme]. [c] nd, not determined. [d] no, not observed.

The reductive half-reaction of the Val464Ala and Val464Thr enzymes with choline was also investigated with a PDA detector in order to gain insights on the UV-visible absorbance spectra of the enzyme-substrate complex species participating in the reaction. Relevant absorbance spectra of the species present right after anaerobic mixing of the enzyme and choline (2.2 ms), at the end of the fast phase of flavin reduction, and at the end of the slow phase of flavin reduction were collected. According to the mechanism of **Scheme 3.3**, only the fully reduced form of enzyme is present at the end of the reaction after both kinetic phases are completed. A mixture of fully reduced enzyme and incompetent enzyme-substrate complex populates the solution at the end of the fast phase of flavin reduction. Finally, a mixture of incompetent and competent enzyme-substrate complexes is present right after anaerobic mixing of the enzyme with choline. The relative amounts of competent and incompetent forms of the enzymes could be estimated from the amplitudes of the kinetic phases observed in the stopped-flow traces, allowing the extraction of the UV-visible absorbance spectra for the competent and incompetent forms of the Val464 variants of choline oxidase in complex with the substrate (eg. The UV-visible absorbance spectrum for $E^*_{ox}S$ can be extracted by taking the spectrum at the end of the fast phase (red traces in **Figures 3.2G-H** inset) and subtracting the quota of the fully reduced spectrum (blue traces in **Figures 3.2G-H** inset) corresponding to the relative amount of

$E_{ox.}$ Subtraction of the extracted spectrum for $E^{*}_{ox}S$ from the initial spectrum (black traces in **Figures 3.2G-H** inset) will in turn yield the $E_{ox}S$ spectrum). As shown in **Figures 3.2G-H**, a significant hypsochromic shift of at least 20 nm is observed in the high energy absorbance band of the incompetent enzyme-substrate complexes as compared to their competent counterparts for both the Val464Ala and Val464Thr enzymes.

Substrate Deuterium Kinetic Isotope Effects. Substrate kinetic isotope effects were employed with the dual goal of assessing the validity of the kinetic mechanism of **Scheme 3.3** and gaining insights into the status of the CH bond of choline in the transition state for the reactions catalyzed by the Val464Ala and Val464Thr enzymes. As shown **in Figures 3.2C-D** a significant decrease in the observed rates for the fast phase of flavin reduction was seen upon substituting choline with 1,2-[$^{2}H_4$]-choline in H_2O, suggesting that the reaction of flavin reduction, which is concomitant to the cleavage of the CH bond of choline, is at least partially rate-limiting for the reductive half-reaction in H_2O. However, when the flavin reduction was performed in D_2O the $^{D}(k_{red})_{D2O}$ values for both investigated enzymes were not significantly different from unity as compared to $^{D}(k_{red})_{H2O}$ values $\geq$2.9, indicating that the cleavage of the substrate CH bond in deuterium oxide is not rate-limiting for the overall reductive half-reaction. In contrast, there was no difference in the observed rates for the slow phase of flavin reduction when choline was substituted with 1,2-[$^{2}H_4$]-choline for both enzymes (**Figures 3.2E-F**) irrespective of the isotopic composition of the solvent. These kinetic data further support the kinetic mechanism of **Scheme 3.3**, for which a significant substrate kinetic isotope effect is predicted for the fast phase of flavin reduction, whereas no substrate isotope effect is expected for the conformational change occurring between the competent and incompetent enzyme

species. **Tables 3.2 and 3.3** summarize the kinetic parameters and the related kinetic isotope effects for the reductive half-reactions of the Val464Ala, Val464Thr and the wild-type (*47*) enzymes determined with choline and 1,2-[$^2H_4$]-choline as substrate.

Table 3.2. Effect of Deuterated Substrate and Solvent on the Reductive Half-reaction of the Val464Ala, Val464Thr and wild-type Enzymes [a].

Parameter	Substrate	solvent	Val464Ala	Val464Thr	Wild-type (*47*)
k_{red}, s^{-1}	Choline	H_2O	50.5 ± 2.4	65.8 ± 0.4	93.1 ± 0.8
k_{red}, s^{-1}	Choline	D_2O	12.0 ± 0.7	11.8 ± 0.3	94.0 ± 1.5
k_{red}, s^{-1}	1,2-[$^2H_4$]-choline	H_2O	17.2 ± 0.7	18.2 ± 0.3	10.3 ± 0.3
k_{red}, s^{-1}	1,2-[$^2H_4$]-choline	D_2O	13.2 ± 0.6	14.5 ± 0.1	10.9 ± 0.3
k_3, s^{-1}	Choline	H_2O	0.013 ± 0.001	0.009 ± 0.002	no[b]
k_3, s^{-1}	Choline	D_2O	0.004 ± 0.001	0.005 ± 0.001	no[b]
k_3, s^{-1}	1,2-[$^2H_4$]-choline	H_2O	0.013 ± 0.001	0.010 ± 0.002	no[b]
k_3, s^{-1}	1,2-[$^2H_4$]-choline	D_2O	0.006 ± 0.001	0.005 ± 0.001	no[b]

[a] Conditions: 50 mM sodium pyrophosphate, 25 °C, pH 10.0. Pre-steady-state kinetic parameters were determined by fitting the kinetic data acquired upon mixing anaerobically the enzyme with the substrate to equations 3 and 4. All fits of the data yielded $R^2 \geq 0.99$. [b] no, not observed.

Table 3.3. Substrate and Solvent Deuterium Kinetic Isotope Effects on the Reductive Half-reaction of the Val464Ala, Val464Thr and Wild type Enzymes.

Parameter	Val464Ala	Val464Thr	Wild-type (*47*)
$^{D}(k_{red})_{H2O}$	2.9 ± 0.1	3.6 ± 0.1	8.9 ± 0.2
$^{D}(k_{red})_{D2O}$	0.9 ± 0.1	0.8 ± 0.1	8.7 ± 0.2
$^{D2O}(k_{red})_{H}$	4.2 ± 0.4	5.6 ± 0.1	0.99 ± 0.1
$^{D2O}(k_{red})_{D}$	1.3 ± 0.1	1.3 ± 0.1	0.94 ± 0.1
$^{D}(k_3)_{H2O}$	1.0 ± 0.1	0.9 ± 0.1	no[b]
$^{D}(k_3)_{D2O}$	0.8 ± 0.2	1.1 ± 0.3	no[b]
$^{D2O}(k_3)_{H}$	3.0 ± 0.4	1.7 ± 0.4	no[b]
$^{D2O}(k_3)_{D}$	2.3 ± 0.4	2.1 ± 0.3	no[b]

[a] Conditions: 50 mM sodium pyrophosphate, 25 °C, pL 10. [b] no, not observed.

Solvent Deuterium Kinetic Isotope Effects. Solvent deuterium kinetic isotope effects were used to probe the status of the OH bond of choline in the transition state for the reaction of hydride transfer catalyzed by the variants of choline oxidase substituted at position 464. The anaerobic flavin reduction reaction was investigated in H_2O and D_2O, and the relevant $^{D2O}(k_{red})$ and $^{D2O}(k_3)$ values were determined at pL 10 and 25 ^{o}C with either choline or 1,2-[$^2H_4$]-choline. As expected, both the Val464Ala and Val464Thr enzymes showed $^{D2O}(k_{red})_{H}$ values of at least 4

with choline as substrate, consistent with these effects directly reporting on the status of the OH bond in the transition state for the reaction catalyzed by the enzymes. When 1,2-[$^2H_4$]-choline was used instead of choline a significant decrease in the $^{D_2O}(k_{red})_D$ to a value of 1.3 was observed with both enzymes (**Table 3.3**), suggesting that slowing down the cleavage of the CH bond of the substrate masks the solvent kinetic isotope effects. The $^{D_2O}(k_3)$ values were significantly larger than unity irrespective of whether choline or 1,2-[$^2H_4$]-choline was used as substrate for the Val464 enzyme variants (**Table 3.3**), consistent with the re-equilibration of the competent and incompetent forms of enzyme being sensitive to the isotopic composition of the solvent.

Solvent Viscosity Effects. The effect of solvent viscosity on the reductive half-reaction of the Val464Thr enzyme was investigated to establish whether the observed solvent kinetic isotope effects are associated with the cleavage of the OH bond of choline or simply due to the increased viscosity of D_2O with respect to H_2O. The reductive half-reaction of the Val464Thr enzyme with choline was consequently investigated at pH 10.0 and 25 ^oC in solutions containing 8% glucose or 0.0211 g/mL PEG-6000, which provide solvent viscosities equivalent to a 100% solution of D_2O. As illustrated in the data of **Table 3.4**, similar k_{red} values, which were smaller than those seen in a control experiment in the absence of viscosigens, were determined in the presence of glucose and PEG-6000, suggesting that no effect other than solvent viscosity was present on the kinetic step of flavin reduction. As summarized in **Table 3.4**, solvent viscosity effects on the k_{red} values of 1.4 were observed with choline as substrate, which were significantly larger than unity and lower than the $^{D_2O}(k_{red})_H$ values of ≥4, suggesting that solvent viscosity plays a significant, but not prominent, role in the kinetic step of cleavage of the substrate OH bond in the reaction catalyzed by the Val464Thr enzyme. In contrast, slightly inverse (i.e., ≤1) effects were seen on

the k_3 values in the presence of glucose or PEG-6000 (**Table 3.4**). These data suggest that the normal (i.e., ≥1) effects observed on the $^{D_2O}(k_3)$ values primarily originate from solvent sensitive steps that directly involve proton abstraction from OH group(s).

Table 3.4. Effect of Glucose and PEG-6000 on the Reductive Half-reaction of the Val464Thr Enzyme with Choline as Substrate [a],

parameter	viscosigen [b]	Val464Thr
$(k_{red})_{glucose}$, s^{-1}	glucose	48.1 ± 0.3
$(k_{red})_{PEG}$, s^{-1}	PEG	48.1 ± 1.6
$(k_3)_{glucose}$, s^{-1}	glucose	0.010 ± 0.003
$(k_3)_{PEG}$, s^{-1}	PEG	0.019 ± 0.003
$k_{red}/(k_{red})_{glucose}$		1.36 ± 0.02
$k_{red}/(k_{red})_{PEG}$		1.37 ± 0.05
$k_3/(k_3)_{glucose}$		0.9 ± 0.3
$k_3/(k_3)_{PEG}$		0.5 ± 0.3

[a] Conditions: 50 mM sodium pyrophosphate, 25 °C, pH 10.0. [b] Solvent contained 8% glucose, equivalent to a relative viscosity of 1.25 (*58*), or 0.0211 g/mL of PEG-6000, equivalent to a relative viscosity of 1.26 (*59*).

Proton Inventories. The reductive half-reaction of the Val464Ala and Val464Thr enzymes was investigated in solutions with varying mole fractions of deuterium oxide to gain insights into the number of exchangeable protons involved in the fast and slow phases of anaerobic flavin reduction. As shown in **Figures 3.4A-B**, linear relationships were seen upon plotting the k_{red} values as a function of the mole fraction of deuterated solvent, suggesting that a single proton is in flight in the transition state for the reaction of flavin reduction catalyzed by the choline oxidase variants containing alanine or threonine at position 464.

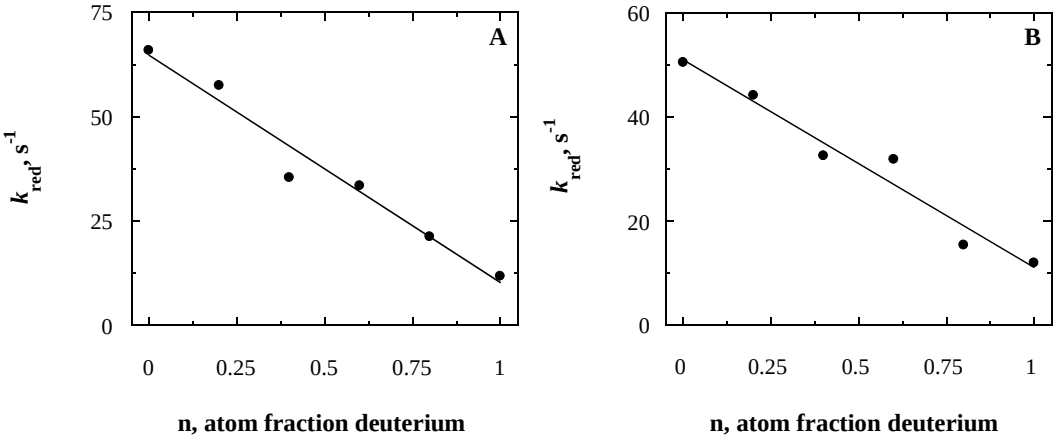

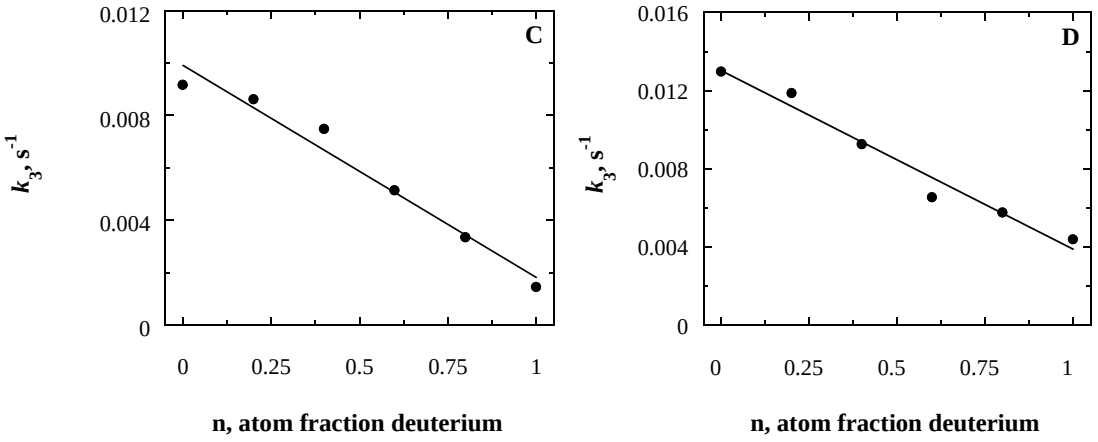

Figure 3.4. The Rates of Anaerobic Flavin Reduction Measured in a Stopped-flow Spectrophotometer as a Function of the Mole Fraction (n) of Deuterium Oxide Associated with the Fast (k_{red}) and Slow (k_3) Phases of Reduction for Val464Thr and Val464Ala. Panel A is the proton inventory of the k_{red} value for Val464Thr. Panel B is the proton inventory of the k_{red} value for Val464Ala.Panel C is the proton inventory of the k_3 value for Val464Thr. Panel D is the proton inventory of the k_3 value for Val464Ala. The lines represent linear fits of the data.

Similar linear relationships were observed with both enzymes in the proton inventories associated with the k_3 value (**Figures 3.4C-D**), also consistent with a single proton being in flight in the kinetic step involving the conformational change of the incompetent enzyme to the competent form of the enzyme.

Effect of pH on the UV-Visible Absorbance Spectra of Free Oxidized Variant Enzymes. The pH dependence of the UV-visible absorbance spectra of the variant enzymes was determined to establish whether the pK_a values for the 8α-N(3)-histidyl-FAD of choline oxidase were affected by replacing the valine at position 464 with alanine or threonine.

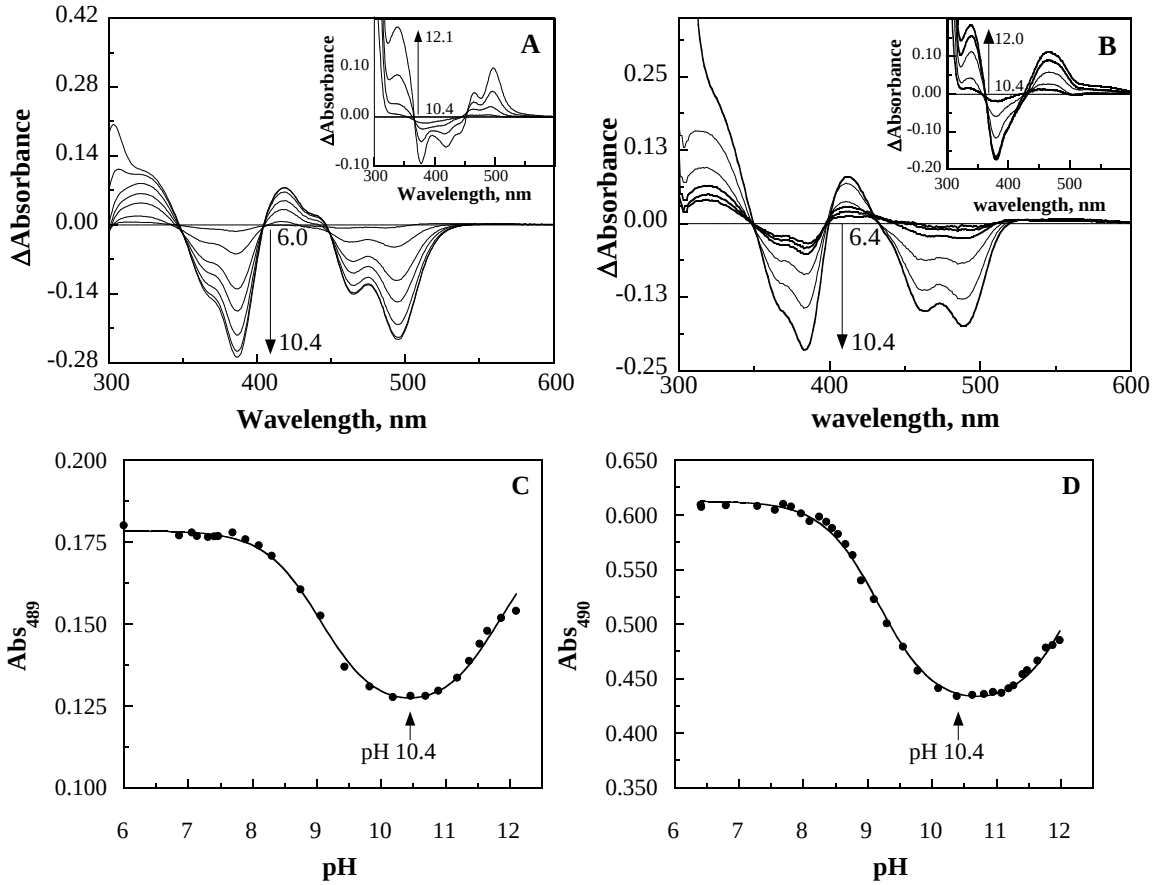

Figure 3.5. pH Dependence of the UV-visible Absorbance Spectra of Val464 Variant Enzymes. Absorbance spectra at varying pH were recorded in 20 mM sodium phosphate, 20 mM sodium pyrophosphate, at 15 °C, starting at pH 6.0 and increasing the pH with addition of NaOH. Panel A shows selected difference absorbance spectra for Val 464Thrspectrum pH x – spectrum pH 6.0) in the pH range from 6.0 to 10.4. *Inset*, shows selected difference absorbance spectra (spectrum pH x – spectrum pH 10.4) in the pH range from 10.4 to 12.1. Panel B shows selected difference absorbance spectrafor Val464Ala. Arrows in panel A and B indicate the direction of increasing pH. Panel C shows the dependence of the UV-visible absorbance values at 489 nm for the Val464Thr enzyme on pH. Panel D shows the dependence of the UV-visible absorbance values at 489 nm for the Val464Ala enzyme on pH The data in panel Cand D were fit with equation 5.

As the pH is increased from 6.0 to ~10.4 a progressive decrease in the absorbance at ~380 nm, ~460 nm, and ~490 nm was observed (**Figures 3.5A-B**). Further increase of the pH above 10.4 yielded an inversion of the spectral changes at the three wavelengths, as clearly shown in **Figures 3.5C-D** for the case of ~490 nm.

The observed spectral changes, along with the fitting of the data with equation 5, are consistent with the presence of two pK_a values associated with the ionization of the histidyl residue linking the flavin to the polypeptide chain (i.e., His99), and the N(3) atom of the isoalloxazine ring of the flavin (*63-66*). The relevant pK_a values for the Val464Ala and Val464Thr enzymes are summarized in **Table 3.5**, along with the previously determined value for the wild-type form of choline oxidase[4].

Table 3.5. Comparison of the pKa Values Associated with the Ionization of the Enzyme-bound Oxidized Form of 8α-N(3)-histidyl-FAD in the Val464Ala, Val464Thr, and His466Ala Enzymes with Wild-type Choline Oxidase [a].

Enzyme	His99	flavin N(3)
Val464Ala	9.1 ± 0.1	≥11.7
Val464Thr	9.1 ± 0.1	≥12
His466Ala [b]	9.3 ± 0.2	nd [c]
wild-type [b]	8.2 ± 0.1	nd [c]

[a] Conditions: 20 mM sodium pyrophosphate, 20 mM sodium phosphate and 15 °C. [b] Data are from (*49*). [c] nd, not determined.

3.6. Discussion

In this study, the hydrophobic residue Val464 lining the top of the active site cavity in proximity of the N(5) atom of the flavin cofactor of choline oxidase was replaced with either threonine or alanine to establish its role in the reductive half-reaction in which a hydride ion is transferred from choline to the flavin. The resulting Val464Thr and Val464Ala enzyme variants are properly folded, stable and functional, as suggested by a number of biophysical and biochemical properties that are in common with the wild-type form of choline oxidase. The

[4] In the course of an independent study on a number of choline oxidase variants in which serine 101 and histidine 99 is replaced with other amino acid residues (Hongling Yuan and Giovanni Gadda; manuscript in preparation), we realized that our initial assignments of the pK_a values associated with the UV-visible absorbance spectra for the wild-type and the variant enzyme His466Ala of choline oxidase published in 49. Ghanem, M., and Gadda, G. (2005) On the catalytic role of the conserved active site residue His466 of choline oxidase, *Biochemistry 44*, 893-904. are incorrect. In that study we erroneously assigned the pK_a values observed at 8.2 and 9.3 to the N(3) atom of the flavin, rather than the histidyl residue covalently linking the flavin to the polypeptide chain (His99).

Val464 variants contain FAD covalently linked to the protein moiety, stabilize an anionic flavosemiquinone at pH 8.0 in the presence of air, display UV-visible absorbance spectra with no sign of protein denaturation, have k_{red}, K_d, and $^{D}k_{red}$ values that are within three-fold from the values shown for the wild-type enzyme. Consequently, the role of the Val464 residue in the reaction of hydride transfer catalyzed by choline oxidase can be established by comparing and contrasting the kinetic and mechanistic properties of the enzyme variants containing threonine or alanine at position 464 with those of the wild-type enzyme containing valine.

The hydrophobic residue at position 464 is important for the proper assembly of the catalytic machinery required for the reaction of choline oxidation catalyzed by choline oxidase. Indeed, the most dramatic effect of replacing Val464 with either a threonine or alanine is the stabilization of a catalytically incompetent form of enzyme that reversibly, slowly equilibrates with a form of enzyme that can oxidize choline. The conformational change that inter-converts the two forms of enzyme occurs on both the free species of choline oxidase devoid of ligands in the active site as well as the enzyme substrate complexes (**Scheme 3.3**), is associated with changes in the ionization state of a group on the enzyme which is not readily available to the bulk solvent. This conclusion is supported by the results of proton inventory on the anaerobic reduction of the flavin with choline, showing a linear dependence on the mole fraction of deuterated solvent of the rate constant for the conversion of the incompetent form of choline oxidase to the active form (k_3). The spectroscopic properties of the Val464 variant enzymes in their catalytically incompetent and active forms further suggest that the ionizable group associated with the loss of catalytic activity must be linked to the flavin cofactor via a covalent bond, one or more hydrogen bonds, or electrostatic interactions. In this regard, upon replacing Val464 with threonine or alanine there is a one unit increase of the pK_a value for the ionization

of the side chain of His99, which is the site of covalent attachment of the polypeptide to the C(8) methyl group of the flavin (*54*). This raises the attractive possibility that His99 may be involved in the formation and stabilization of the incompetent form of choline oxidase (*see below*). In support of this hypothesis is the 20 nm hypsochromic shift of the high energy band of FAD seen in the UV-visible absorbance spectra of the catalytically incompetent form of the Val464Ala and Val464Thr enzymes with respect to the active form, which is expected for a change in the ionization of an 8α-N(3)-histidyl-flavin (*64-66*). Further evidence of a change in ionization being involved in the inactivation of the enzyme is observed in the difference in the relative amounts of active and inactive forms of the investigated Val464 variant enzymes at pH 6.0 and 10.0.

Replacement of Val464 with threonine or alanine significantly slows down the cleavage of the OH bond of choline in the oxidation reaction catalyzed by choline oxidase. In this regard, in the wild-type enzyme it was previously shown that the cleavage of the OH bond is considerably faster than the cleavage of the CH bond of choline, as indicated by $^{D_2O}(k_{red})_H$ values of 0.99 and $^{D}(k_{red})_{H_2O}$ values of 8.9 (*47*). In contrast, in the reactions catalyzed by the Val464Ala and Val464Thr enzymes the abstraction of the hydroxyl proton and the cleavage of the CH bond are both associated with deuterium kinetic isotope effects significantly larger than unity, with $^{D_2O}(k_{red})_H$ values $\geq$4.2 and $^{D}(k_{red})_{H_2O}$ values between 2.9 and 3.6. Interestingly, both cleavages of the OH and CH bonds contribute to different extents to the overall rate of flavin reduction depending upon the isotopic composition of the solvent or the substrate, consistent with the two steps having rate constants of similar magnitude. The similar increases of the pK_a values for the 8-α-N(3)-histidyl-flavin seen upon replacing Val464 with threonine or alanine and His466 with alanine (*49*) suggest that the slower rate of hydroxyl proton abstraction in the valine substituted enzymes may be due to a different positioning of His466, the flavin N(5) atom, or both with

respect to the initial alcohol substrate, as His466 was previously shown to facilitate hydroxyl proton abstraction by stabilizing the alkoxide species in catalysis (*49*).

Substitution of Val464 with alanine or threonine has a minimal effect on the rate of hydride ion transfer from the α-carbon of the alkoxide species formed in catalysis and the N(5) atom of the flavin cofactor. Evidence supporting this conclusion comes from the comparison of the k_{red} values with 1,2-[$^2H_4$]-choline, which primarily reflect the cleavage of the substrate CH bond, for the Val464Ala or Val464Thr enzymes with earlier data obtained with the wild-type enzyme, showing comparable rate constants (i.e., ~17 s^{-1} for the Val464 variants, as compared to 10.4 s^{-1} for the wild-type enzyme (*47*)).

The abstraction of the hydroxyl proton of choline in the enzyme variants substituted on Val464 is associated with an isomerization of the enzyme-substrate complex, as suggested by the effects of solvent viscosity on the rate constant for flavin reduction decreasing by ~40% in the presence of viscosigens. Since a reaction of hydroxyl proton abstraction per se is not expected to depend on the viscosity of the solvent, the effect of solvent viscosity must arise from a solvent sensitive internal equilibrium between a choline-enzyme complex and a choline alkoxide-protonated enzyme complex. An internal equilibrium of the enzyme-substrate complex was proposed earlier for the wild-type form of choline oxidase based on the enthalpy of activation ($\Delta H^{\ddagger}$) for the reaction of hydride ion transfer under reversible catalytic regime being significantly larger than the $\Delta H^{\ddagger}$ value for the reaction under irreversible catalytic regime (*53*). In that case, it was demonstrated that the environmental organization required in the enzyme-substrate complex to bring the hydride donor and acceptor in a preorganized configuration suitable for environmentally assisted tunneling is linked to the conformational change associated with the hydroxyl proton abstraction (*48, 53*). Furthermore, both solvent viscosity and substrate

kinetic isotope effects on the steady state kinetic parameters for the reaction of a choline oxidase variant in which Glu312 is substituted with aspartate were also interpreted with the presence of an internal equilibrium of the enzyme-substrate complex preceding the hydride transfer reaction (*54*).

The structural information on the wild-type form of choline oxidase provides a solid framework to substantiate the hypothesis of an involvement of His99 in the inactivation of the enzyme. Indeed, the N(1) atom of His99 is located in a small cavity that is completely secluded from the bulk solvent, in hydrogen bonding distance (2.9 Å) with a structural water molecule (W2110). This water molecule, in turn, is in hydrogen bonding distance with the peptidyl oxygen atoms of Leu64 (3.1 Å) and Tyr69 (3.0 Å) located on a long loop (residues 64-95) covering the active site of the enzyme (**Figure 3.6**) (*54*). A change in the ionization state of His99 is expected to affect the hydrogen bonding pattern around W2110, conceivably resulting in a change in the conformation of the enzyme. The link between Val464 and His99, which are spatially located 10.6 Å away from one another, is likely provided by His466. Since the C(2) atom of His466 is in van der Waals contact with a methyl group of Val464 (3.2 Å) and its N(3) atom is in hydrogen bonding distance from the N(1) atom of the flavin (3.2 Å) (**Figure 3.6**), it is expected that substitution of the hydrophobic side chain at position 464 (Val) with a hydrophilic side chain (Thr) or with an amino acid with a shorter side chain (Ala) would affect the interaction of His466 with the flavin isoalloxazine moiety. In support of this conclusion is the observation that both the replacements of Val464 with threonine or alanine and of His466 with alanine have the same effect of increasing the pK_a value for the ionization of the N(1) atom of His99 from 8.2 to ~9.1

(*49*).

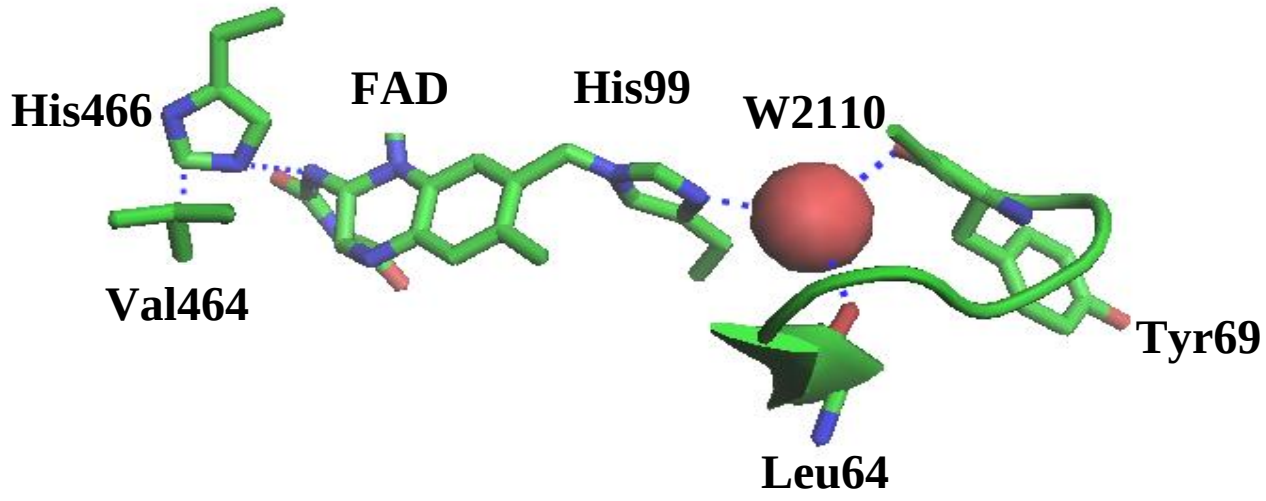

Figure 3.6. Close-up View of the Active Site of the Wild-type Form of Choline Oxidase Showing the Hydrogen Bonding Interactions Involving the N(1) atom of His99, a Structural Water Molecule (W2110) Secluded from the Bulk Solvent, the Peptidyl Oxygen Atoms of Leu64 and Tyr69, the van der Waals Interaction Between a Methyl Group of Val464 and the C(2) Atom of His466, and the Hydrogen Bonding Interaction of the N(3) Atom of His466 and the N(1) Atom of the Flavin Cofactor (PDB entry 2jbv).

In conclusion, the results presented in this study on the enzyme variants of choline oxidase in which Val464 has been replaced with alanine or threonine allow to conclude that the hydrophobic residue Val464 lining the active site cavity close to the N(5) atom of the flavin, although not directly participating in catalysis, is important for the positioning of the catalytic groups in the active site of the enzyme. Replacement of Val464 with alanine or threonine has uncovered a kinetically slow equilibrium between a catalytically incompetent form of enzyme and a form of enzyme that maintains the ability to efficiently oxidize the alcohol substrate. From a mechanistic standpoint, a major effect of the presence of a hydrophilic residue at position 464 is to considerably decrease the rate of hydroxyl proton abstraction from the substrate in the reaction of choline oxidation, with a minimal effect on the rate of hydride ion transfer from the

alkoxide species to the N(5) flavin atom. The replacement of Val464 with threonine or alanine is likely to affect the preorganization of the enzyme-substrate complex that undergoes the hydride transfer reaction. In this respect, it will be of interest to tailor future studies towards addressing to which extent a mutation of a residue not directly participating in catalysis, such as Val464, may affect the mode of hydride ion transfer.

3.7. Appendix

The proposed mechanism for the reaction catalyzed by the choline oxidase variants Val464Ala and Val464Thr in which both the free enzymes and enzyme-substrate complexes can interconvert (*61*). The derivation of the equation that describes the rate of the second phase of flavin reduction follows the logic described by Frederick and Palfey (*61*) and the method laid forth by Cha (*60*).

Scheme A1. Pre-steady State Mechanism of Val464 variant Enzymes.

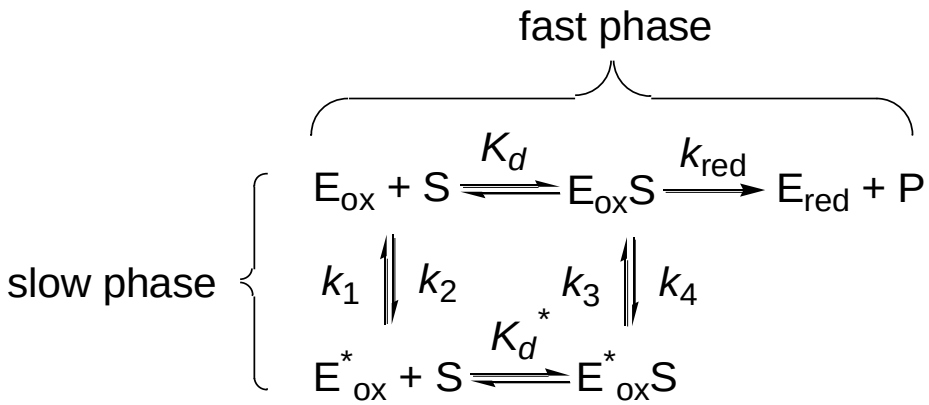

Assumptions:

Free E_{ox} and E_{ox}* binding with substrate is in rapid equilibrium. This allows for the simplification (*60*) of **Scheme A1** to yield a partial equilibrium mechanism shown in **Scheme A2**.

Scheme A2. Simplified Mechanism for Derivation of Pre-steady State Equations for Val464 Variant Enzymes.

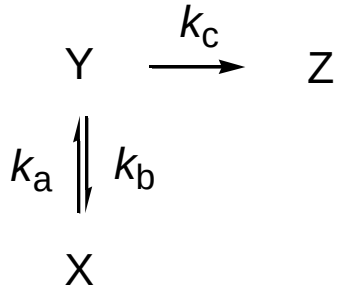

In **Scheme A2**, X represents the rapid equilibrium segment for E_{ox}* binding to substrate, Y represents the rapid equilibrium segment for E_{ox} binding to substrate and Z is the reduced enzyme and product. The rate constants k_a and k_b are apparent rate constants that represent the rate of interconversion of the two rapid equilibrium segments and k_c is the apparent rate of flavin reduction.

$$k_a = k_3 f_{E^*_{ox}S} + k_1 f_{E^*_{ox}} \quad \text{(A1)}$$

$$k_b = k_4 f_{E_{ox}S} + k_2 f_{E_{ox}} \quad \text{(A2)}$$

$$k_c = k_{red} f_{E_{ox}S} \quad \text{(A3)}$$

Where $f_{E^*_{ox}S}$, $f_{E^*_{ox}}$, $f_{E_{ox}S}$ and $f_{E_{ox}}$ are fractional concentration factors defining the fraction of the total enzyme within a rapid equilibrium segment of a given enzyme species.

$$f_{E^*_{ox}S} = \frac{[s]}{[s] + K^*_d} \quad \text{(A4)}$$

$$f_{E^*_{ox}} = \frac{K^*_d}{[s] + K^*_d} \quad \text{(A5)}$$

$$f_{E_{ox}S} = \frac{[s]}{[s] + K_d} \quad \text{(A6)}$$

$$f_{E_{ox}} = \frac{K_d}{[s] + K_d} \tag{A7}$$

The change of the relative amounts of enzyme in a given rapid equilibrium segment can be described by the following differential equations:

$$\frac{dX}{dt} = -k_a X + k_b Y \tag{A8}$$

$$\frac{dY}{dt} = k_a X - (k_b + k_c) Y \tag{A9}$$

$$\frac{dZ}{dt} = k_c Y \tag{A10}$$

The fast reaction is ~5000 times faster when substrate is saturating $([s] >> K_d$ and $K_d^*)$ than the slow reaction, meaning that the initial amount of Y, Y_0 has reacted completely before any significant fraction of incompetent enzyme is converted to the competent form. This means upon onset of the second phase the initial amount of X, X_0 will either still be in the form of X or have converted to Y or Z.

$$X_0 = X + Y + Z \Leftrightarrow X = X_0 - Y - Z \tag{A11}$$

Assuming steady state for Y.

$$\frac{dY}{dt} = 0 \tag{A12}$$

Insert the above expression for X (A11) into the differential equation for Y (A12).

$$0 = k_a (X_0 - Y - Z) - (k_b + k_c) Y \Leftrightarrow$$

$$Y = \frac{k_a (X_0 - Z)}{(k_a + k_b + k_c)} \tag{A13}$$

Insert expression for Y (A13) into the differential equation for Z (A10) and solve for Z.

$$\frac{dZ}{dt} = k_c Y = k_c \frac{k_a (X_0 - Z)}{(k_a + k_b + k_c)} = \frac{k_c k_a X_0}{(k_a + k_b + k_c)} - \frac{k_c k_a}{(k_a + k_b + k_c)} Z = kX_0 - kZ = k(X_0 - Z) \Leftrightarrow$$

$$\frac{dZ}{X_0 - Z} = kdt \Leftrightarrow$$

$$\int \frac{dZ}{X_0 - Z} = \int kdt \Leftrightarrow$$

$$-\ln(X_0 - Z) = kt + c \text{ , t} = 0 \Rightarrow \text{Z} = 0 \Leftrightarrow$$

$$Z = X_0 - X_0 e^{kt}, k = \frac{k_c k_a}{(k_a + k_b + k_c)} \qquad \text{(A14)}$$

Insert the expressions for k_a, k_b and k_c (A1-A3) into the term for the observed rate (A14):

$$k_{obs_2} = \frac{k_a k_c}{k_a + k_b + k_c} = \frac{\frac{k_3[s] + k_1 K_d^*}{K_d^* + [s]} \cdot \frac{k_{red}[s]}{K_d + [s]}}{\frac{k_3[s] + k_1 K_d^*}{K_d^* + [s]} + \frac{k_2 K_d + k_4[s]}{K_d + [s]} + \frac{k_{red}[s]}{K_d + [s]}} \Leftrightarrow$$

$$k_{obs_2} = \frac{\left(k_3[s] + k_1 K_d^*\right)\left(k_{red}[s]\right)}{\left(k_3[s] + k_1 K_d^*\right)\left(K_d + [s]\right) + \left(k_2 K_d + k_4[s]\right)\left(K_d^* + [s]\right) + k_{red}[s]\left(K_d^* + [s]\right)} \Leftrightarrow$$

$$k_{obs_2} = \frac{k_{red} k_3 [s]^2 + k_{red} k_1 K_d^* [s]}{\left(k_3 + k_4 + k_{red}\right)[s]^2 + \left(\left(k_3 + k_2\right) K_d + \left(k_1 + k_4 + k_{red}\right) K_d^*\right)[s] + \left(k_1 + k_2\right) K_d K_d^*}$$

$k_{red} >> k_1, k_2, k_3, k_4$ allowing to reduce the equation to :

$$k_{obs_2} = \frac{k_{red} k_3 [s]^2 + k_{red} k_1 K_d^* [s]}{k_{red}[s]^2 + \left(\left(k_3 + k_2\right) K_d + \left(k_{red}\right) K_d^*\right)[s] + \left(k_1 + k_2\right) K_d K_d^*}$$

At [S] >> K_d and K_d^*, allowing to reduce the equation to :

$$k_{obs_2} = \frac{k_{red}k_3[s]^2 + k_{red}k_1K_d^*[s]}{k_{red}[s]^2 + \left(\left(k_3 + k_2\right)K_d + \left(k_{red}\right)K_d^*\right)[s]}$$

set $K_d = \alpha K_d^*$

$$k_{obs_2} = \frac{k_{red}k_3[s]^2 + k_{red}k_1K_d^*[s]}{k_{red}[s]^2 + \left(\left(k_3 + k_2\right)\alpha K_d^* + \left(k_{red}\right)K_d^*\right)[s]} = \frac{k_{red}k_3[s]^2 + k_{red}k_1K_d^*[s]}{\left(k_{red}\right)[s]^2 + \left(\left(\alpha k_3 + \alpha k_2 + k_{red}\right)K_d^*\right)[s]} \Leftrightarrow$$

$$k_{obs_2} = \frac{k_{red}k_3[s]^2 + k_{red}k_1K_d^*[s]}{k_{red}[s]^2 + \left(k_{red}K_d^*\right)[s]} = \frac{k_3[s] + k_1K_d^*}{[s] + K_d^*} \quad \text{(A15)}$$

The limiting values for the observed rate of flavin reduction:

$$\lim_{[s]\to\infty} k_{obs_2} = k_3 \quad \text{(A16)}$$

$$\lim_{[s]\to 0} k_{obs_2} = k_1 \quad \text{(A17)}$$

3.8. Acknowledgements

The authors thank Andrea Pennati, Hongling Yuan, Kevin Francis, Osbourne Quaye, and Kunchala Rungsrisuriyachai for helpful discussions. We also thank Kevin Francis for the critical reading of the manuscript.

3.9. References

1. Csonka, L. N., and Epstein, W. (1996) Osmoregulation, In *Escherichia coli and Salmonella: Cellular and Molecular Biology* (Neidhardt, F. C., Curtiss III, R., Ingraham,

J. L., Lin, E. C. C., Low, K. B., Magasanik, B., Reznikoff, W. S., Riley, M., Schaechter, M., and Umbarger, H. E., Eds.), pp 1210-1223, ASM Press, Washington, D.C.

2. Burg, M. B., Kwon, E. D., and Kultz, D. (1997) Regulation of gene expression by hypertonicity, *Annu Rev Physiol 59*, 437-455.
3. Kempf, B., and Bremer, E. (1998) Uptake and synthesis of compatible solutes as microbial stress responses to high-osmolality environments, *Arch Microbiol 170*, 319-330.
4. McNeil, S. D., Nuccio, M. L., and Hanson, A. D. (1999) Betaines and related osmoprotectants. Targets for metabolic engineering of stress resistance, *Plant Physiol 120*, 945-950.
5. Bremer, E., and Kramer, R. (2000) Coping with Osmotic Challanges: Osmoregulation through Accumulation and Release of Compatible Solutes in Bacteria., In *Bacterial Stress Response* (Storz, G., and Hengge-Areonis, R., Eds.), pp 79-97, ASM Press, Washington, D.C.
6. Sakamoto, A., Alia, Murata, N., and Murata, A. (1998) Metabolic engineering of rice leading to biosynthesis of glycinebetaine and tolerance to salt and cold, *Plant Mol Biol 38*, 1011-1019.
7. Waditee, R., Bhuiyan, N. H., Hirata, E., Hibino, T., Tanaka, Y., Shikata, M., and Takabe, T. (2007) Metabolic engineering for betaine accumulation in microbes and plants, *J Biol Chem 282*, 34185-34193.
8. Quan, R., Shang, M., Zhang, H., Zhao, Y., and Zhang, J. (2004) Engineering of enhanced glycine betaine synthesis improves drought tolerance in maize, *Plant Biotechnol J 2*, 477-486.

9. Sakamoto, A., Valverde, R., Alia, Chen, T. H., and Murata, N. (2000) Transformation of Arabidopsis with the codA gene for choline oxidase enhances freezing tolerance of plants, *Plant J 22*, 449-453.

10. Alia, Kondo, Y., Sakamoto, A., Nonaka, H., Hayashi, H., Saradhi, P. P., Chen, T. H., and Murata, N. (1999) Enhanced tolerance to light stress of transgenic Arabidopsis plants that express the codA gene for a bacterial choline oxidase, *Plant Mol Biol 40*, 279-288.

11. Holmstrom, K. O., Somersalo, S., Mandal, A., Palva, T. E., and Welin, B. (2000) Improved tolerance to salinity and low temperature in transgenic tobacco producing glycine betaine, *J Exp Bot 51*, 177-185.

12. Deshnium, P., Gombos, Z., Nishiyama, Y., and Murata, N. (1997) The action in vivo of glycine betaine in enhancement of tolerance of Synechococcus sp. strain PCC 7942 to low temperature, *J Bacteriol 179*, 339-344.

13. Deshnium, P., Los, D. A., Hayashi, H., Mustardy, L., and Murata, N. (1995) Transformation of Synechococcus with a gene for choline oxidase enhances tolerance to salt stress, *Plant Mol Biol 29*, 897-907.

14. Lisa, T. A., Casale, C. H., and Domenech, C. E. (1994) Cholinesterase, acid phosphatase, and phospholipase C of *Pseudomonas aeruginosa* under hyperosmotic conditions in a high-phosphate medium, *Curr. Microbiol. 28*, 71-76.

15. Pesin, S. R., and Candia, O. A. (1982) Acetylcholine concentration and its role in ionic transport by the corneal epithelium, *Invest Ophthalmol Vis Sci 22*, 651-659.

16. Wright, J. R., and Clements, J. A. (1987) Metabolism and turnover of lung surfactant, *Am Rev Respir Dis 136*, 426-444.

17. Kilbourne, J. P. (1978) Bacterial content and ionic composiiton of sputum in cystic fibrosis, *Lancet i*, 334.

18. Peddie, B. A., Chambers, S. T., and Lever, M. (1996) Is the ability of urinary tract pathogens to accumulate glycine betaine a factor in the virulence of pathogenic strains?, *J Lab Clin Med 128*, 417-422.

19. Culham, D. E., Emmerson, K. S., Lasby, B., Mamelak, D., Steer, B. A., Gyles, C. L., Villarejo, M., and Wood, J. M. (1994) Genes encoding osmoregulatory proline/glycine betaine transporters and the proline catabolic system are present and expressed in diverse clinical Escherichia coli isolates, *Can J Microbiol 40*, 397-402.

20. Kunin, C. M., and Rudy, J. (1991) Effect of NaCl-induced osmotic stress on intracellular concentrations of glycine betaine and potassium in Escherichia coli, Enterococcus faecalis, and staphylococci, *J Lab Clin Med 118*, 217-224.

21. Landfald, B., and Strom, A. R. (1986) Choline-glycine betaine pathway confers a high level of osmotic tolerance in Escherichia coli, *J Bacteriol 165*, 849-855.

22. Lucht, J. M., and Bremer, E. (1994) Adaptation of Escherichia coli to high osmolarity environments: osmoregulation of the high-affinity glycine betaine transport system proU, *FEMS Microbiol Rev 14*, 3-20.

23. Badger, J. L., and Kim, K. S. (1998) Environmental growth conditions influence the ability of Escherichia coli K1 to invade brain microvascular endothelial cells and confer serum resistance, *Infect Immun 66*, 5692-5697.

24. Schwan, W. R., Lee, J. L., Lenard, F. A., Matthews, B. T., and Beck, M. T. (2002) Osmolarity and pH growth conditions regulate fim gene transcription and type 1 pilus expression in uropathogenic Escherichia coli, *Infect Immun 70*, 1391-1402.

25. Rachid, S., Ohlsen, K., Witte, W., Hacker, J., and Ziebuhr, W. (2000) Effect of subinhibitory antibiotic concentrations on polysaccharide intercellular adhesin expression in biofilm-forming Staphylococcus epidermidis, *Antimicrob Agents Chemother 44*, 3357-3363.

26. Bajaj, V., Lucas, R. L., Hwang, C., and Lee, C. A. (1996) Co-ordinate regulation of Salmonella typhimurium invasion genes by environmental and regulatory factors is mediated by control of hilA expression, *Mol Microbiol 22*, 703-714.

27. Basso, H., Rharbaoui, F., Staendner, L. H., Medina, E., Garcia-Del Portillo, F., and Guzman, C. A. (2002) Characterization of a novel intracellularly activated gene from Salmonella enterica serovar typhi, *Infect Immun 70*, 5404-5411.

28. Leclerc, G. J., Tartera, C., and Metcalf, E. S. (1998) Environmental regulation of Salmonella typhi invasion-defective mutants, *Infect Immun 66*, 682-691.

29. Tartera, C., and Metcalf, E. S. (1993) Osmolarity and growth phase overlap in regulation of Salmonella typhi adherence to and invasion of human intestinal cells, *Infect Immun 61*, 3084-3089.

30. Lamark, T., Rokenes, T. P., McDougall, J., and Strom, A. R. (1996) The complex bet promoters of Escherichia coli: regulation by oxygen (ArcA), choline (BetI), and osmotic stress, *J Bacteriol 178*, 1655-1662.

31. Rokenes, T. P., Lamark, T., and Strom, A. R. (1996) DNA-binding properties of the BetI repressor protein of Escherichia coli: the inducer choline stimulates BetI-DNA complex formation, *J. Bacteriol. 178*, 1663-1670.

32. Ko, R., Smith, L. T., and Smith, G. M. (1994) Glycine betaine confers enhanced osmotolerance and cryotolerance on Listeria monocytogenes, *J Bacteriol 176*, 426-431.

33. Smith, L. T. (1996) Role of osmolytes in adaptation of osmotically stressed and chill-stressed Listeria monocytogenes grown in liquid media and on processed meat surfaces, *Appl Environ Microbiol 62*, 3088-3093.

34. Bayles, D. O., and Wilkinson, B. J. (2000) Osmoprotectants and cryoprotectants for Listeria monocytogenes, *Lett Appl Microbiol 30*, 23-27.

35. Sakamoto, A., and Murata, N. (2001) The use of bacterial choline oxidase, a glycinebetaine-synthesizing enzyme, to create stress-resistant transgenic plants, *Plant Physiol 125*, 180-188.

36. Ikuta, S., Imamura, S., Misaki, H., and Horiuti, Y. (1977) Purification and characterization of choline oxidase from Arthrobacter globiformis, *J Biochem (Tokyo) 82*, 1741-1749.

37. Yamada, H., Mori, N., and Tani, Y. (1979) properties of choline oxidase of Cylyndrocarpon didymum M-1, *Agric. Biol. Chem. 43*, 2173-2177.

38. Ohta-Fukuyama, M., Miyake, Y., Emi, S., and Yamano, T. (1980) Identification and properties of the prosthetic group of choline oxidase from Alcaligenes sp, *J Biochem (Tokyo) 88*, 197-203.

39. Perrino, L. A., and Pierce, S. K. (2000) Choline dehydrogenase kinetics contribute to glycine betaine regulation differences in chesapeake bay and atlantic oysters, *J Exp Zool 286*, 250-261.

40. Perrino, L. A., and Pierce, S. K. (2000) Betaine aldehyde dehydrogenase kinetics partially account for oyster population differences in glycine betaine synthesis, *J Exp Zool 286*, 238-249.

41. Velasco-Garcia, R., Mujica-Jimenez, C., Mendoza-Hernandez, G., and Munoz-Clares, R. A. (1999) Rapid purification and properties of betaine aldehyde dehydrogenase from Pseudomonas aeruginosa, *J Bacteriol 181*, 1292-1300.

42. Ghanem, M., Fan, F., Francis, K., and Gadda, G. (2003) Spectroscopic and kinetic properties of recombinant choline oxidase from *Arthrobacter globiformis*, *Biochemistry 42*, 15179-15188.

43. Tsuge, H., Nakano, Y., Onishi, H., Futamura, Y., and Ohashi, K. (1980) A novel purification and some properties of rat liver mitochondrial choline dehydrogenase, *Biochimica et biophysica acta 614*, 274-284.

44. Russell, R., and Scopes, R. K. (1994) Use of hydrophobic chromatography for purification of the membrane- located choline dehydrogenase from a Pseudomonas strain, *Bioseparation 4*, 279-284.

45. Fan, F., Ghanem, M., and Gadda, G. (2004) Cloning, sequence analysis, and purification of choline oxidase from Arthrobacter globiformis: a bacterial enzyme involved in osmotic stress tolerance, *Archives of biochemistry and biophysics 421*, 149-158.

46. Gadda, G., Powell, N. L., and Menon, P. (2004) The trimethylammonium headgroup of choline is a major determinant for substrate binding and specificity in choline oxidase, *Archives of biochemistry and biophysics 430*, 264-273.

47. Fan, F., and Gadda, G. (2005) On the catalytic mechanism of choline oxidase, *J. Am. Chem. Soc. 127*, 2067-2074.

48. Fan, F., and Gadda, G. (2005) Oxygen- and temperature-dependent kinetic isotope effects in choline oxidase: correlating reversible hydride transfer with environmentally enhanced tunneling, *Journal of the American Chemical Society 127*, 17954-17961.

49. Ghanem, M., and Gadda, G. (2005) On the catalytic role of the conserved active site residue His466 of choline oxidase, *Biochemistry 44*, 893-904.

50. Fan, F., Germann, M. W., and Gadda, G. (2006) Mechanistic studies of choline oxidase with betaine aldehyde and its isosteric analogue 3,3-dimethylbutyraldehyde, *Biochemistry 45*, 1979-1986.

51. Gadda, G., Fan, F., and Hoang, J. V. (2006) On the contribution of the positively charged headgroup of choline to substrate binding and catalysis in the reaction catalyzed by choline oxidase, *Archives of biochemistry and biophysics 451*, 182-187.

52. Ghanem, M., and Gadda, G. (2006) Effects of reversing the protein positive charge in the proximity of the flavin N(1) locus of choline oxidase, *Biochemistry 45*, 3437-3447.

53. Fan, F., and Gadda, G. (2007) An internal equilibrium preorganizes the enzyme-substrate complex for hydride tunneling in choline oxidase, *Biochemistry 46*, 6402-6408.

54. Quaye, O., Lountos, G. T., Fan, F., Orville, A. M., and Gadda, G. (2008) Role of Glu312 in binding and positioning of the substrate for the hydride transfer reaction in choline oxidase, *Biochemistry 47*, 243-256.

55. Rungsrisuriyachai, K., and Gadda, G. (2008) On the role of histidine 351 in the reaction of alcohol oxidation catalyzed by choline oxidase, *Biochemistry 47*, 6762-6769.

56. Hoang, J. V., and Gadda, G. (2007) Trapping choline oxidase in a nonfunctional conformation by freezing at low pH, *Proteins 66*, 611-620.

57. Schowen, K. B., and Schowen, R. L. (1982) Solvent isotope effects on enzyme systems, In *Methods Enzymol.* (Purich, D. L., Ed.), pp 551-606, Academic Press, New York.

58. Lide, D. R. (2000) Handbook of Chemistry and Physics, pp 8-57, CRC Press, Boca Raton, Fl.

59. Stanislava Kirini, C. K. (1999) Viscosity of aqueous solutions of poly(ethylene glycol)s at 298.15 K, *Fluid Phase Equilibria 155*, 311-325.

60. Cha, S. (1968) A simple method for derivation of rate equations for enzyme-catalyzed reactions under the rapid equilibrium assumption or combined assumptions of equilibrium and steady state, *The Journal of biological chemistry 243*, 820-825.

61. Frederick, K. K., and Palfey, B. A. (2005) Kinetics of proton-linked flavin conformational changes in p-hydroxybenzoate hydroxylase, *Biochemistry 44*, 13304-13314.

62. Fersht, A. (1999) Structure and mechanism in protein science, pp 125-132, W. H. Freeman and Company.

63. Massey, V., and Ganther, H. (1965) On the interpretation of the absorption spectra of flavoproteins with special reference to D-amino acid oxidase, *Biochemistry 4*, 1161-1173.

64. De Francesco, R., and Edmondson, D. E. (1988) pKa values of the 8 alpha-imidazole substituents in selected flavoenzymes containing 8 alpha-histidylflavins, *Archives of biochemistry and biophysics 264*, 281-287.

65. De Francesco, R., Tollin, G., and Edmondson, D. E. (1987) Influence of 8 alpha-imidazole substitution of the FMN cofactor on the rate of electron transfer from the neutral semiquinones of two flavodoxins to cytochrome c, *Biochemistry 26*, 5036-5042.

66. Williamson, G., and Edmondson, D. E. (1985) Effect of pH on oxidation-reduction potentials of 8 alpha-N-imidazole-substituted flavins, *Biochemistry 24*, 7790-7797.

CHAPTER IV

ROLE OF VAL464 IN THE FLAVIN OXIDATION REACTION CATALYZED BY CHOLINE OXIDASE

(This chapter has been submitted for publication verbatim in Finnegan, S, Agniswamy, J, Weber, I and Gadda, G., (2010), *Biochemistry*)

4.1.Abbreviations

DMB, 3,3-dimethyl-butan-1-ol. FAD, flavin adenine dinuclotide, TMA, trimethylamine

4.1.Abstract

The oxidation of reduced flavin cofactors by oxygen is a very important reaction that is central to the chemical versatility of hundreds of flavoproteins classified as monooxygenases and oxidases. These enzymes are characterized by bimolecular rate constants $\geq 10^5$ $M^{-1}s^{-1}$, and produce water and hydrogen peroxide, respectively. A hydrophobic cavity close to the reactive flavin C(4a) atom has been previously identified in the 3D structure of monooxygenases, but not in flavoprotein oxidases. In the present study, we have investigated by X-ray crystallography, mutagenesis, steady state and rapid reaction approaches the role of Val464, which is <6 Å from the flavin C(4a) atom in choline oxidase. The 3D structure of the Val464Ala enzyme was essentially identical to that of the wild-type enzyme as shown by X-ray crystallography. Time-resolved anaerobic substrate reduction of the enzymes showed that replacement of Val464 with alanine or threonine did not affect the reductive half-reaction. Steady state and rapid kinetics as well as enzyme monitored turnovers indicated that the oxidative half-reaction in the Ala464 and Thr464 enzymes was decreased by ~50-fold with respect to the wild-type enzyme. We propose that the side chain of Val464 in choline oxidase provides a non-polar site that is required to guide

oxygen in proximity of the C(4a) atom of the flavin, where it will subsequently react via electrostatic catalysis. Visual analysis of available structures suggests that analogous non-polar sites are likely present in most flavoprotein oxidases. Mechanistic considerations provide rationalization for the differences between sites in monooxygenases and oxidases.

4.2.Introduction

The oxidation of reduced flavin cofactors by molecular oxygen, or the lack thereof, is a very important chemical reaction that is at the core of the chemical versatility displayed by flavoenzymes. Flavoenzymes comprise hundreds of enzymes catalyzing the most diverse biochemical reactions. Depending upon the ability to react with oxygen and the product of oxygen reduction, three general classes of flavoenzymes are distinguished (*1-2*). Flavoprotein dehydrogenases show very little or no reactivity with oxygen, thereby requiring other electron acceptors for catalytic turnover. On the other hand, monooxygenases and oxidases show high reactivity with oxygen, which is usually characterized by second-order rate constants $\geq 10^5$ $M^{-1}s^{-1}$, with water and hydrogen peroxide being produced in the reactions, respectively (*1*). Reduced flavins existing free in solution, i.e., not associated with a protein, also reduce oxygen, but with much slower bimolecular rate constants of 2.5×10^2 $M^{-1}s^{-1}$ (*3*). It is therefore the protein microenvironment surrounding the flavin in flavoprotein dehydrogenases, monooxygenases and oxidases that modulates the extent to which the reduced flavin reacts with oxygen in these different classes of enzymes (*2, 4-5*).

Several studies on a number of enzymes have contributed to the current knowledge of the features in the active sites of flavoenzymes that contribute to the up- and down-modulation of oxygen reactivity. A classical example of a dehydrogenase, where oxygen reactivity is suppressed due to ligand binding, is mammalian medium-chain acyl-CoA dehydrogenase, where

the presence of the ligand has been shown to increase the redox potential of the flavin and to desolvate the active site (*6-7*). Lack of oxygen reactivity can also be due to steric effects arising from the presence of amino acid side chains that physically prevent oxygen from approaching the reactive C(4a) atom of the reduced flavin (see **Scheme 4.1** for flavin numbering), as in the case of the alanine residues in the active sites of a mutant form of L-lactate monooxygenase (*8*) and L-galactono-γ-lactone dehydrogenase (*9*).

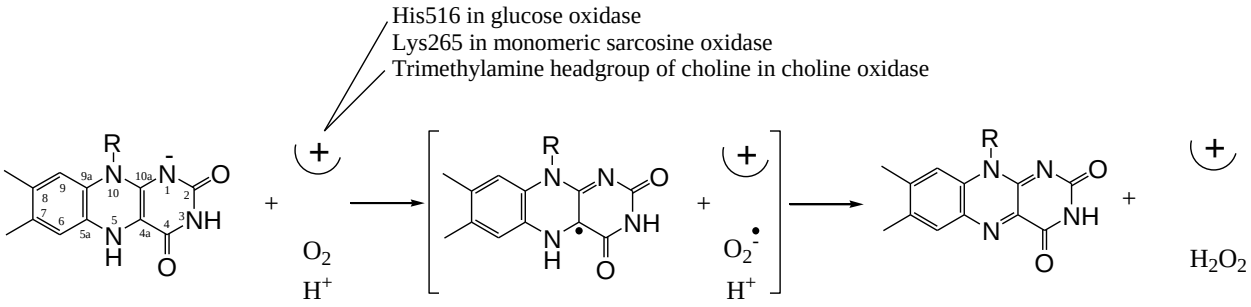

Scheme 4.1. Activation of Oxygen by a Positively Charged Group in Glucose Oxidase, monomeric Sarcosine Oxidase, and Choline Oxidase.

On the other hand, studies on glucose oxidase using mechanistic and structural approaches have established that the presence of a positive charge on a histidine residue in proximity of the flavin C(4a) atom is required to stabilize the negatively charged superoxide species that is formed transiently in the reaction of the reduced flavin with oxygen (**Scheme 4.1**) (*10-13*). Similar activations of molecular oxygen have been proposed in monomeric sarcosine oxidase and choline oxidase, where the positive charge is provided by an active site lysine in the former and the trimethylammonium moiety of the enzyme-bound substrate in the latter (**Scheme 4.1**) (*14-16*). Based on a combination of site-directed mutagenesis with mechanistic and structural investigations, a hydrophobic tunnel has been proposed to guide oxygen to the C(4a) atom of the reduced flavin in cholesterol oxidase (*17*). More recently, an integrated approach based on X-ray crystallography, enhanced-statistics molecular dynamics simulations, kinetics and site-directed

mutagenesis, allowed the authors to propose the presence of multiple diffusion pathways that converge to the reactive center on the flavin in the monooxygenase component C_2 of *p*-hydroxyphenylacetate hydroxylase and alditol oxidase (*18*). In this respect, the three-dimensional structure of the monooxygenase component C_2 of *p*-hydroxyphenylacetate hydroxylase also shows the presence of a hydrophobic cavity with proper geometry in proximity of the C(4a) atom of the flavin, a feature that is not structurally apparent in flavoprotein oxidases (*19*). These results collectively present general principles for the reaction with oxygen or lack thereof in flavoproteins. They do not, however, directly address whether the site in flavoprotein oxidases where oxygen reacts with the reduced flavin has some non-polar character in addition to the positively charged group that is required for the activation of oxygen (**Scheme 4.1**).

Our group has investigated the reaction of alcohol oxidation catalyzed by the FAD-containing choline oxidase from *Arthrobacter globiformis* using biochemical (*20-23*), structural (*24-25*), site-directed mutagenic (*15*, *21*, *25-28*), and mechanistic (*29-35*) approaches. The enzyme catalyzes the two-step, flavin-linked oxidation of choline to glycine betaine, with betaine aldehyde as intermediate and molecular oxygen as electron acceptor (**Scheme 4.2**).

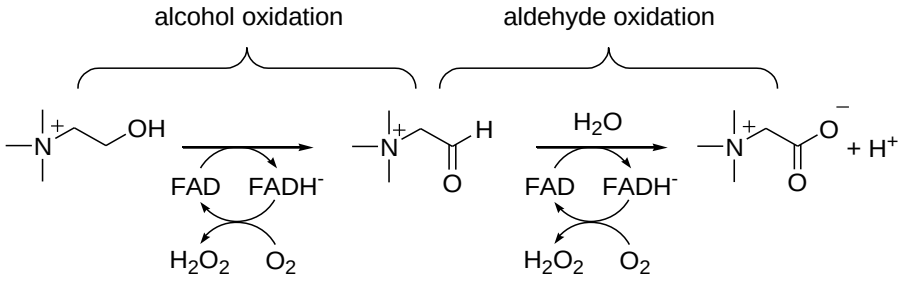

Scheme 4.2. Two-step Oxidation of Choline Catalyzed by Choline Oxidase.

A detailed mechanistic understanding of the reductive half-reaction where a hydride ion is transferred from choline to the enzyme-bound flavin has emerged from these studies (for a recent review see (*36*)). The subsequent oxidation of the enzyme-bound, reduced flavin with oxygen

occurs while the active site is still occupied with the aldehyde intermediate of the reaction, as suggested by steady state kinetic studies with choline and a number of substrate analogues (*15-16, 23, 31, 34*). In this respect, site-directed mutagenesis studies where each of the three histidine residues located in the active site of the enzyme were individually replaced indicated that these residues do not contribute to oxygen activation, as the bimolecular rate constants for oxygen reaction (k_{cat}/K_{oxygen}) were not significantly altered in the mutant enzymes from the value of ~10^5 $M^{-1}s^{-1}$ of the wild-type enzyme (*27, 37-38*). In contrast, substitution of the positively charged substrate with the isosteric analogue devoid of charge 3,3-dimethyl-butan-1-ol yielded k_{cat}/K_{oxygen} values of ~10^3 $M^{-1}s^{-1}$, consistent with activation of oxygen for reaction with the reduced flavin being exerted by the enzyme-bound ligand (*15-16*). In agreement with this conclusion, the His99Asn, His351Ala, His466Ala and wild-type forms of choline oxidase showed k_{cat}/K_{oxygen} values that are independent of pH, since the trimethylammonium moiety of the substrate cannot ionize (*15, 23, 27, 32, 37-38*). In the X -ray structure of choline oxidase previously solved to a resolution of 1.86 Å (*24-25*), Val464 lies in the active site cavity close to the C(4a)-N(5) atoms of the flavin, with its hydrophobic side chain in van der Waals contact with the C(2) atom of the conserved His466.

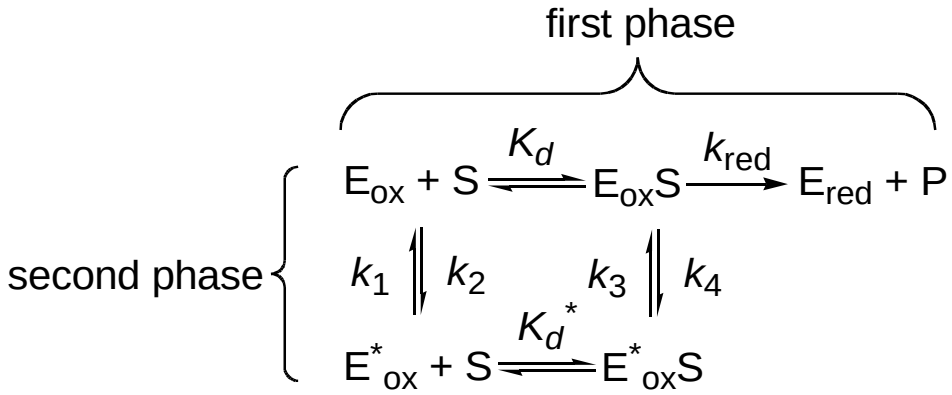

Scheme 4.3. Minimal Kinetic Mechanism for Reductive Half-reaction of the Val464Ala and Val464Thr Enzymes. E_{ox}, catalytically competent oxidized enzyme; E_{ox}*, catalytically incompetent enzyme; S, choline; E_{red}, reduced enzyme.

Replacement of Val464 with threonine or alanine results in the ensuing variant enzymes having a catalytically incompetent form of enzyme in equilibrium with a competent form (**Scheme 4.3**) that is able to efficiently oxidize choline with rates similar to those determined for the wild-type enzyme (*28*).

In the present study, we have used X-ray crystallography, site-directed mutagenesis, and both steady state and rapid kinetics approaches to investigate the role of the hydrophobic residue Val464 in the active site of choline oxidase. The three-dimensional structure of the Val464Ala enzyme was solved by X-ray crystallography to a resolution of 2.2 Å, and the oxidative half-reactions, steady state kinetic mechanisms and enzyme monitored turnovers were investigated for the Val464Ala and Val464Thr variants along with the wild-type enzyme for comparison. Moreover, pH profiles of the k_{cat}/K_{oxygen} values with choline as substrate and the effect of substituting choline with 3,3-dimethyl-butan-1-ol on the k_{cat}/K_{oxygen} values were investigated in the Val464Ala enzyme. The results presented established the hydrophobic side chain of Val464 as being important in the oxidative half-reaction of choline oxidase, with minimal effects on the reaction of choline oxidation and, most importantly, the three-dimensional structure of the enzyme. A role is proposed for Val464 in the flavin oxidation reaction catalyzed by choline oxidase. Analysis of the three-dimensional structures of several flavoprotein oxidases suggests that hydrophobic residues in the active site of these enzymes may have roles similar to that of Val464 in choline oxidase in the reaction of the reduced flavin with oxygen.

4.3.Experimental procedures

Materials. *Escherichia coli* strain Rosetta(DE3)pLysS was from Novagen (Madison, WI). DNase was from Roche (Indianapolis, IN). The QuikChange site-directed mutagenesis kit was

from Stratagene (La Jolla, CA). The QIAprep Spin Miniprep kit was from Qiagen (Valencia, CA). Oligonucleotides used for sequencing of the mutant genes were custom synthesized by Sigma Genosys (Woodland, TX). Choline chloride was from ICN Pharmaceutical Inc (Irvine, CA). 3,3-Dimethyl-butan-1-ol (DMB), glucose, glucose oxidase and betaine aldehyde were from Sigma (St. Louis, MO). All other reagents were of the highest purity commercially available.

Site-Directed Mutagenesis. The Val464Ala, Val464Thr, and Val464Leu enzymes were prepared using the pET/*codA* plasmid harboring the wild-type gene for choline oxidase as template for site-directed mutagenesis as previously described, and the presence of the desired mutation was confirmed by sequencing as described (*21-22, 25, 28*).

Enzyme Expression and Purification. The Val464Ala, Val464Thr and wild-type enzymes were expressed and purified to homogeneity using the procedure described previously for the purification of the wild-type enzyme (*16, 22*). Attempts to purify the Val464Leu enzyme were unsuccessful; stable and active enzyme could not be obtained due to protein instability during protein purification, thereby preventing the characterization of the Val→Leu substitution at position 464.

Crystallization, X-ray Data Collection and Refinement of the Val464Ala Enzyme. Crystals of theVal464Ala enzyme were grown aerobically at room temperature by hanging drop vapor diffusion from 10-15% (v/v) polyethylene glycol MW 6000, 50-200 mM magnesium acetate and 200 mM trimethylamine in 0.08 M sodium cacodylate, pH 6.0. Single crystals were transferred from the mother liquor into a cryoprotectant consisting of mother liquor with 25% (v/v) glycerol

and allowed to soak for approximately 2 min prior to flash-freezing in liquid nitrogen. Diffraction data were collected at 100 K on beamline 22-ID of the Southeast Regional Collaborative Access Team (SER-CAT) at the Advanced Photon Source, Argonne National Laboratory. The data were integrated and scaled with HKL2000 (*39*).

The crystal structure of the Val464Ala enzyme was solved by molecular replacement using PHASER (*40*) in the CCP4i suite of programs using as the starting model the structure of wild-type choline oxidase (PDB code 2JBV) (*25*). The structure was subjected to several rounds of refinement in REFMAC (*41*) of CCP4. The molecular graphics programs O 9.0 (*42*) and Coot 0.33 (*43*) were used in model rebuilding. The solvent molecules were inserted at stereochemically reasonable positions based on the peak height of the $2F_o$-F_c and F_o-F_c electron density maps, hydrogen bond interactions and inter-atomic distances. The geometry of the refined structures was validated according to the Ramachandran plot criteria (*44*). Molecular figures were prepared with MOLSCRIPT, RASTER3D (*45*) and PyMol (http://www.pymol.org).

Enzyme Monitored Turnover. Enzyme monitored turnover experiments were carried out by monitoring the absorbance at 455 nm as a function of time using an SF-61DX2 HI-TECH KinetAsyst high performance stopped-flow spectrophotometer thermostated at 25 °C. The aerobic enzyme solution was mixed with an aerobic solution of 20 mM choline, both prepared in 50 mM sodium pyrophosphate, pH 10.0. The final [oxygen] was 0.25 mM; the final [choline] was 10 mM.

Enzyme Kinetics. Steady state kinetic measurements were carried out by using the method of initial rates using a computer-interfaced Oxy-32 oxygen-monitoring system (Hansatech

Instrument Ltd.) (*46*). The pH dependence of the bimolecular rate constants for reaction of the reduced flavin with oxygen (k_{cat}/K_{oxygen}) was determined by measuring enzymatic activity at varying concentrations of choline and oxygen in the pH range between 5.0 to 10.0 in 50 mM sodium pyrophosphate at 25 °C, with the exception of pH 7.0 where sodium phosphate was used. The assay reaction mixture was equilibrated at the desired oxygen concentration by bubbling with an O_2/N_2 gas mixture for at least 10 min before the reaction was started with the addition of the enzyme.

Oxidative half-reaction measurements for the wild-type, Val464Ala and Val464Thr enzymes were carried out using an SF-61DX2 HI-TECH KinetAsyst high performance stopped-flow spectrophotometer thermostated at 25 °C, in 50 mM sodium pyrophosphate buffer, pH 10.0. The rate constants for flavin oxidation were measured by monitoring the increase in absorbance at 455 nm that results from the mixing of anaerobic reduced enzyme in 50 mM buffer with 50 mM buffer which was equilibrated at varying oxygen concentrations by sparging with an O_2/N_2 gas mixture for at least 10 min prior to mixing. The enzymes were previously reduced by anaerobic mixing of the oxidized enzymes with a 1.1-molar excess of betaine aldehyde.

Data Analysis. Kinetic data were fit with KaleidaGraph (Synergy Software, Reading, PA) or the Hi-Kinetic Studio Software Suite (Hi-Tech Scientific, Bradford on Avon, U.K.). A first attempt at the determination of the steady state kinetic parameters for the Val464Ala and Val464Thr enzymes at varying concentrations of both choline and oxygen was carried out by fitting the initial rates to eq 1, which describes a steady state kinetic mechanism with formation of a ternary complex. $K_{choline}$ and K_{oxygen} are the Michaelis constants for choline and oxygen, respectively, and k_{cat} is the true turnover number of the enzyme (*e*) at saturating concentrations of

both choline and oxygen. This approach yielded estimated K_{oxygen} values in the 5-8 mM range, which were ≥5-fold higher than the highest concentration of oxygen that was used in the experiments, thereby preventing saturation of the enzyme with oxygen. Thus, the true value for k_{cat}, as well as the derivative parameter $k_{cat}/K_{oxygen,}$ could not be determined by using eq 1. Since the k_{cat}/K_{oxygen} value represents the bimolecular rate constant for the capture of oxygen onto the enzyme when [oxygen] $<K_{oxygen}$, it could be determined graphically as described below (eq 2). Here, the k_{cat}/K_{oxygen} values were determined from the reciprocal of the *y*-intercept of a secondary plot of the slopes of the lines obtained from the primary double reciprocal plot of e/v_o versus 1/[oxygen] (i.e., $slope_{1/[oxygen]}$) as a function of 1/[choline] (*47*):

$$\frac{v}{e} = \frac{k_{cat}[choline][oxygen]}{K_{choline}[oxygen] + K_{oxygen}[choline] + [choline][oxygen] + K_{ia}K_{oxygen}} \quad (1)$$

$$\text{slope}_{1/[\text{oxygen}]} = \frac{K_{oxygen}}{k_{cat}} + \left(\frac{K_{iA}K_{oxygen}}{k_{cat}}\right)\frac{1}{[choline]} \quad (2)$$

Stopped-flow traces for the oxidative half-reaction were fit with eq 3, which describes a single-exponential process in which k_{obs} is the observed rate constant for the increase in absorbance at 455 nm, *A* is the absorbance at time *t*, *B* is the amplitude of the absorbance change, and *C* is an offset value that accounts for the non-zero absorbance value at infinite time.

$$A = B\exp(-k_{obs}t) + C \quad (3)$$

The pre-steady state bimolecular rate constant for flavin oxidation was determined with eq 4. Here, the k_{obs} value is the observed rate constant associated with flavin oxidation at any given concentration of oxygen, k_{ox} is the second-order rate constant for flavin oxidation.

$$k_{obs} = k_{ox}[\text{oxygen}] \quad (4)$$

4.4.Results

Determination of the Crystal Structure of the Val464Ala Enzyme[1]. The Val464Ala enzyme was crystallized in the tetragonal space group $P4_32_12$ with a homodimer in the asymmetric unit. The structure was refined to the resolution of 2.2 Å and R-factor of 16.5 %. The X-ray diffraction data and refinement statistics are listed in **Table 4.1**.

Table 4.1. Crystallographic Data Collection and Refinement Statistics

	Choline Oxidase Val464Ala
Space group	$P4_32_12$
a = b (Å)	87.04
c (Å)	353.07
Resolution range	50-2.2
Total observations	411,516
Unique reflections	67,756
Completeness	96.0 (99.5)[a]
$\langle I/\sigma(I)\rangle$	12.3 (5.5)
R_{sym} (%)[b]	13.4 (37.6)
Resolution range	50-2.2
R_{cryst} (%)[c]	16.5
R_{free} (%)[d]	22.7
Mean B-factor (Å^2)	19.4
Number of atoms	
Protein	8302
FAD	106
Water	472
r.m.s. deviations	
Bond length (Å)	0.025
Angles (°)	2.08

[a]Values in parentheses are given for the highest resolution shell
[b]$R_{sym} = \Sigma_{hkl}|I_{hkl} - \langle I_{hkl}\rangle|/\Sigma_{hkl}I_{hkl}$.
[c]$R = \Sigma|F_{obs}-F_{cal}|/\Sigma F_{obs}$.
[d]$R_{free} = \Sigma_{test}(|F_{obs}|-|F_{cal}|)^2/\Sigma_{test}|F_{obs}|^2$.

Although the replacement of the side chain on residue 464 from valine to alanine results in loss of van der Waals interactions between Ala464 and His310, Glu312, His351 and Asn378,

[1] The atomic coordinates and structure factors have been deposited in the Protein Data Bank as entry 3LJP

these residues are located in the same position in the mutant and wild-type enzymes (2JBV) (**Figure 4.1**).

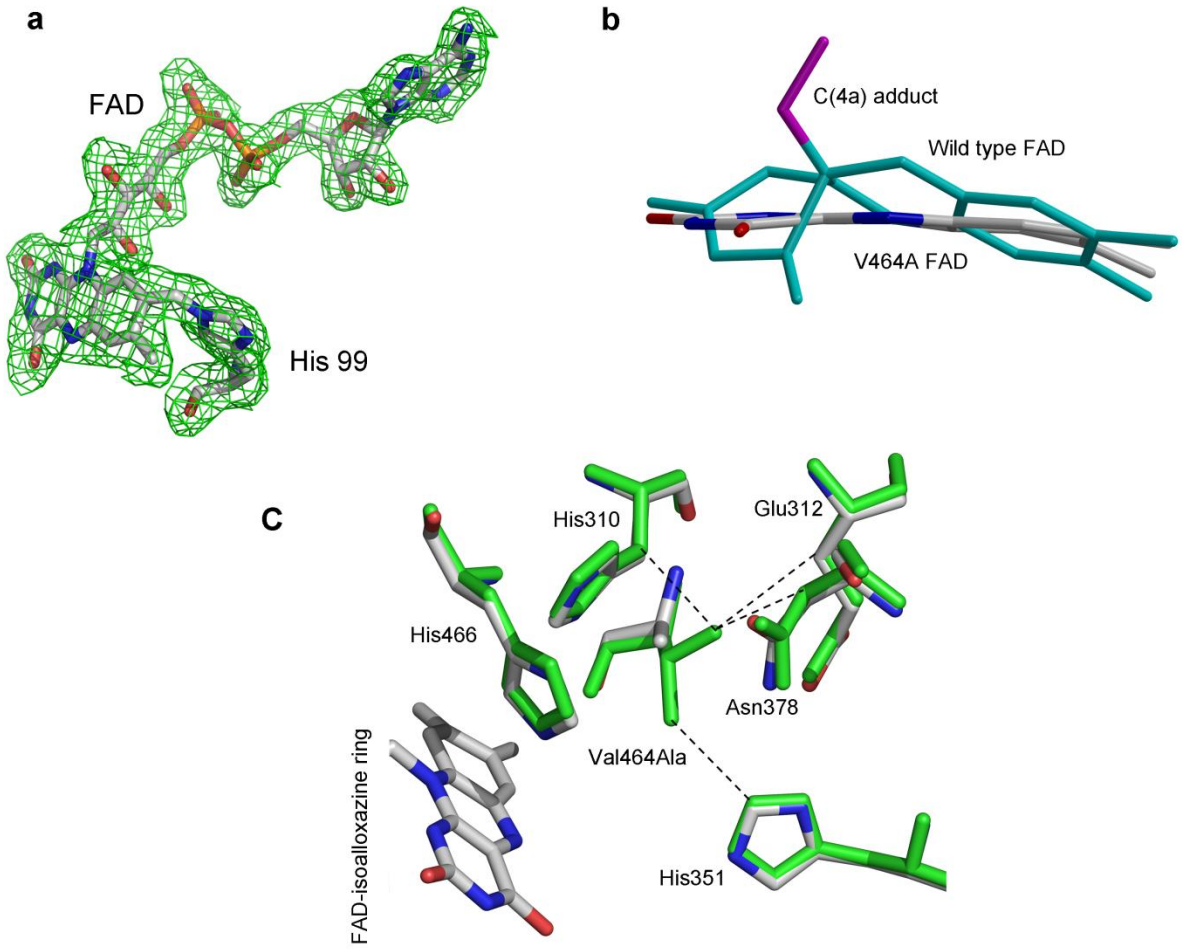

Figure 4.1. Crystal Structure of Val464Ala Mutant**.** Panel A shows the $2F_o$-F_c electron density map of FAD contoured at a level of 1 σ. The FAD is covalently bound to His99. Panel B illustrates the superposition of the FAD isoalloxazine ring from the wild-type (cyan) and the Val464Ala enzymes (colored by element type) of choline oxidase. The C(4a) oxygen adduct of wild-type FAD is shown in magenta. Note that the isoalloxazine ring of the Val464Ala enzyme is more planar than that of the wild-type structure. Panel C shows the Val464Ala mutation site. The van der Waals interactions between the side chains of Val464 (green) and residues His310, Glu312, His351 and Asn378, indicated by broken lines, are lost in the structure of the Val464Ala enzyme. Despite the loss of these interactions, these residues in the Val464Ala enzyme maintain virtually identical conformations and positions to those in the wild-type enzyme.

The homodimers of the Val464Ala enzyme could be superimposed with those of the wild-type enzyme with an rmsd value of 0.67 Å for 1056 topologically equivalent Cα atoms, consistent with the overall structure of the Val464Ala enzyme being essentially identical to that of the wild-type choline oxidase (2JBV) previously reported. The individual monomers of the Val464Ala enzyme are even more similar to those of the wild-type choline oxidase with rmsd values of 0.29 Å and 0.25 Å for the A and B chain, respectively. Furthermore, the two monomers within the structure of the Val464Ala enzyme are very similar to one another, as evident from the rmsd values of 0.22 for 528 common Cα atoms.

The FAD in the Val464Ala enzyme is covalently bound to the Nε2 atom of His 99 as in the case of wild-type (*25*). The $2F_o$- F_c electron density map of FAD contoured at 1σ is shown in **Figure 4.1**. A striking difference between the structures of the Val464Ala and wild-type enzymes is the absence of the C(4a) oxygen adduct on the *re*-face of the FAD cofactor, observed in the wild-type enzyme, on the FAD cofactor in the Val464Ala variant enzyme, resulting in the isoalloxazine moiety of the FAD cofactor in the variant enzyme being more planar than that in the wild-type (**Figure 4.1B**). This difference is consistent with the C(4a) atom of the of the FAD cofactor being sp^3 hybridized in the wild-type enzyme due to the presence of the C(4a) adduct as compared to sp^2 hybridized in the Val464Ala enzyme. For the wild-type choline oxidase the enzyme-bound FAD is likely reduced in the X-ray beam during data collection and the reduced FAD then forms either a C(4a)-OH or C(4a)-OO(H) adduct but an insufficient proton inventory prevents the FAD reoxidation to proceed (*24*). The absence of the FAD C(4a) adduct in the crystal structure of the Val464Ala enzyme is most likely due to the lowered apparent affinity for oxygen in the Val464Ala variant enzyme as compared to the wild-type enzyme as observed by the inability to saturate the Val464Ala enzyme with oxygen in the steady state kinetic studies.

Alternatively, it may simply be due to the FAD not being reduced during the data collection and thus making the formation of the C(4a) adduct impossible in the synchotron. The crystallization conditions for both the wild-type and the variant enzyme do not contain any reagents known to form C(4a) adducts with FAD.

Overall, with the exception of the point mutation that replaces Val464 with alanine, the orientation and position of all the amino acid residues in the active site and in the vicinity of the Ala464 position in the Val464Ala enzyme are closely identical to those of the wild-type form of choline oxidase, as illustrated in **Figure 4.1**. The point mutation at position 464 results in an important difference observable in the structures of the Val464Ala variant and the wild-type enzyme, which is a significant increase in the size of the pocket on the *re*-face directly above the C(4a)-N(5) atoms of the flavin. This pocket is defined by His351, Ala464, and His466, and is the location where the C(4a) oxygen adduct is observed in the crystal structure of the wild-type enzyme, consistent with this being the site of oxygen reduction. In this regard, a 2 Å increase is seen in the distance between the C(4a)-N(5) atoms of FAD and the nearest side chain atom CB of Ala464 with respect to the distance to side chain atom CG1 of Val464 in the wild-type enzyme.

Interestingly, only one form of the Val464Ala variant enzyme is observable in the crystal structure solved even though the enzyme has previously been shown to exist in an equilibrium between an incompetent and a competent form (*28*). The crystallization conditions for Val464Ala included 200 mM trimethylamine, which is a substrate analog known to be a competitive inhibitor of the wild-type choline oxidase (*16*). Although trimethylamine is not observed in the 3D X-ray crystal structure of the enzyme, it may have contributed to the selective crystallization of only one form of the Val464Ala variant enzyme. Alternatively, the ΔH_{fusion} for

the phase change associated with the crystallization may be sufficient to shift the equilibrium during this process to a point where the crystal only contains one form of enzyme.

Steady State Kinetic Mechanism of Val464Ala and Val464Thr Enzymes. The steady state kinetic mechanisms of the Val464Ala and Val464Thr enzymes were investigated with the method of the initial rates by monitoring the rates of oxygen consumption in a Clark oxygen electrode, in the pH-range from pH 5.0 till pH 10.0, at varying concentrations of both choline and oxygen. The analysis of the collected data is shown here exemplified by the data collected at pH 8.0 and 25 ^{o}C .With both enzymes, a double reciprocal plot of the initial rates of reaction as a function of [choline] yielded intersecting lines, as previously reported for the wild-type and several mutants of choline oxidase (*25, 27, 37-38, 48-50*). Therefore, the k_{cat}/K_{oxygen} value is not independent of the concentration of choline, unless oxygen is saturating (*47*). The data with the Val464Ala enzyme were fit well with eq 1, yielding, however, computer-estimated K_{oxygen} values in the 5-8 mM range, which was at least 5-fold larger than the highest [oxygen] used (i.e., 1 mM). Lack of enzyme saturation with oxygen thereby prevented the use of eq 1 for the determination of the steady state kinetic parameters of the enzyme. The k_{cat}/K_{oxygen} values were therefore determined graphically with the data at hand by using eq 2, as described in the Experimental Procedures. This yielded a k_{cat}/K_{oxygen} value of 1,500 ± 150 $M^{-1}s^{-1}$ at pH 8.0.

With the Val464Thr enzyme, the dependences of the initial rates of reaction on [oxygen] at different concentrations of choline showed sigmoidal rather than hyperbolic patterns (**Figure 4.2**) and were fit best to a Hill equation. As for the case of the Val464Ala enzyme, the estimated K_{oxygen} values were well above the maximal [oxygen] of ~1 mM that was used, thereby precluding the determination of meaningful kinetic parameters. Moreover, the sigmoidal kinetic

patterns prevented the determination of the k_{cat}/K_{oxygen} values for the Val464Thr enzyme by using the graphical methods employed for the Val464Ala enzyme.

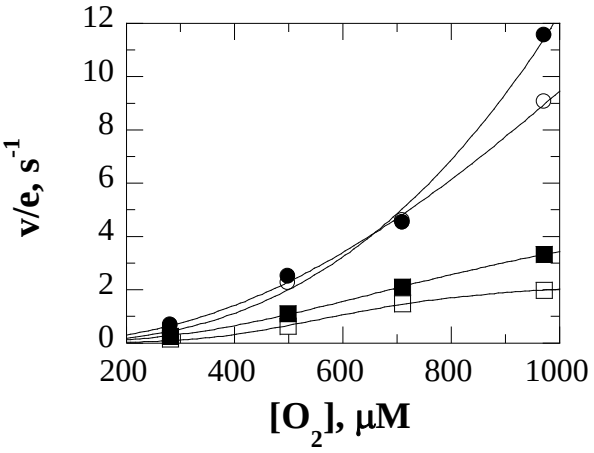

Figure 4.2. Dependence of the Initial Rates of Reaction with Choline as Substrate for the Val464Thr Enzyme as a Function of [Oxygen] in 50 mM Sodium Pyrophosphate, pH 10.0 and 25 °C. Choline concentrations were: 5 mM (●), 1 mM (○), 0.1 mM (■), and 0.05 mM (□). The curves are independent fits of the data to the Hill equation ($v/e=k_{cat}[\text{oxygen}]^h/(K_{oxygen}{}^h+[\text{oxygen}]^h)$.

A kinetic behavior similar to that shown by the Val464Thr enzyme was recently reported for selected active site variants of cholesterol oxidase, where the observations were explained with a rate-limiting interconversion of multiple forms of enzyme reacting differently with oxygen (*17*). Although this interpretation could satisfactorily explain the steady state kinetic pattern of the Val464Thr enzyme, lack of saturation of the enzyme with oxygen did not allow us to further investigate the steady state kinetic mechanism and draw conclusions on the steady state behavior of the Val464Thr enzyme.

pH Dependence of the k_{cat}/K_{oxygen} Values of Val464Ala Enzyme. The effect of pH on the k_{cat}/K_{oxygen} values of the Val464Ala enzyme is shown in **Figure 4.3**. As for the case of the wild-type enzyme (*32*), the Val464Ala enzyme had k_{cat}/K_{oxygen} values that were independent of the pH

between 5.0 and 10.0, however with an average value of 1,700 ± 150 $M^{-1}s^{-1}$. This value is ~50-fold lower than the pH independent k_{cat}/K_{oxygen} value of 90,000 $M^{-1}s^{-1}$ that was previously reported for the wild-type enzyme (*32*), indicating that the oxidative half-reaction in choline oxidase is affected substantially by the replacement of Val464 with alanine.

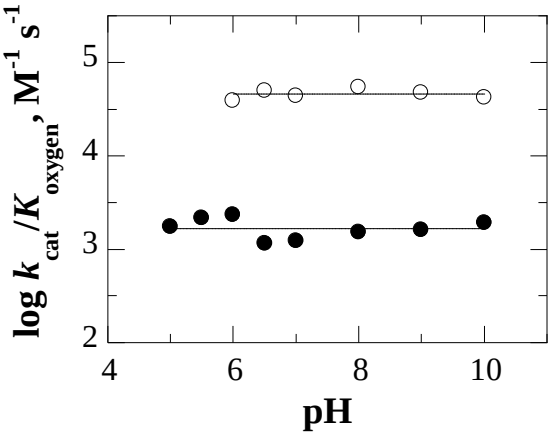

Figure 4.3. Effect of pH on the k_{cat}/K_{oxygen} Values with Choline as Substrate for the Val464Ala Enzyme (●) Compared to Wild-type Enzyme (○). The lines that fit the k_{cat}/K_{oxygen} values represent the average of the values. Data for wild-type enzyme are from (*32*).

Oxidative Half-reactions of Wild-type, Val464Ala and Val464Thr Enzymes at pH 10.0.

The oxidative half-reactions where the reduced Val464Ala, Val464Thr and the wild-type enzymes were oxidized with oxygen were investigated using a stopped-flow spectrophotometer. The rate constants for flavin oxidation were measured from the increase in absorbance at 455 nm of the flavin cofactor at various concentrations of oxygen at pH 10.0 and 25 ^{o}C. As shown in **Figure 4.4,** for all three investigated enzymes the oxidation of the flavin from the hydroquinone to the fully oxidized state was monophasic, without formation of any detectable transient species. The monophasic behavior of FAD oxidation is consistent with the mechanism shown in **Scheme 4.3**, showing that upon complete reduction of the FAD cofactor by the substrate only one form of reduced enzyme is present.

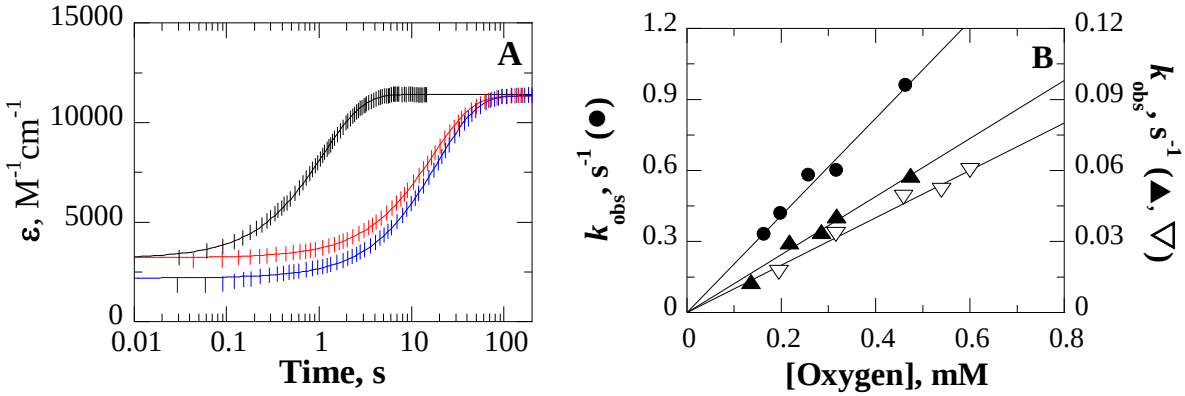

Figure 4.4. Time-resolved, Flavin Oxidation of the Val464Ala, Val464Thr and Wild-type Enzymes with Oxygen in 50 mM Sodium Pyrophosphate, pH 10.0 and 25 °C, Monitored at 455 nm in a Stopped-flow Spectrophotometer. Panel A shows the oxidation traces of the wild-type enzyme with 460 µM oxygen (black), Val464Thr with 475 µM oxygen (red) and Val464Ala with 460 µM oxygen (blue). All traces were fit to eq 3, yielding R^2-values > 0.999. For clarity, only one experimental point out of every two points is shown for the wild-type enzyme (vertical lines) and one out of ten points are shown for both Val464Ala and Val464Thr. The time indicated is after the end of flow, i.e., 2.2 ms. Panel B shows the dependence of the observed rate constants for flavin oxidation as a function of the concentration of oxygen for the wild-type (●), Val464Ala (▽) and Val464Thr (▲) enzymes. For each enzyme the observed rate constants were fit to eq 4.

With all investigated enzymes, the observed rate constants for flavin oxidation (k_{obs}) when plotted as a function of the concentration of oxygen defined second order processes (**Figure 4.4**). For the wild-type enzyme the k_{ox} was 1900 ± 40 $M^{-1}s^{-1}$, whereas for the Val464Ala and Val464Thr enzymes it was 100 ± 2 $M^{-1}s^{-1}$ and 125 ± 4 $M^{-1}s^{-1}$, respectively. These k_{ox} values refer to the free enzymes and therefore do not reflect the values that would be measured in enzymatic turnover where oxygen reacts with the reduced flavin when the active site is occupied with the product of the oxidation reaction; however, they demonstrate that the Val464Ala and Val464Thr enzymes are impaired to similar extents in their ability to react with oxygen with respect to the wild-type enzyme, with a significant decrease in the k_{ox} values. Attempts to determine the k_{ox} values for the three enzymes with the substrate bound were unsuccessful, due to inability to obtain a stable reduced enzyme-substrate complex.

Enzyme Monitored Turnover of Val464Ala, Val464Thr, and Wild-type Enzymes. Enzyme monitored turnovers were carried out on the Val464Ala and Val464Thr enzymes under atmospheric oxygen conditions (i.e., 0.25 mM oxygen) with 10 mM choline at pH 10.0 in a stopped-flow spectrophotometer. As shown in **Figure 4.5**, the enzymes reached steady state conditions of turnover with choline and oxygen when the absorbance at 455 nm was about 2/3 that of the fully oxidized, resting enzymes.

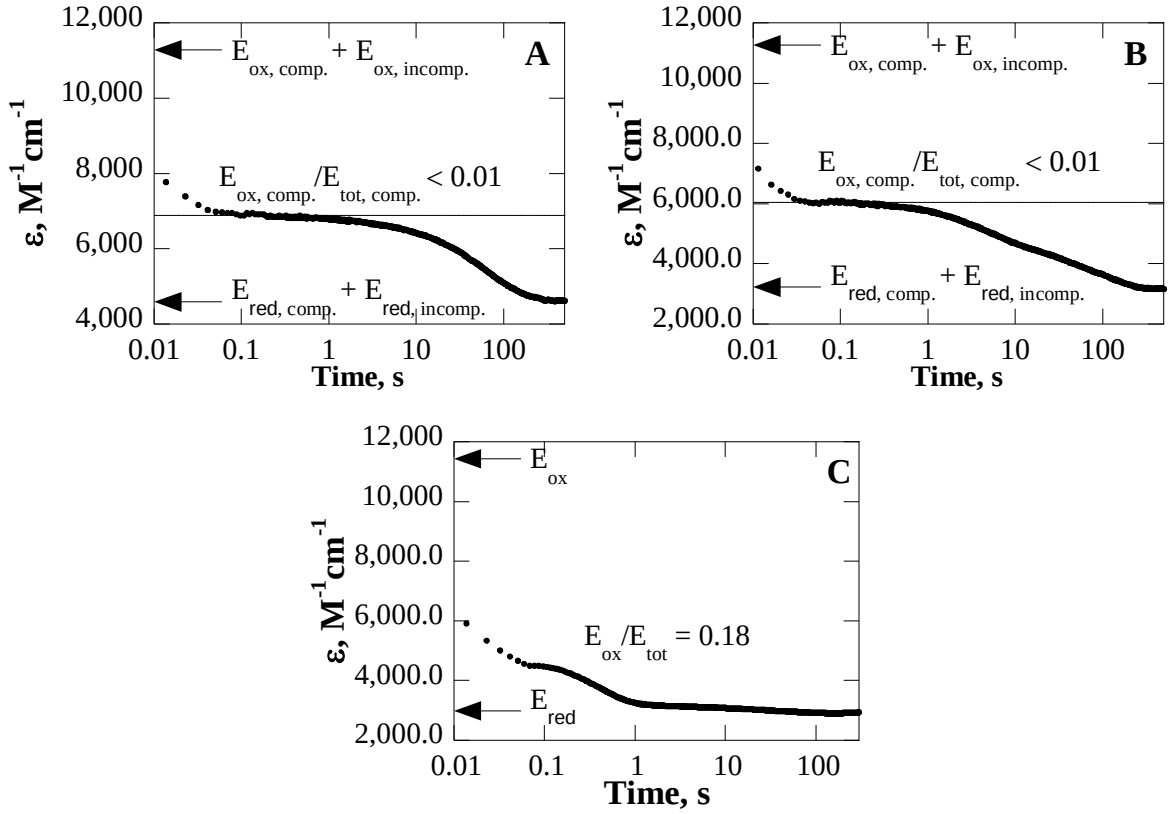

Figure 4.5. Enzyme Monitored Turnovers with Choline and Oxygen as Substrates for the Val464Ala (panel A), Val464Thr (panel B), and Wild-type (panel C) Enzymes. In all cases, [choline] = 10 mM, [oxygen] = 0.25 mM, pH 10.0 and 25 ^{o}C. The top arrow corresponds to the extinction coefficient at 455 nm of the fully oxidized enzyme (both the catalytically competent and incompetent forms for the Val464 substituted enzymes), while the bottom arrow corresponds to the fully reduced enzyme after oxygen depletion in the reaction mixture (and also full conversion of the incompetent to catalytically competent forms for the Val464 substituted enzymes). The horizontal lines in panels A and B define the expected absorbance during turnover of the Val464Ala and Val464Thr enzyme when all of the catalytically competent form of the enzyme is in the reduced state and the incompetent form of the enzyme, which does not undergo turnover, is still present in the oxidized form before slowly converting to the

catalytically competent form. The ratios E_{ox}/E_{tot} are estimations of the fraction of oxidized (catalytically competent) enzyme with respect to the total enzyme that is catalytically competent for turnover.

This value corresponded well with the fraction of enzyme that is present in the catalytically competent form (i.e., 65%), which was previously determined for both the Val464Ala and Val464Thr enzymes (*28*). Since complete conversion of the incompetent to competent forms of the Val464 variant enzymes occurs over several seconds (*28*), during the steady state catalytic turnover of **Figure 4.5** the majority of the enzyme-bound flavin was in the reduced form in the Val464Ala and Val464Thr enzymes that are competent for catalysis. The reductive half-reaction in both the Val464 substituted enzymes is minimally affected with respect to the wild-type enzyme (*28*), and the two enzymes also show similar behavior in the enzyme monitored turnover. Hence, it can be concluded that the oxidative half-reactions are affected to similar extents in the Val464Ala and Val464Thr enzymes with respect to the wild-type choline oxidase. In this respect, a control experiment with the wild-type enzyme showed that ~20% of the enzyme-bound flavin is in the oxidized state under catalytic turnover of the enzyme in the same conditions (**Figure 4.5**), consistent with the much higher bimolecular rate constant k_{cat}/K_{oxygen} for the oxidative half-reaction of the wild-type enzyme (*32*).

k_{cat}/K_{oxygen} Values of Val464Ala Enzyme with 3,3-Dimethyl-butan-1-ol as Substrate. The k_{cat}/K_{oxygen} values of the Val464Ala enzyme were also determined with 3,3-dimethyl-butan-1-ol, an isosteric analogue of choline that contains a *tert*-butyl headgroup devoid of charge. The effect of the substrate analog on k_{cat}/K_{oxygen} for the Val464Ala enzyme was determined at pH 8.0 in order for it to be directly compared to a previous study performed on the wild-type enzyme (*16*). As for the case of choline as substrate, the Val464Ala enzyme could not be saturated with

oxygen due to K_{oxygen} being significantly larger than the highest [oxygen] of ~1 mM that was attainable in the experiment (data not shown). Consequently, the apparent k_{cat}/K_{oxygen} values were determined by measuring initial rates of reaction as a function of [oxygen] at fixed saturating concentrations of 3,3-dimethyl-butan-1-ol. As shown in **Table 4.2**, similar $^{app}(k_{cat}/K_{oxygen})$ values were determined with 10 mM, 30 mM and 40 mM 3,3-dimethyl-butan-1-ol, establishing a true k_{cat}/K_{oxygen} value of 31 ± 2 $M^{-1}s^{-1}$ at pH 8.0 for the reaction of the Val464Ala enzyme with 3,3-dimethyl-butan-1-ol as substrate.

Table 4.2. $^{app}(k_{cat}/K_{oxygen})$ for the Val464Ala Enzyme at Fixed Saturating Concentrations of 3,3-dimethyl-butan-1-ol as Substrate [a].

[3,3-dimethyl-butan-1-ol], mM	$^{app}(k_{cat}/K_{oxygen})$, $M^{-1}s^{-1}$
10	33 ± 1
30	30 ± 1
40	31 ± 1

[a] Conditions: 50 mM sodium pyrophosphate, 25 °C, pH 8.0.

Thus, the lack of positive charge on the organic substrate bound at the active site of the enzyme results in a further decrease of ~55-fold in the k_{cat}/K_{oxygen} value of the Val464Ala enzyme (i.e., 1,700 $M^{-1}s^{-1}$ with choline as substrate). For comparison, a similar decrease of ~55-fold was previously reported for the wild-type enzyme with the substrate devoid of positive charge (i.e., 90,000 $M^{-1}s^{-1}$ and 1,600 $M^{-1}s^{-1}$ with choline and 3,3-dimethyl-butan-1-ol, respectively) (*15-16*). In contrast, the k_{cat}/K_{oxygen} values for a number of active site variants of choline oxidase with point mutations of residues shown to be important for catalysis either in direct contact with or further removed from Val464 (i.e., His99Asn, Gly312Asp, His351Ala, and His466Ala) were shown previously not to be significantly different from the wild-type, as summarized in **Figure 4.6** (*1, 15, 25-27, 38*).

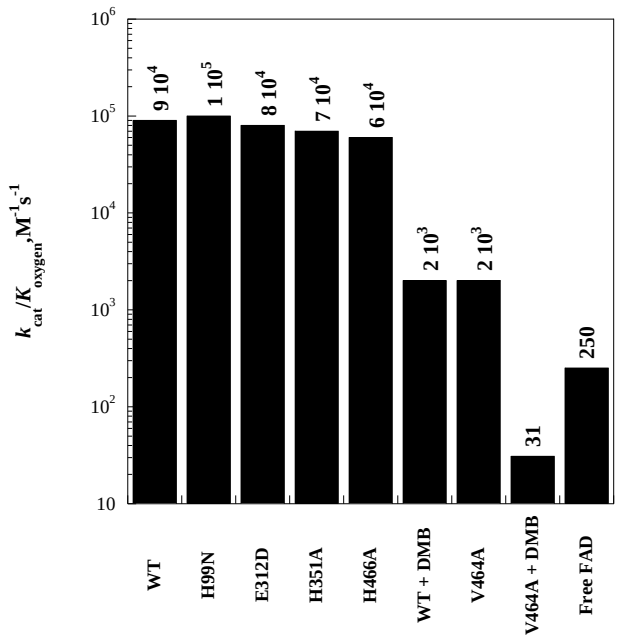

Figure 4.6. k_{cat}/K_{oxygen} Values for the Wild-type Enzyme as well as Variant Forms of Choline Oxidase with Mutations in the Active Site at pH 10.0 and 25°C with the Exception of WT + DMB and V464A + DMB which are at pH 8.0 and 25°C. As a reference the rate of oxidation of free flavin by oxygen at pH 6.5 is added. Data are from this study and ref. *1, 15, 25-27, 38 (16).*

4.5.Discussion

In this study, the role of Val464 in the reaction of flavin oxidation catalyzed by choline oxidase was investigated with site-directed mutagenesis, steady state and rapid kinetics, and X-ray crystallography. Val464, which sits in the active site of the enzyme on the *re*-face at ~5.0 Å from the C(4a) and the N(5) atoms of the flavin, was replaced with alanine or threonine and the effects of the mutations on the properties of the enzyme were investigated. The overall three-dimensional structure, as well as the location and conformation of all the active site residues in the Val464Ala enzyme, were shown by X-ray crystallography to be essentially identical to those of the wild-type enzyme (*25*). Consistent with an unaltered enzyme structure, a number of functional properties were shared by the mutant and wild-type enzymes, as demonstrated in this and a previous study (*28*). The Val464Ala and the wild-type enzymes catalyze the oxidation of

choline through a sequential steady-state kinetic mechanism, consistent with a similar order of substrate binding and product release during turnover. In addition, the Val464Ala enzyme shows a pH-independent k_{cat}/K_{oxygen} value with choline and a significantly lower k_{cat}/K_{oxygen} value with 3,3-dimethyl-butan-1-ol with respect to choline as substrate, as does the wild-type enzyme. Finally, a recent study showed that the competent forms of Ala464 and Thr464 variants of choline oxidase contain covalently bound FAD, stabilize an anionic flavosemiquinone in the presence of air, have UV-visible absorbance spectra with no sign of protein denaturation, and kinetic isotope effects on the k_{red} values at pH 10.0 that are within 3-fold from the values of the wild-type enzyme (*28*). These structural and functional observations unequivocally establish that the role of Val464 in the reaction of flavin oxidation catalyzed by choline oxidase can be elucidated by comparing and contrasting the mechanistic properties of the Val464Ala and Val464Thr enzymes with those of the wild-type enzyme.

The active site residue Val464 is important for the oxidation of the reduced flavin by molecular oxygen, but not for substrate binding or the hydride ion transfer reaction that occurs between the choline substrate and the flavin cofactor. Evidence in support of this conclusion comes from the comparison of the kinetic data of the Val464Ala and Val464Thr enzymes with those for the wild-type form of choline oxidase. In summary, replacement of Val464 with alanine or threonine results in a 2-fold decrease in the limiting rate constant for flavin reduction (k_{red}) and less than 5-fold decrease in the equilibrium constant for formation of the enzyme-substrate complex (K_d) (*28*). In the Val464Ala variant enzyme the substitution of the valine with an alanine results in a 50-fold decrease in the bimolecular rate constant for reaction with oxygen, k_{cat}/K_{oxygen}. In the Val464Thr variant enzyme a direct measurement of the k_{cat}/K_{oxygen} values could not be carried out due to the inability to saturate the enzyme with oxygen and the sigmoidal

kinetic patterns of the initial rates of reaction as a function of oxygen concentration. However, the similar kinetic behavior of the Val464Thr and Val464Ala enzymes in enzyme monitored turnover experiments, along with the rate oxidation of the free form of enzyme and reduction also being similar for the two enzymes, is consistent with them having similar overall rates for flavin oxidation. At pH 10.0, an in-depth mechanistic investigation of the reductive half-reaction of the mutant enzymes using solvent and substrate kinetic isotope effects previously established that the replacement of Val464 with alanine or threonine significantly slows down the cleavage of the OH bond of choline, but has a minimal effect on the rate of hydride ion transfer that is associated with the cleavage of the CH bond of choline (*28*).

We propose that the role of Val464 in the oxidation reaction where the reduced flavin reacts with oxygen is to provide a non-polar site that is proximal to the C(4a) atom of the flavin in order to guide oxygen at the site where the presence of the nearby positively charged catalyst will subsequently activate it to the superoxide species. Evidence for this conclusion comes from the effect on the bimolecular rate constant for reaction of the reduced flavin with oxygen upon replacing Val464 with alanine, which results in a 50-fold decrease in the k_{cat}/K_{oxygen} value. As shown by the comparison of the crystallographic structures of the mutant and the wild-type enzyme, such an amino acid substitution increases the size of the cavity on the *re*-face of the flavin that is proximal to the C(4a)-N(5) atoms, where the C(4a) oxygen adduct is observed in the wild-type enzyme, but produces no other observable changes in the structure of the active site. Evidence for the importance of a non-polar site in proximity of the C(4a) atom of the flavin comes from the similar effect on the oxidative half-reaction that is seen in the enzymes containing alanine or threonine at residue 464. Additionally, no significant effects on k_{cat}/K_{oxygen} are observed upon mutating the remaining residues (His351 and His466) that define the cavity on

the *re*-face directly above the C(4a)-N(5) atoms of the flavin or any of the other active site residues that have been shown to participate in catalysis (*27, 38*).

The requirement in choline oxidase for a non-polar site in proximity of the C(4a) atom of the flavin is not associated with the presence of the electrostatic catalyst that will subsequently activate oxygen for the reaction with the flavin. In this regard, previous studies established that the positive charge that is required to activate oxygen in choline oxidase is provided by the trimethylammonium group of the enzyme-bound substrate and not by a side chain of an amino acid in the active site of the enzyme (*15, 27, 37-38*). Evidence for the effect of the non-polar site being independent of the charge that activates oxygen comes from the comparison of the k_{cat}/K_{oxygen} values of the wild-type and Val464Ala enzymes determined with choline and 3,3-dimethyl-butan-1-ol as substrate. Replacement of Val464 with alanine results in a $\Delta\Delta G$ of 2.3 ± 0.2 kcal mol^{-1} as calculated from the ratio of the k_{cat}/K_{oxygen} values determined with choline as substrate for the wild-type and Val464Ala enzymes. Analogously, a $\Delta\Delta G$ of 2.4 ± 0.2 kcal mol^{-1} can be estimated for the wild-type enzyme upon taking the ratio of the k_{cat}/K_{oxygen} values determined with 3,3-dimethyl-butan-1-ol and choline. These values define the individual energetic contributions of the residue at position 464 and the charge harbored on the substrate towards the reaction of the reduced flavin with oxygen. When both contributions are taking into account, by taking the ratio of the k_{cat}/K_{oxygen} values determined with choline as substrate for the wild-type enzyme and 3,3-dimethyl-butan-1-ol as substrate for the Val464Ala enzyme, a $\Delta\Delta G$ of 4.7 ± 0.5 kcal mol^{-1} can be estimated. This experimental value agrees well with the sum of the individual contributions (i.e., 4.7 ± 0.6 kcal mol^{-1}), consistent with the two effects being additive and independent of one another (*51*).

Analysis of a number of flavoprotein oxidases whose three-dimensional structure is known suggests that a non-polar site of the type identified in this study in choline oxidase is likely a general feature in the class of enzymes. Here, we will limit our discussion to the cases of glucose oxidase and monomeric sarcosine oxidase, for which experimental evidence for activation of oxygen by a positive charge has been previously provided (*11-14*). In the three-dimensional structure of glucose oxidase, Val560 is ~4.7 Å away from the side chain of His516, which provides the positive charge for oxygen activation (*11-13*), and less than 6.5 Å from the C(4a) atom of the flavin. Similarly, in the active site of monomeric sarcosine oxidase Phe256 is less than 4 Å away from the side chain of Lys265, which has been shown to activate oxygen for reaction with the reduced flavin with its positive charge (*14*), and less than 6 Å from the C(4a) atom of the flavin. A possible rationale for why these sites in oxidases are not as immediately evident from the structure as in the case of the monooxygenase component C_2 of *p*-hydroxyphenylacetate hydroxylase (*19*), but require a mechanistic investigation of the enzymes, is likely that in oxidases the requirement of a non-polar cavity that encapsulates and stabilizes crucial reaction intermediates is not as stringent as in monooxygenases. Monooxygenases are required to completely desolvate the cavity surrounding the C(4a) atom of the flavin to allow longer life-times for reaction intermediates such as C(4a)-(hydro)peroxides and C(4a)-hydroxides (*19*). Most likely oxidases do not share this requirement, either because oxygen reduction occurs through outer-sphere electron transfers with no formation of any C(4a)-flavin adduct with the flavin (*10*), or simply because once oxygen is activated for reaction there is no need to prolong the life-time of C(4a)-flavin adduct intermediates that will decay to hydrogen peroxide without being used to hydroxylate organic substrates.

In conclusion the results of the mechanistic and structural investigation of active site mutant enzymes where the hydrophobic side chain on Val464 is replaced with either alanine or threonine are consistent with the presence of a non-polar site in proximity of the C(4a)-N(5) atoms of the flavin in choline oxidase. The presence of such a non-polar site is important for the oxidative half-reaction in which the enzyme-bound reduced flavin reacts with molecular oxygen to produce hydrogen peroxide and complete the catalytic cycle. It is proposed that the function of the non-polar, amino acyl side-chain is to guide oxygen at the site where it subsequently will be activated to a superoxide species through electrostatic catalysis exerted by a positive charge. The results also suggest that these two events in the reaction with oxygen catalyzed by choline oxidase are independent of one another. It is expected that non-polar sites of the kind identified in this study in choline oxidase will be identified through mechanistic investigation in a number of flavoprotein oxidases with various overall folding topologies including PHBH-folds and $(\alpha/\beta)_8$-barrels, as suggested from visual surveys of available crystal structures of flavin dependent oxidases, such as old yellow enzyme, glycolate oxidase, cholesterol oxidase and vanillyl-alcohol oxidase.

4.6.Acknowledgements

The authors thank Jane V. Hoang for the site-directed mutagenesis to prepare the Val464Ala enzyme and for the pH profile of the k_{cat}/K_{oxygen} values, and Andrea Pennati for help in the site-directed mutagenesis of the Val464Leu enzyme. We thank the staff at the SER-CAT beamlines at the Advanced Photon Source, Argonne National Laboratory, for assistance during X-ray data collection. Use of the Advanced Photon Source was supported by the U. S.

Department of Energy, Basic Energy Sciences, Office of Science, under Contract No. W-31-109-Eng-38.

4.7.References

1. Massey, V. (1994) Activation of molecular oxygen by flavins and flavoproteins, *J Biol Chem 269*, 22459-22462.
2. Mattevi, A. (2006) To be or not to be an oxidase: challenging the oxygen reactivity of flavoenzymes, *Trends Biochem Sci 31*, 276-283.
3. Kemal, C., and Bruice, T. C. (1976) Simple synthesis of a 4a-hydroperoxy adduct of a 1,5-dihydroflavine: preliminary studies of a model for bacterial luciferase, *Proc Natl Acad Sci U S A 73*, 995-999.
4. Massey, V. (2000) The chemical and biological versatility of riboflavin, *Biochem Soc Trans 28*, 283-296.
5. Ghisla, S., and Massey, V. (1989) Mechanisms of flavoprotein-catalyzed reactions, *Eur J Biochem 181*, 1-17.
6. Wang, R., and Thorpe, C. (1991) Reactivity of medium-chain acyl-CoA dehydrogenase toward molecular oxygen, *Biochemistry 30*, 7895-7901.
7. DuPlessis, E. R., Pellett, J., Stankovich, M. T., and Thorpe, C. (1998) Oxidase activity of the acyl-CoA dehydrogenases, *Biochemistry 37*, 10469-10477.
8. Sun, W., Williams, C. H., Jr., and Massey, V. (1996) Site-directed mutagenesis of glycine 99 to alanine in L-lactate monooxygenase from Mycobacterium smegmatis, *J Biol Chem 271*, 17226-17233.

9. Leferink, N. G., Fraaije, M. W., Joosten, H. J., Schaap, P. J., Mattevi, A., and van Berkel, W. J. (2009) Identification of a gatekeeper residue that prevents dehydrogenases from acting as oxidases, *J Biol Chem 284*, 4392-4397.

10. Klinman, J. P. (2007) How do enzymes activate oxygen without inactivating themselves?, *Acc Chem Res 40*, 325-333.

11. Roth, J. P., Wincek, R., Nodet, G., Edmondson, D. E., McIntire, W. S., and Klinman, J. P. (2004) Oxygen isotope effects on electron transfer to O2 probed using chemically modified flavins bound to glucose oxidase, *J Am Chem Soc 126*, 15120-15131.

12. Roth, J. P., and Klinman, J. P. (2003) Catalysis of electron transfer during activation of O2 by the flavoprotein glucose oxidase, *Proc Natl Acad Sci U S A 100*, 62-67.

13. Su, Q., and Klinman, J. P. (1999) Nature of oxygen activation in glucose oxidase from Aspergillus niger: the importance of electrostatic stabilization in superoxide formation, *Biochemistry 38*, 8572-8581.

14. Zhao, G., Bruckner, R. C., and Jorns, M. S. (2008) Identification of the oxygen activation site in monomeric sarcosine oxidase: role of Lys265 in catalysis, *Biochemistry 47*, 9124-9135.

15. Gadda, G., Fan, F., and Hoang, J. V. (2006) On the contribution of the positively charged headgroup of choline to substrate binding and catalysis in the reaction catalyzed by choline oxidase, *Arch Biochem Biophys 451*, 182-187.

16. Gadda, G., Powell, N. L., and Menon, P. (2004) The trimethylammonium headgroup of choline is a major determinant for substrate binding and specificity in choline oxidase, *Arch Biochem Biophys 430*, 264-273.

17. Chen, L., Lyubimov, A. Y., Brammer, L., Vrielink, A., and Sampson, N. S. (2008) The binding and release of oxygen and hydrogen peroxide are directed by a hydrophobic tunnel in cholesterol oxidase, *Biochemistry 47*, 5368-5377.

18. Baron, R., Riley, C., Chenprakhon, P., Thotsaporn, K., Winter, R. T., Alfieri, A., Forneris, F., van Berkel, W. J., Chaiyen, P., Fraaije, M. W., Mattevi, A., and McCammon, J. A. (2009) Multiple pathways guide oxygen diffusion into flavoenzyme active sites, *Proc Natl Acad Sci U S A 106*, 10603-10608.

19. Alfieri, A., Fersini, F., Ruangchan, N., Prongjit, M., Chaiyen, P., and Mattevi, A. (2007) Structure of the monooxygenase component of a two-component flavoprotein monooxygenase, *Proc Natl Acad Sci U S A 104*, 1177-1182.

20. Hoang, J. V., and Gadda, G. (2007) Trapping choline oxidase in a nonfunctional conformation by freezing at low pH, *Proteins 66*, 611-620.

21. Ghanem, M., and Gadda, G. (2006) Effects of reversing the protein positive charge in the proximity of the flavin N(1) locus of choline oxidase, *Biochemistry 45*, 3437-3447.

22. Fan, F., Ghanem, M., and Gadda, G. (2004) Cloning, sequence analysis, and purification of choline oxidase from Arthrobacter globiformis: a bacterial enzyme involved in osmotic stress tolerance, *Arch Biochem Biophys 421*, 149-158.

23. Ghanem, M., Fan, F., Francis, K., and Gadda, G. (2003) Spectroscopic and kinetic properties of recombinant choline oxidase from *Arthrobacter globiformis*, *Biochemistry 42*, 15179-15188.

24. Orville, A. M., Lountos, G. T., Finnegan, S., Gadda, G., and Prabhakar, R. (2009) Crystallographic, spectroscopic, and computational analysis of a flavin C4a-oxygen adduct in choline oxidase, *Biochemistry 48*, 720-728.

25. Quaye, O., Lountos, G. T., Fan, F., Orville, A. M., and Gadda, G. (2008) Role of Glu312 in binding and positioning of the substrate for the hydride transfer reaction in choline oxidase, *Biochemistry 47*, 243-256.

26. Gadda, G., Quaye, O., and Cowins, S. (2009) Contribution of flavin covalent linkage with histidine 99 to the reaction catalyzed by choline oxidase, *J Biol Chem*.

27. Rungsrisuriyachai, K., and Gadda, G. (2008) On the role of histidine 351 in the reaction of alcohol oxidation catalyzed by choline oxidase, *Biochemistry 47*, 6762-6769.

28. Finnegan, S., and Gadda, G. (2008) Substitution of an active site valine uncovers a kinetically slow equilibrium between competent and incompetent forms of choline oxidase, *Biochemistry 47*, 13850-13861.

29. Fan, F., and Gadda, G. (2007) An internal equilibrium preorganizes the enzyme-substrate complex for hydride tunneling in choline oxidase, *Biochemistry 46*, 6402-6408.

30. Fan, F., Germann, M. W., and Gadda, G. (2006) Mechanistic studies of choline oxidase with betaine aldehyde and its isosteric analogue 3,3-dimethylbutyraldehyde, *Biochemistry 45*, 1979-1986.

31. Fan, F., and Gadda, G. (2005) Oxygen- and temperature-dependent kinetic isotope effects in choline oxidase: correlating reversible hydride transfer with environmentally enhanced tunneling, *J Am Chem Soc 127*, 17954-17961.

32. Fan, F., and Gadda, G. (2005) On the catalytic mechanism of choline oxidase, *J. Am. Chem. Soc. 127*, 2067-2074.

33. Gadda, G. (2003) pH and deuterium kinetic isotope effects studies on the oxidation of choline to betaine-aldehyde catalyzed by choline oxidase, *Biochim Biophys Acta 1650*, 4-9.

34. Gadda, G. (2003) Kinetic mechanism of choline oxidase from Arthrobacter globiformis, *Biochim Biophys Acta 1646*, 112-118.

35. Quaye, O., and Gadda, G. (2009) Effect of a conservative mutation of an active site residue involved in substrate binding on the hydride tunneling reaction catalyzed by choline oxidase, *Arch Biochem Biophys 489*, 10-14.

36. Gadda, G. (2008) Hydride transfer made easy in the reaction of alcohol oxidation catalyzed by flavin-dependent oxidases, *Biochemistry 47*, 13745-13753.

37. Quaye, O., Cowins, S., and Gadda, G. (2009) Contribution of flavin covalent linkage with histidine 99 to the reaction catalyzed by choline oxidase, *J Biol Chem 284*, 16990-16997.

38. Ghanem, M., and Gadda, G. (2005) On the catalytic role of the conserved active site residue His466 of choline oxidase, *Biochemistry 44*, 893-904.

39. Minor, Z. O. a. W. (1997) Processing of X-ray Diffraction Data Collected in Oscillation Mode., *Methods in Enzymology 276*, 307-326.

40. McCoy, A. J., Grosse-Kunstleve, R. W., Storoni, L. C., and Read, R. J. (2005) Likelihood-enhanced fast translation functions, *Acta Crystallogr D Biol Crystallogr 61*, 458-464.

41. Murshudov, G. N., Vagin, A. A., and Dodson, E. J. (1997) Refinement of macromolecular structures by the maximum-likelihood method, *Acta Crystallogr D Biol Crystallogr 53*, 240-255.

42. Jones, T. A., Zou, J. Y., Cowan, S. W., and Kjeldgaard, M. (1991) Improved methods for building protein models in electron density maps and the location of errors in these models, *Acta Crystallogr A 47 (Pt 2)*, 110-119.

43. Emsley, P., and Cowtan, K. (2004) Coot: model-building tools for molecular graphics, *Acta Crystallogr D Biol Crystallogr 60*, 2126-2132.

44. Lovell, S. C., Davis, I. W., Arendall, W. B., 3rd, de Bakker, P. I., Word, J. M., Prisant, M. G., Richardson, J. S., and Richardson, D. C. (2003) Structure validation by Calpha geometry: phi,psi and Cbeta deviation, *Proteins 50*, 437-450.

45. Merritt, E. A., and Murphy, M. E. (1994) Raster3D Version 2.0. A program for photorealistic molecular graphics, *Acta Crystallogr D Biol Crystallogr 50*, 869-873.

46. Allison, D. R., and Purich, D. L. (1979) Practical considerations in the design of initial velocity enzyme rate assays, In *Methods Enzymol.* (Purich, D. L., Ed.), pp 3-19, Academic Press, New York.

47. Cook, P. F., and Cleland, W. W. (2007) *Enzyme kinetics and mechanism*, Garland Science, London and New York.

48. Fan, F., and Gadda, G. (2005) On the catalytic mechanism of choline oxidase, *J Am Chem Soc 127*, 2067-2074.

49. Ghanem, M., Fan, F., Francis, K., and Gadda, G. (2003) Spectroscopic and kinetic properties of recombinant choline oxidase from Arthrobacter globiformis, *Biochemistry 42*, 15179-15188.

50. Gadda, G. (2003) Kinetic mechanism of choline oxidase from Arthrobacter globiformis, *Biochim Biophys Acta 1646*, 112-118.

51. Mildvan, A. S. (2004) Inverse thinking about double mutants of enzymes, *Biochemistry 43*, 14517-14520.

CHAPTER V

ON THE IMPORTANCE OF SER101 FOR OVERALL TURNOVER IN CHOLINE OXIDASE

(Publication in preparation 2010 verbatim by Finnegan, S., Yuan, H., Wang, Y., Orville, A.M., Weber, I. and Gadda, G.)

5.1.Abstract

Choline oxidase is a homodimer of 120 kDa, with each subunit containing covalently bound FAD in an 8R-N(1)-histidyl linkage. This oxidase catalyzes the oxidation of choline to glycine betaine through two sequential flavin-linked hydride transfers from choline and the ensuing betaine aldehyde intermediate to the flavin cofactor. The chemical factors affecting how flavin dependent enzymes achieve bimolular rate constants $\geq 10^5$ $M^{-1}s^{-1}$ for the reaction of the reduced flavin with oxygen are not fully understood and as such represent one of the challenging questions in modern flavoenzymology. In the X-ray structure of choline oxidase previously reported, Ser101 is located in proximity of the C(4a) flavin atom, suggesting it may participate in flavin oxidation. Kinetic data show that mutation of Ser101 to alanine in choline oxidase results in an increase in oxygen reactivity, as seen in the second order rate constant for oxygen capture, k_{cat}/K_{oxygen}. Here, we report the three dimensional structure of the Ser101Ala enzyme to a resolution of 2.5 Å. A comparison of the structures of the Se101Ala and wild-type enzymes is also presented.

5.2.Introduction

The reaction of choline oxidation catalyzed by choline oxidase (E.C. 1.1.3.17; choline-oxygen oxidoreductase) has been extensively characterized (*1*). In brief, the reaction includes

two reductive half-reactions where the FAD cofactor is reduced in subsequent steps by the alcohol substrate and the aldehyde intermediate (**Scheme 5.1**) (*2*).

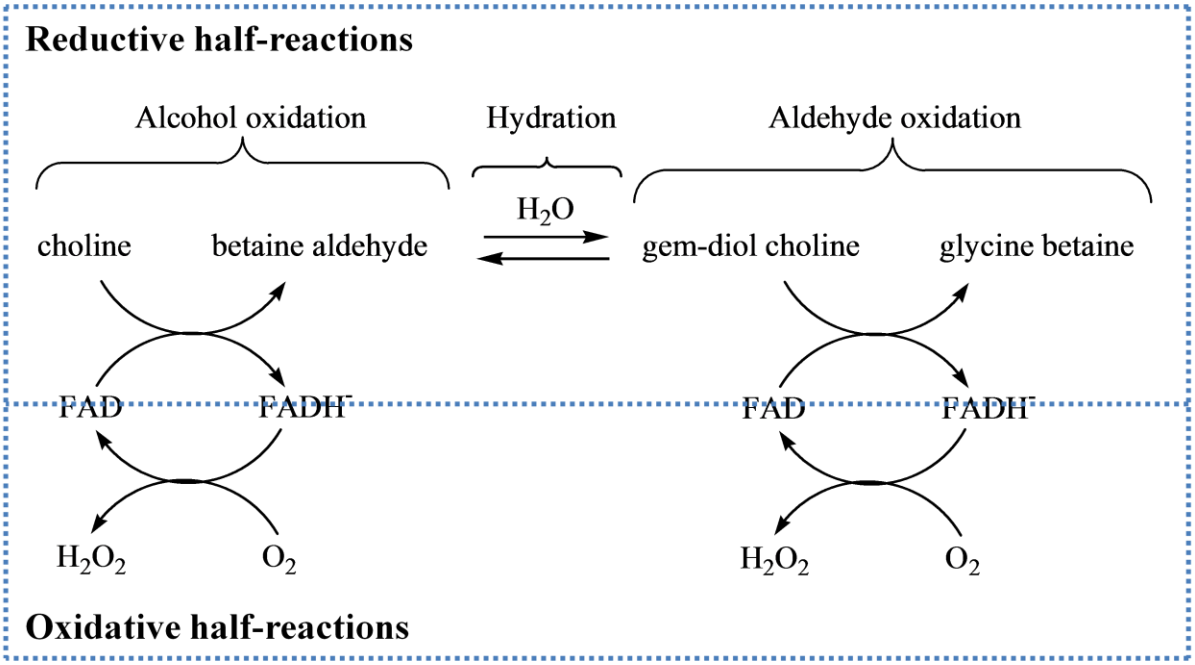

Scheme 5.1: The Steady-state Kinetic Mechanism of Choline Oxidation Catalyzed by Choline Oxidase.

Each reductive half reaction is followed by an oxidative half-reaction where the reduced FAD cofactor is oxidized by molecular oxygen with formation of hydrogen peroxide (*2*). In the wild-type enzyme, the first reductive half-reaction is initiated by a kinetically fast abstraction of the hydroxyl proton of choline, which results in the formation of a transient alkoxide intermediate (*2*). This is followed by a rate-limiting hydride ion transfer from the α-carbon of the alkoxide intermediate to the N(5) atom of the flavin resulting in the oxidation of choline to betaine aldehyde and reduction of the flavin (*2*). Betaine aldehyde is subsequently hydrated in the active site to form *gem*-diol choline (*3*). In the second reductive half-reaction, the *gem*-diol choline is oxidized to the product, glycine betaine. In the oxidative half-reactions the reduced flavin reacts with oxygen by transferring a hydride equivalent to form oxidized flavin and

hydrogen peroxide (*4*). The enzyme must therefore balance the requirements that each of these half-reactions have in order to achieve maximum overall rate of catalysis.

In the crystal structure of wild-type choline oxidase the side chain of Ser101 is less than 4 Å from the N(5) atom of FAD and within hydrogen bonding distance (i.e., <3 Å) of the oxygen atom of DMSO, a ligand that was used in the crystallization of the enzyme (*5*). This suggests that Ser101 may be actively involved in the oxidation of choline catalyzed by the enzyme. Here, we report the overexpression, purification, crystal structure and kinetic characterization of the Ser101Ala variant of the enzyme with choline and betaine aldehyde as substrate. The results are consistent with replacement of the active site serine with alanine yielding a tenfold decrease in both the reductive half-reactions and a threefold to fourfold increase in both the oxidative half-reactions catalyzed by the enzyme. This, in turn, results in a tenfold decrease in the overall turnover of the enzyme, consistent with Ser101 being important to balance and optimize the overall turnover rather than any of the half-reactions that are catalyzed by chorine oxidase.

5.3.Experimental Procedures

The mutant gene for the choline Ser101Ala enzyme was prepared using the QuikChange™ Site-Directed Mutagenesis kit following the manufacturer's instructions in the presence of 2% DMSO, as previously described (*6*-*7*). The pET/*codA*mg plasmid harboring the wild-type gene was used as template (*6*). Upon mutagenesis, the entire mutant gene (pET/*codA*mg-Ser101Ala) was sequenced at the DNA Core Facility of Georgia State University to confirm the presence of the desired mutation. As an expression host, competent *Escherichia coli* strain Rosetta(DE3)pLysS cells were transformed with the mutant plasmid by electroporation. The

mutant enzyme was expressed and purified to homogeneity as previously described for wild-type choline oxidase (*6*-*8*).

Crystals of the Ser101Ala enzyme were grown by the hanging-drop vapor-diffusion method at room temperature. Purified Ser101Ala (2 μL) at a concentration of 5 mg mL^{-1} was mixed with 2 μL from the 500 μL reservoir solution which consisted of 80 mM sodium cacodylate, 20% v/v PEG6000, 20% v/v glycerol, 150 mM Mg-Acetate at pH 6.0.Single crystals were transferred into a cryoprotectant consisting of reservoir solution containing 25% (v/v) glycerol and allowed to soak for approximately 2 min prior to flash-freezing in liquid nitrogen for data collection at Beamline 12B of the National Synchrotron Light Source at *Brookhaven* National Laboratory, NY. The data were integrated, scaled, and merged using the HKL2000 package (*9*). The structures were solved by molecular replacement with PHASER (*10*) using the structure of wild-type choline oxidase (2JBV from the Protein Data Bank) as the starting model (*11*). Refinement was carried out using Refmac5 (*12*) in CCP4 (*13*-*14*) and manual adjustment used the molecular graphics program COOT (*15*). Structural figures were made by PyMol (*16*).

Steady state kinetic parameters were measured with the method of the initial rates (*17*) at varying concentrations of both choline, or betaine aldehyde, and oxygen in 50 mM sodium pyrophosphate, pH 10.0, at 25 ^{o}C. Kinetic assays were performed at pH 10.0 because at this pH value the kinetic parameters k_{cat} and k_{cat}/K_m of choline oxidase are maximal and independent of pH (*4*). Initial rates were determined by monitoring the rate of oxygen consumption with a computer-interfaced Oxy-32 oxygen monitoring system (Hansatech Instrument Ltd.) thermostated at 25 °C. The assay reaction mixture was equilibrated at the desired concentration of oxygen by sparging the appropriate O_2/N_2 gas mixture for 10 min before the reaction was started by the addition of the enzyme. The initial rates measured with choline were fit to eq 1,

which describes a sequential steady state kinetic mechanism in which $K_{choline}$ and K_{oxygen} are the Michaelis constants and k_{cat} is the overall turnover number of the enzyme when saturated with both substrates (e). The initial rates measured with betaine aldehyde were fit to eq 2, which describes a sequential steady state kinetic mechanism where $K_{aldehyde} \ll K_{oxygen}K_{iA}$.

$$\frac{v}{e} = \frac{k_{cat}[choline][oxygen]}{K_{choline}[oxygen] + K_{oxygen}[choline] + [choline][oxygen] + K_{iA}K_{oxygen}} \quad (1)$$

$$\frac{v}{e} = \frac{k_{cat}[betainealdehyde][oxygen]}{K_{aldehyde}[oxygen] + K_{oxygen}[betainealdehyde] + [betainealdehyde][oxygen]} \quad (2)$$

Reductive half-reactions with betaine aldehyde as substrate were carried out by using a Hi-Tech SF-61 stopped-flow spectrophotometer thermostated at 25 °C and pH 10.0. The rate of flavin reduction was measured by monitoring the decrease in absorbance at 454 nm that results from the anaerobic mixing of the enzyme and betaine aldehyde, as previously described for the wild-type enzyme (*2*). Glucose (5 mM) and glucose oxidase (0.5 μM) were added to the substrate and enzyme solutions to scavenge possible trace amounts of oxygen. The mutant enzyme Ser101Ala was mixed anaerobically with an equal volume of betaine aldehyde, obtaining reaction mixtures with 10 μM enzyme and 0.2-5 mM betaine aldehyde. For each concentration of the substrates, the rate constants for flavin reduction were recorded in triplicate, with measurements usually differing by ≤5 %. Stopped-flow traces were fit to eq 3, which describes a single exponential process where k_{obs} is the observed first-order rate constant for flavin reduction, *A* is the value of absorbance at the specific wavelength of interest at time *t*, *B* is the amplitude of the absorbance change, and *C* is an offset value that accounts for the non-zero

absorbance value at infinite time. Kinetic parameters for the reductive half-reactions were determined by using eq 4, where k_{obs} is the observed first-order rate constant for the reduction of the enzyme-bound flavin at any given concentration of substrate, k_{red} is the limiting first-order rate constant for flavin reduction at saturated substrate concentration, and K_d is the macroscopic dissociation constant for binding of the substrate to the enzyme.

$$A = B\exp(-k_{obs}t) + C \quad (3)$$

$$k_{obs} = \frac{k_{red}[betainealdehyde]}{K_d + [betainealdehyde]} \quad (4)$$

5.4.Results

The Ser101Ala enzyme crystallized in the primitive monoclinic space group $P2_1$ with eight subunits in the asymmetric unit. Data to 2.5 Å were used to refine the structure of the Ser101Ala enzyme to a final R-factor of 22.8% **(Table 5.1)**. The final model consisted of residues 1-530[6], the FAD, and ligand acetate in the active site of the enzyme. When the homodimers of the Ser101Ala enzyme were superimposed with those of the wild-type enzyme the average rmsd values were 0.41 Å for 527 equivalent Cα atoms in each chain, showing no significant structural differences between the two enzymes. The active sites of the two structures are compared in **Figure 5.1**, showing no differences in the relative location of the flavin and the active site residues in the two enzymes. Interestingly, although the replacement of the side chain on residue 101 from serine to alanine resulted in loss of hydrogen bonds with His351 and DMSO, a

[6] It is quite common having some disorder at the terminals in crystal structures and as such it is not concerning that only 530 residues are distinguishable in the structure of Ser101Ala, even though the amino acid sequence of choline oxidase contains 546 residues. In fact the wild-type enzyme only has reported coordinates for 528 residues. For the the structures of Ser101Ala and wild-type it is the last 16 or 18 C-terminal residues that are missing, respectively.

cryoprotectant used in the crystallization of the wild-type enzyme, all of the active site residues locate in the same position in the mutant and wild-type enzymes. Moreover, the electron density maps clearly indicate that FAD in the Ser101Ala enzyme is covalently linked to the His99 Nϵ2 atom as seen in the wild-type (*5*).

Table 5.1. Crystallographic Data Collection and Refinement Statistics for Ser101Ala

Space group	$P2_1$
Unit cell dimensions: (Å)	
A	69.26
B	346.03
C	105.92
β	94.33
Unique reflections	150,964
R_{merge} (%) overall (final shell)	11.1(25.8)[a]
I/σ(I) overall (final shell)	14 (3.2)
Completeness (%) overall (final shell)	90.4 (50.3)
Data range for refinement (Å)	10-2.47
R_{cryst} (%)[b]	22.8
R_{free} (%)[c]	29.2
No. of solvent atoms	333
(total occupancies)	(207.3)
RMS deviation from ideality	
Bonds (Å)	0.014
Angle distance (Å)	0.021
Average B-factors (Å^2)	
Main-chain atoms	26.4
Side-chain atoms	27.2
FAD	18.5
Solvent	20.3

[a] Values in parentheses are given for the highest resolution shell

[b] $R_{cryst} = \Sigma|F_{obs}-F_{cal}|/\Sigma F_{obs}$.

[c] $R_{free} = \Sigma_{test}(|F_{obs}|-|F_{cal}|)^2/\Sigma_{test}|F_{obs}|^2$.

A notable difference between the wild-type and the Ser101Ala enzymes is that the isoalloxazine moiety of the FAD cofactor in the variant enzyme is more planar than that of the wild-type. In the latter enzyme, the C(4a) atom was shown to be in an sp^3 hybridization due to the presence of an oxygen adduct that is not observed in the Ser101Ala variant enzyme resulting in the C(4a) atom being sp^2 hybridized (*5, 18*). In the Ser101Ala enzyme the isoalloxazine ring

system showed a slight bend between the two planes containing the benzene and pyrimidine moieties defining an 8^{o} angle along the N(5)-N(10) axis (**Figure 5.1**). A similar bend was previously observed in the structure of another active site mutant form of choline oxidase, where Val464 is replaced with alanine, for which the C(4a) atom of FAD was also shown to be sp^2 hybridized (*19*). All taken together, the major differences observable in the structures of the Ser101Ala and wild-type enzymes are the hybridization of the flavin C(4a) atom and the loss of the hydroxyl group of Ser101.

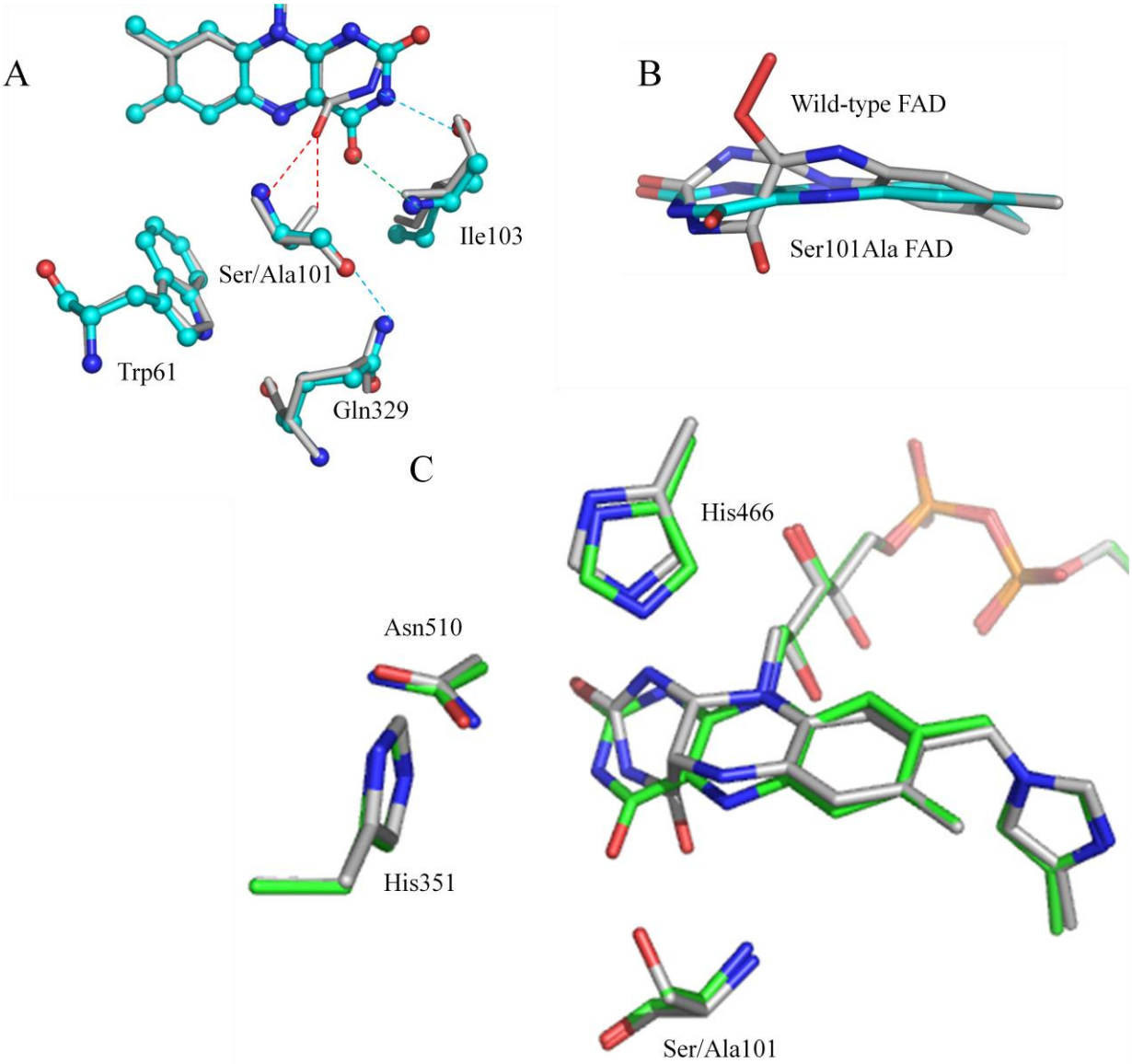

Figure 5.1. Comparison of Crystal Structures of the Ser101Ala and Wild-type Enzymes of

Choline Oxidase. The residues with carbons in green represent the Ser101Ala structure, whereas the carbon atoms for the wild-type enzyme are in gray. Panel A shows the interactions at the Ser101Ala mutation site. Proposed hydrogen bonds in the wild-type enzyme only are colored red, those in the Ser101Ala enzyme are colored green, and those proposed in both enzymes are colored cyan. Panel B illustrates the superposition of the FAD isoalloxazine ring from the wild-type (grey) and the Ser101Ala enzymes (colored by element type) of choline oxidase. Note that the isoalloxazine ring of the Ser101Ala enzyme is more planar than that of the wild-type structure. Panel C shows a comparison of the active sites of wild-type and Ser101Ala choline oxidase. The wild-type enzyme structure is from pdb file 2jbv (*5*).

The steady state kinetic parameters with choline and betaine aldehyde as substrate for the Ser101Ala enzyme were determined (by a colleague graduate student, Ms. Hongling Yuan) at varying concentrations of oxygen, by measuring the initial rates of oxygen consumption with a Clark-type oxygen electrode at pH 10.0 and 25 ^{o}C. As for the case previously reported for the wild-type enzyme (*4*, *20*), the best fits of the data were obtained with eq 1 for choline and eq 2 for betaine aldehyde (**Figure 5.2**).

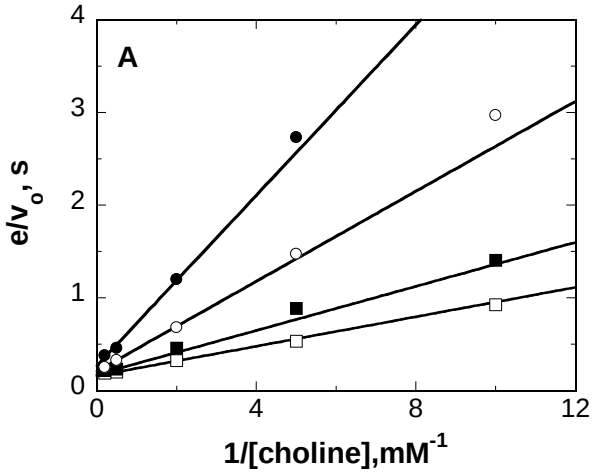

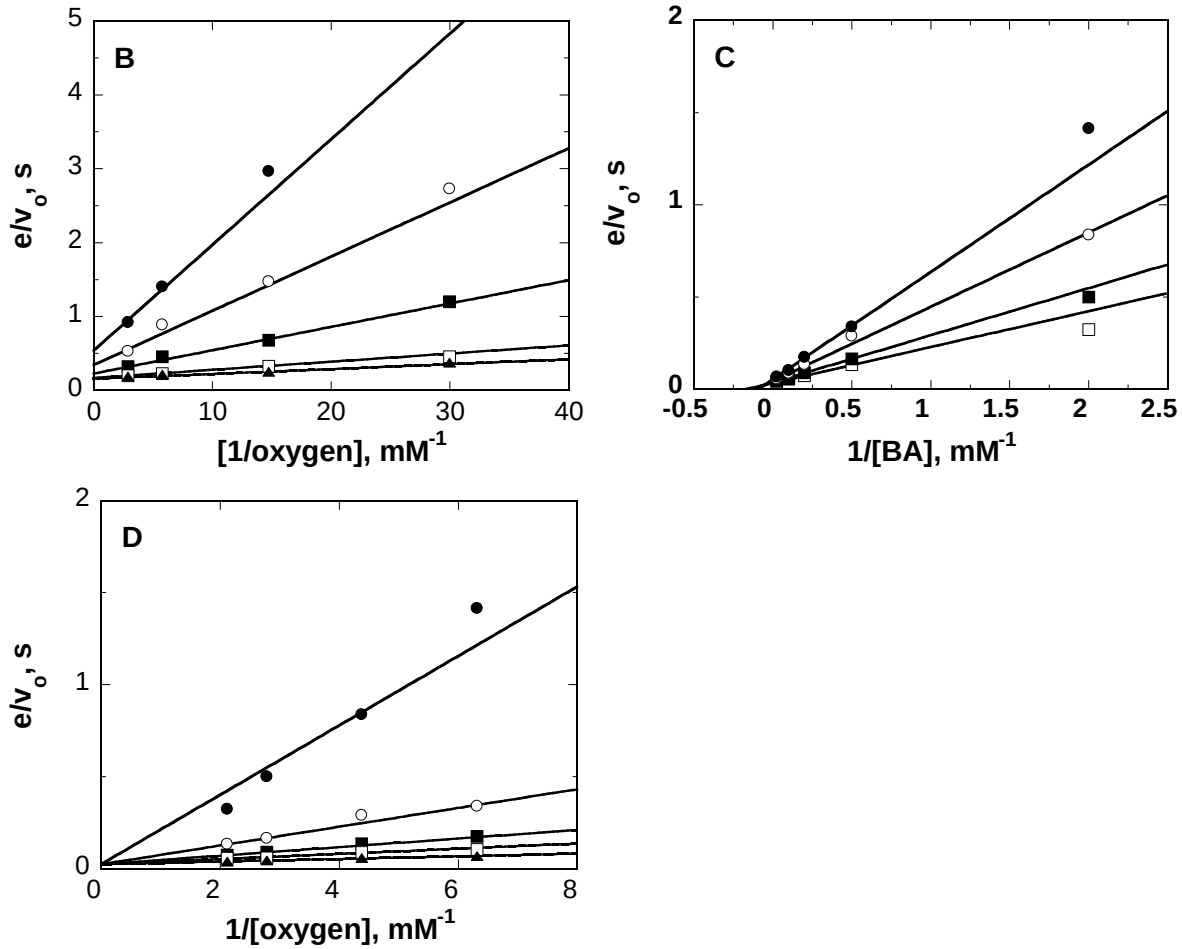

Figure 5.2. Double Reciprocal Plots of CHO-Ser101Ala Catalyzed Oxidation of Choline and Betaine Aldehyde. Choline oxidase activity was measured at varying concentration of both choline and oxygen or betaine aldehyde and oxygen in 100 Mm sodium pyrophosphate, pH 10.0, at 25 ^{o}C, respectively. Panel A, e/v_o as a function of the inverse choline concentration determined at several fixed concentrations oxygen: (●) 0.033 mM; (○) 0.068 mM; (■) 0.172 mM; (□) 0.344 mM. Panel B, e/v_o as a function of the inverse oxygen concentration determined at several fixed concentrations choline: (●) 0.1 mM; (○) 0.2 mM; (■) 0.5 mM; (□) 2 mM; (▲) 5 mM. Panel C, e/v_o as a function of the inverse betaine aldehyde concentration determined at several fixed concentrations oxygen: (●) 0.16 mM; (○) 0.23 mM; (■) 0.36 mM; (□) 0.47 mM. Panel D, e/v_o as a function of the inverse oxygen concentration determined at several fixed concentrations betaine aldehyde: (●) 0.5 mM; (○) 2 mM; (■) 5 mM; (□) 10 mM; (▲) 40 mM.

As summarized in **Table 5.2**, the Ser101Ala enzyme showed between threefold and fourfold increases in the k_{cat}/K_{oxygen} values with choline and betaine aldehyde, and tenfold decrease in both the $k_{cat}/K_{choline}$ and k_{cat} values with choline as substrate.

Table 5.2. Comparison of the Kinetic Parameters of Ser101Ala[a] and Wild-type[b] Choline Oxidase at pH 10.0.

Substrate	kinetic parameters	Ser101Ala	wild-type
Choline	k_{cat}, s^{-1}	6.7 ± 0.1	60 ± 1
	k_{cat}/K_m, $M^{-1}s^{-1}$	25,600 ± 2000	237,000 ± 9000
	k_{cat}/K_{oxygen}, $M^{-1}s^{-1}$	261,000 ± 6500	86,400 ± 3600
	K_m, mM	0.26 ± 0.02	0.25 ± 0.01
	K_{oxygen}, mM	0.026 ± 0.001	0.69 ± 0.03
betaine aldehyde	k_{cat}, s^{-1}	43 ± 3	133 ± 4
	k_{cat}/K_{oxygen}, $M^{-1}s^{-1}$	203,400 ± 33,400	53,400 ± 1600
	K_{oxygen}, mM	0.2 ± 0.03	2.5 ± 0.01
	k_{red}	47 ± 2	135 ± 4
	K_d	0.9 ± 0.1	0.45 ± 0.1

[a] Conditions: 50 mM sodium pyrophosphate, pH 10.0, at 25 °C. [b] From ref (*2*)

Since the $k_{cat}/K_{betaine\ aldehyde}$ value could not be determined by using a steady state kinetic approach due to $K_{aldehyde} \ll K_{oxygen}K_{ia}$, the reductive half-reaction with betaine aldehyde was investigated by mixing anaerobically the enzyme and the substrate in a stopped-flow spectrophotometer at pH 10.0 and 25 °C. As for the case previously reported for the wild-type enzyme (*2*), the absorbance at 454 nm of the Ser101Ala enzyme decreased in a single exponential manner upon mixing with betaine aldehyde (**Figure 5.3**). A plot of the k_{obs} for flavin reduction as a function of the concentration of betaine aldehyde followed saturation kinetics, allowing the determination of the limiting rate constant for flavin reduction at saturated substrate (k_{red}) and the apparent thermodynamic equilibrium constant for the formation of the enzyme-betaine aldehyde complex (K_d). As summarized in **Table 5.2**, the k_{red} and K_d values with betaine aldehyde as substrate for the Ser101Ala enzyme differed by less than threefold from the values

previously determined for the wild-type form of choline oxidase.

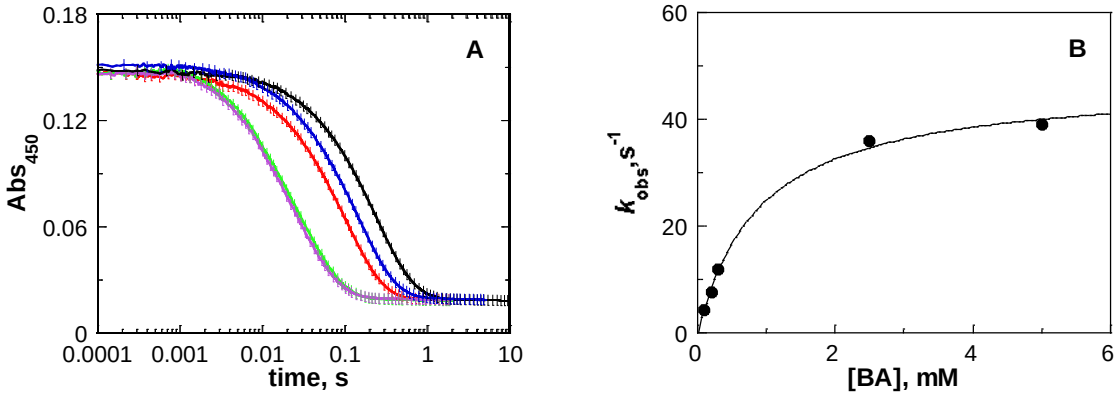

Figure 5.3. Reductive Half-reaction of the Ser101Ala Enzyme with Betaine Aldehyde. Panel a shows the reduction traces with 0.1 mM (black), 0.2 mM (blue), 0.3 mM (red), 2.5 mM (green) and 5 mM (fuscia) betaine aldehyde. All traces were fit to eq 3. Time indicated is after the end of flow, i.e., 2.2 mm. For clarity, one experimental point every 5 is shown (vertical lines). Panel B shows the observed rate constants for flavin reduction as a function of the concentration of betaine aldehyde. Data were fit to eq 4. Buffer used was 50 mM sodium pyrophosphate, pH 10.0.

5.5.Discussion

In choline oxidase, the requirements that each half-reaction have are balanced not to maximize each half-reaction individually but rather to achieve the most efficient overall catalysis. The results presented here indicate that the lack of a hydroxyl group on residue 101 does not result in any overall structural changes to the protein with respect to the wild-type enzyme. In the X-ray crystallographic data of the Ser101Ala enzyme it is seen from the inter atom distance and the orientation of the ligand, acetate, in the active site that, it is likely hydrogen bonded to the N(5) atom of the flavin cofactor as well as the N(3) atoms of the side-chains of Histidine 351 and histidine 466, similar to the DMSO in the active site of the crystal structure of the wild-type choline oxidase.

One observable difference in the structures for the wild-type and the Ser101Ala variant enzymes is the absence of a the C(4a) oxygen adduct, observed in the wild-type enzyme (*5*), on

the FAD cofactor in the Ser101Ala variant enzyme. For the wild-type choline oxidase the enzyme-bound FAD is likely reduced in the X-ray beam during data collection and the reduced FAD then forms either a C(4a)-OH or C(4a)-OO(H) adduct but an insufficient proton inventory prevents the FAD reoxidation to proceed (*18*). The absence of the FAD C(4a) adduct in the Ser101Ala variant enzyme is due to the FAD either not being reduced during the data collection or simply to the presence of a proper proton inventory for a C(4a) oxygen adduct to decay. Alternatively, the C(4a) oxygen adduct may not be as stabilized in the Ser101Ala variant enzyme due to the loss of possible hydrogen bond to the hydroxyl group of the serine 101 in the variant enzyme. Regardless of the reason for the absence of the C(4a) oxygen adduct in the Ser101Ala variant enzyme, the point mutation does not affect the overall structure of the protein moiety of choline oxidase and as such any kinetic differences between the Ser101Ala and the wild-type enzymes can be attributed to the removal of a hydroxyl group at position 101.

Kinetically, there are no significant changes in the K_m value for choline between the Ser101Ala and wild-type enzymes. In contrast, the overall rate of catalysis (k_{cat}) in the Ser101Ala enzyme is significantly slower, whilst having a faster oxidative half-reaction (k_{cat}/K_{oxygen}). Thus, in the Ser101Ala enzyme the requirements for each half-reaction are no longer optimized to yield the highest overall rate of catalysis, but instead the oxidative half-reaction is favored, at the expense of a lowered overall rate of catalysis, meaning the reductive half-reaction must be impaired as compared to the wild-type enzyme. The kinetic favoring of the oxidative half-reaction in the Ser101Ala variant enzyme is likely due to a change in the FAD micro-environment caused by the mutation of serine 101 to an alanine resulting in a change of the redox potential of FAD to make it a stronger reducing agent. Alternatively the increased k_{cat}/K_{oxygen} value in Ser101Ala could be due to increased oxygen accessibility to the C(4a)-N5

region of the flavin or the presence of a water molecule in place of the hydroxyl group of serine 101 being able to stabilize the reaction intermediates of the flavin reoxidation more effectively.

Choline oxidase and numerous choline oxidase variants with mutations in the active site have been investigated thus far and the mutation of Ser101 to an alanine is the only variant that has resulted in a shift of the balance to favor the oxidative half-reaction, thus making the Ser101Ala variant enzyme a very interesting enzyme for further studies on the role of serine in the reaction catalyzed by choline oxidase (*5, 21-23*).

5.6.Acknowledgement

Use of the National Synchrotron Light Source, Brookhaven National Laboratory was supported by the U.S. Department of Energy, Office of Science, Office of Basic Energy Sciences, under Contract No. DE-AC02-98CH10886.

5.7.References

1. Gadda, G. (2008) Hydride transfer made easy in the reaction of alcohol oxidation catalyzed by flavin-dependent oxidases, *Biochemistry 47*, 13745-13753.
2. Fan, F., and Gadda, G. (2005) On the catalytic mechanism of choline oxidase, *J Am Chem Soc 127*, 2067-2074.
3. Fan, F., Germann, M. W., and Gadda, G. (2006) Mechanistic studies of choline oxidase with betaine aldehyde and its isosteric analogue 3,3-dimethylbutyraldehyde, *Biochemistry 45*, 1979-1986.
4. Ghanem, M., Fan, F., Francis, K., and Gadda, G. (2003) Spectroscopic and kinetic properties of recombinant choline oxidase from Arthrobacter globiformis, *Biochemistry 42*, 15179-15188.

5. Quaye, O., Lountos, G. T., Fan, F., Orville, A. M., and Gadda, G. (2008) Role of Glu312 in binding and positioning of the substrate for the hydride transfer reaction in choline oxidase, *Biochemistry 47*, 243-256.

6. Fan, F., Ghanem, M., and Gadda, G. (2004) Cloning, sequence analysis, and purification of choline oxidase from Arthrobacter globiformis: a bacterial enzyme involved in osmotic stress tolerance, *Arch Biochem Biophys 421*, 149-158.

7. Ghanem, M., and Gadda, G. (2006) Effects of reversing the protein positive charge in the proximity of the flavin N(1) locus of choline oxidase, *Biochemistry 45*, 3437-3447.

8. Gadda, G., Powell, N. L., and Menon, P. (2004) The trimethylammonium headgroup of choline is a major determinant for substrate binding and specificity in choline oxidase, *Arch Biochem Biophys 430*, 264-273.

9. Otwinowski, Z., and Minor, W. (1997) Processing of X-ray diffraction data collected in oscillation mode, *Methods Enzymol 276*, 307-326.

10. McCoy, A. J., Grosse-Kunstleve, R. W., Adams, P. D., Winn, M. D., Storoni, L. C., and Read, R. J. (2007) Phaser crystallographic software, *J Appl Crystallogr 40*, 658-674.

11. Berman, H. M., Westbrook, J., Feng, Z., Gilliland, G., Bhat, T. N., Weissig, H., Shindyalov, I. N., and Bourne, P. E. (2000) The Protein Data Bank, *Nucleic Acids Res 28*, 235-242.

12. Murshudov, G. N., Vagin, A. A., and Dodson, E. J. (1997) Refinement of macromolecular structures by the maximum-likelihood method, *Acta Crystallogr D Biol Crystallogr 53*, 240-255.

13. (1994) The CCP4 suite: programs for protein crystallography, *Acta Crystallogr D Biol Crystallogr 50*, 760-763.

14. Potterton, E., Briggs, P., Turkenburg, M., and Dodson, E. (2003) A graphical user interface to the CCP4 program suite, *Acta Crystallogr D Biol Crystallogr 59*, 1131-1137.

15. Emsley, P., and Cowtan, K. (2004) Coot: model-building tools for molecular graphics, *Acta Crystallogr D Biol Crystallogr 60*, 2126-2132.

16. DeLano, W. L. (2002) *The pymol molecular graphics system*, San Carlos, CA.

17. Allison, R. D., and Purich, D. L. (1979) Practical considerations in the design of initial velocity enzyme rate assays, *Methods Enzymol 63*, 3-22.

18. Orville, A. M., Lountos, G. T., Finnegan, S., Gadda, G., and Prabhakar, R. (2009) Crystallographic, spectroscopic, and computational analysis of a flavin C4a-oxygen adduct in choline oxidase, *Biochemistry 48*, 720-728.

19. Finnegan, S., Agniswamy, J., Weber, I. T., and Gadda, G. (2010) Role of Val464 in the Flavin Oxidation Reaction Catalyzed by Choline Oxidase, *Biochemistry*.

20. Gadda, G. (2003) Kinetic mechanism of choline oxidase from Arthrobacter globiformis, *Biochim Biophys Acta 1646*, 112-118.

21. Quaye, O., Cowins, S., and Gadda, G. (2009) Contribution of flavin covalent linkage with histidine 99 to the reaction catalyzed by choline oxidase, *J Biol Chem 284*, 16990-16997.

22. Rungsrisuriyachai, K., and Gadda, G. (2008) On the role of histidine 351 in the reaction of alcohol oxidation catalyzed by choline oxidase, *Biochemistry 47*, 6762-6769.

23. Ghanem, M., and Gadda, G. (2005) On the catalytic role of the conserved active site residue His466 of choline oxidase, *Biochemistry 44*, 893-904.

CHAPTER VI

ON THE ROLE OF THE ACTIVE SITE RESIDUE HIS310 OF CHOLINE OXIDASE

(This chapter contains data (**Figures 6.6 and 6.7**) from experiments conducted by Dr M. Ghanem, which have been added for completeness. The data presented in **Figures 6.6 and 6.7** were also acquired subsequently by Steffan Finnegan)

6.1.Abstract

The presence of a protein positive charge close to the N(1)-C(2) locus of the flavin cofactor is a common characteristic feature of many flavoprotein oxidases. In choline oxidase (E.C. 1.1.3.17) from *Arthrobacter globiformis* studies have revealed that the positive charge in the active site is provided by His466, which is located at a distance of ~3.3 Å from the N(1)-C(2) locus of the enzyme-bound flavin (His466$^{N\varepsilon 2}$-N(1)-FAD). From the X-ray crystal structure of choline oxidase a second histidine residue, His310, is located ~2.9 Å from His466. The orientation of the side-chains of both histidine residues suggests the presence of a His466$^{N\delta 1}$-His310$^{N\delta 1}$ hydrogen bond. To assess the contribution made by His310 to catalysis, mutant forms of the enzyme were prepared in which the active site residue His310 was substituted with alanine, asparagine or aspartate. Upon purification of the Ala310, Asn310 and Asp310 variant enzymes polarographic measurements showed no catalytic activity with choline as substrate, suggesting His310 being essential for catalysis. However, spectrophotometrically, the FAD cofactor in the variant enzymes were still able to be reduced with rate constants ~ 10^5 time slower than the wild-type enzyme under anaerobic conditions upon mixing with choline. Choline being able to reduce the FAD cofactor is consistent with the variant enzymes retaining the ability to bind choline upon mutation of His310. The results obtained herein also indicated the involvement of His310 in the flavinylation process in choline oxidase, as the mutation of His310 resulted in a significant alteration of the stoichiometric amount of the flavin. Therefore, these

results together with the structural information suggest an important role of His310 in catalysis and the modulation of the microenvironment of the enzyme-bound flavin. The existence of a proton transfer network consisting of the side-chains of His466, His310 and the backbone carbonyl oxygen atoms of Thr380 and Val507 is proposed as the basis for the mechanism by which His310 affects catalysis in choline oxidase.

6.2.Introduction

Choline oxidase (E.C. 1.1.3.17) from *Arthrobacter globiformis* is a flavin-dependent cytosolic enzyme that catalyzes the oxidation of choline to glycine betaine via an enzyme-bound aldehyde intermediate (**Scheme 6.1**). Choline oxidase has been characterized in its biophysical, structural, and mechanistic properties. The enzyme is a homodimer with a mass of 120 kDa (*1*), containing a covalently linked FAD in a 1:1 stoichiometry (*1*), that during turnover cycles between its fully oxidized and reduced states (*2-3*). A detailed picture of the mechanism of the reaction catalyzed by choline oxidase was obtained from the biophysical, kinetic, structural and mechanistic studies of the wild-type choline oxidase as well as selected mutant forms of the enzyme (*2-9*). In summary, during the reductive half-reaction, the alcohol substrate, choline, is activated through proton abstraction from its hydroxyl group by an unidentified active site base with pK_a of 7.4 with the subsequent formation of an alkoxide species (*2*). This choline alkoxide intermediate species is transiently stabilized in the active site through electrostatic interaction with the protonated imidazole side-chain of His466 (**Figure 6.1**) (*8*). A hydride transfer from the α-carbon of the substrate to the N(5) atom of the isoalloxazine nucleus of the enzyme-bound FAD occurs quantum mechanically from the activated choline alkoxide species (*4*). The

positively charged trimethylammonium headgroup of the substrate is the major determinant for substrate binding and specificity, with little participation of the ethyl moiety (*7*).

The presence of a protein positive charge close to the N(1) atom of the bound flavin is a common feature of many flavoprotein oxidases. Studies have shown that this positive charge is provided by His466 in choline oxidase (*10*, *11*), which is located at a distance of ~3.3 Å from the N(1) locus of the enzyme-bound flavin (His466$^{N\varepsilon 2}$-N(1)-FAD) (*10*). The X-ray crystal structure of choline oxidase also showed that another histidine residue, His310, is at a distance of ~2.9 Å from His466 (**Figure 6.2**). In addition, the X-ray crystallographic data of the wild-type enzyme also showed that the N(3) atom of His310 is located at a distance of ~2.8 Å from the carbonyl main chain oxygen atoms of Thr380 and Val507 (**Figure 6.2**). These structural data suggest that His466 is hydrogen bonded to both N(1)-FAD and His310$^{N\delta 1}$ through its N(3) and N(1) atoms, respectively. Moreover, these data also suggest that His310 is hydrogen bonded to the peptidyl oxygen atoms of Thr380 and Val507 through its N(3) atom (**Figure 6.2**).

In the present study, to assess the contribution made by His310 in catalysis, mutant forms of choline oxidase were prepared in which His310 was substituted with alanine, asparagine or aspartate.

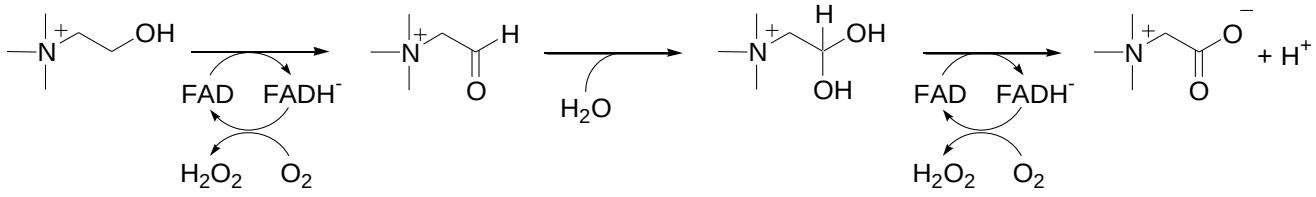

Scheme 6.1. Reaction Catalyzed by Choline Oxidase.

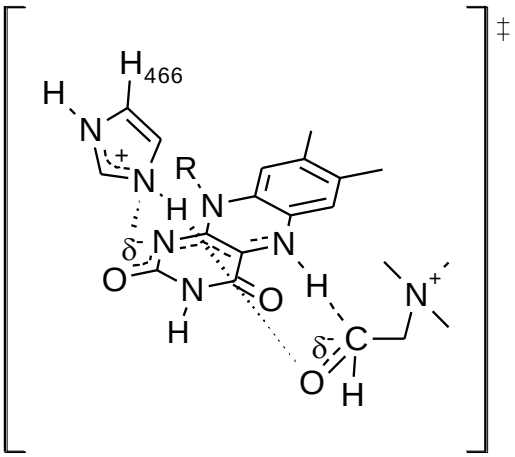

Figure 6.1. Line Drawing Showing the Interaction of His466 with the N(1)−C(2)═O Locus of FAD and the Intermediate Alkoxide Species in the Transition State for the Oxidation of Choline Catalyzed by Choline Oxidase. The positioning of His466 relative to the flavin is from the X-ray crystallographic structure of the enzyme (*10*), the positioning of choline is arbitrary.

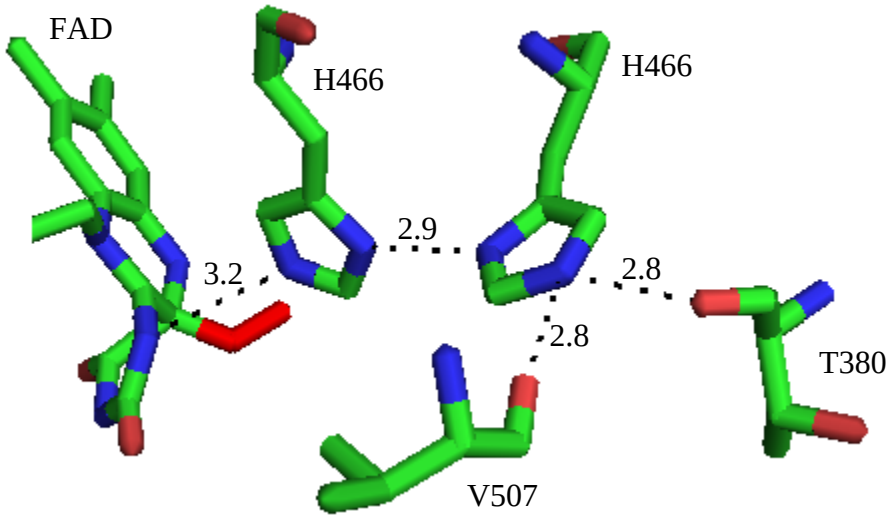

Figure 6.2. Crystal Structure of Choline Oxidase. X-ray Crystallographic Structure of the Active Site of Choline Oxidase Determined at 1.86 Å Resolution (*10*).

6.3.Experimental Procedures

Materials. *Escherichia coli* strain Rosetta(DE3)pLysS was from Novagen (Madison, WI). DNase was from Roche (Indianapolis, IN). The QuikChange site-directed mutagenesis kit was from Stratagene (La Jolla, CA). The QIAprep Spin Miniprep kit was from Qiagen (Valencia, CA). Oligonucleotides used for sequencing of the mutant genes were custom synthesized by

Sigma Genosys (Woodland, TX). Choline chloride was from ICN Pharmaceutical Inc (Irvine, CA). All other reagents were of the highest purity commercially available.

Site-Directed Mutagenesis. The His310Ala, His310Asp, and His310Asn variant enzymes were prepared using the pET/*codAmg* plasmid harboring the wild-type gene for choline oxidase as template for site-directed mutagenesis as previously described (*8*). The presence of the desired mutations were confirmed by sequencing the entire mutagenized genes. *Escherichia coli* strain Rosetta(DE3)pLysS competent cells were transformed with the mutant plasmids by electroporation (*1, 10-12*).

Enzyme Expression and Purification. The His310Ala, His310Asp, and His310Asn variant enzymes were expressed and purified to homogeneity using the procedure described previously for the purification of the wild-type enzyme with the modification of adding 10% glycerol to all solutions (*1, 3, 8*). The protein concentrations of the variant enzymes were determined with the method of Bradford (*13*). Expression levels and purity were determined using SDS-PAGE (*14*). *Spectrophotometric Studies.* The UV-visible absorbance spectra of the His310Ala, His310Asp, and His310Asn variant enzymes were acquired in 20 mM Tris-Cl and 10% glycerol, pH 8.0, at 15 °C. The extinction coefficient of the three variant and the wild-type enzymes were determined in 20 mM sodium pyrophosphate and 10% glycerol, pH 8.0 after denaturation of the enzymes by incubation at 40 °C for 1 h in the presence of 4M urea, based upon the ε_{450} value of 11.3 mM^{-1} cm^{-1} for free FAD (*15*). For the quantification of the ratio of the covalently bound flavin to the enzyme, enzymes were incubated on ice for 30 min after the addition of 10 % trichloroacetate,

followed by removal of precipitated protein by centrifugation, and the determination of the concentration of FAD in the ensuing supernatant solution.

The oxidized flavin content per enzyme active site was determined spectrophotometrically as previously described for the wild-type enzyme (*3*).

Enzyme Assays. The enzymatic activities of the His310Ala, His310Asp, and His310Asn variant enzymes were measured by the method of initial rates as described for the wild-type enzyme (*3, 16*) using a computer-interfaced Oxy-32 oxygen-monitoring system (Hansatech Instrument Ltd.). The effect of incubation with exogenous imidazole on this catalytic activity of the His310Ala enzyme was determined by measuring the enzymatic activity with 10 mM choline as substrate for the enzyme in the presence of 100 mM of imidazole in air-saturated 50 mM sodium pyrophosphate, pH 6.0 or 10.0.

The anaerobic reductions of the His310Ala, His310Asp, and His310Asn variant enzymes with choline as a reductant were measured in 20 mM Tris-Cl and 10% glycerol, pH 8.0 and 15 ^{o}C. The reaction mixtures were made anaerobic by a 25-cycle treatment of alternating evacuation and re-equilibration with oxygen-free argon (pre-treated with an oxygen scrubbing cartridge, Agilent, Palo Alto, Ca) in an anaerobic cell equipped with two side arms. The organic substrate, choline, was loaded into one side arm and the enzyme was loaded into the main chamber. Upon completion of the 25-cycle anaerobic treatment, the enzyme and substrate were mixed and incubated anaerobically for 16-40 h. The progress of the FAD reduction was monitored using an Agilent Technologies diode-array spectrophotometer Model HP 8453. Upon complete reduction, the reduced enzyme mixture was exposed to atmospheric oxygen and was monitored for 12-24 h in an Agilent Technologies diode-array spectrophotometer Model HP 8453.

Data Analysis. Reduction data traces were fit with equation 1, which describes a double-exponential process, in which k_{obs1} and k_{obs2} are the observed rate constants for the change in absorbance of the flavin peak centered around 455 nm, *A* is the value of absorbance at the specific wavelength of interest at time *t*, B and C are the amplitudes of the absorbance changes for the fast and slow observed phases, and D is an offset value that accounts for the non-zero absorbance value at infinite time.

$$A = B\exp(-k_{obs1}t) + C\exp(-k_{obs2}t) + D \quad (1)$$

Data points obtained for the observed rate of flavin reduction were fit to eq 2, where k_{obs} is the observed rate for the reduction of enzyme bound flavin, k_{red} is the limiting first-order rate constant for flavin reduction at saturating substrate concentrations, and K_d is the macroscopic dissociation constant for binding of choline to the active enzyme.

$$k_{obs} = \frac{k_{red}[choline]}{K_d + [choline]} \quad (2)$$

6.4.Results

Expression and Purification. The His310Ala, His310Asp, and His310Asn variant enzymes were expressed and purified to high degree and quantity, as established by SDS-page, Bradford assay and spectrophotometrically, using the same protocol established for the wild-type choline oxidase (*1, 3, 8*). Polarographically, neither of the variant enzymes, at final concentrations as high as 20 μM of purified enzyme, with and without exogenous imidazole incubation, showed any catalytic activity toward its organic substrate choline at final concentrations of 20-30 mM at pH 7.0, at 25 °C. In comparison, the wild-type enzyme, at a final concentration of 0.1 μM purified enzyme, typically shows a catalytic activity of ~15 s^{-1} with 10 mM choline (*16*).

Flavin Properties. The UV-visible absorbance spectra of the oxidized and fully reduced forms of the variant enzymes at pH 8.0 are shown in **Figure 6.3**. The spectra for the oxidized form of the variant enzymes are consistent with the typical spectrum of the oxidized flavin with absorbance peaks centered at 365 nm and 455 nm, suggesting that the enzyme-bound flavin cofactor in the variant enzymes is purified in the oxidized redox state (*17-18*).

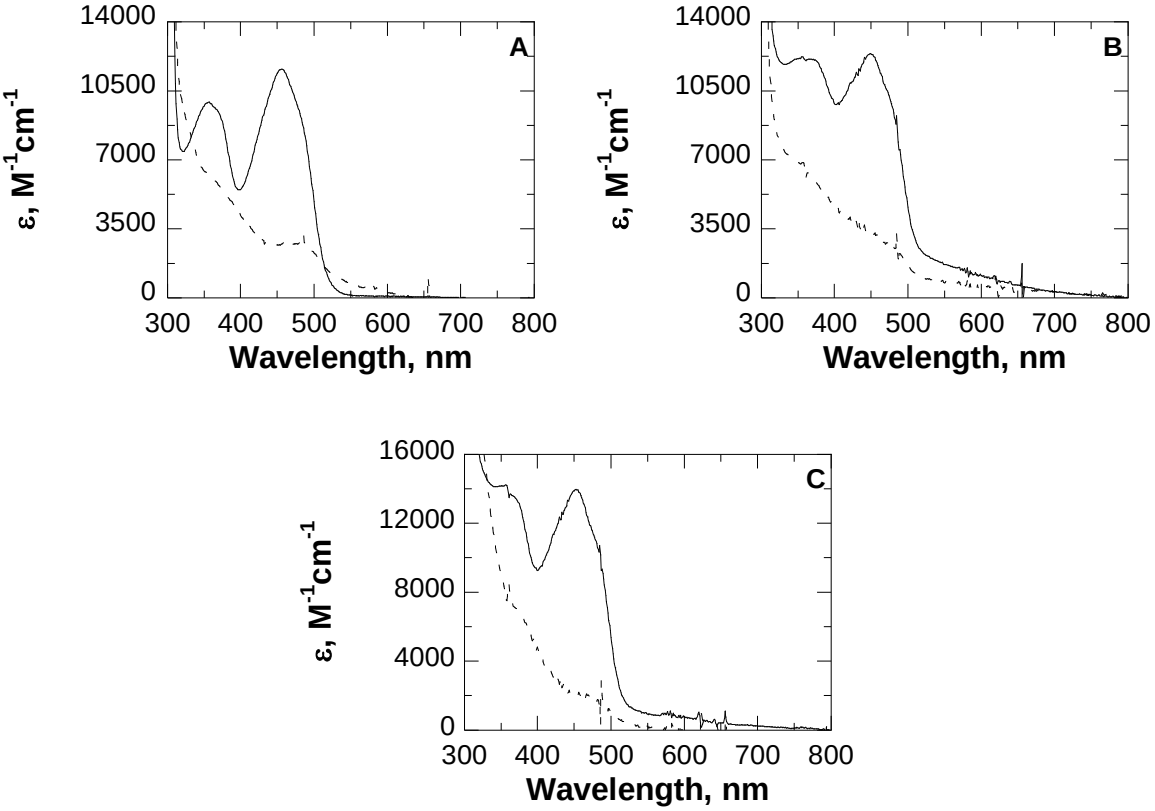

Figure 6.3. Spectral Properties of the His310 Variant Enzymes. Panel A shows the spectra for the oxidized and the reduced forms of His310Ala, Panel B shows the same spectra for His310Asp, and Panel C shows the spectra for His310Asn. Solid curves, UV-visible absorbance spectrum of oxidized form of variant enzymes in 20 mM Tris-Cl and 10% glycerol, pH 8.0; dashed curves, reduced form of variant enzymes in 20 mM Tris-Cl and 10% glycerol, pH 8.0.

The spectra for the reduced form of the variant enzymes show that the variant enzymes stabilize the neutral form of the hydroquinone (characterized by no peak at ~340 nm and the

presence of a shoulder at ~450 nm) as compared to the anionic hydroquinone (characterized by a peak at ~340 nm and no shoulder at ~450 nm) in the wild-type enzyme (*17-18*).

Small changes in the extinction coefficients for the flavin peak around 455 nm were determined for the variant enzymes as compared to the wild-type enzyme. Additionally, the FAD cofactor was determined to be covalently bound in the variant enzymes, however, with a significantly lower stoichiometry of the FAD/active site as compared to the wild-type enzyme as summarized in **Table 6.1**. A stoichiometry of ~0.3 FAD per monomer of protein was previously determined for two choline oxidase variant enzymes with point mutations of histidine 466 (*8-9*).

Table 6.1. Flavin Properties of the His310Ala, His310Asp, and His310Asn Variant Enzymes

Enzyme	**Stoichiometry (FAD/monomer)**	**ε $M^{-1}cm^{-1}$**	**Reduced form**
His310Ala	0.1	11,600 (457 nm)	Neutral hydroquinone
His310Asp	0.1	12,400 (454 nm)	Neutral hydroquinone
His310Asn	0.1	13,900(452 nm)	Neutral hydroquinone
Wild-type (*1*)	0.9	11,400 (452 nm)	Anionic hydroquinone

The folding topology of the histidine 310 variant enzymes was probed with near and far UV circular dichroism as well as FAD and tryptophan flouresence (**Figure 6.4**). However, the collected spectra were all inconclusive (spectra contained similar peaks, but with a significant variation in the peak heights) regarding the similarity of the folding between the wild-type and variant enzymes. As a consequence, the crystal structure of the variant enzymes is required for comparison and establishing the degree of similarity of the structures of the wild-type and the variant enzyme.

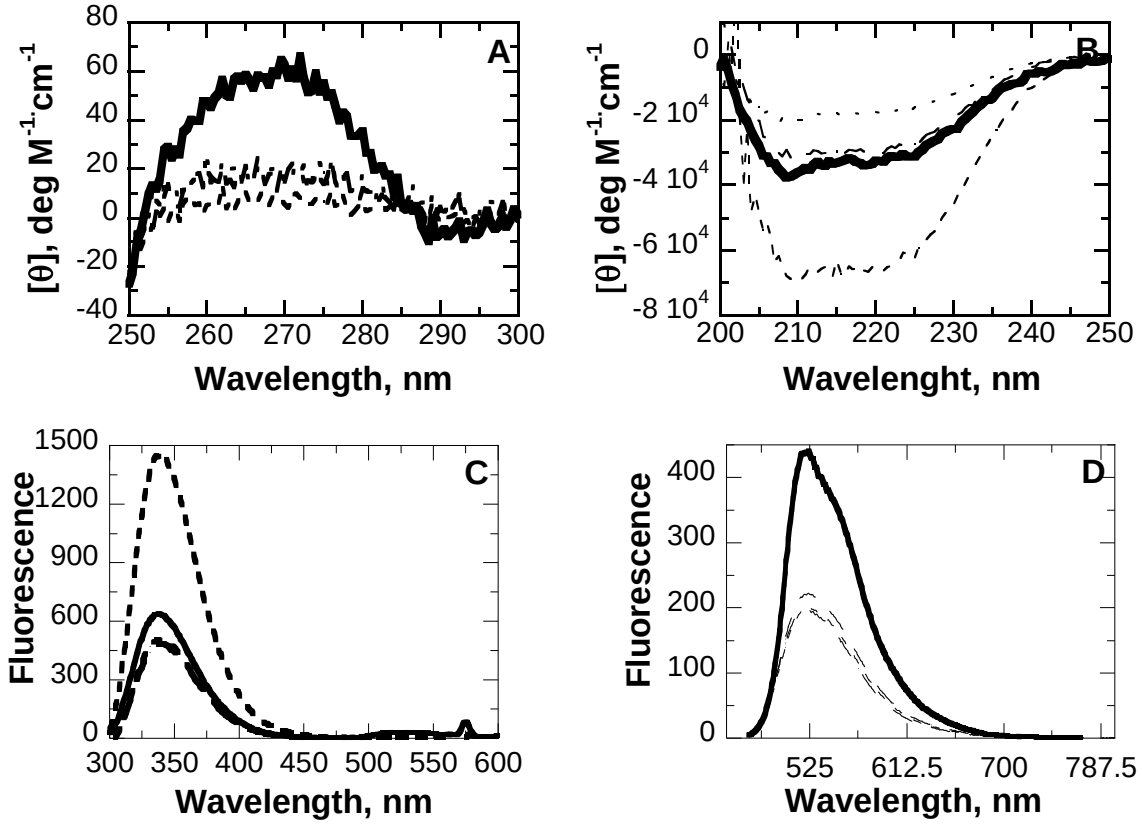

Figure 6.4. Circular Dichroism and Fluorescence of the His310Ala, His310Asp and His310Asn Variant Enzymes as well as the Wild-type Enzyme. Panel A shows the near UV circular dichroism spectra at pH 6.0, panel B shows the far UV circular dichroism spectra at pH 6.0, panel C shows the tryptophan fluorescence at pH 6.0 and panel D shows the FAD fluorescence at pH 6.0. Solid curves, wild-type choline oxidase; dashed curves, histidine 310 variant enzymes.

Reaction of Variant Enzymes with Choline. Purified His310Ala, His310Asp, and His310Asn variant enzymes at final concentrations as high as 20 μM showed no oxygen consumption when assayed with 20-30 mM choline as a substrate at pH 7.0 and 25 °C.

However, anaerobic mixing of the variant enzymes with choline at a final concentration of 10 mM resulted in a biphasic reduction (**Figure 6.5**) of the oxidized enzyme-bound flavin. The fast phase started right after mixing the enzyme with its organic substrate and lasted for ~30 min and the second phase lasted in excess of 16 h resulting in the full reduction of the bound flavin.

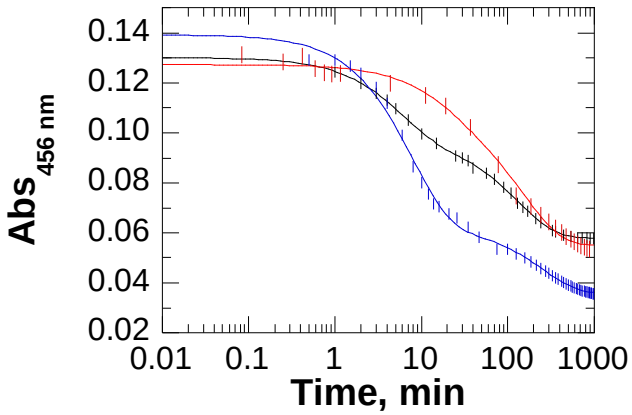

Figure 6.5. Time Resolved, Anaerobic Reduction of the His310Ala, His310Asp and His310Asn Variant Enzymes with Choline in 20 mM Tris-Cl, pH 7.0 and at 15 °C Monitored at 456 nm in a Spectrophotometer. The reduction traces for the His310Ala enzyme with 10 mM choline (black), the His310Asp enzyme with 10 mM choline (red) and the His310Asn enzyme with 10 mM choline (blue). All traces were fit with eq. 1.

The reductive half-reactions in which the His310Ala and His310Asn variant enzymes are reduced anaerobically with choline were investigated using a stopped-flow spectrophotometer by measuring the rates of decrease in absorbance at 456 nm as a function of the concentration of choline in 20 mM Tris-Cl, pH 8.0 and 25 ^{o}C, under pseudo-first order conditions (i.e., 20 μM enzyme and ≥100 μM substrate). For both variant enzymes anaerobic mixing with choline at final concentrations ranging from 0.75 to 20 mM displayed a biphasic reduction lasting for ~16-40 h resulting in the bound flavin being reduced to the neutral hydroquinone. The spectra of the oxidized and the reduced forms a His310Ala, for each of the choline concentrations tested, are shown in **Figure 6.6** and the corresponding reduction traces are shown in **Figure 6.7**. Interestingly, for all histidine 310 variant enzymes investigated, no flavin reoxidation was detectable upon exposing the fully reduced enzymes to atmospheric oxygen for more than 12 hours.

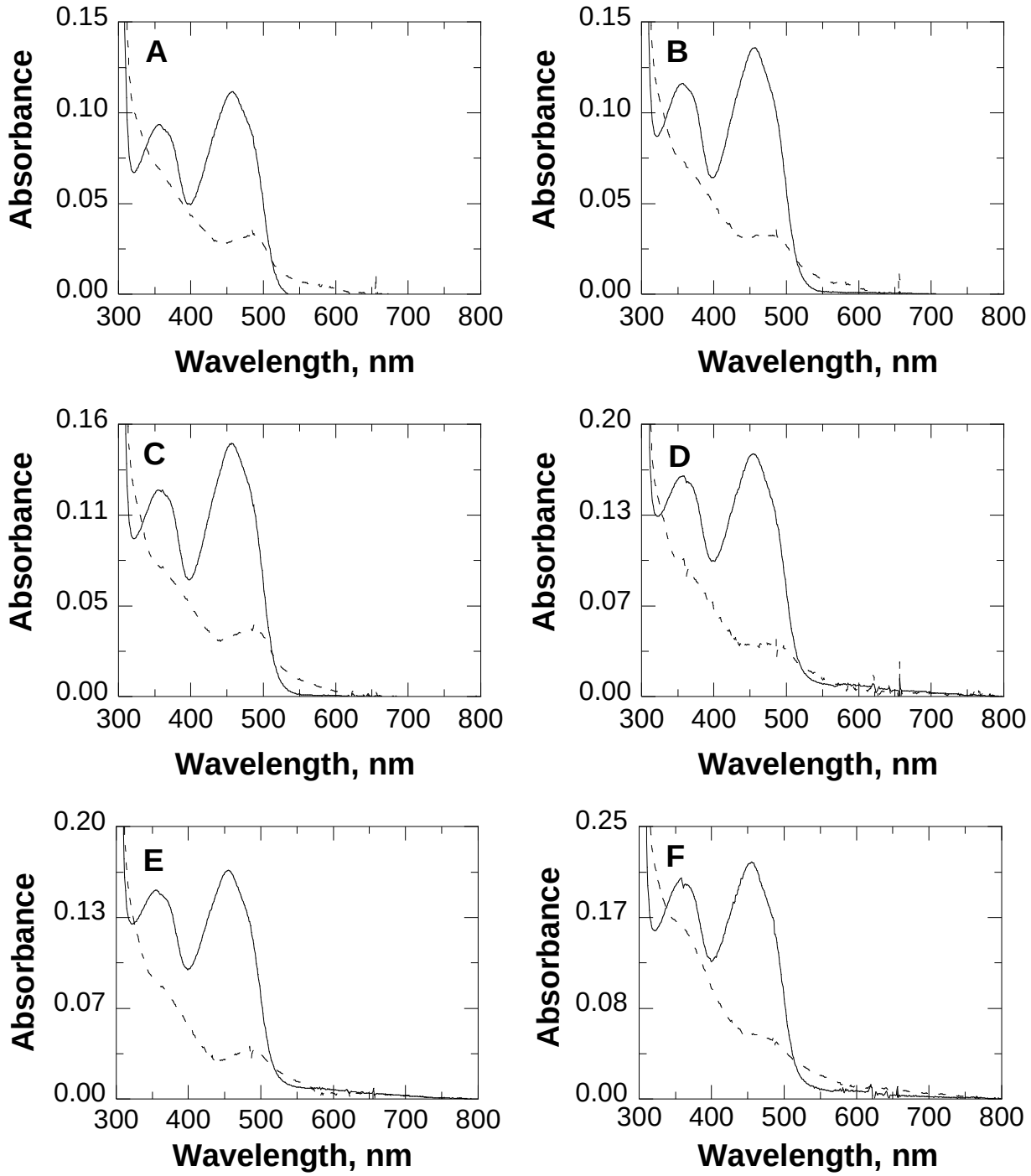

Figure 6.6. Anaerobic Spectra of the Oxidized and Reduced Form of the His310Ala Variant Enzyme, pH 8.0, at 15 °C. *Solid curves*, UV-visible absorbance spectra of the oxidized form of His310Ala prior to mixing with choline; *dashed curves*, UV-visible absorbance spectra of the reduced form of His310Ala post anaerobic mixing with 0.75 mM of choline for 40 h (*panel A*), 1 mM choline for 16 h (*panel B*), 1.5 mM choline for 16 h (*panel C*), 2 mM choline for 16 h (*panel D*), 5 mM choline for 16 h (*panel E*), and 10 mM choline for 5.5 h (*panel F*). (Modified from (*19*))

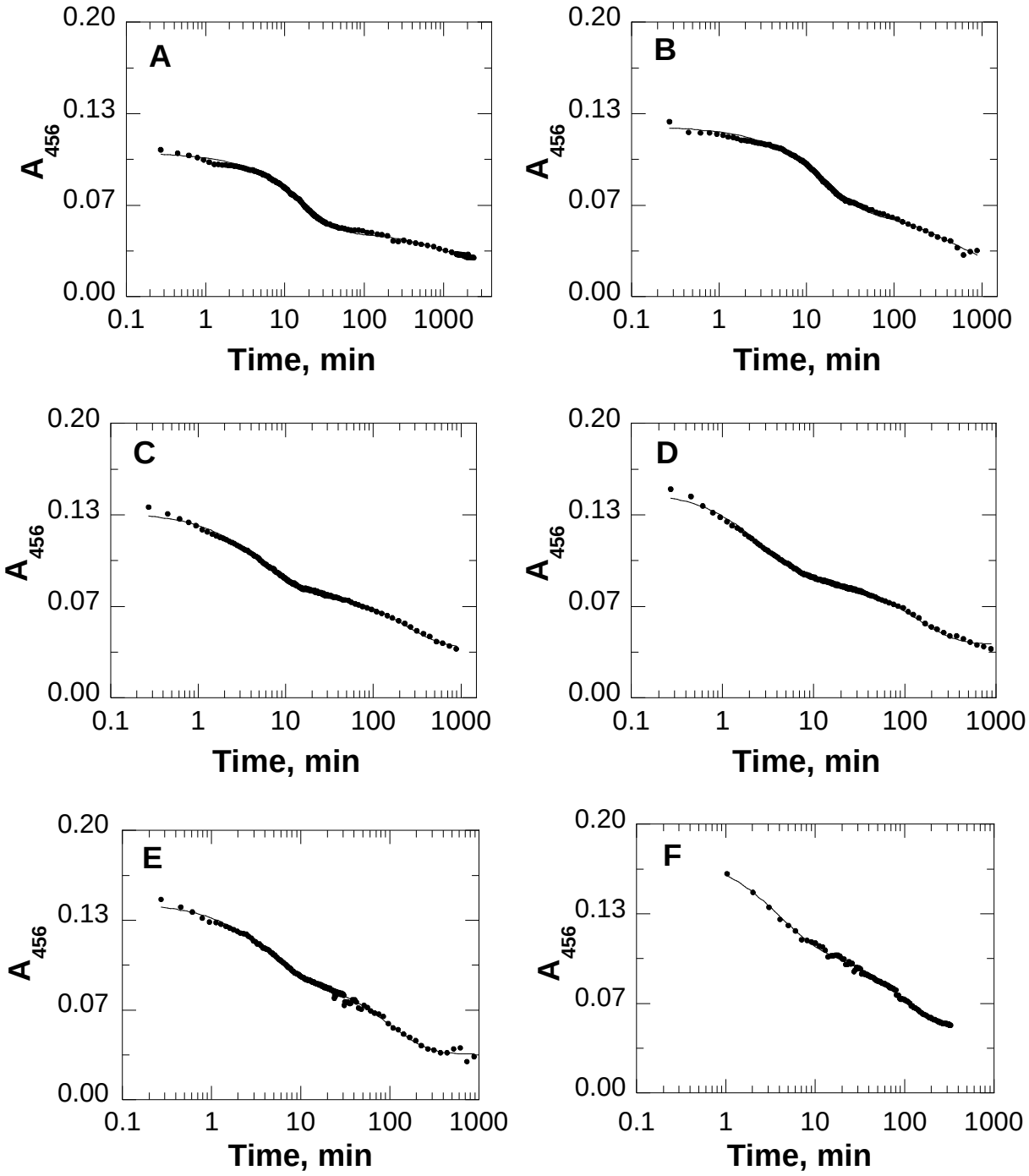

Figure 6.7. Anaerobic Reduction Traces of the His310Ala Variant Enzyme with Choline, pH 8.0, at 15 °C. UV-visible absorbance values (•) at 456 nm as a function of time after the anaerobic mixing of the variant enzyme with 0.75 mM of choline for 40 h (panel A), 1 mM choline for 16 h (panel B), 1.5 mM choline for 16 h (panel C), 2 mM choline for 16 h (panel D), 5 mM choline for 16 h (panel E), and 10 mM choline for 5.5 h (panel F). The reduction traces were all fit with eq 1. (Modified from (19))

The results of the FAD reduction in the His310Asn and His310Ala variant enzymes with choline are summarized in **Table 6.2**.

The ability of the His310Asn and His310Ala variant enzymes to be reduced upon mixing with the organic substrate choline suggests that although they do not show any catalytic activity toward choline as measured polarographically, they are still capable of binding and oxidizing choline.

Table 6.2. Anaerobic Reduction of His310Ala and His310Asn with Choline [a]

	Wild-type[c]	**His310Ala**		**His310Asn**	
[Choline], mM	k_{red} s^{-1}	Fast phase k_{obs1}, min^{-1}	Slow phase $k_{obs2} \times 10^3$, min^{-1}	Fast phase k_{obs1}, min^{-1}	Slow phase $k_{obs2} \times 10^3$, min^{-1}
0.75		0.06 ± 0.001	1.0 ± 0.1	Nd.[b]	Nd.[b]
1		0.06 ± 0.001	2.0 ± 0.3	0.10 ± 0.002	12 ± 0.5
1.5		0.19 ± 0.002	4.0 ± 0.1	0.16 ± 0.010	27 ± 2.0
2		0.35 ± 0.005	7.0 ± 0.2	0.12 ± 0.006	34 ± 0.1
5		0.23 ± 0.005	10 ± 0.3	1.08 ± 0.06	66 ± 1.1
10		0.26 ± 0.01	11 ± 0.2	2.64 ± 0.30	48 ± 1.4
20	93	0.13 ± 0.005	6.0 ± 0.5	0.48 ± 0.005	74 ± 3.5

[a] Enzyme concentrations were ~20 μM in 20 mM Tri-Cl and 10 % glycerol, pH 8.0, at 15 °C. [b]Not determined. [c]Limiting rate of reduction, k_{red} at pH 10.0 (*20*).

The data points obtained for the observed rate of the fast phase of anaerobic flavin reduction, k_{obs1}, for His310Ala and His310Asn as a function of choline concentration were scattered and did not allow the determination of the k_{red} and the K_d by fitting with equation 2 (**Figure 6.8A and C**). Even though the data points obtained for the slow phase of flavin reduction for both His310Ala and His310Asn variant enzymes are scattered, the overall trend is consistent with what is expected for a first-order rate constant and as such, it is reasonable to fit the data with

equation 2. The value obtained for k_{red} for His310Ala was ~550,000-fold lower than that for wild-type enzyme at pH 10.0 and 25 °C (2×10^{-4} s^{-1} *vs.* 93 s^{-1}), and the value determined for K_d was at ~5-fold higher than that of wild-type enzyme (1.8 mM *vs.* 0.3 mM) (*2*). For the His310Asn variant enzyme k_{red} was ~70,000-fold lower than that for wild-type enzyme at pH 10.0 and 25 °C (1×10^{-3} s^{-1} *vs.* 93 s^{-1}), and the value determined for K_d was approximately one order of magnitude larger than that of wild-type enzyme (2.9 mM *vs.* 0.3 mM).

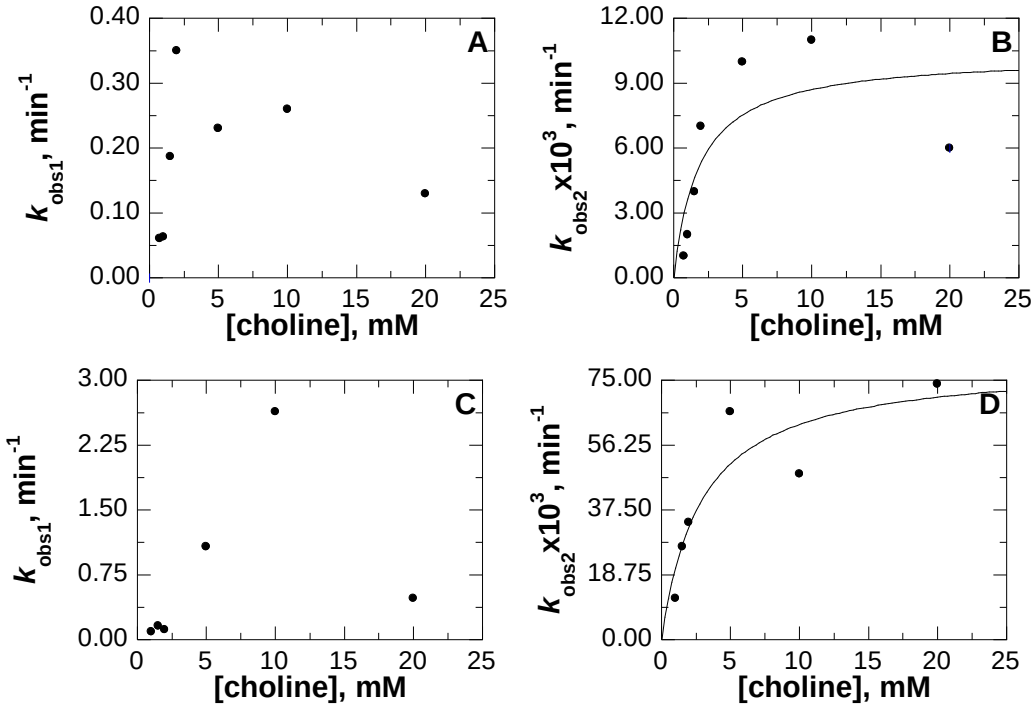

Figure 6.8. Anaerobic Flavin Reduction of His310Ala and His310Asn. Observed Rate (•) of the Decrease of Absorbance at 456 nm as a Function of Choline Concentration for the Fast Phase of His310Ala (*panel A*), for the slow phase of His310Ala (*panel B*), for the fast phase of His310Asn (*panel C*) and for the slow phase of His310Asn (*panel D*).

The scattering of the data points pertaining to the fast phase of flavin reduction could be attributed either to the rate of reduction of being substrate independent, or to the variant enzymes undergoing a conformational change prior to flavin reduction as a result of the substitution of residue His310.

6.5.Discussion

Even though the choline oxidase variant enzymes with the histidine residue at position 310 replaced with alanine, asparagine or aspartate show no catalytic activity toward its organic substrate choline as measured polarographically, the anaerobic reduction results clearly suggest that they are still capable of binding and oxidizing choline. The mutation of residue 310 resulted in changes to the flavin microenvironment that caused the flavin cofactor to be reduced to the neutral hydroquinone in the variant enzymes rather than the anionic hydroquinone as in the wild-type enzyme. Additionally, a significantly lowered ratio of holoenzyme/apoenzyme suggests that histidine 310 significantly affects the flavinylation and the cofactor binding in choline oxidase.

The location of His310 ~2.9 Å behind His466 observed in the X-ray crystal structure of the wild-type choline oxidase, effectively prevents His310 from directly affecting the flavin microenvironment (**Figure 6.2**) and as such it must exert its effect through histidine 466. Studies in which His466 was replaced with alanine or aspartate showed that His466 needs to be protonated and that, in addition to stabilizing the transient alkoxide species that is formed during enzyme turnover, it also modulates the electrophilicity of the enzyme-bound flavin and the polarity of the active site (*8*). Furthermore, His466 was shown to be responsible for stabilizing the negative charge that develops on the flavin during enzyme turnover (*9*). The X-ray crystal structure of the wild-type enzyme along with the studies on the role of the active site His466 residue suggest the existence of a proton-transfer network between the protonated active site residue His466 and His310; the latter residue being hydrogen bonded to the peptidyl oxygen atoms of Thr380 and Val507 through its N(3) atom (**Figure 6.2**). The main role of the proton-transfer network between the side-chains of His466, His310 and the backbone peptidyl oxygen atoms of Thr380 and Val507 is proposed to ensure the correct orientation and protonation state

of His466 for efficient catalysis. This highly coordinated hydrogen bonding network ensures that His466 is in the correct orientation to abstract a proton from the hydroxyl group of choline. Upon proton abstraction the proposed proton transfer network functions by facilitating a proton being transferred from the protonated His466 to His310 during the reductive half-reaction, and transferring the proton back again during the oxidative half-reaction. Thereby, preventing the premature deprotonation of His466 through a proton transferring to the anionic reduced flavin.

The anaerobic reduction results obtained herein showed a significantly impaired reductive half-reaction in the variant enzymes, as seen by the rate of reduction being ~10^5 times slower as compared to that for the wild-type enzyme. This finding is consistent with a proton transfer network being disrupted upon substituting the active site residue His310 of choline oxidase resulting in His466 not being positioned properly to abstract the proton from choline and stabilize the transient alkoxide intermediate or the developing negative charge on the N(1)-C(2)=O locus of the flavin. Additionally, a disruption of the proposed proton network would likely result in the reduced flavin being the neutral hydroquinone, and thus having a significant impact on the oxidative half-reaction, as is the case in the data presented.

The proposed model of the reaction mechanism for the oxidation of choline catalyzed by choline oxidase that includes the proton-transfer network between His466 and His310 is shown in **Scheme 6.2**. In summary, during the reductive half-reaction, an active site base (His466) activates the alcohol substrate with the formation of an alkoxide species, which subsequently transfers a hydride ion from the α-carbon to the N(5) atom of the bound flavin (species 1 and 2 in **Scheme 6.2**) (*2*-*3*). The alkoxide intermediate is transiently stabilized in the active site through electrostatic interaction with the Nε2 atom of the protonated side chain of His466 (*8*). The protonated His466 also electrostatically stabilizes the negative charge developing at the N(1)-

C(2)=O locus of the flavin (species 3 in **Scheme 6.2**) (*9*). Concomitant with the hydride transfer a proton is transferred from His466 to His310, triggered by the conformational change of Glu312 relayed to His310 via Pro311. This conformational change results in a minor change of the microenvironment of His310 causing its pK_a to shift, thereby favoring a proton being transferred from His466 to His310. The negative charge at the N(1)-C(2)=O locus of the anionic hydroquinone can still be stabilized through hydrogen bonding with Nε2 atom of the imidazole side-chain of His466 (species 4 in **Scheme 6.2**), however not as effectively as the protonated His466. In the oxidative half-reaction, electron delocalization from the N(1) locus of the anionic hydroquinone along with a proton transfer from the catalytic base results in the formation of the C(4a)-hydroperoxo-flavin. Concomitantly a proton is transferred back from His310 to His466 (species 5 in **Scheme 6.2**). Finally the highly unstable C(4a)-hydroperoxo-flavin abstracts a second proton from the N(5) locus of the flavin with the subsequent release of H_2O_2 and the formation of oxidized flavin (species 6 and 7 in **Scheme 6.2**).

In conclusion, the kinetic and spectral data collected for the practically inactive variant enzymes are consistent with the presence of the proposed proton transfer network between His466, His310, Thr380 and Val507 that has been disrupted due to the mutation of histidine 310. The disruption of the proposed proton transfer network would likely result in an incorrect positioning of His466, thereby explaining the lowered rate of flavin reduction. Further, a disruption of the proposed proton transfer network would also likely result in the premature deprotonation of His466 by the reduced anionic flavin effectively cutting off the oxidative half-reaction, as observed for the His310 variant enzymes.

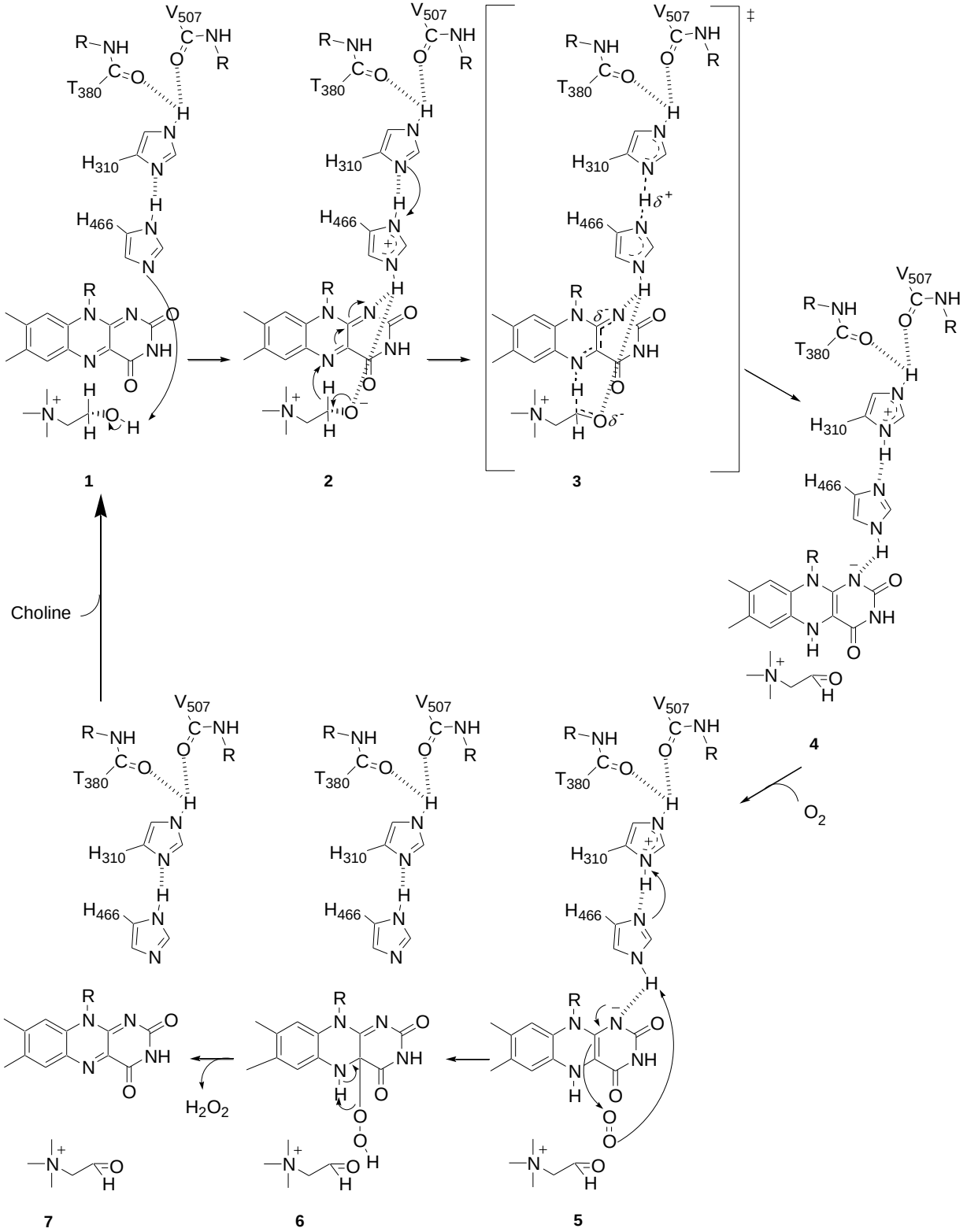

Scheme 6.2. Proposed Reaction Mechanism for the Reaction Catalyzed by Choline Oxidase (modified from (*19*)).

6.6. References

1. Fan, F., Ghanem, M., and Gadda, G. (2004) Cloning, sequence analysis, and purification of choline oxidase from Arthrobacter globiformis: a bacterial enzyme involved in osmotic stress tolerance, *Arch Biochem Biophys 421*, 149-158.
2. Fan, F., and Gadda, G. (2005) On the catalytic mechanism of choline oxidase, *J. Am. Chem. Soc. 127*, 2067-2074.
3. Ghanem, M., Fan, F., Francis, K., and Gadda, G. (2003) Spectroscopic and kinetic properties of recombinant choline oxidase from *Arthrobacter globiformis*, *Biochemistry 42*, 15179-15188.
4. Fan, F., and Gadda, G. (2005) Oxygen- and temperature-dependent kinetic isotope effects in choline oxidase: correlating reversible hydride transfer with environmentally enhanced tunneling, *J. Am. Chem. Soc. 127*, 17954-17961.
5. Gadda, G. (2003) Kinetic mechanism of choline oxidase from *Arthrobacter globiformis*, *Biochim. Biophys. Acta 1646*, 112-118.
6. Gadda, G. (2003) pH and deuterium kinetic isotope effects studies on the oxidation of choline to betaine-aldehyde catalyzed by choline oxidase, *Biochim. Biophys. Acta 1650*, 4-9.
7. Gadda, G., Powell, N. L., and Menon, P. (2004) The trimethylammonium headgroup of choline is a major determinant for substrate binding and specificity in choline oxidase, *Arch. Biochem. Biophys. 430*, 264-273.
8. Ghanem, M., and Gadda, G. (2005) On the catalytic role of the conserved active site residue His466 of choline oxidase, *Biochemistry 44*, 893-904.

9. Ghanem, M., and Gadda, G. (2006) Effects of reversing the protein positive charge in proximity of the N(1)-flavin locus of choline oxidase, *Biochemistry*, in press.

10. Quaye, O., Lountos, G. T., Fan, F., Orville, A. M., and Gadda, G. (2008) Role of Glu312 in binding and positioning of the substrate for the hydride transfer reaction in choline oxidase, *Biochemistry 47*, 243-256.

11. Ghanem, M., and Gadda, G. (2006) Effects of reversing the protein positive charge in the proximity of the flavin N(1) locus of choline oxidase, *Biochemistry 45*, 3437-3447.

12. Finnegan, S., and Gadda, G. (2008) Substitution of an active site valine uncovers a kinetically slow equilibrium between competent and incompetent forms of choline oxidase, *Biochemistry 47*, 13850-13861.

13. Bradford, M. M. (1976) A rapid and sensitive method for the quantitation of microgram quantities of protein utilizing the principle of protein-dye binding, *Anal Biochem 72*, 248-254.

14. Shapiro, A. L., Vinuela, E., and Maizel, J. V., Jr. (1967) Molecular weight estimation of polypeptide chains by electrophoresis in SDS-polyacrylamide gels, *Biochem Biophys Res Commun 28*, 815-820.

15. Whitby, L. G. (1953) A new method for preparing flavin-adenine dinucleotide, *Biochem. J. 54*, 437-442.

16. Fan, F., Ghanem, M., and Gadda, G. (2004) Cloning, sequence analysis, and purification of choline oxidase from *Arthrobacter globiformis*: a bacterial enzyme involved in osmotic stress tolerance, *Arch. Biochem. Biophys. 421*, 149-158.

17. Massey, V., and Palmer, G. (1966) On the existence of spectrally distinct classes of flavoprotein semiquinones. A new method for the quantitative production of flavoprotein semiquinones, *Biochemistry 5*, 3181-3189.

18. Ghisla, S., and Massey, V. (1986) New flavins for old: artificial flavins as active site probes of flavoproteins, *Biochem J 239*, 1-12.

19. Ghanem, M. (2006) On the Mechanistic Roles of the Protein Positive Charge Close to the N(1) Flavin Locus in Choline Oxidase, In *Chemistry*, p 341, Georgia State University, Atlanta.

20. Fan, F., and Gadda, G. (2005) On the catalytic mechanism of choline oxidase, *J Am Chem Soc 127*, 2067-2074.

CHAPTER VII

THE NATURE OF THE KINETICALLY SLOW EQUILIBRIUM BETWEEN TWO CONFORMERS OF THE VAL464ALA VARIANT CHOLINE OXIDASE

7.1.Abstract

The importance of residues in the active site that do not directly participate in catalysis is often overlooked in terms of studies trying to pinpoint key residues for enzymatic turnover, as they would likely only exert a minimal effect on the overall catalysis. However, studies in which valine 464 in the active site of choline oxidase has been replaced with either alanine or threonine have revealed that this hydrophobic residue lining the active site cavity close to the N(5) atom of the flavin plays several important roles. The replacement of Val464 with threonine or alanine in choline oxidase resulted in a significantly lowered oxygen reactivity and establishment of a kinetically slow equilibrium between a catalytically competent and incompetent form of enzyme. It is the nature of this equilibrium that is the subject of investigation in the present study. Rapid kinetic approaches revealed that the interconversion of the two forms of enzyme is independent of the isotopic composition of the substrate and that a protonated group is needed for maximum rate of interconversion.

7.2.Introduction

Choline oxidase (CHO; E.C. 1.1.3.17) from *Athrobacter globiformis* is a homodimer with molecular weight of 120 kDa that contains a covalently linked FAD in a 1:1 stoichiometry (*1*).

The enzyme catalyzes the reaction shown in **Scheme 7.1** that converts choline to glycine betaine through four-electron oxidation with betaine aldehyde as a reaction intermediate (*2-3*).

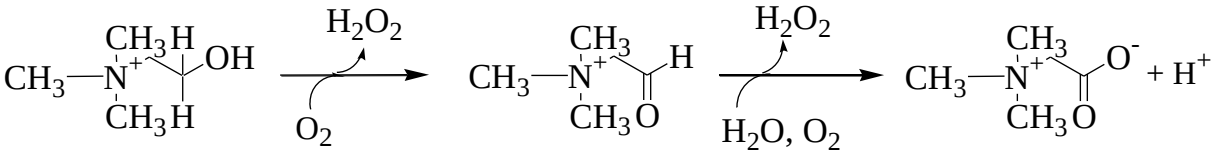

Scheme 7.1. The Two-step Reaction for the Oxidation of Choline to Glycine Betaine Catalyzed by Choline Oxidase.

The reaction catalyzed by choline oxidase is of interest as glycine betaine has been found in bacteria and plants in response to water deficit or salt stress (*4-8*). Additionally, based on the amino acid sequence of choline oxidase, similarities can be seen with other enzymes belonging to the GMC oxidoreductase enzyme superfamily, such as glucose oxidase, cholesterol oxidase, and cellobiose dehydrogenase. Another common aspect for these enzymes is that they all have FAD as a cofactor for catalysis and have non-activated primary alcohols substrates (*2, 9-11*). As such, a detailed elucidation of the catalytic mechanism of choline oxidase may provide insights into the kinetic mechanisms of a large family of enzymes.

Studies based on steady state kinetics, rapid kinetics, pH, mutagenesis, substrate deuterium and solvent isotope effects as well as viscosity effects have through the years provided a much more detailed understanding of the reaction shown in **Scheme 7.1** (*1, 12-22*), which have been summarized in a recent review by G. Gadda published in *Biochemistry (2009) 47*, 13745-13753 (*23*).

A recent study on the role of the hydrophobic residue at position 464 revealed that it is important for the proper assembly of the catalytic machinery required for the reaction catalyzed by choline oxidase (*19*). Evidence for this was that upon replacing Val464 with either a threonine

or alanine (Val464Ala andVal464Thr) a catalytically incompetent form of enzyme that reversibly equilibrated with a form of enzyme that could efficiently oxidize choline was stabilized. It was shown that, both in the free variant enzyme devoid of ligands in the active site as well as the enzyme-substrate complex a conformational change was involved in the interconversion of the catalytically competent and incompetent forms of enzyme (**Scheme 7.2**).

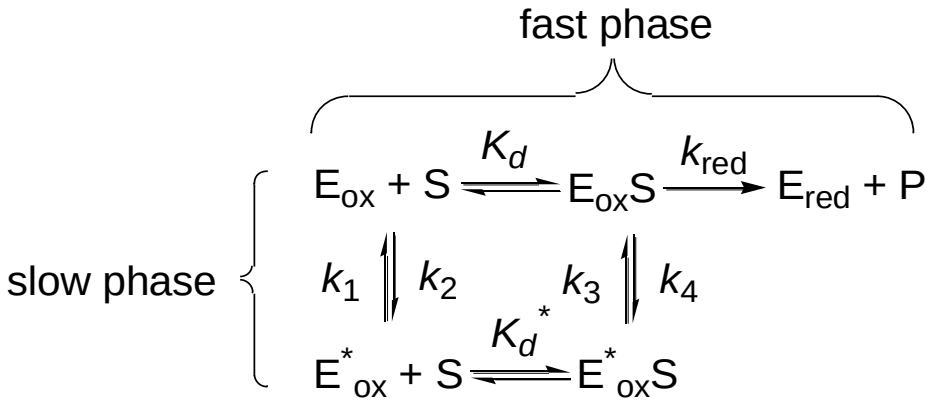

Scheme 7.2. Proposed Kinetic Mechanism for Choline Oxidation Catalyzed by the Val464Thr and Val464Ala Enzymes. E_{ox}, catalytically competent enzyme; E^*_{ox}, catalytically incompetent enzyme; S, substrate; k_{red}, first-order rate constant for flavin reduction; K_d, macroscopic dissociation constant for substrate binding to the competent enzyme; K_d^*, macroscopic dissociation constant for substrate binding to the incompetent enzyme; k_1 and k_3, first-order rate constants for the conversion of catalytically inert to competent enzyme; k_2 and k_4, first-order rate constants for the conversion of catalytically competent to inert enzyme (*19*).

From proton inventory and spectroscopic studies on the Val464Ala and Val464Thr variant enzymes it was shown that this conformational change is associated with changes in the ionization state of a group, linked to the flavin cofactor of the variant enzyme, that is not readily available to the bulk solvent. His99, which is the site of covalent attachment of the polypeptide to the C(8) methyl group of the flavin (*13*), was proposed to be involved in the formation and stabilization of the incompetent form of choline oxidase (*19*).

The structural information on the Val464Ala variant of choline oxidase (Protein Data Bank as entry 3LJP) provides a solid framework to substantiate the hypothesis of an involvement of

His99 in the inactivation of the enzyme. Indeed, the N(1) atom of His99 is located in a small cavity that is completely secluded from the bulk solvent, in hydrogen bonding distance (2.8 Å) with a structural water molecule (W780). This water molecule, in turn, is in hydrogen bonding distance with the peptidyl oxygen atoms of Leu64 (3.4 Å) and Tyr69 (3.1 Å) located on a long loop (residues 64-95) covering the active site of the enzyme (**Figure 7.1**) (*24*).

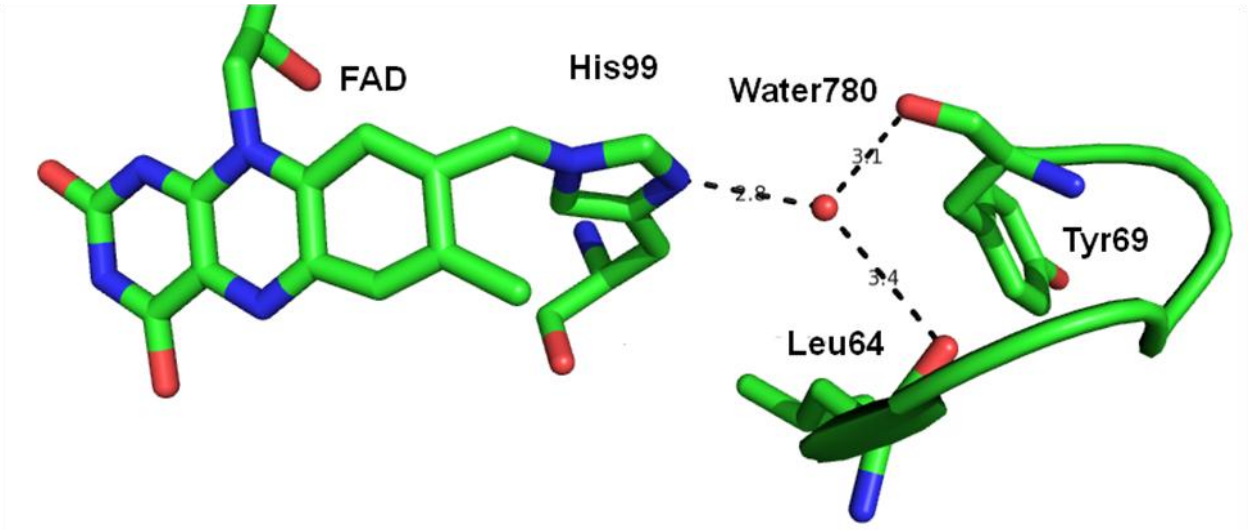

Figure 7.1. Close-up View of the Active Site of the Val464Ala Variant Form of Choline Oxidase Showing the Hydrogen Bonding Interactions Involving the N(1) Atom of His99, a Structural Water Molecule (W780) Secluded from the Bulk Solvent, the Peptidyl Oxygen Atoms of Leu64 and Tyr69 (PDB entry 3LJP).

A change in the ionization state of His99 is expected to affect the hydrogen bonding pattern around W780, conceivably resulting in a change in the conformation of the enzyme. The link between Ala464 and His99, which are spatially removed from each other, is likely provided by His466, which is in van der Waals contact with Ala464 and in hydrogen bonding distance of the flavin cofactor. The presence of such a link is supported by the observation that both the replacements of Val464 with threonine or alanine and of His466 with alanine have the same effect of increasing the pK_a value for the ionization of the N(1) atom of His99 from 8.2 to ~9.1 (*18-19*).

In summary, the replacement of Val464 with alanine or threonine showed that the hydrophobic residue Val464 lining the active site cavity close to the N(5) atom of the flavin is important for the correct positioning of the catalytic groups in the active site of choline oxidase. Replacement of Val464 with alanine or threonine also resulted in the reductive half-reaction showing a significantly decreased rate of hydroxyl proton abstraction, while minimally affecting the rate of hydride ion transfer from choline to the flavin (*19*). It was further determined, that the replacement of Val464 with alanine or threonine resulted in establishment of a kinetically slow equilibrium between a catalytically competent and an incompetent form of enzyme (*19*).

In the present study, the kinetic behavior of the competent and incompetent form of the Val464Ala variant enzyme is investigated by means of rapid kinetics and substrate deuterium isotope effects in the pH range from pH 5.5 to 10.0.

7.3.Experimental Procedures

Materials. *Escherichia coli* strain Rosetta(DE3)pLysS was from Novagen (Madison, WI). DNase was from Roche (Indianapolis, IN). The QuikChange site-directed mutagenesis kit was from Stratagene (La Jolla, CA). The QIAprep Spin Miniprep kit was from Qiagen (Valencia, CA). Oligonucleotides used for sequencing of the mutant genes were custom synthesized by Sigma Genosys (Woodland, TX). Choline chloride was from ICN Pharmaceutical Inc (Irvine, CA). 1,2-[$^{2}H_{4}$]-choline bromide (98%) was from Isotec Inc. (Miamisburg, OH). All other reagents were of the highest purity commercially available.

Site-Directed Mutagenesis. Val464Ala variant form of choline oxidase was prepared using the pET/*codA*mg plasmid harboring the wild-type gene for choline oxidase as template, as previously described (*13, 17, 25*). The presence of the desired mutation was confirmed by

sequencing the entire mutagenized gene. *Escherichia coli* strain Rosetta(DE3)pLysS competent cells were transformed with the mutant plasmid by electroporation.

Enzyme Expression and Purification. The Val464Ala enzyme was expressed and purified to homogeneity as previously described (*19, 25-26*). The protein concentration of the variant enzyme was determined using the Bradford assay (*27*). Expression levels and purity were determined using SDS-PAGE (*28*) and the oxidized flavin content per enzyme active site was determined spectrophotometrically as previously described for the wild-type enzyme (*29*).

Enzyme Assays. Reductive half-reaction measurements were carried out using an SF-61DX2 HI-TECH KinetAsyst high performance stopped-flow spectrophotometer thermostated at 25 °C, in 50 mM buffer, at pH 5.5 to pH 10.0. The rate of flavin reduction was measured by monitoring the decrease in absorbance at 455 nm that results from the anaerobic mixing of enzyme with the organic substrate as previously described for the wild-type enzyme (*30*). After anaerobic mixing in the stopped-flow spectrophotometer the final concentration of the enzyme was ~10 μM, whereas those of the organic substrates were between 0.05 to 10 mM, thereby maintaining pseudo-first order kinetic conditions.

Data Analysis. Kinetic data were fit with KaleidaGraph (Synergy Software, Reading, PA) and the Hi-Kinetic Studio Software Suite (Hi-Tech Scientific, Bradford on Avon, U.K.). Stopped-flow data traces were fit with equation 1, which describes a double-exponential process, in which k_{obs1} and k_{obs2} are the observed rate constants for the change in absorbance at 455 nm, *A* is the value of absorbance at time *t*, B and C are the amplitudes of the absorbance changes for the fast and slow observed phases, and D is an offset value that accounts for the non-zero absorbance

value at infinite time. The kinetic parameters of the reductive half-reaction were determined by using equations 2 and 3, which apply to the kinetic mechanism of **Scheme 7.2**. In equation 2, k_{obs1} is the observed first-order rate associated with the fast phase of flavin reduction at any given concentration of substrate, k_{red} is the limiting first-order rate constant for flavin reduction at saturating substrate concentrations, S is substrate concentration and K_d is the macroscopic dissociation constant for binding of the substrate to the active enzyme. In equation 3, k_{obs2} is the observed first-order rate associated with the slow phase of flavin reduction at any given concentration of substrate, k_1 is the first-order rate constant for the conversion of the E^*_{ox} to E_{ox}, k_3 is the first-order rate constant for the reverse conversion, K_d* represents the macroscopic dissociation constant for binding of the substrate to the inactive enzyme, and S is substrate concentration (*19*).

$$A = B\exp(-k_{obs1}t) + C\exp(-k_{obs2}t) + D \quad (1)$$

$$k_{obs1} = \frac{k_{red}S}{K_d + S} \quad (2)$$

$$k_{obs2} = \left(\frac{k_3 S + k_1 K_d^*}{S + K_d^*}\right) \quad (3)$$

The pH profiles of the K_d, K_d*, k_1 and k_3_values were determined by fitting the data to Equation 4, where Y_L and Y_H are the limiting values at low and high pH, respectively, and K_a is the dissociation constant for the ionization of groups that are relevant to the kinetic parameter analyzed.

$$\log Y = \log\frac{Y_L + Y_H\left[1+\left(\frac{pK_a}{pH}\right)\right]}{1+\left(\frac{pK_a}{pH}\right)} \quad (4)$$

The pH profiles for the k_{red}, $^{D}k_{red}$, $^{D}K_d$*, $^{D}k_1$ and $^{D}k_3$ values were determined by fitting the data to the average value for all their respective data values.

Finally the pH profile for $^{D}K_d$ values was determined by fitting the data to equation 5, which describes a 3rd order polynomial.

$$Y = ax^3 + bx^2 + cx + d \quad (5)$$

7.4.Results

Expression and Purification. A variant form of choline oxidase was engineered using site-directed mutagenesis to replace a valine at position 464 with alanine. The enzyme was expressed in *Escherichia coli* strain Rosetta(DE3)pLysS, and purified by salting out with ammonium sulfate followed by ion exchange chromatography using a DEAE-sepharose column as previously described for the wild-type enzyme (*25*). As previously reported, the Val464Ala variant enzyme has its flavin cofactor covalently bound and has a 25-fold decrease of the specific activity at pH 7.0 as compared to the wild-type enzyme (*19*).

pH-dependence of the Reductive Half-reaction. The reductive half-reaction in which the Val464Ala enzyme is reduced anaerobically with both choline and 1,2-[$^{2}H_4$]-choline as substrates was investigated using a stopped-flow spectrophotometer by measuring the rates of decrease in absorbance at 455 nm as a function of the substrate concentration of choline at 25 ^{o}C in the pH range 5.5 to 10.0, under pseudo-first order conditions (i.e., 10 μM enzyme and ≥50 μM substrate). For all investigated pH values, the Val464Ala enzyme was reduced to the hydroquinone state in a biphasic pattern, with the observed rates for the fast phase of flavin reduction defining a rectangular hyperbola when plotted as a function of the concentration of

organic substrate. In contrast the observed rates for the slow phase of flavin reduction yielded an inverse hyperbolic dependency of substrate concentration, with the observed rates decreasing to an asymptotic value with increasing concentration of organic substrate. These kinetic data can be accounted for with the kinetic mechanism of **Scheme 7.2** (*19*), which is the proposed mechanism for the reductive half-reaction of Val464Ala at pH 10.0. The data collected are consistent with the Val464Ala enzyme utilizing the same mechanism for choline oxidation throughout the pH range investigated.

The kinetic data associated to the fast phase of flavin reduction were fitted with equation 2 allowing for the determination of the first-order rate constant for flavin reduction (k_{red}), and the dissociation constant for the catalytically competent enzyme-substrate Michaelis complex (K_d) for all investigated pH values. The determined kinetic parameters for the fast phase with both choline and 1,2-[$^2H_4$]-choline are plotted as a function of pH in **Figure 7.2A and** B.

The kinetic data associated with the slow phase of flavin reduction were fitted with equation 3 allowing for the determination of the first-order rate constants for the conversion of the incompetent form of enzyme to the competent form of enzyme (k_1 and k_3), and of the dissociation constant for the catalytically incompetent enzyme-substrate complex (K_d^*). The requirement for pseudo-first order conditions in the anaerobic reduction of the enzyme with the organic substrate dictated that the concentration of substrate $\geq$ 50 μM (5-times [enzyme]) and the computer estimated K_d^*-value was $\leq$ 80 μM, thereby preventing an accurate determination of the first-order rate constant for the conversion of the E^*_{ox} form of choline oxidase to the E_{ox} species (k_1) at pH 10.0. As a result, the data shown for k_1 at this one pH is the estimated value from equation 2. At all other pH-values investigated the K_d^*-value $\geq$ 120 μM and an accurate determination of k_1

was possible. The kinetic parameters for the slow phase with both choline and 1,2-[$^2H_4$]-choline are plotted as a function of pH in **Figure 7.2C-E.**

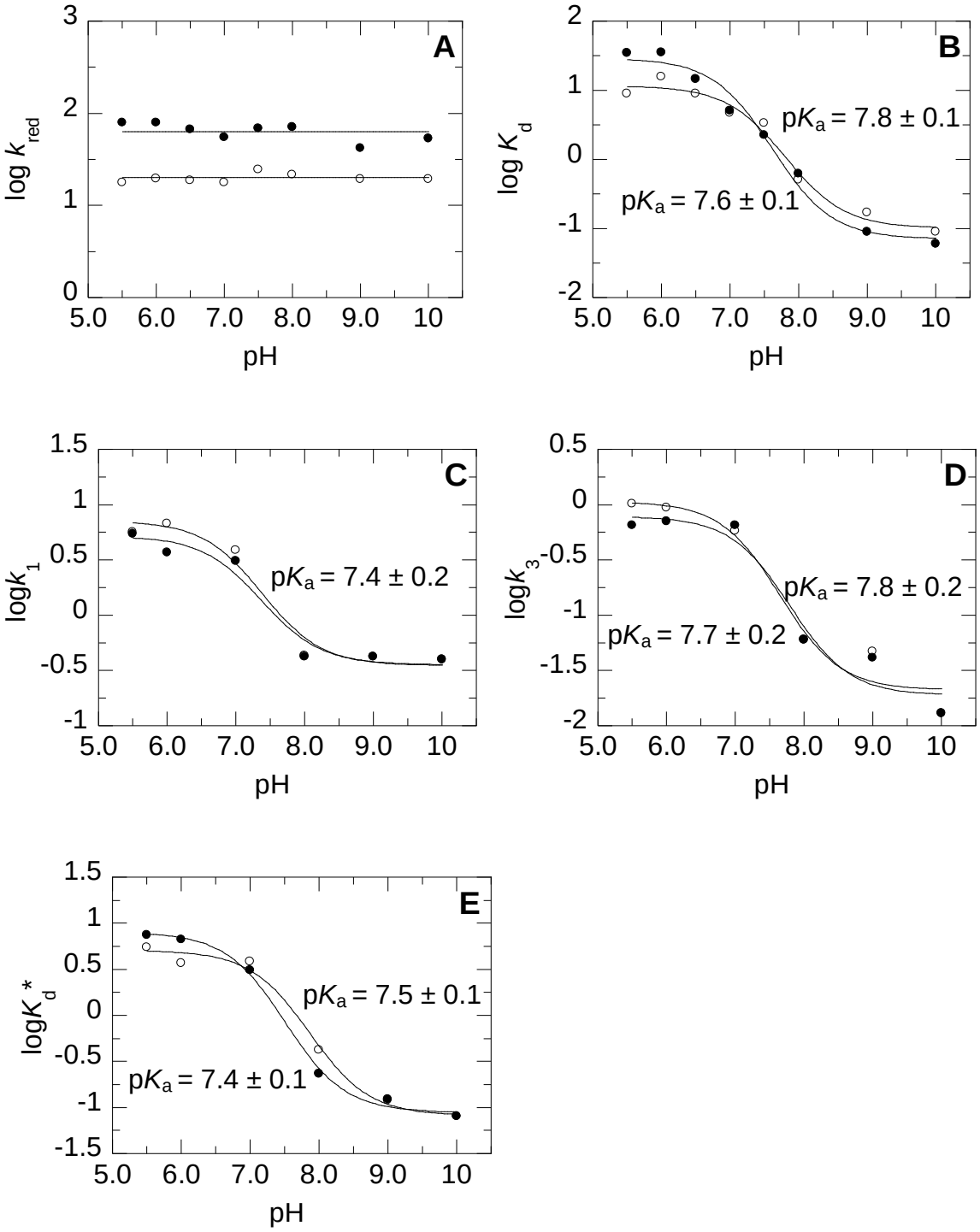

Figure 7.2. pH Dependence of the k_{red} (panel A), K_d (panel B), k_1 (panel C), k_3 (panel D) and K_d^* (panel E) Values with Choline (●) and 1,2-[$^2H_4$]-choline (○) as Substrate for Choline Oxidase.

Activity assays were performed in a stopped-flow spectrophotometer in 50 mM buffer, at 25 ºC. Data for K_d, k_1, k_3 and K_d^* were fit with eq. 4.

From the pH profiles of the kinetic parameters for the biphasic reduction of the Val464Ala enzyme with both choline and 1,2-[$^2H_4$]-choline it is seen that k_{red} is pH independent between pH 5.5 and 10.0, whereas both k_1 and k_3 show the need for a group to be protonated with pK_a values of 7.4 and 7.8 with choline as a substrate and 7.4 and 7.7 with 1,2-[$^2H_4$]-choline as a substrate respectively. The pH profiles for the macroscopic dissociation constants, K_d and K_d^*, show an unprotonated group with pK_a values of 7.8 and 7.5 with choline and 7.6 and 7.4 with 1,2-[$^2H_4$]-choline as a substrate, respectively, needed for organic substrate binding.

pH-dependence of the Substrate Deuterium Kinetic Isotope Effects. The pH-dependence of the substrate kinetic isotope effects were employed with the goal of gaining insights into whether there is a change in the rate-limiting steps for the reductive half-reaction of the Val464Ala enzyme as pH changes. As shown in **Figure 7.3A-E** one observable substrate deuterium isotope effect is for the rate of flavin reduction of the fast phase, k_{red} between pH 5.5 and 10.0 with an average magnitude for $^Dk_{red}$ of 3.2 ± 0.3 between pH 5.5 and 10.0 (**Figure 7.3A)**[7]. This substrate deuterium isotope effect is consistent with the cleavage of the CH bond of choline being at least partially rate-limiting in the reductive half-reaction for the investigated pH-range. A second observeable substrate deuterium isotope effect is seen at the extremes of the pH range investigated for the macroscopic dissociation constant for the fast phase of flavin reduction (K_d) (**Figure 7.3B).** In contrast, no substrate deuterium isotope effect is observed between pH 5.5 and

[7] $^Dk_{red}$ is pH independent in the pH range investigated, as seen from k_{red} being pH independent with both choline and 1,2-[$^2H_4$]-choline as substrates. The representation of the pH dependence of $^Dk_{red}$ in Figure 7.3A gives the impression that there is a pH dependence at low pH, but this is merely an artifact arising from the scattering of the datapoints for k_{red} with choline and 1,2-[$^2H_4$]-choline as substrates.

10.0 for the rates of the slow phase of flavin reduction (k_1 and k_3) or for the macroscopic dissociation constant (K_d^*) **Figure 7.3C-E**.

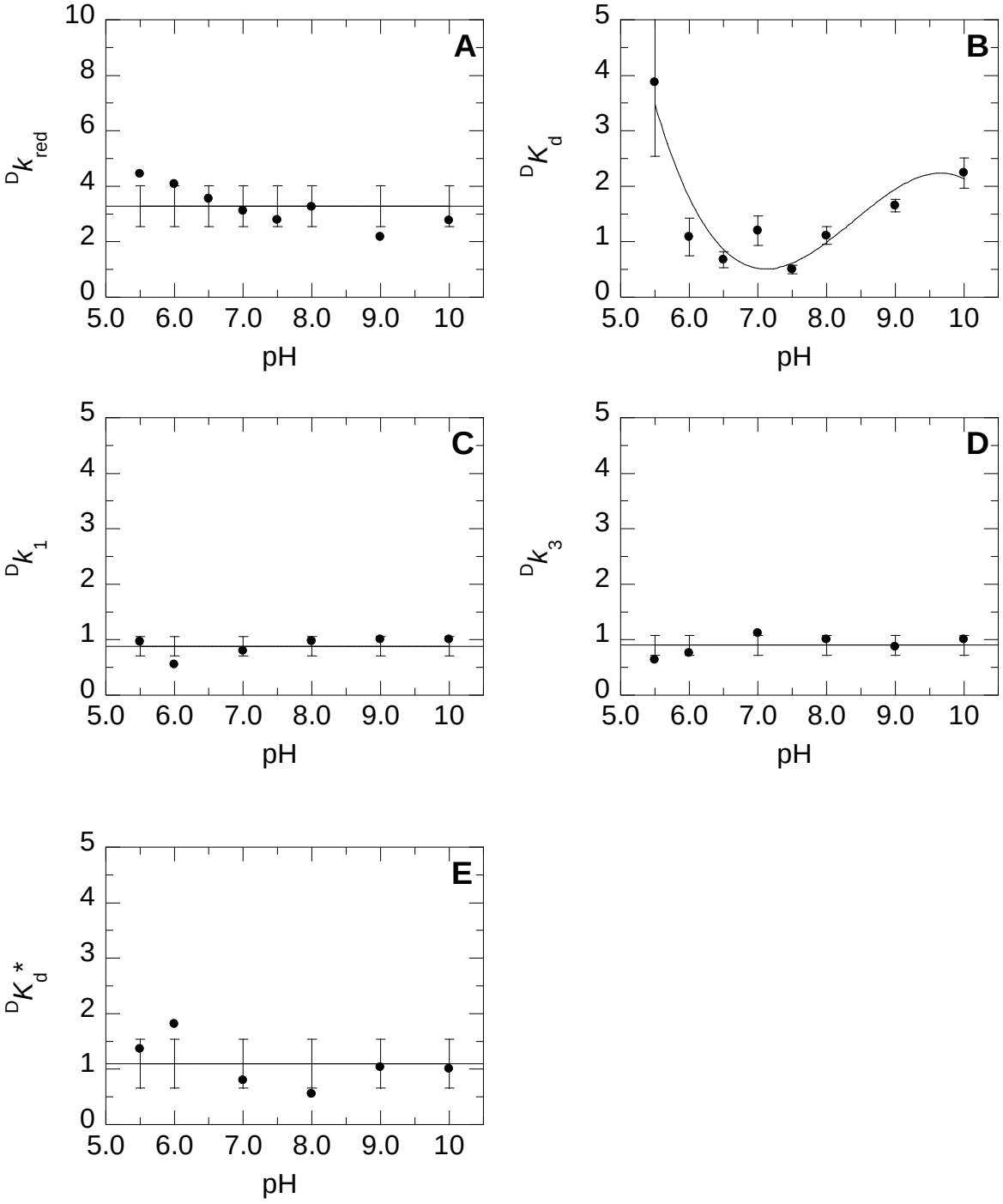

Figure 7.3. pH Dependence of Substrate Deuterium Isotope Effects of the $^{D}k_{red}$ (panel A), $^{D}K_d$ (panel B) (here fitted with $y = -0.2x^3 + 5.3x^2 - 43.2x + 116.5$), $^{D}k_1$ (panel C), $^{D}k_3$ (panel D) and

$^{D}K_{d}^{*}$ (panel E) Values. Activity assays were performed in a stopped-flow spectrophotometer in 50 mM buffer, at 25 ºC.

pH-dependence of the Equilibrium between the two Enzyme Forms. The biphasic flavin reduction in the Val464Ala enzyme has been attributed to the enzyme existing in an equilibrium between a competent (E_{ox}) and an incompetent form (E^{*}_{ox}) (*19*). The relative amplitudes of the kinetic phases seen in the stopped-flow traces can be used to quantitate the relative amounts of each form of enzyme. As shown in **Table 7.1** the relative amount of E_{ox} is independent of pH between pH 6.5 and 10.0 with an average value of 86 ± 8 % and then dropping to an average value of 47 ± 1 % at pH 5.5 and 6.0.

Table 7.1. Effect pH Dependence of the Ratio of Competent Enzyme to Total Enzyme.

pH	E_{ox}/E_{total}, %
10.0	76 ± 5
9.0	80 ± 6
8.0	94 ± 7
7.5	94 ± 7
7.0	83 ± 6
6.5	90 ± 6
6.0	48 ± 10
5.5	46 ± 9

[a] Conditions: 50 mM buffer, 25 °C, pH 10.0. Pre-steady-state kinetic parameters were determined by fitting the kinetic data acquired upon mixing anaerobically the enzyme with the choline to equations 1.

7.5.Discussion

In a recent study, the replacement of Val464 with alanine resulted in the establishment of a kinetically slow equilibrium between a catalytically competent and an incompetent form of enzyme (*19*), with each form having a separate conformation, with only one being congruent with efficient choline oxidation. It was proposed that the conformational change associated with the conversion of the incompetent form to the competent conformation involves the change of ionization state of a group linked to the flavin cofactor. The pH profiles presented here for the

rate of interconversion for both the free enzyme as well as the enzyme-substrate complex (k_1 and k_3 in **Scheme 7.2**) show that a protonated group is indeed needed for maximum rate of interconversion, which is consistent with previous findings at pH 10.0 that the interconversion involves a single proton changing position (*19*). The pK_a value for the group that needs to be protonated of around 7.6 would predict that the relative amount of the competent form of the enzyme, E_{ox} would increase as pH is lowered; however this is not the case as seen in **Table 7.1**. This could be a result of the group that needs to be protonated not being accessible to the bulk solvent, and as such not affected by the pH. However, this seems unlikely in the light of the interconversion of the enzyme-substrate complex (k_3) being sensitive to the isotopic composition of the solvent at pH 10.0, as seen by a solvent deuterium isotope effect with choline as a substrate of 3 (*19*). A more likely explanation is based on the principle of thermodynamic cycles, which in the case of the Val464Ala enzyme where the two forms of enzyme are linked by an ionizable group can be shown as **Scheme 7.3** (*31*).

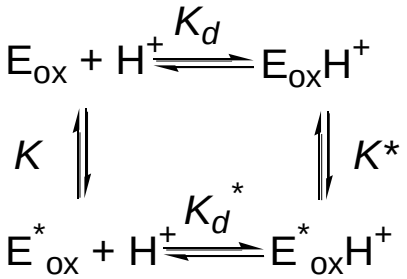

Scheme 7.3. The Thermodynamic Cycle Linking Ionization and Equillibria for the Competent and Incompetent form of Val464Ala.

The thermodynamic cycle for the equilibrium of the two forms of the Val464Ala enzyme predicts that at low pH:

$$K_{app} = \frac{K \cdot K_d}{K_d^*}$$

And at high pH:

$$K_{app} = K$$

Meaning that the ratio of E_{ox}/E_{total} should be pH independent at high pH. Whereas at low pH only if $K_d = K_d^*$ would the ratio of E_{ox}/E_{total} be pH independent. In order for the ratio of E_{ox}/E_{total} to be pH independent throughout the pH range investigated the equilibrium constant for the free form of enzyme, *K* must also be pH independent. If the before mentioned conditions are not met, then the ratio of E_{ox}/E_{total} will be pH dependent. K_d, K_d^* and the rate of free enzyme interconversion (k_1) have been shown to be dependent on pH with different pK_a values, as such a pH dependence of the ratio of E_{ox}/E_{total} is expected, which is consistent with the data summarized in **Table 7.1**.

Based on a previous study (*19*) that determined that an ionizable group interacting with the flavin cofactor is involved in the interconversion of the two forms of the Val464Ala enzyme and the crystal structure of the wild-type enzyme, His99 and His466 are identified as likely candidates for being the ionizable group involved. One experiment that could potentially help determine which residue is involved in the interconversion of the two forms of enzyme in the Val464Ala enzyme would be the determination of the pH-dependence of the UV-spectra of the Val464Ala with glycine betaine in the active site. This experiment would be expected to yield a pK_a value for the N(1) atom of His99 similar to the one determined for the ionizable group needed for efficient interconversion of the enzyme forms in the Val464Ala enzyme determined in the pH-profiles for k_1 and k_3. Based on another previous study which showed no effect on k_{cat} by adding exogenous imidazole to the reaction mixture for the His466Ala variant enzyme, but saw a rescuing effect upon adding imidazolium (*18*), a second set of experiments can be devised. These experiments would entail the investigation of the reductive half-reaction for His466Ala at high pH with exogenous imidazole. At high pH, only a fraction of the added imidazole would be protonated and as such, if His466 is the ionizable group involved in the interconversion of the

two enzyme forms of Val464Ala, a biphasic flavin reduction of His466Ala under anaerobic conditions upon mixing with choline would be expected. This reasoning is based on, only the enzyme interacting with imidazolium would be in a competent conformation and the enzyme interacting with imidazole would have to undergo a conformational change similar to the one observed for the Val464Ala enzyme.

The rate of flavin reduction in the fast phase (k_{red}) is seen to be pH independent for both choline and 1,2-[$^2H_4$]-choline and as such the substrate deuterium isotope effect is also pH independent. The pH independence and magnitude of the substrate deuterium isotope effect is consistent with the rate of hydride transfer being partially rate-limiting throughout the pH range investigated. It is also seen that the dissociation constants for the two phases of flavin reduction with both choline and 1,2-[$^2H_4$]-choline require an unprotonated group for the substrate binding.

In conclusion, the presented pH studies on the Val464Ala variant enzyme showed that the flavin reduction is biphasic as a result of the enzyme existing as a pH-independent kinetically slow equilibrium between a catalytically competent and incompetent form. The biphasic behavior displayed throughout the pH range investigated can be explained by the mechanism determined for the Val464Ala enzyme at pH 10.0. The fast phase, being the reduction of the flavin cofactor in the competent form was seen to be dependent on the isotopic composition of the substrate but independent of pH. Contrary to this, the reduction of the flavin for the incompetent form (slow phase) was pH-dependent, but independent of the isotopic composition of the substrate. The pH dependence of the slow phase showed that a protonated group is needed for maximum rate of conversion to the competent form. These findings coincide well with findings for Val464Ala at pH 10.0, that a single proton in flight is involved in the conformational

change associated with the interconversion of the incompetent and competent form of the enzyme.

7.6.References

1. Fan, F., Ghanem, M., and Gadda, G. (2004) Cloning, sequence analysis, and purification of choline oxidase from *Arthrobacter globiformis*: a bacterial enzyme involved in osmotic stress tolerance, *Arch. Biochem. Biophys. 421*, 149-158.
2. Cavener, D. R. (1992) GMC oxidoreductases. A newly defined family of homologous proteins with diverse catalytic activities, *J Mol Biol 223*, 811-814.
3. Ikuta, S., Matuura, K., Imamura, S., Misaki, H., and Horiuti, Y. (1977) Oxidative pathway of choline to betaine in the soluble fraction prepared from Arthrobacter globiformis, *J Biochem (Tokyo) 82*, 157-163.
4. Boch, J., Kempf, B., Schmid, R., and Bremer, E. (1996) Synthesis of the osmoprotectant glycine betaine in Bacillus subtilis: characterization of the gbsAB genes, *J Bacteriol 178*, 5121-5129.
5. Canovas, D., Vargas, C., Csonka, L. N., Ventosa, A., and Nieto, J. J. (1998) Synthesis of glycine betaine from exogenous choline in the moderately halophilic bacterium halomonas elongata, *Appl Environ Microbiol 64*, 4095-4097.
6. Cosquer, A., Pichereau, V., Le Mee, D., Le Roch, M., Renault, J., Carboni, B., Uriac, P., and Bernard, T. (1999) Toxicity and osmoprotective activities of analogues of glycine betaine obtained by solid phase organic synthesis towards Sinorhizobium meliloti, *Bioorg Med Chem Lett 9*, 49-54.

7. Kappes, R. M., Kempf, B., and Bremer, E. (1996) Three transport systems for the osmoprotectant glycine betaine operate in Bacillus subtilis: characterization of OpuD, *J Bacteriol 178*, 5071-5079.

8. Peddie, B. A., Lever, M., Hayman, C. M., Randall, K., and Chambers, S. T. (1994) Relationship between osmoprotection and the structure and intracellular accumulation of betaines by Escherichia coli, *FEMS Microbiol Lett 120*, 125-131.

9. Higham, C. W., Gordon-Smith, D., Dempsey, C. E., and Wood, P. M. (1994) Direct 1H NMR evidence for conversion of beta-D-cellobiose to cellobionolactone by cellobiose dehydrogenase from Phanerochaete chrysosporium, *FEBS Lett 351*, 128-132.

10. Tsuge, H., Nakano, Y., Onishi, H., Futamura, Y., and Ohashi, K. (1980) A novel purification and some properties of rat liver mitochondrial choline dehydrogenase, *Biochim Biophys Acta 614*, 274-284.

11. Weibel, M. K., and Bright, H. J. (1971) The glucose oxidase mechanism. Interpretation of the pH dependence, *J Biol Chem 246*, 2734-2744.

12. Rungsrisuriyachai, K., and Gadda, G. (2008) On the role of histidine 351 in the reaction of alcohol oxidation catalyzed by choline oxidase, *Biochemistry 47*, 6762-6769.

13. Quaye, O., Lountos, G. T., Fan, F., Orville, A. M., and Gadda, G. (2008) Role of Glu312 in binding and positioning of the substrate for the hydride transfer reaction in choline oxidase, *Biochemistry 47*, 243-256.

14. Quaye, O., and Gadda, G. (2009) Effect of a conservative mutation of an active site residue involved in substrate binding on the hydride tunneling reaction catalyzed by choline oxidase, *Arch Biochem Biophys 489*, 10-14.

15. Quaye, O., Cowins, S., and Gadda, G. (2009) Contribution of flavin covalent linkage with histidine 99 to the reaction catalyzed by choline oxidase, *J Biol Chem 284*, 16990-16997.

16. Orville, A. M., Lountos, G. T., Finnegan, S., Gadda, G., and Prabhakar, R. (2009) Crystallographic, spectroscopic, and computational analysis of a flavin C4a-oxygen adduct in choline oxidase, *Biochemistry 48*, 720-728.

17. Ghanem, M., and Gadda, G. (2006) Effects of reversing the protein positive charge in the proximity of the flavin N(1) locus of choline oxidase, *Biochemistry 45*, 3437-3447.

18. Ghanem, M., and Gadda, G. (2005) On the catalytic role of the conserved active site residue His466 of choline oxidase, *Biochemistry 44*, 893-904.

19. Finnegan, S., and Gadda, G. (2008) Substitution of an active site valine uncovers a kinetically slow equilibrium between competent and incompetent forms of choline oxidase, *Biochemistry 47*, 13850-13861.

20. Fan, F., Germann, M. W., and Gadda, G. (2006) Mechanistic studies of choline oxidase with betaine aldehyde and its isosteric analogue 3,3-dimethylbutyraldehyde, *Biochemistry 45*, 1979-1986.

21. Fan, F., and Gadda, G. (2007) An internal equilibrium preorganizes the enzyme-substrate complex for hydride tunneling in choline oxidase, *Biochemistry 46*, 6402-6408.

22. Fan, F., and Gadda, G. (2005) Oxygen- and temperature-dependent kinetic isotope effects in choline oxidase: correlating reversible hydride transfer with environmentally enhanced tunneling, *J Am Chem Soc 127*, 17954-17961.

23. Gadda, G. (2008) Hydride transfer made easy in the reaction of alcohol oxidation catalyzed by flavin-dependent oxidases, *Biochemistry 47*, 13745-13753.

24. Finnegan, S., Agniswamy, J., Weber, I. T., and Gadda, G. (2010) Role of Val464 in the Flavin Oxidation Reaction Catalyzed by Choline Oxidase, *Biochemistry*.

25. Fan, F., Ghanem, M., and Gadda, G. (2004) Cloning, sequence analysis, and purification of choline oxidase from Arthrobacter globiformis: a bacterial enzyme involved in osmotic stress tolerance, *Archives of biochemistry and biophysics 421*, 149-158.

26. Gadda, G., Powell, N. L., and Menon, P. (2004) The trimethylammonium headgroup of choline is a major determinant for substrate binding and specificity in choline oxidase, *Archives of biochemistry and biophysics 430*, 264-273.

27. Bradford, M. M. (1976) A rapid and sensitive method for the quantitation of microgram quantities of protein utilizing the principle of protein-dye binding, *Anal Biochem 72*, 248-254.

28. Shapiro, A. L., Vinuela, E., and Maizel, J. V., Jr. (1967) Molecular weight estimation of polypeptide chains by electrophoresis in SDS-polyacrylamide gels, *Biochem Biophys Res Commun 28*, 815-820.

29. Ghanem, M., Fan, F., Francis, K., and Gadda, G. (2003) Spectroscopic and kinetic properties of recombinant choline oxidase from Arthrobacter globiformis, *Biochemistry 42*, 15179-15188.

30. Fan, F., and Gadda, G. (2005) On the catalytic mechanism of choline oxidase, *J. Am. Chem. Soc. 127*, 2067-2074.

31. Fersht, A. (1999) Structure and mechanism in protein science, pp 125-132, W. H. Freeman and Company.

CHAPTER VIII

GENERAL DISCUSSION AND CONCLUSIONS.

As the understanding of enzymes and how they achieve large rate enhancements of reactions has evolved, the complexity of enzyme catalysis has become very apparent, as exemplified by the studies on choline oxidase, where several residues have been shown to affect catalysis, and often multiple aspects of it (*1-16*). The need for an in-depth understanding of the kinetic mechanism as well as the mechanistic properties of enzymes become necessary, as the net rate enhancement achieved during catalysis as compared to the uncatalyzed reaction is the result of the combination of multiple effects exerted by a great number of residues in the protein matrix. This dissertation utilized the well characterized and extensively studied choline oxidase as a model enzyme to contribute to the understanding of enzyme catalysis by investigating the effects on the overall reaction kinetics of residues in the protein matrix that do not directly participate in catalysis. A combination of steady state kinetics, rapid kinetics, pH, mutagenesis, substrate deuterium and solvent isotope effects, viscosity effects as well as X-ray crystallography were used to investigate the roles of histidine at position 310, valine at position 464 and serine at position 101.

From the crystal structure of the wild-type choline oxidase solved to 1.86 Å resolution (*2*) a histidine residue, His310, not in direct contact with neither the active site nor the flavin cofactor, is seen to be located ~2.9 Å from His466. His466 has been shown to provide a positive charge in the active site needed for catalysis. The orientation of the side-chains of both histidine residues indicate the presence of a $His466^{N\delta1}$-$His310^{N\delta1}$ hydrogen bond. To assess the contribution made by this hydrogen bond to catalysis, mutant forms of the enzyme were prepared in which His310 was substituted with alanine, asparagine or aspartate.

Similarly from the crystal structure of the wild-type choline oxidase a pocket, defined by His351, Val464, and His466, on the *re*-face directly above the C(4a) atom of the flavin, where the C(4a) oxygen adduct is observed, can be identified (*2, 5*). Previous studies have established the important roles of His466 and His351 (*1, 6-7*) in the reaction catalyzed by choline oxidase, thus leaving the role of hydrophobic Val464 to be explored. This was done by replacing the valine residue with an alanine or a threonine.

Finally, the role of serine 101, seen to be less than 4 Å from the N(5) atom of FAD and within hydrogen bonding distance of the active site, was done by replacing the serine with an alanine.

The ensuing variant enzymes were investigated kinetically as well as structurally. The crystal structures for the Ser101Ala and Val464Ala variant enzymes were successfully attained, while the one for any of the His310 variant enzymes remains elusive.

The Val464Ala enzyme crystallized as a homodimer, with each monomer being superimposable with its corresponding complement in the wild-type enzyme with an rmsd value of 0.67 Å for 1056 topologically equivalent Cα atoms, consistent with the overall structures of the Val464Ala and the wild-type enzymes being essentially identical. The FAD cofactor in the Val464Ala enzyme is covalently bound to the Nε2 atom of His99 as in the case of wild-type (*2, 17*).

The homodimers seen in the crystal structure for the Ser101Ala enzyme were also superimposable with those of the wild-type enzyme with an average rmsd value of 0.41 Å for 527 equivalent Cα atoms in each monomer, showing no significant structural differences between the two enzymes. Additionally, the electron density maps clearly indicated that FAD in the Ser101Ala enzyme is also covalently linked to the His99 Nϵ2 atom (*17*).

For both variant enzymes, the overall structures determined were identical to the one for the wild-type enzyme. Further it was seen that the orientations of the residues in and around the active site were also similar to those in the wild-type enzyme. The major difference observed for both variant enzymes was that the isoalloxazine moiety of the FAD cofactor was more planar than that of the wild-type. In the latter enzyme, the C(4a) atom has been shown to be sp^3 hybridized due to the presence of an oxygen adduct that is not observed in neither of the variant enzymes resulting in the C(4a) atom being sp^2 hybridized (*2*, *5*).

Kinetically, the His310 (His310Ala, His310Asn and His310Asp), Ser101 (Ser101Ala) and Val464 (Val464Ala and Val464Thr) variant enzymes were distinct, each with kinetic parameters differing significantly from those of the wild-type enzyme.

Of the presented variant enzymes, the variant enzymes where Val464 was replaced with either alanine or threonine were the most extensively investigated. The substitution of valine to alanine or threonine resulted in the reductive half-reaction showing a significantly decreased rate of the initial hydroxyl proton abstraction, while minimally affecting the rate of the subsequent hydride ion transfer and the overall net rate of the reductive half-reaction. However, where the hydroxyl proton abstraction and the hydride transfer proceeds via stepwise mechanism in the wild-type enzyme (*18*), the mechanism is not unequivocal in the Val454Ala variant enzyme as seen by the presence of both substrate and solvent deuterium isotope effects (*12*). The isotope effect results are ambiguous in that they are consistent with both a stepwise mechanism and a mechanism where the synchronicity of the hydroxyl proton abstraction and the hydride transfer display some degree of temporal overlap. As such, the hydride ion transfer in the Val464Ala variant enzyme is at least partially rate limiting as compared to fully rate limiting in the wild-type enzyme. It was further determined that the replacement of Val464 resulted in the

establishment of a kinetically slow equilibrium between a catalytically competent and an incompetent form of enzyme, where the incompetent form is converted to the competent one through a conformational change involving a proton transfer during anaerobic oxidation of the organic substrate.

For the oxidative half-reaction, steady state, rapid kinetics and enzyme monitored turnovers indicated that the reactivity of the reduced form of the Val464 variant enzymes with oxygen is decreased ~50-fold with respect to that of the wild-type enzyme.

In summary, the Val464 variant enzymes exist as an equilibrium of two interconvertible forms of enzyme with the reductive half-reaction proceeding at similar rates for the competent form. Contrary to this, the oxidative half-reaction is significantly impaired upon substitution of Val464. Overall, these results are consistent with valine at position 464 being important for the preorganization of the active site for efficient catalysis, and providing a non-polar site in proximity of the C(4a) atom of the flavin, that is required to guide oxygen to the site of reduction.

In the variant enzyme where His310 was replaced with either an alanine, asparagine or aspartate no catalytic activity with choline as substrate could be detected polarographically. Nevertheless, spectrophotometrically, the variant enzymes were able to be reduced under anaerobic conditions upon mixing with choline, indicating that the they retained the ability to bind choline upon mutation of His310. However, the rates of reduction were estimated to be 70,000 to 550,000 times slower than in the wild-type enzyme. The substitution of His310 also resulted in a significant increased ratio of apoenzyme/holoenzyme thereby implicating His310 in the flavinylation process in choline oxidase. Finally, the reduced form of the variant enzymes

was seen to be the neutral hydroquinone as compared to the anionic form in the wild-type enzyme, and when exposed to atmospheric oxygen no reoxidation of the reduced variant enzymes occurred. Therefore, these results together with the structural information of the wild-type enzyme suggest an important role of His310 in catalysis and the modulation of the micro-environment of the enzyme-bound flavin. The existence of a proton transfer network consisting of the side-chains of His466, His310 and the backbone carbonyl oxygen atoms of Thr380 and Val507 is proposed as the basis for the mechanism by which His310 affects catalysis in choline oxidase.

Overall the His310 variant enzymes are able to bind and be reduced anaerobically by the organic substrate, but show no activity towards the second substrate oxygen. These results are consistent with histidine at position 310 being part of a proton-transfer network, between the side-chains of His466, His310 and the backbone carbonyl oxygen atoms of Thr380 and Val507, whose main purpose is to ensure correct positioning and protonation state of His466. In order to substantiate this hypothesis, the X-ray crystal structure of one of the His310 variant enzymes is required, in order to attribute the kinetic differences of the His310 variant enzymes and the wild-type enzyme to the role exerted by His310 rather than being the result of structural differences between the two enzymes.

For the variant enzyme where Ser101 was replaced with an alanine, preliminary kinetic characterization showed no significant changes in the K_m value for choline between the Ser101Ala and wild-type enzymes. In contrast, the overall rate of catalysis (k_{cat}) in the Ser101Ala enzyme is an order of magnitude slower, whilst having the rate of the reductive half-reaction with betaine aldehyde as a substrate lowered only 3-fold as compared to the rate determined for

the wild-type enzyme. Finally, the oxidative half-reaction showed a 3-4 fold rate increase as compared to the wild-type enzyme.

In summary, preliminary kinetic data suggests that the Ser101 variant enzyme has an improved oxidative half-reaction at the expense of a lowered reductive half-reaction. This kinetic favoring of the oxidative half-reaction is likely due to a change in the FAD micro-environment resulting in an elevation of the reduction potential of FAD cofactor.

Overall, the results presented in this dissertation have provided insight into the role of several residues in close proximity to the flavin cofactor in choline oxidase. One being His310, which is a not in direct contact with the flavin, but can affect the flavin micro-environment through His466. His310 is likely involved in maintaining the correct protonation state of His466, which has been shown to be important for electrostatic stabilization of the reaction intermediate as well as the developing negative charge on the N(1) atom of the flavin during catalysis (*7*). A second residue being Val464, that along with His351 and His466 defines the cavity on the *re*-face directly above the C(4a)-N(5) atoms of the flavin, where the C(4a)-oxygen adduct is observed in the crystal structure of the wild-type enzyme (*2*). Val464 is seen to be important for the oxidation of the reduced flavin by molecular oxygen, but not for substrate binding or the hydride ion transfer reaction that occurs between the choline substrate and the flavin cofactor (*12*). Finally Ser101, which is less than 4 Å from the N(5) atom of FAD and within hydrogen bonding distance of the ligand in the active site of wild-type choline oxidase (*2*), is seen to promote the oxidative half-reaction while demoting the hydride ion transfer reaction in the reaction catalyzed by choline oxidase.

With the elucidation of the large effects on catalysis exerted by the residues presented in this dissertation, it is apparent that efficient catalysis in enzymes, at least in choline oxidase, is achieved through the combination of a large number of effects exerted by multiple residues. This dissertation clearly illustrates the complexity of how enzymes achieve large rate enhancements of reactions and that the residues having prominent roles during catalysis is not limited to active site residues.

References

1. Rungsrisuriyachai, K., and Gadda, G. (2008) On the role of histidine 351 in the reaction of alcohol oxidation catalyzed by choline oxidase, *Biochemistry 47*, 6762-6769.
2. Quaye, O., Lountos, G. T., Fan, F., Orville, A. M., and Gadda, G. (2008) Role of Glu312 in binding and positioning of the substrate for the hydride transfer reaction in choline oxidase, *Biochemistry 47*, 243-256.
3. Quaye, O., and Gadda, G. (2009) Effect of a conservative mutation of an active site residue involved in substrate binding on the hydride tunneling reaction catalyzed by choline oxidase, *Arch Biochem Biophys 489*, 10-14.
4. Quaye, O., Cowins, S., and Gadda, G. (2009) Contribution of flavin covalent linkage with histidine 99 to the reaction catalyzed by choline oxidase, *J Biol Chem 284*, 16990-16997.
5. Orville, A. M., Lountos, G. T., Finnegan, S., Gadda, G., and Prabhakar, R. (2009) Crystallographic, spectroscopic, and computational analysis of a flavin C4a-oxygen adduct in choline oxidase, *Biochemistry 48*, 720-728.
6. Ghanem, M., and Gadda, G. (2006) Effects of reversing the protein positive charge in the proximity of the flavin N(1) locus of choline oxidase, *Biochemistry 45*, 3437-3447.

7. Ghanem, M., and Gadda, G. (2005) On the catalytic role of the conserved active site residue His466 of choline oxidase, *Biochemistry 44*, 893-904.

8. Ghanem, M., Fan, F., Francis, K., and Gadda, G. (2003) Spectroscopic and kinetic properties of recombinant choline oxidase from Arthrobacter globiformis, *Biochemistry 42*, 15179-15188.

9. Gadda, G., Fan, F., and Hoang, J. V. (2006) On the contribution of the positively charged headgroup of choline to substrate binding and catalysis in the reaction catalyzed by choline oxidase, *Arch Biochem Biophys 451*, 182-187.

10. Gadda, G. (2003) Kinetic mechanism of choline oxidase from Arthrobacter globiformis, *Biochim Biophys Acta 1646*, 112-118.

11. Gadda, G. (2003) pH and deuterium kinetic isotope effects studies on the oxidation of choline to betaine-aldehyde catalyzed by choline oxidase, *Biochim Biophys Acta 1650*, 4-9.

12. Finnegan, S., and Gadda, G. (2008) Substitution of an active site valine uncovers a kinetically slow equilibrium between competent and incompetent forms of choline oxidase, *Biochemistry 47*, 13850-13861.

13. Fan, F., Ghanem, M., and Gadda, G. (2004) Cloning, sequence analysis, and purification of choline oxidase from Arthrobacter globiformis: a bacterial enzyme involved in osmotic stress tolerance, *Arch Biochem Biophys 421*, 149-158.

14. Fan, F., Germann, M. W., and Gadda, G. (2006) Mechanistic studies of choline oxidase with betaine aldehyde and its isosteric analogue 3,3-dimethylbutyraldehyde, *Biochemistry 45*, 1979-1986.

15. Fan, F., and Gadda, G. (2007) An internal equilibrium preorganizes the enzyme-substrate complex for hydride tunneling in choline oxidase, *Biochemistry 46*, 6402-6408.

16. Fan, F., and Gadda, G. (2005) Oxygen- and temperature-dependent kinetic isotope effects in choline oxidase: correlating reversible hydride transfer with environmentally enhanced tunneling, *J Am Chem Soc 127*, 17954-17961.

17. Finnegan, S., Agniswamy, J., Weber, I. T., and Gadda, G. (2010) Role of Val464 in the Flavin Oxidation Reaction Catalyzed by Choline Oxidase, *Biochemistry*.

18. Fan, F., and Gadda, G. (2005) On the catalytic mechanism of choline oxidase, *J Am Chem Soc 127*, 2067-2074.